PROBING THE DENATURED STATE ENSEMBLE WITH FLUORESCENCE

A Dissertation

by

ROY WILLIS ALSTON

Submitted to the Office of Graduate Studies of
Texas A&M University
in partial fulfillment of the requirements for the degree of

DOCTOR OF PHILOSOPHY

May 2004

Major Subject: Biochemistry

PROBING THE DENATURED STATE ENSEMBLE WITH FLUORESCENCE

A Dissertation

by

ROY WILLIS ALSTON

Submitted to Texas A&M University
in partial fulfillment of the requirements
for the degree of

DOCTOR OF PHILOSOPHY

Approved as to style and content by:

C. Nick Pace (Chair of Committee)	Gregory D. Reinhart (Member)
J. Martin Scholtz (Member)	Gary R. Kunkel (Member)
Gregory D. Reinhart (Head of Department)	

May 2004

Major Subject: Biochemistry

ABSTRACT

Probing the Denatured State Ensemble with Fluorescence. (May 2004)

Roy Willis Alston, B.S.E., University of Arkansas;

M.S., Indiana State University;

M.S., Texas A&M University

Chair of Advisory Committee: Dr. C. Nick Pace

To understand protein stability and the mechanism of protein folding, it is essential that we gain a better understanding of the ensemble of conformations that make up the denatured state of a protein. The primary goal of the research described here was to see what we might learn about the denatured state using fluorescence. To this end, tryptophan was introduced at five sites in Ribonuclease Sa (RNase Sa): D1W, Y52W, Y55W, T76W, and Y81W. The fluorescent properties of the denatured states of these five proteins were studied and compared to the fluorescent properties of eight model compounds: N-acetyl-tryptophan-amide (NATA), N-acetyl-Ala-Trp-Ala-amide (AWA), N-acetyl-Ala-Ala-Trp-Ala-Ala-amide (AAWAA), and five pentapeptides based on the sequence around the original tryptophan substitutions in RNase Sa.

Regardless of the denaturant, λ_{max} for the proteins and model compounds differed very little, 349.3 ± 1.2 nm. However, significant differences were observed in the fluorescence intensity at λ_{max} (I_F), suggesting that I_F is more sensitive to the immediate environment than λ_{max}. The differences in I_F are due in part to quenching by neighboring side chains. More importantly, I_F was always significantly greater in the protein than in its corresponding pentapeptide, indicating that the protein exerts an effect on the tryptophan, which cannot be mimicked by the pentapeptide models.

Acrylamide and iodide quenching experiments were also performed on the model compounds and proteins. Significant differences in the Stern-Volmer quenching constant (K_{SV}) were also observed between the proteins and between the proteins and their corresponding pentapeptides. Importantly, the K_{SV} for the protein was always less than in its corresponding pentapeptide. These data along with the I_F data show that non-local structure in the unfolded state influences tryptophan fluorescence and accessibility.

In summary, these and our other studies show that fluorescence can be used to gain a better understanding of the denatured states of proteins.

DEDICATION

Dedicated to my family:

For their love and support.

And to Dr. Pace:

For his faith and belief in me.

ACKNOWLEDGEMENTS

There are so many people who have helped me get to this point, but most importantly, I am indebted to Dr. Nick Pace. Regardless of the career choice, you have to have someone who will give you an opportunity and believe in you. He allowed me to complete a Master's and Ph.D. in his lab. Dr. Pace's love of science, patience with his students, and leadership in the lab are second to none. Dr. Pace is more than my mentor, though. I am honored to call him a friend. I am grateful to Dr. Gary R. Kunkel, Dr. Gregory D. Reinhart, and Dr. J. Martin Scholtz for serving on my committee. Their expertise lent so much to my research. I am grateful to Dr. Art Johnson. Although he didn't serve on my committee, his door was always open and his expertise was invaluable. My thanks also goes to Saul Trevino. Saul was very instrumental in helping me express and purify the proteins in the charge-reversal background. Certainly, many members, past and present, of the Pace and Scholtz labs at one time or another have been extremely generous with their time and helpful to me. There are two people who helped me get here: Dr. Bret Shirley of Altus Biologics, Inc. and Dr. Don England of Harding University. Bret is as close a friend as anyone could hope for, and Dr. England's love of chemistry and pride in me caused me to want to strive for more. Alas, this would be incomplete without thanking my family. Their love and encouragement have kept me going. I couldn't have done this without them!

TABLE OF CONTENTS

Page

Page

LIST OF FIGURES

FIGURE Page

FIGURE Page

FIGURE Page

FIGURE Page

FIGURE Page

FIGURE Page

FIGURE Page

FIGURE Page

FIGURE Page

FIGURE Page

LIST OF TABLES

TABLE Page

INTRODUCTION

> … proteins dissolved in concentrated guanidine hydrochloride (GuHCl) lose essentially all elements of their native structure, and exist as random coiled chains in which no important noncovalent interactions remain (Nozaki and Tanford 1967).

The Denatured State

In the 1960's, Tanford's group published a series of studies aimed at better characterizing the denatured states of proteins. The major conclusion was that proteins in 6 M GdnHCl with their disulfide bonds broken closely approach a randomly coiled conformation. Even with their disulfide bonds intact, proteins seemed to unfold as completely as possible given the restraints imposed by the disulfide bonds (Tanford 1968). It is debatable whether Tanford fully believed that, because he did note from other work that polypeptides such as polyleucine and polyphenylalanine retain structured regions in 6 M GuHCl, at least at room temperature (Auer and Doty 1966; Sage and Fasman 1966). Furthermore, Tanford went on to say, "Structured regions may therefore be expected in proteins, too, if long segments of a polypeptide chain consist entirely or predominantly of highly hydrophobic amino acid residues (Tanford et al. 1967)."

Several papers have been published in the past few years addressing the exisitance of residual structure in the denatured state and how it plays an important role in folding and stability of proteins. Shortle's group suggested that the denatured states of proteins were more complicated than previously thought. They stated, "There is now considerable evidence that even in strong denaturants such as 6 M GdnHCl and 9 M

This dissertation follows the style and format of *Protein Science*.

urea, some structure may remain in protein chains (Dill and Shortle 1991)."

Evidence from other proteins also suggests that the denatured state is not a random coil but may have fluctuating pockets of structure (Kemmink et al. 1993; Shortle 1993; Lumb and Kim 1994; Smith et al. 1996). These pockets of structure often include aromatic amino acids (Neri et al. 1992; Schwalbe et al. 1997).

Why study the denatured state? One reason is their role in protein folding and stability. In their review, Dill and Shortle state, "The denatured states of proteins are equal in importance to the native states in determining the stability of a protein, since stability is defined as the difference in free energies between native and denatured states (Dill and Shortle 1991)." Baldwin states, "Today there are strong suspicions that the seeds of folding process are already present in the denatured protein (Baldwin 2002)." Other reviews have addressed the possible role of residual structure in protein folding (Miranker and Dobson 1996; Shortle 1996). Residual structure in the denatured state could act as initiation sites allowing the polypeptide chain to form the first elements of secondary structure through short-range interactions (Garcia et al. 1998).

Tryptophan Fluorescence

Tryptophan fluorescence of proteins has been used for many years to gain insight into a protein's structure and dynamics. In 2001, Vivian and Callis stated that some 300 papers per year abstracted in Biological Abstracts reported work that exploits or studies tryptophan fluorescence in proteins. Among the properties studied are changes in the fluorescence intensity, wavelength of maximal intensity (λ_{max}), band shape, anisotropy, lifetimes (τ), and energy transfer. The studies are applied to protein folding, substrate binding, external quencher accessibility, etc. (Vivian and Callis 2001). However, understanding tryptophan fluorescence is a complicated subject. Many

papers in the past several years have demonstrated that the fluorescence of tryptophan residues is strongly dependent on their environment (Chen et al. 1996; Callis 1997; Callis and Burgess 1997; Chen and Barkley 1998; Meagher et al. 1998).

Tryptophan is the most important of the intrinsic fluorescence probes in proteins: it has a larger molar absorption coefficient (Table 1), it serves as an energy transfer acceptor for the other aromatic amino acids, it can be selectively excited at long wavelengths (e.g., >296 nm), and its fluorescence intensity (I_F) and the intensity wavelength maximum (λ_{max}) are sensitive to the microenvironment of the indole side chain (Weinryb and Steiner 1971; Lakowicz 1983; Beechem and Brand 1985; Eftink 1991). Table 2 gives the λ_{max} values of tryptophan, NATA, and a tripeptide, N-acetyl-AWA-amide, in various solvents.

Table 1. Aromatic amino acids, their residue volumes, mean percent buried in proteins, hydrophobicity, absorbance and fluorescence properties.

Amino Acid	Volume ($Å^3$)[a]	Mean Percent Buried[b]	Hydrophobicity (kcal mol^{-1})[c]	Absorbance[d]		Fluorescence[e]	
				λ_{max}[f]	ε_{max}[g]	λ_{max}[f]	φ_F
Tryptophan	232	87	3.1	280	5600	353	0.13
Tyrosine	197	77	1.3	275	1400	304	0.14
Phenylalanine	194	88	2.4	258	200	282	0.02

[a](Harpaz et al. 1994)
[b]The mean fraction buried in a sample of 61 proteins (Lesser and Rose 1990)
[c](Fauchere and Pliska 1983)
[d](Schmid 1997)
[e](Lakowicz 1999)
[f]nm
[g]M^{-1} cm^{-1}

Table 2. λ_{max} values for tryptophan and two tryptophan models in various solvents.

Compound	λ_{max} (nm) in Various Solvents[a]					
	Hexane	Dioxane	Ethanol	Acetonitrile	Water	9 M Urea
NATA[b]	320	328	337	335	351	348
AWA[b]	322	327	337	335	351	349
NATA[c]		329	340	334	352	
Trp[d]		329	338		350[e]	

[a]The dielectric constants for the solvents are: hexane, 1.9; dioxane, 2.2; ethanol, 24; acetonitrile, 38; Water, 78; 9 M Urea, 99.
[b]This paper: NATA is N-acetyl-Trp-amide; AWA is N-acetyl-Ala-Trp-Ala-amide.
[c](Ross et al. 1997).
[d](Konev 1967)
[e]In 0.1 M Tris, pH 7.0.

To help in the understanding of the fluorescence properties of tryptophans, attempts have been made to classify tryptophans. One of the first to suggest discrete discrete classes of tryptophans was Konev in 1967, who suggested two main classes, involving the parameters λ_{max} and quantum yield (q). One of the classes included tryptophans inside the protein in a non-polar, hydrophobic environment with a shorter wavelength of fluorescent maximum (λ_{max} of ~330 nm) and a rather low quantum yield (0.04 to 0.07). The second class consisted of exposed tryptophan residues in a polar aqueous environment with a long wavelength fluorescence maximum (λ_{max} ~350 nm) and a quantum yield equal or higher than that of free aqueous tryptophan (~0.13 to 0.17). This idea was based on the observation that protein spectra shift toward 350 nm upon denaturation by urea, and toward 330 nm upon addition of anionic detergents (Reshetnyak and Burstein 2001). In 2001, Callis stated that the most common use of tryptophan fluorescence λ_{max} information is to assign a tryptophan as buried in a non-polar environment if λ_{max} is < 330 nm or as exposed in a polar environment if λ_{max} is

longer than ~330 nm (Vivian and Callis 2001). However, classifying tryptophans into one of these two classes is surely too restrictive. For example, Konev's hypothesis could not explain proteins with high quantum yield and an intermediate λ_{max}. For example, Ribonuclease T1 has a quantum yield of 0.31 and a λ_{max} of 322 nm (Eftink 1991). Furthermore, Callis demonstrated that mere exposure to water may or may not create a large red shift (Vivian and Callis 2001).

In 1973 and later refined in 2001, Burstein and co-workers revised and extended Konev's hypothesis of discrete classes of tryptophan residues in proteins and suggested a new model using some additional spectral parameters and approaches (Burstein et al. 1973; Burstein et al. 2001; Reshetnyak and Burstein 2001; Reshetnyak et al. 2001). A detailed characterization of the environment of the tryptophan in each class was made in terms of hydrogen bonding, solvent accessibility, packing density, relative polarity, temperature factor, and dynamic accessibility. Burstein assigns tryptophans to one of five discrete classes (Reshetnyak and Burstein 2001; Reshetnyak et al. 2001). This division into classes should allow researchers to better compare tryptophans in various proteins. As Engelborghs states, "This work represents an important achievement in the characterization of the environment of each tryptophan and the linkage to the spectral properties (Engelborghs 2003)." We will now turn our attention to what specific factors contribute to λ_{max} and fluorescence intensity at λ_{max} (I_F).

Spectral Moment and λ_{max}

The fluorescence intensity wavelength maximum, λ_{max}, for tryptophans in proteins ranges from 308 to 355 nm (Eftink 1991; Vivian and Callis 2001). As previously stated, it is generally thought that there is a relationship between λ_{max} and the solvent exposure of tryptophans in proteins (Burstein et al. 1973; Turoverov and

Kuznetsova 2003). For example, Callis wrote: “The wavelength of maximum fluorescence intensity (λ_{max}) is universally and unquestioningly used as an indicator of exposure to water, i.e., as an indicator of how deeply the tryptophan is buried in the protein (Callis 1997).” In fact, indole has been shown to be extremely sensitive to hydrogen-bonding solvents. For example, one study demonstrated that as small amounts (< 5%) of ethanol were added to cyclohexane, indole’s λ_{max} shifted significantly to the red (Gryczynski et al. 1988).

More recently, Vivian and Callis have reported calculations that suggest that the observed shifts in λ_{max} can be largely accounted for by differences in the electrostatic interactions of the ground state and the ^1L_a excited state of the tryptophan and the surrounding protein/solvent environment (Vivian and Callis 2001). They consider the question, “Why so few blue shifts from protein?” One possibility they suggest is that the ground state dipole of tryptophan is oriented to give a favorable electrostatic interaction with the protein and since the ^1L_a excited state has a larger dipole and is nearly parallel to that of the ground state, we expect an even more favorable electrostatic interaction with the excited state and hence a red shift in most proteins.

I_F

According to current knowledge, the quantum yield primarily depends on the existence of quenching groups in the microenvironment, on long-range effects such as Trp-Trp non-radiative energy transfer, and on excited-state electron transfer from the indole ring to an electron acceptor (Turoverov and Kuznetsova 2003). Chen and Barkley identified eight amino acid side chains representing six functional groups which quenched 3-methylindole with a 100-fold range in quenching rate constants. Those amino acids side chains included the amide groups of glutamine and asparagine, the

carboxyl groups of glutamic and aspartic acids, ε-amino group of lysine, phenol ring of tyrosine, sulfhydryl of cysteine, and the protonated group of histidine imidazole (Chen and Barkley 1998). It is important to note that they do not all quench 3-methylindole to the same degree. Although, arginine and phenylalanine were not found to quench 3-methylindole in their work, they have been shown to be an effective quenchers in other studies (Clark et al. 1996; Lakowicz 1999). Additionally, peptide bonds have also been shown to quench tryptophan fluorescence (Chen et al. 1996; Adams et al. 2002). However, peptide bond quenching seems to be very dependent upon the rotamer of the tryptophan (Adams et al. 2002). The experimental (Chen and Barkley 1998; Sillen et al. 2000; Adams et al. 2002) and theoretical (Callis and Vivian 2003) evidence suggests that electron transfer to the carbonyl carbon of a neighboring peptide group may be the most important mechanism for intramolecular quenching of Trp fluorescence.

Additionally, Cowgill observed that as the dielectric constant of the solvent decreased, the λ_{max} of indole decreased and the quantum yield increased (Table 3).

Table 3. Comparison of the dielectric constant, λ_{max}, and quantum yield for indole in various solvents (Cowgill 1967).

Solvent	Dielectric Constant	λ_{max}, nm	Quantum Yield
Water	78.5	350	0.40
n-Butanol	17.1	330	0.58
p-Dioxane	2.2	315	0.62
n-Hexane	1.9	300	

Small Molecule Extrinsic Quenching

As stated previously, fluorescence can be quenched by many groups. In this section, we will focus primarily on quenching resulting from collisional encounters between the fluorophores and small molecule, extrinsic quenchers (e.g. acrylamide,

iodide, etc.), which is referred to as collisional or dynamic quenching. For collisional quenching to occur, the quencher must encounter the fluorophore during the lifetime of the excited state. Upon contact, the fluorophore returns to the ground state without emission of a photon. Static quenching may also occur, which is the formation of a complex between the fluorophores and the quencher, resulting in a non-fluorescent complex (Lakowicz 1999). For either static or dynamic quenching to occur though, there must be contact between the fluorophore and the quencher. Studying this molecular contact yields insight into the accessibility of fluorophores to quenchers.

The exposure or accessible surface area of an atom or residue can be calculated from an x-ray crystal structure (Lee and Richards 1971). Because the calculations are derived from a crystal structure, these calculations represent a static view of the molecule, when in fact, proteins are by no means static, but engage in internal motions of many kinds (Gurd and Rothgeb 1979; Karplus and McCammon 1981; Maity et al. 2003). As a result of this mobility, a residue that appears buried in the crystal structure may become periodically exposed to solvent in solution. Therefore, an excellent way to experimentally determine the degree of exposure of tryptophanyl residues in solution is by fluorescence quenching (Lehrer 1971; Eftink and Ghiron 1977). Iodide and acrylamide have been shown to quench tryptophan fluorescence in numerous studies (Eftink and Ghiron 1976; Komath and Swamy 1999), and they are the quenchers studied here.

Lakowicz and Weber suggested that O_2 might easily penetrate into proteins and this was later confirmed by others (Lakowicz and Weber 1973b; a; Calhoun et al. 1983; Gratton et al. 1984). This concept was later extended to small molecules, such as acrylamide (Eftink and Ghiron 1981). If this was true, the rate of true penetration

reactions should be sensitive to molecular characteristics of the quencher such as size, polarity, and charge. Calhoun and co-workers concluded that when quenching is observed, the pathway involves encounters with tryptophans that are partially exposed at the protein's surface, so that protein penetration need not be invoked (Calhoun et al. 1986).

Collisional quenching experiments by steady-state fluorescence are described by the Stern-Volmer equation:

$$\frac{F_0}{F_I} = K_{SV}[Q] + 1$$

where F_0 and F_I are the fluorescence of the sample in the absence of quencher and in the presence of quencher, respectively, K_{SV} is the Stern-Volmer quenching constant, and [Q] is the quencher concentration. A plot of F_0/F_I as a function of quencher concentration, [Q], is expected to be linear, with a y-intercept of one and slope equal to K_{SV}. A deviation from the linearity of the plot would suggest that a static and a dynamic component exist.

Ribonuclease Sa

Ribonucleases (RNases) may be the oldest enzymes, so perhaps it is not surprising that they are involved in such a wide range of functions (Schein 1997). The *Streptomyces* are Gram-positive filamentous bacteria that are used industrially for the production of several antibiotics. Strains of *Streptomyces aureofaciens* are used to produce the antibiotic chlortetracycline, and they also synthesize and secrete into the growth medium a small RNase (Bacova et al. 1971). The RNases from three of these strains have been characterized and named RNase Sa, RNase Sa2, and RNase Sa3

(Hartley et al. 1996; Hebert et al. 1997). These Sa RNases are members of the microbial RNase family (Hartley 1980; Hill et al. 1983).

The amino acid sequences of RNases Sa, Sa2, Sa3, Ba, and T1 are aligned in Figure 1 with the proposed tryptophan substitutions boxed. All five of these enzymes cleave single-stranded RNA molecules specifically on the 3' side of guanosine nucleotides. Compared to the 96 residues of RNase Sa, the percent identities are shown in Table 4.

Table 4. Sequence identity of the five microbial RNases.

RNase	Sequence Identity
Sa	100 %
Sa3	69 %
Sa2	56 %
Ba	23 %
T1	11 %

Figure 2 shows the secondary structure representation of RNase Sa. RNases Sa, Ba, and T1 have remarkably similar tertiary structures in the β-sheet regions near the active sites, but there are substantial difference in the α-helices and turns as shown in Figure 3.

Several of the microbial RNases have been studied as models for protein folding, especially RNase T1 by our lab (Pace 1990; Yu et al. 1994; Mullins et al. 1997; Myers et al. 1997; Giletto and Pace 1999) and Ba by the Fersht lab (Bond et al. 1997; Soler-Gonzalez and Fersht 1997; Killick et al. 1998; Axe et al. 1999). RNase Sa has been studied less, but has many features that make it a good model for protein folding studies, too (Pace et al. 2000; Pace 2001; Takano et al. 2003). RNase Sa is the smallest member of the microbial RNase family, with just 96 amino acids. Crystal

structures of native at 1.2 Å resolution (pdb1rgg.ent) and most recently, a 1.0 Å resolution (pdb1lni.ent) have been determined (Sevcik et al. 1991; Sevcik et al. 1996; Sevcik et al. 2002). A solution structure was also recently determined by NMR (Laurents et al. 2001). NMR has also been used to measure the pK values of the ionizable residues in RNase Sa (Huyghues-Despointes et al. 2003; Laurents et al. 2003). The thermodynamics of folding have been studied and the conformational stability of RNase Sa is 6.0 kcal mol^{-1} at 25 ^{o}C and pH 7.0 (Pace et al. 1998).

All members of the microbial RNase family have a relatively high content of aromatic amino acids, especially tyrosine. However, RNase Sa has no tryptophan residues. Table 5 shows the aromatic amino acid content of various RNases as well as that of an average protein.

Table 5. Aromatic amino acid composition for the various RNases and the average composition for a protein.

	Tryptophan	Tyrosine	Phenylalanine	Total
Sa	0 (0.0%)	8 (8.3%)	3 (3.1%)	11/96 (11.5%)
Sa2	1 (1.0%)	7 (7.2%)	3 (3.1%)	11/97 (11.3%)
Sa3	1 (1.0%)	8 (8.1%)	4 (4.0%)	13/99 (13.1%)
T1	1 (1.0%)	9 (8.7%)	3 (2.9%)	13/104 (12.5%)
Ba	3 (2.7%)	7 (6.4%)	4 (3.6%)	14/110 (12.7%)
Average[a]	1.3%	3.2%	3.9%	8.4%

[a](McCaldon and Argos 1988)

```
Sa                                                  DVSGTVCLSAL   11
Sa2                                               ADPALADVCRTKL   13
Sa3                                             ASVKAVGRVCYSAL    14
Ba   AQVINTFDGVADYLQTYHKLPNDYITKSEAQA   32
T1                                 ACDYTCGSNCYSS  SDVST   18

Sa   PPEATDTLNLIASDGPFPYSQDGVVFQNRESV   43
Sa2  PSQAQDTLALIAKNGPYPYNRDGVVFENRESR   45
Sa3  PSQAHDTLDLIDEGGPFPYSQDGVVFQNREGL   46
Ba   LGWVASKGNLADVA  PG  KSIGGDIFSNREGK   62
T1     AQAAGYQLHEDGETVGSNSYPHKYNNYEGF   48

Sa   LPTQSYGY[Y]HE[Y]TV          ITPGARTRGTRR   69
Sa2  LPKKGNGYYHEFTV          VTPGSNERGTRR   71
Sa3  LPAHSTGYYHEYTV          ITPGSPTRGARR   72
Ba   LPGKSGRTWREADI        NYTSGF    RNSDR   87
T1   DFSVSSP  YYEWPILSSGDVYSGGSP    GADR   77

Sa   IITGEA[T]QEDY[Y]TGDHYA       TFSLIDQTC    96
Sa2  VVTG  GYGEQYWSPDHYA       TFQEIDPRC    97
Sa3  IITGQQWQEDYYTADHYA       SFRRVDFAC    99
Ba   ILYSSDW  LIYKTTDHYQ       TFTKIR       110
T1   VVFNENN  QLAGVITHTGASGNNFVECT       104
```

Figure 1. Sequence alignment of RNases Sa, Sa2, Sa3, Ba, and T1 with the proposed tryptophan substitutions boxed (Hill et al. 1983; Hebert et al. 1997).

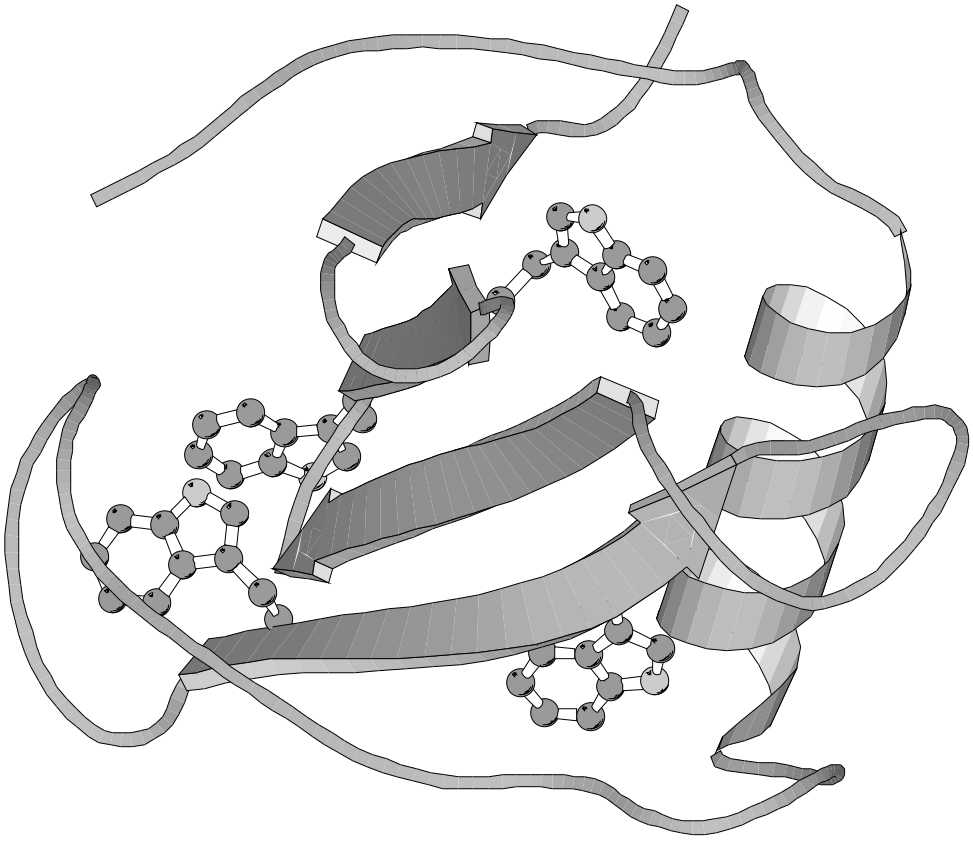

Figure 2. Secondary structure representation of RNase Sa with the tryptophan substitutions. This plot was prepared using the program *MOLSCRIPT* (Kraulis 1991).

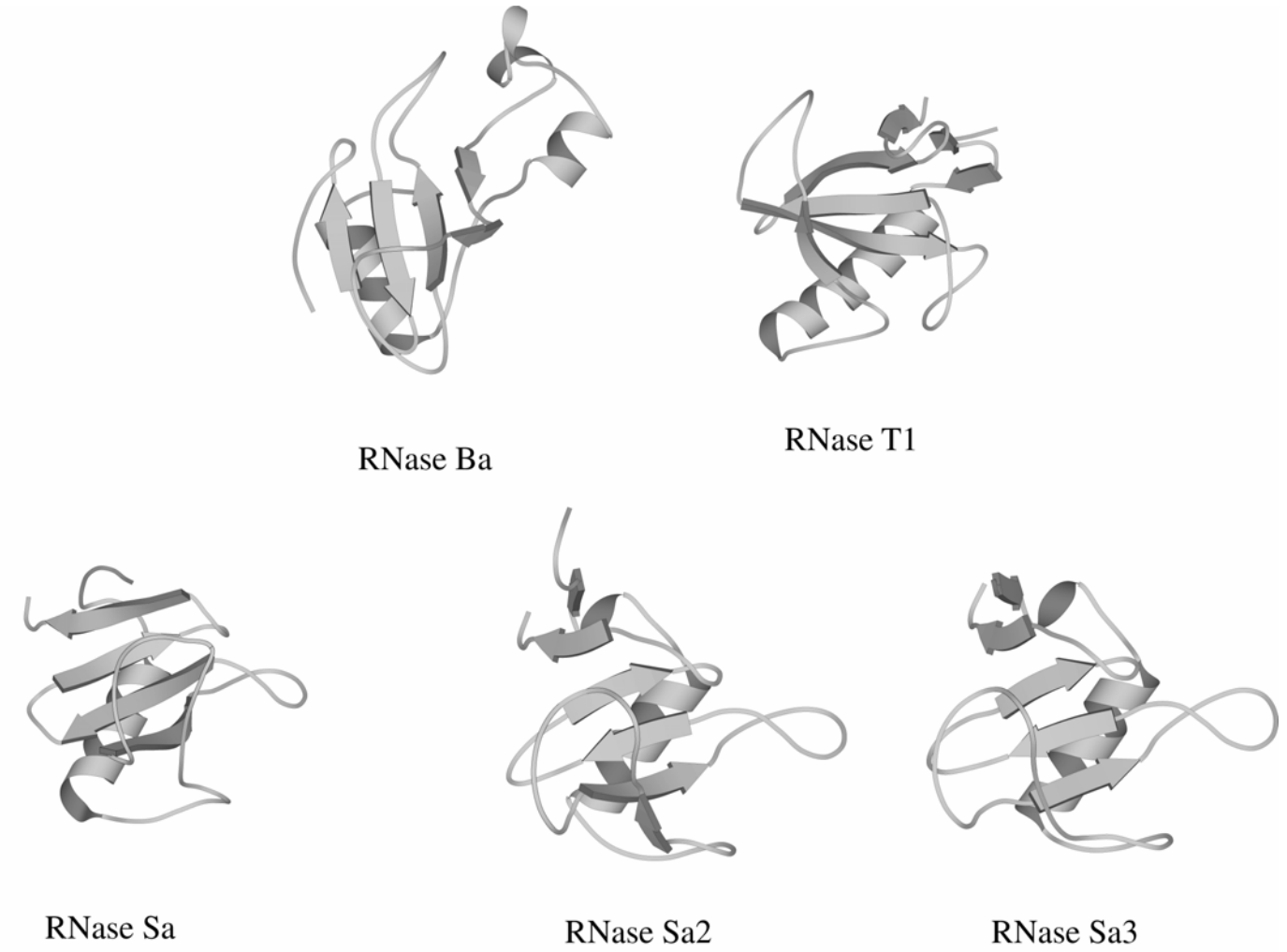

Figure 3. The secondary structure representation of RNase Sa compared to Ba, T1, Sa2, and Sa3. This plot was prepared using the program *MOLSCRIPT* (Kraulis 1991).

Previous Research

Introduction

Since RNase Sa has no tryptophans, we previously inserted tryptophan residues at sites (Y52W, Y55W, T76W, and Y81W) equivalent to those where tryptophans are found in other RNases (Figure 1). This was done to allow us the ability to compare four different folded environments in RNases Sa, with the folded environments in the proteins on which the tryptophan sites were based. One of the main goals of this previous work was to improve our understanding of the influence of the environment on the fluorescence properties of tryptophan residues. Tables and figures relating to research done previously are found in Appendix A.

Stability of the Single Tryptophan Variants of RNase Sa

Tryptophan has the largest and most hydrophobic side chain of all of the amino acids (Fauchere and Pliska 1983). Because of its size, when a tryptophan residue replaces any other residue in a protein it may cause a conformational change and decrease the stability for steric reasons. Our four tryptophan containing variants retain their enzyme activity, indicating that their conformation has not been changed to a great extent. Three of the tryptophan variants are less stable than wild-type RNase Sa (Appendix A, Table 26) (Alston 1999). In these cases, tryptophan was substituted for a tyrosine at a largely buried site in RNase Sa (Table 6). Additionally, Tyr52 and Tyr81 both form intramolecular hydrogen bonds. We proposed that in T76W, the tryptophan is partially buried and makes a favorable contribution to the stability. Additionally, in Y52W, Y55W, and Y81W, the tryptophan residues are largely buried, but the hydrogen bonding and van der Waals interactions are not as favorable as they are for the tyrosine residues they replace in RNase Sa or as they are for the tryptophan residues in the

parent proteins. Interestingly, of all the variants our lab has made in RNase Sa, Y52W has one of the largest decreases in stability.

Table 6. Accessibility of the residue to be substituted with tryptophan in RNase Sa and of the tryptophan in the parent RNase.

Residue in RNase Sa	% Buried	Trp in the parent RNase	% Buried
Tyr 52	98%	RNase Ba Trp 71	98%
Tyr 55	89%	RNase T1 Trp 59	100%
Thr 76	10%	RNase Sa3 Trp 79	0%
Tyr 81	89%	RNase Sa2 Trp 82	94%

[a]Percent buried calculated by the Lee & Richards algorithm (Lee and Richards 1971).

Fluorescence Properties of the Tryptophan Containing Variants, λ_{max}

The λ_{max} values for the native states range from 309 for Y52W to 335 nm for T76W (Appendix A, Figure 29 and Appendix A, Table 27) (Alston 1999). It is very surprising that the tryptophan of Y52W is blue shifted to such an extent. The largest blue shift observed to date is to 308 nm for Trp48 in Azurin. Note that the tyrosine it replaces in RNase Sa is 98% buried and the corresponding tryptophan in barnase is also 98% buried but has a λ_{max} of 332 nm. We think our data supports the idea proposed by Vivian and Callis (2001). We have substituted tryptophans at sites selected for other residues, so it is unlikely that the tryptophan side chain would have favorable electrostatic interactions with the protein. This might explain why the newly-introduced tryptophan residues are all blue shifted with respect to the tryptophan residues in the parent proteins.

Trp59 in RNase T1 is one of the most studied tryptophan residues in proteins (Longworth 1971; Axelsen and Prendergast 1989; Eftink 1991; Vivian and Callis 2001). It is 100% buried, but the N in the indole ring is hydrogen bonded to a water molecule (Martinez-Oyanedel et al. 1991). Its native emission λ_{max} is 318 nm (Table 3), but when

we place a tryptophan at the equivalent position in RNase Sa (Y55W), the fluorescence intensity is markedly reduced and λ_{max} appears to be lowered to near 310 nm. However, it appears that the tryptophan fluorescence is quenched to such an extent that we are mainly observing a very weak tryptophan fluorescence superimposed on the fluorescence of the tyrosine residues. This is supported by the observation that λ_{max} shifts from 310 nm to 322 nm when the exciting wavelength is increased from 280 nm to 296 nm. Similar results were observed when Tyr 92 in RNase A was replaced by a tryptophan (Sendak et al. 1996).

Our λ_{max} values are in good agreement with previous data for both NATA and tryptophan in the same solvents (Table 2). These data clearly show that more polar solvents have favorable interactions with the large dipole of the ^1L_a excited state of the indole ring to give large red shifts in λ_{max}, and that in solvents such as hexane where only dipole-induced dipole interactions are possible the red shifts are smaller. The smaller red shifts observed in our folded parent RNases suggest that the environment of most tryptophan residues is designed to favor interactions with the smaller ground state dipole and the interactions with the excited state – while favorable – are not as favorable as can be achieved in a polar solvent. The red shifts are even smaller for the RNase Sa variants because the indole side chains are now in environments selected for other side chains.

Fluorescence Properties of the Tryptophan Containing Variants, I_F

Adding a tryptophan to RNase Sa markedly increases the fluorescence of Y52W, T76W, and Y81W, but not Y55W (Appendix A, Figure 29 and Appendix A, Table 27) (Alston 1999). At identical concentrations, the fluorescence intensities of the folded proteins vary more than 10 fold from 8150 (Y55W) to 82,800 (RNase T1). The

tryptophan in folded RNase Sa3 is completely exposed to solvent so, as expected, the fluorescence intensity is almost the same in the folded and unfolded state. However, when a tryptophan is added to the equivalent position in RNase Sa, the fluorescence intensity is substantially higher in the folded protein. It appears that the newly introduced tryptophan (T76W) is partially buried in RNase Sa, as the increased stability discussed above also indicated.

Of the seven single tryptophan proteins, the tryptophan of RNase T1 has the greatest fluorescence intensity, but when a tryptophan is added to the equivalent position in RNase Sa (Y55W), the tryptophan has the lowest intensity of any of the proteins (Appendix A, Table 27) (Alston 1999). The tryptophan in Y55W appears to be almost completely quenched. There is a phenylalanine is the immediate vicinity of Y55W, which may be doing the quenching. We are currently trying to solve the crystal structures of the tryptophan variants. It will be interesting to see if we can understand the strong quenching of the tryptophan in Y55W once we know the structure.

Circular Dichroism of the Tryptophan Containing Variants

Some proteins, including most of the microbial RNases, have positive CD bands in the far UV spectra between 220 and 235 nm, and Woody has proposed that tryptophan can make a significant contribution to this band (Woody 1994). RNase Sa has a positive CD band at 234 nm that is lost when the protein unfolds and the CD change is so large that this is the wavelength we use to follow unfolding. Most of the proteins with these positive CD bands contain tryptophan, but RNase Sa does not. In a previous study, we showed that when Tyr52 was replaced with phenylalanine the positive CD band was shifted slightly to longer wavelengths and the magnitude was substantially reduced (Hebert 1997). In this study, without exception, the presence of

tryptophan in the variants increased the mean residue ellipticity at 234 nm (Appendix A, Figure 30). The largest change is for Y81W where the mean residue ellipticity is more than double the value for wild-type RNase Sa. Our results show that both tyrosine and tryptophan residues contribute to positive CD band at 234 nm observed in the microbial ribonuclease family.

The Charge-Reversal Project

The conformational stability of a globular protein may be defined as the free energy change for the reaction: folded, native (F) ↔ unfolded, denatured (U). To increase the stability of a protein there are two choices, increase the free energy of U or decrease the free energy of F. Two recent papers came out of our lab, addressing the possibility of increasing a protein's stability by reversing the charge on an exposed amino acid side chain to make the coulombic interactions among the charged groups on the proteins more stabilizing (Grimsley et al. 1999; Pace et al. 2000).

Coulomb's Law ($E = q_1q_2 / Dr$) is defined as the energy required to bring two unit charges, q_1 and q_2, from infinity to a distance r apart in a medium with a dielectric constant, D. At neutral pH, the side chains of Asp and Glu will have a negative charge, the side chains of Lys and Arg will have a positive charge, and the side chain of His will have a partial positive charge. Consequently, both attractive and repulsive charge-charge interactions exist. When a protein unfolds, the charges might be further apart and the effective dielectric constant increased; consequently, coulombic interactions will be substantially reduced. In general, then, coulombic interactions will contribute favorably to protein stability (Grimsley et al. 1999).

Introducing favorable coulombic interactions was used on two single-site variants of RNase Sa, D25K and E41K with success. At pH 7, the net charge or RNase

Sa is ≈ -7. Consequently, to stabilize these proteins by improving electrostatic interactions, a negative charge was replaced with a positive charge. Additionally, these substitutions were chosen because both are relatively accessible to solvent, not hydrogen bonded, and predicted by Coulomb's Law to have a stability increase of over 1 kcal/mol when the negative charge is removed (Appendix A, Table 28). We observed that the stability of both variants increased by about 1 kcal/mol when the negative charge in wild-type RNase Sa was replace by a positive charge in the variants (Appendix A, Table 28).

However, this approach is not always successful. Two other single-site charge-reversal variants of RNase Sa, D17K and E41K, were prepared. They too, are relatively accessible to solvent, not hydrogen bonded, and predicted by Coulomb's Law to have an increase in stability when the negative charge is removed. However, both of these variants had a decrease in stability with the charge-reversal substitutions. We concluded that for the variants with decreased stability, the electrostatic interactions were more favorable in the denatured state than for wild-type RNase Sa. Two other observations supported this conclusion, *m*-values and salt screening.

Research Objectives

One of the major goals of the present study was to gain a better understanding of how the environment influences λ_{max}, fluorescence intensity, and extrinsic quenching of the tryptophans in the denatured state. Additionally, by placing the single-site tryptophan variants in the wild-type and charge-reversal backgrounds, we hope to observe the subtle differences between these two backgrounds in the denatured state ensemble.

MATERIALS AND METHODS

Materials

N-acetyl-L-tryptophan-amide was obtained from Sigma-Aldrich (St. Louis, MO). N-acetyl-Ala-Trp-Ala-amide, N-acetyl-Ala-Ala-Trp-Ala-Ala-amide, Trp-Val-Ser-Gly-Thr-amide, N-acetyl-Gly-Tyr-Trp-His-Glu-amide, N-acetyl-His-Glu-Trp-Thr-Val-amide, N-acetyl-Glu-Ala-Trp-Gln-Glu-amide, N-acetyl-Asp-Tyr-Trp-Thr-Gly-amide were synthesized by AnaSpec, Inc. (San Jose, CA) with > 99% purity. Ultra-pure urea was obtained from Nacalai Tesque, Inc. (Kyoto, Japan), and ultra-pure guanidine hydrochloride was obtained from ICN Biomedicals, Inc. (Auroa, OH). MOPS (3-[N-morpholino] propanesulfonic acid was obtained from Sigma. Enzymes for the manipulation of DNA were from Promega Corporation (Madison, WI). All other reagents were of analytical grade.

Oligonucleotides

Oligonucleotides were made at the 40 nanomole scale by the Gene Technologies Laboratory, Texas A&M University (College Station, Texas) or 25 nanomole scale by Integrated DNA technologies, Inc. (Coralville, IA), and were used without further purification. Oligonucleotides used for the construction, mutagenesis and sequencing of DNA used are shown in Table 7. Concentration of oligonucleotide stocks were measured on a Gilford Model 250 Spectrophotometer using a 1 cm cuvette and an absorption coefficient for single-stranded DNA of 0.05 mg^{-1} ml cm^{-1} at 260 nm.

Site-Directed Mutagenesis

The NovaBlue cells were prepared and made competent, and the plasmid DNA was prepared as previously described (Hebert et al. 1997). Variants of RNase Sa were made using the four primer polymerase chain reaction (PCR) overlapping extension

technique (Ho et al. 1989). Three separate reactions were needed for each variant. The first and second reactions produced the 5' and 3' ends of the gene and incorporated a mutated primer in each. The final reaction resulted in the complete amplification of the altered sequence. Five pmol of primer, 10 ng pEH100, 200 mM dNTPs, and 2.5 U Vent polymerase were included in a 100 μl reaction volume for PCR. The thermal cycler profile was 94 ^{o}C (2.5 minutes) for 1 cycle, followed by 25 cycles of 94 ^{o}C (0.5 minutes), 68 ^{o}C (0.5 minutes), and 72 ^{o}C (0.5 minutes). Finally, there was a 5.0 minute extension period at 72 ^{o}C. Samples were frozen at -20 ^{o}C until needed. PCR products were analyzed by running 5 μl of the reaction on a 1.5 or 2% agarose gel (0.5X TBE, 0.25 μg/ml ethidium bromide) (Sambrook et al. 1989).

Table 7. Oligonucleotides used in the construction, mutagenesis and sequencing of RNase Sa vectors.

Oligo[a]	Sequence
D1W+	5' -GTGACAAAAGCCTGGGTCTCTGGTACC- 3'
D1W-	5' -GGTACCAGAGACCCAGGCTTTTGTCAC- 3'
Y52W+	5'-CCAGTCATATGGTTACTGGCACGAATACACCGTG- 3'
Y52W-	5'-CACGGTGTATTCGTGCCAGTAACCATATGACTGG- 3'
Y55W+	5' -TACTACCACGAATGGACCGTGATCACC- 3'
Y55W-	5' -GGTGATCACGGTCCATTCGTGGTAGTA- 3'
T76W+	5' -ACCGGTGAAGCTTGGCAGGAAGACTAC- 3'
T76W-	5' -GTAGTCTTCCTGCCAAGCTTCACCGGT- 3'
Y81W+	5' -CAGGAAGACTACTGGACCGGTGACCAC- 3'
Y81W-	5' -GTGGTCACCGGTCCAGTAGTCTTCCTG- 3'
D17R+	5' -CCGGAAGCTACCCGTACCCTGAACC- 3'
D17R-	5' -CGTTCAGGGTACGGGTAGCTTCCGG- 3'

[a]The + and - symbols in each label describe the complementarity of the oligonucleotide to the coding and non-coding strands of the gene, respectively.

The final PCR product from the mutagenesis reaction was purified using a Qiagen PCR Purification Kit.

The purified PCR product was digested first with *Xba* I and then precipitated with 95% ethanol, *d*H_2O, 7.5M ammonium acetate, and $MgCl_2$. The PCR product was then

digested with *Eco*R I and precipitated again the same way. This purified vector was used in the ligation of mutated phoA-RNase Sa gene cassette recreating pEH100 with the desired mutation. Ligated vector was transformed into competent NovaBlue cells and assumed variants were screened using DNA sequencing. The protein was then purified as described previously with minor modifications (Hebert et al. 1997).

Protein Purification

Cell Growth

For each purification, a freshly transformed stock of *E. coli* NovaBlue cells carrying the wild-type or variant RNase Sa vector was prepared. Freshly transformed cells were grown overnight in 50 ml of LB medium, then diluted 1:10 into 500 ml of terrific medium. This culture was grown at 30 ^{o}C to an OD_{600} of 0.6 and subsequently diluted into 10.5 L of terrific broth medium in an 11 L benchtop fermentor (New Brunswick Scientific, Inc., Model 19). The culture was shaken at 350 rpm and aerated with pressurized air at 12 L per minute filtered through an Acro 50 PTFE filter. Growth was continued at 30 ^{o}C to an OD_{600} of 0.6. At this time, production of RNase Sa expression was induced by the addition of IPTG to a final concentration of 0.1 mM for pEH100 vectors. An additional aliquot of ampicillin (25 μg/ml) was also added at this time. Cultures were grown an additional 12 hours before cells were harvested.

Osmotic Shock

RNase Sa was released from the periplasmic space of *E. coli* NovaBlue cells using an osmotic shock treatment (Neu and Heppel 1965). Cells were harvested in a Beckman JS-4.2 rotor at 4,000 rpm for 25 minutes. Cell pellets were resuspended by vigorous shaking in 2000 ml of 20% sucrose, 15 mM Tris pH 7.4, 3 mM Na_2EDTA and transferred to GSA bottles. After centrifugation in a Sorvall GSA rotor at 10,000 rpm for

30 minutes at 4 ^{o}C, the supernatant was saved and the cell pellets resuspended rapidly by vigorous shaking in 2000 ml of 15 mM Tris pH 7.4, 3 mM Na_2EDTA. After incubation for 20 minutes on ice, cells were pelleted in a Sorvall GSA rotor as before, and this supernatant was added to the first supernatant.

Acid Precipitation and Ion Exchange

The combined supernatants (4000 ml of periplasmic fraction) were acidified by adding 10.8 g disodium succinate and 18.8 g succinic acid (final concentrations: 20 mM sodium/50 mM succinate). The final pH was adjusted to 3.25 with concentrated HCl and any precipitate formed was removed by centrifugation in a Sorvall GSA rotor at 10,000 rpm for 20 minutes at 4 ^{o}C.

SP Sephadex C25 Cation Exchange Chromatography

Cation exchange chromatography was performed using a 5 x 10 cm SP-Sephadex gravity column. The SP-Sephadex C25 resin was preequilibrated with 20 mM sodium/50 mM succinate buffer pH 3.25. After loading, the column was washed with 1 L of the low pH buffer. Elution was performed using a pH gradient from pH 3.25 to pH 6.0 in succinate buffer using a total volume of 1 L. Fraction volumes of 12 ml were collected. All cation exchange chromatography runs were performed at room temperature. Fractions containing RNase activity were pooled and freeze dried.

G-50 Sephadex Exclusion Chromatography

The freeze dried RNase Sa sample from the ion exchange step was dissolved in a solution containing 2-5 ml of 2 M Tris pH 10.5 and 20 ml of 50 mM ammonium bicarbonate buffer (final pH ~7.0). The sample was loaded on a 4.8 x 110 cm Sephadex G-50 column and eluted with 50 mM ammonium bicarbonate buffer pH 7.0.

All G-50 runs were performed at room temperature. Fraction volumes of 12 ml were collected. Fractions containing RNase activity were pooled and freeze dried.

Protein Gel Analysis

Protein purity was examined by running the isolated proteins on Bio-Rad 4-20% Tricine-HCl SDS-PAGE Ready Gel. Gels were stained using standard Coomassie Brilliant Blue R-250 (Sambrook et al. 1989).

Enzyme Activity

Enzymatic activity for RNase Sa was measured using the method of Uchida and Egami (Uchida and Egami 1967) with minor modifications. Five microliters of sample were added to 0.75 ml of 0.2 M Tris-HCl pH 7.5, 20 mM EDTA assay buffer. The reaction was initiated by adding 0.25 ml of a 12 mg ml^{-1} solution of RNA (Torula Yeast or Baker's Yeast). After incubation for 30 minutes at 25 ^{o}C, the reaction was stopped by adding 0.25 ml of uranyl reagent (0.75% uranyl acetate, in 25% perchloric acid (v/v)). Samples were incubated on ice for 10 minutes and centrifuged (13,000 rpm for 6 minutes in a microfuge). Two hundred microliters of the supernatant was diluted into 5.0 ml distilled water and the A_{260} was measured against a blank consisting of the complete reaction mixture minus enzyme sample.

Preparation of Stock Solutions

Urea stock solutions were prepared by weight, and the molarity of the solutions was calculated using the equation (Kawahara and Tanford 1966):

$$\frac{d}{d_o} = 1 + 0.2658W + 0.0330W^2 \qquad (1)$$

where d is the urea solution density, d_o is the density of water, and W is the weight fraction of denaturant in the solution. The molarities, M, were confirmed by calculating the molarities using the equation:

$$M = 117.66(\Delta N) + 29.753(\Delta N)^2 + 185.56(\Delta N)^3 \quad (2)$$

where ΔN is the difference between the refractive indices of the denaturant and buffer solutions measured at the sodium D line (Warren and Gordon 1966). All refractive indices were measured with an American Optical Abbe refractometer. Urea stock solutions were used if the molarities from the two approaches agreed to within 1%. Urea stock solutions were used within 24 hours after preparation (Hagel et al. 1971). Guanidine hydrochloride stock solutions were prepared similarly, except with the following equation (Nozaki 1972):

$$\frac{d}{d_o} = 1 + 0.2710W + 0.0330W^2 \quad (3)$$

$$M = 57.147(\Delta N) + 38.68(\Delta N)^2 - 91.6(\Delta N)^3 \quad (4)$$

Protein concentrations of RNase Sa solutions were determined spectrophotometrically using an Agilent 8453 spectrophotometer. The molar absorption coefficient of ε_{280} = 12045 M^{-1} cm^{-1} was used for wild-type RNase Sa (Hebert et al. 1997). For the tyrosine to tryptophan variants and the threonine to tryptophan variant, the molar absorption coefficients, ε_{280} = 16055 M^{-1} cm^{-1} and ε_{280} = 17545 M^{-1} cm^{-1}, were used, respectively. These are based on the average molar absorption coefficients observed for Tyr and Trp residues in proteins (Pace et al. 1995). The error in determining the protein concentration using these predicted extinction coefficients will be less than 3%. For the peptides with the tryptophan as the only aromatic group, ε_{280} =

5630 M^{-1} cm^{-1} was used and for peptides which contained a single tryptophan and a single tyrosine, ε_{280} = 6845 M^{-1} cm^{-1} was used.

Fluorescence Emission Spectra

Protein samples with 10 μM concentration in 30 mM MOPS, pH 7.0, 25 ^{o}C were studied under denatured conditions (8.5 M urea and 6 M guanidine hydrochloride). All fluorescence measurements were made on an SLM 8100 Spectrofluorometer. The samples were excited at 300 nm and the emission was recorded from 310 to 500 nm every one nm using four nanometer emission and four nanometer excitation bandwidths and a one second integration time. Temperature was controlled using a Brinkman Lauda RM refrigerated water bath. The fluorescence contribution from the MOPS and urea or guanidine hydrochloride was subtracted from that of the samples, and instrument corrections were applied. Emission spectra were corrected for wavelength dependent instrument response. The emission λ_{max} is the wavelength where the greatest fluorescence intensity, I_F, was observed. The spectral moment was calculated using the following formula:

$$SpectralMoment = \frac{\sum_{i=310}^{500} \lambda_i I_{F,i}}{\sum_{i=310}^{500} I_{F,i}} \quad (5)$$

Fluorescence Anisotropy

Anisotropy measurements were made using an excitation wavelength of 300 nm and an emission wavelength of 350 nm at 5 μM. Anisotropy is determined by:

$$R = \frac{I_{VV} - GI_{VH}}{I_{VV} + 2GI_{VH}} \quad (6)$$

where the two subscripts (V and H) indicate the orientation of the excitation and emission polarizers, respectively, and G is the ratio of the sensitivities of the detection system for vertically and horizontally polarized light:

$$G = \frac{I_{HV}}{I_{HH}} \tag{7}$$

Anisotropy measurements were performed at least twice for improved precision.

Iodide and Acrylamide Quenching

The fluorescence quenching experiments were carried out under the following conditions. The quenching experiments were done on both native (oxidized) and denatured (oxidized and reduced) forms of the proteins (10 μM), at pH 7.0. For the native proteins, experiments were done in 30 mM MOPS. Quenching for the denatured, reduced (10 mM TCEP) forms of the proteins was done in both 7.6 M urea and 3.8 M GndHCl at 25 ^{o}C. For the denatured, oxidized forms of the proteins, 8.5 M urea and 6 M GndHCl were used. The change in concentrations of the denaturants for the quenching on the oxidized and reduced states of the proteins (e.g. 7.6 M urea for the reduced proteins and 8.5 M urea for the oxidized proteins) was a consequence of solubility issues with iodide and urea and iodide and guanidine hydrochloride.

All samples were equilibrated for one hour before any data was collected. Depending on the experiment, either acrylamide or iodide was titrated into each sample in incremental steps, from 0 M to ~0.20 M. Constant stirring and temperature were maintained. For iodide quenching, an equal molar concentration of potassium chloride was used as a counter ion, and iodide quenching was only performed in the presence of a reducing agent (either 10 mM TCEP for the denatured, reduced proteins or 2 mM sodium thiosulfate for the native, oxidized proteins). (For the denatured proteins, iodide

quenching was only performed on their reduced states. For the native proteins, 2 mM sodium thiosulfate is not sufficient enough reductant to reduce our proteins.) After each titration, samples were equilibrated for three minutes. The samples were then excited at 300 nm, with a 350 nm emission, while a time trace was run for thirty seconds, integrating over five second intervals. Four nanometer excitation and emission slit widths were used. The average time was recorded. After blank subtraction, F_0/F_I was plotted as a function of quencher concentration with the slope of the line being the Stern-Volmer quenching constant:

$$\frac{F_0}{F_I} = K_{SV}[Q] + 1 \tag{8}$$

where F_0 and F_I are the fluorescence of the sample in the absence of quencher and in the presence of quencher, respectively, K_{SV} is the Stern-Volmer quenching constant, and [Q] is the quencher concentration. Each experiment was performed at least twice for improved precision.

Modeling of the Peptides

Peptides were modeled in an extended conformation using Insight 2000. The geometric center of the tryptophan ($C_{X,Y,Z}$) was determined by:

$$C_{X,Y,Z} = \frac{\sum X_i}{n}, \frac{\sum Y_i}{n}, \frac{\sum Z_i}{n} \tag{9}$$

where X_i, Y_i, and Z_i represent the coordinates of the atoms of the indole ring (CG, CD1, CD2, NE1, CE2, CE3, CZ2, CZ3, CH2), and n is the number of atoms forming the indole ring (n=9).

Denaturation Curves

The stability of the wild type and variant proteins was determined by analyzing urea, guanidine hydrochloride, and thermal denaturation curves. Denaturation curves were determined using circular dichroism measurements at 234 nm as described previously (Pace et al. 1998).

Analysis of the denaturation curves was performed using the two-state unfolding model and the linear extrapolation method. These two methods were combined into a single equation to describe the shape of the urea and guanidine hydrochloride denaturation curve (Santoro and Bolen 1988):

$$y = \frac{\left(y_f + m_f[urea]\right) + \left(y_u + m_u[urea]\right)\exp^{m\left([urea]-[D]_{1/2}\right)/(RT)}}{1+\exp^{m\left([urea]-[D]_{1/2}\right)/(RT)}} \quad (10)$$

where y is the observed measured parameter, m_f and y_f are the slope and intercept, respectively, of the pre-transition baseline, m_u and y_u are the slope and intercept, respectively, of the post-transition baseline, *m* is the dependence of free energy of unfolding on urea concentration, and $D_{1/2}$ is the midpoint of the denaturation curve. The free energy of unfolding in the absence of denaturant, $\Delta G^o(H_2O)$, (defined as the conformational stability of the protein) is the product of *m* and $D_{1/2}$. Thermal denaturation curves were fit to:

$$y = \frac{\left(y_f + m_f T\right) + \left(y_u + m_u T\right)\exp^{\frac{-\Delta H_m}{R}\left(\frac{1}{T}+\frac{1}{T_m}\right)}}{1+\exp^{\frac{-\Delta H_m}{R}\left(\frac{1}{T}+\frac{1}{T_m}\right)}} \quad (11)$$

where y is the observed measured parameter, m_f and y_f are the slope and intercept, respectively, of the pre-transition baseline, m_u and y_u are the slope and intercept, respectively, of the post-transition baseline, T_M is the midpoint of the thermal unfolding,

and ΔH^0_M is the enthalpy of unfolding at T_M. The experimental curves were fit to the above equation using Origin and SigmaPlot data analysis software. Denaturation curves were performed at least twice for each variant.

Circular Dichroism

Circular Dichroism spectra were measured in 0.1 cm quartz cuvettes in 30 mM MOPS buffer, pH 7, and 25°C using an Aviv 202 CD spectrophotometer. Measured circular dichroism ellipticity values were converted to mean reside ellipticity, [θ], in deg cm^2 $decimol^{-1}$ using the equation:

$$[\theta] = \frac{100\Delta\theta}{Cnl} \tag{12}$$

where $\Delta\theta$ is the difference in millidegrees between the protein sample and the buffer sample, C is the concentration of protein in mM, *n* is the number of residues in the protein, and *l* is the path length of the cuvette in cm.

RESULTS

Introduction

The aim of this research was to use fluorescence to study the denatured state ensembles of ten single tryptophan containing variants of RNase Sa. They are D1W, Y52W, Y55W, T76W, and Y81W. Note that the single-site tryptophan variants were studied in two backgrounds, wild-type and a charge-reversal (D17R) background. Those conditions were urea and guanidine hydrochloride, reduced and oxidized, pH 7.0, and 25 °C. For comparison, we carried out similar studies on eight model compounds: NATA, AWA, AAWAA, WVSGT (D1W), GYWHE (Y52W), HEWTV (Y55W), EAWQE (T76W), and DYWTG (Y81W). The latter five were chosen since they have the same sequences as those surrounding the tryptophans in the proteins.

We analyzed the fluorescence spectra to determine λ_{max}, spectral moment, fluorescence intensity at λ_{max}, and relative quantum yields. We also examined the acrylamide and iodide quenching of fluorescence, as well as fluorescence anisotropy under the same conditions. These results are summarized in Table 8 through Table 11. To aid the reader in the Results section, we only include the data in tabular form. However, all of the graphical data may be found in the appendices. Appendix B contains the peptide data at pH 7.0, and Appendix C contains the protein data at pH 7.0. For the Results section, we will only state the general trends revealed by the data in the tables. A more complete analysis will be given in the Discussion section.

Peptides, pH 7.0

Table 8 and Table 9 summarize the parameters characterizing the fluorescence of the peptides in urea and guanidine hydrochloride, pH 7.0 and 25 °C. The spectral moments and λ_{max} do not differ significantly among the peptides; however there are differences in fluorescence intensity at λ_{max} and quenching between the peptides. Additionally, the spectral moments and λ_{max} for each peptide do not differ significantly between the peptide in either urea or guanidine hydrochloride; however, there are differences in fluorescence intensity at λ_{max} between the two denaturants. Fluorescence intensity at λ_{max} is always greater in urea than in guanidine hydrochloride for the peptides.

For acrylamide quenching, the Stern-Volmer quenching constants are higher in urea than in guanidine hydrochloride and are higher than the Stern-Volmer quenching constants from iodide quenching. For iodide quenching, the Stern-Volmer quenching constants are higher in urea for AAWAA, WVSGT (1), HEWTV (55), and DYWTG (81). However, NATA, AWA, GYWHE (52), and EAWQE (76) had higher Stern-Volmer quenching constants from iodide quenching in guanidine hydrochloride.

Table 8. Parameters characterizing the fluorescence of the peptides in urea[a], pH 7.0, and 25 °C.

Peptide	Trp	SM[b] (nm)	λ_{max}[c] (nm)	I_F at λ_{max}[d]	Acrylamide K_{SV}[e] (M^{-1})	Iodide K_{SV}[f] (M^{-1})	Anisotropy
NATA		363	352	49000	19.86 ± 0.48	8.85 ± 0.05	0.009 ± 0.002
AWA		362	349	24400	9.84 ± 0.22	3.95 ± 0.03	0.023 ± 0.001
AAWAA		362	350	28500	9.86 ± 0.18	4.03 ± 0.03	
WVSGT	1	361	347	23900	12.81 ± 0.09	7.73 ± 0.20	
GYWHE	52	361	347	24600	7.90 ± 0.11	2.63 ± 0.02	
HEWTV	55	361	349	30800	10.06 ± 0.14	3.72 ± 0.02	
EAWQE	76	361	347	32300	9.59 ± 0.15	2.92 ± 0.02	
DYWTG	81	361	347	21500	8.39 ± 0.13	2.49 ± 0.02	

Table 9. Parameters characterizing the fluorescence of the peptides in guanidine hydrochloride[g], pH 7.0, and 25 °C.

Peptide	Trp	SM[b] (nm)	λ_{max}[c] (nm)	I_F at λ_{max}[d]	Acrylamide K_{SV}[e] (M^{-1})	Iodide K_{SV}[f] (M^{-1})	Anisotropy
NATA		364	351	35500	16.89 ± 0.55	6.81 ± 0.03	0.006 ± 0.005
AWA		362	346	22100	9.80 ± 0.27	3.42 ± 0.01	0.019 ± 0.009
AAWAA		362	350	23100	8.66 ± 0.17	3.19 ± 0.03	
WVSGT	1	363	350	22100	10.52 ± 0.28	5.35 ± 0.07	
GYWHE	52	361	347	23100	7.60 ± 0.16	2.86 ± 0.02	
HEWTV	55	362	349	25700	8.85 ± 0.18	3.39 ± 0.03	
EAWQE	76	362	348	24900	8.08 ± 0.13	3.07 ± 0.02	
DYWTG	81	362	347	18400	7.20 ± 0.11	2.36 ± 0.03	

[a]The urea concentrations used were 8.5 M for the emission scans, anisotropy and oxidized quenching, and 7.6 M for reduced quenching.
[b]Spectral Moment (SM) is the wavelength at which the area under the emission spectrum is divided into two equal areas.
[c]λ_{max} is the wavelength of maximal intensity of the emission spectrum. We estimate the error to be ± 2 nm.
[d]I_F at λ_{max} is the fluorescence intensity at λ_{max}. We estimate the error to be 3%.
[e]Acrylamide K_{SV} is the Stern-Volmer quenching constant derived from the acrylamide quenching data (Equation 8).
[f]Iodide K_{SV} is the Stern-Volmer quenching constant derived from the iodide quenching data (Equation 8).
[g]The guanidine hydrochloride concentrations used were 6 M for the emission scans, anisotropy and oxidized quenching, and 3.8 M for reduced quenching.

Protein Denatured States, pH 7.0

Table 10 and Table 11 summarize the parameters characterizing the fluorescence of the proteins in urea, guanidine hydrochloride, pH 7.0 and 25 ºC. The spectral moments and λ_{max} do not differ significantly among the proteins; however there are differences in fluorescence intensity at λ_{max} and quenching between the proteins. Additionally, the spectral moments and λ_{max} for each protein do not differ significantly between the protein in either urea or guanidine hydrochloride; however, there are differences in fluorescence intensity at λ_{max} between the two denaturants. Fluorescence intensity at λ_{max} is generally greater in urea than in guanidine hydrochloride for the proteins.

With acrylamide quenching, the Stern-Volmer quenching constants for acrylamide quenching are higher in urea than in guanidine hydrochloride and are higher than the Stern-Volmer quenching constants from iodide quenching. With iodide quenching, the Stern-Volmer quenching constants are higher in urea for D1W, Y55W, and T76W (wild-type background). However, Y52W, T76W (charge-reversal background), and Y81W had higher Stern-Volmer quenching constants from iodide quenching in guanidine hydrochloride.

Generally, we observed small differences between the oxidized and reduced states of the proteins with fluorescence intensities at λ_{max} and greater differences in acrylamide quenching, especially in guanidine hydrochloride. RNase D1W, T76W, and Y81W were the variants which showed some change. Finally, with the exception of the fluorescence intensity at λ_{max} at Y55W and quenching data from D1W, generally, no significant differences were observed between the wild-type and charge-reversal background.

The thermal unfolding of the tryptophan variants in both backgrounds was compared. Generally, we saw no significant difference between the two backgrounds with stability (Table 12).

Table 10. Parameters characterizing the fluorescence of the proteins[a] in urea[b], pH 7.0, and 25 °C.

Protein[a]		SM[c] (nm)	λ_{max}[d] (nm)	I_F at λ_{max}[e]	Acrylamide K_{SV}[f] (M^{-1})	Iodide K_{SV}[g] (M^{-1})	Anisotropy
D1W	WR	361	345	25900	10.04 ± 0.07	5.23 ± 0.09	0.043 ± 0.007
	WO	360	347	25300	9.17 ± 0.04		0.073 ± 0.001
	RR	362	348	26200	11.99 ± 0.09	5.83 ± 0.08	0.045 ± 0.004
	RO	360	349	24800	9.51 ± 0.02		0.054 ± 0.001
Y52W	WR	360	348	34600	7.20 ± 0.10	2.77 ± 0.03	0.090 ± 0.001
	WO	360	348	35600	7.44 ± 0.07		0.096 ± 0.001
	RR	360	345	34400	7.03 ± 0.09	2.63 ± 0.05	0.087 ± 0.001
	RO	359	346	36000	7.29 ± 0.07		0.096 ± 0.004
Y55W	WR	360	350	41200	8.52 ± 0.12	3.33 ± 0.04	0.072 ± 0.001
	WO	360	347	42400	8.65 ± 0.10		0.076 ± 0.001
	RR	361	350	38700	8.32 ± 0.09	3.41 ± 0.04	0.076 ± 0.001
	RO	360	349	41300	8.29 ± 0.08		0.080 ± 0.002
T76W	WR	360	346	40700	7.92 ± 0.12	3.04 ± 0.02	0.079 ± 0.001
	WO	359	346	42400	8.26 ± 0.07		0.093 ± 0.002
	RR	360	348	41400	7.41 ± 0.09	2.70 ± 0.04	0.076 ± 0.003
	RO	359	346	44100	7.78 ± 0.06		0.082 ± 0.006
Y81W	WR	359	347	28700	6.15 ± 0.08	1.87 ± 0.02	0.085 ± 0.004
	WO	358	346	30800	6.53 ± 0.07		0.099 ± 0.002
	RR	360	349	29300	6.37 ± 0.08	2.09 ± 0.02	0.089 ± 0.005
	RO	359	345	32100	6.68 ± 0.03		0.043 ± 0.007

[a]WR and WO are wild-type background, reduced and oxidized, respectively. RR and RO are the charge-reversal background, reduced and oxidized respectively.
[b]The urea concentrations used were 8.5 M for the emission scans, anisotropy and oxidized quenching, and 7.6 M for reduced quenching.
[c]Spectral Moment (SM) is the wavelength at which the area under the emission spectrum is divided into two equal areas.
[d]λ_{max} is the wavelength of maximal intensity of the emission spectrum. We estimate the error to be ± 2 nm.
[e]I_F at λ_{max} is the fluorescence intensity at λ_{max}. We estimate the error to be 3%.
[f]Acrylamide K_{SV} is the Stern-Volmer quenching constant derived from the acrylamide quenching data (Equation 8).
[g]Iodide K_{SV} is the Stern-Volmer quenching constant derived from the iodide quenching data (Equation 8).

Table 11. Parameters characterizing the fluorescence of the proteins[a] in guanidine hydrochloride[b], pH 7.0, and 25 °C.

Protein[a]		SM[c] (nm)	λ_{max}[d] (nm)	I_F at λ_{max}[e]	Acrylamide K_{SV}[f] (M^{-1})	Iodide K_{SV}[g] (M^{-1})	Anisotropy
D1W	WR	363	351	25000	8.38 ± 0.25	4.59 ± 0.05	0.032 ± 0.004
	WO	363	351	28000	9.05 ± 0.03		0.054 ± 0.003
	RR	363	350	24400	9.45 ± 0.28	4.70 ± 0.05	0.037 ± 0.010
	RO	363	350	26800	9.23 ± 0.04		0.036 ± 0.003
Y52W	WR	360	347	30700	6.87 ± 0.20	3.06 ± 0.02	0.095 ± 0.001
	WO	360	349	31500	6.13 ± 0.06		0.090 ± 0.019
	RR	360	346	30200	6.85 ± 0.16	3.02 ± 0.03	0.094 ± 0.002
	RO	360	345	31500	5.99 ± 0.06		0.098 ± 0.003
Y55W	WR	361	346	33800	7.97 ± 0.20	3.22 ± 0.04	0.080 ± 0.002
	WO	361	346	35000	6.82 ± 0.06		0.113 ± 0.039
	RR	361	348	32100	7.62 ± 0.18	3.31 ± 0.03	0.074 ± 0.001
	RO	361	348	33500	6.93 ± 0.09		0.072 ± 0.004
T76W	WR	361	346	31100	7.57 ± 0.15	2.92 ± 0.03	0.060 ± 0.009
	WO	361	347	31500	6.23 ± 0.06		0.083 ± 0.004
	RR	361	347	32100	6.97 ± 0.13	2.92 ± 0.04	0.078 ± 0.003
	RO	361	349	33000	6.23 ± 0.06		0.084 ± 0.001
Y81W	WR	360	346	26000	5.96 ± 0.10	2.47 ± 0.02	0.082 ± 0.003
	WO	360	345	27100	5.30 ± 0.05		0.092 ± 0.009
	RR	361	347	26400	6.15 ± 0.11	2.49 ± 0.03	0.117 ± 0.044
	RO	361	347	27500	5.69 ± 0.04		0.095 ± 0.005

[a]WR and WO are wild-type background, reduced and oxidized, respectively. RR and RO are the charge-reversal background, reduced and oxidized respectively.

[b]The guanidine hydrochloride concentrations used were 6 M for the emission scans, anisotropy and oxidized quenching, and 3.8 M for reduced quenching.

[c]Spectral Moment (SM) is the wavelength at which the area under the emission spectrum is divided into two equal areas.

[d]λ_{max} is the wavelength of maximal intensity of the emission spectrum. We estimate the error to be ± 2 nm.

[e]I_F at λ_{max} is the fluorescence intensity at λ_{max}. We estimate the error to be 3%.

[f]Acrylamide K_{SV} is the Stern-Volmer quenching constant derived from the acrylamide quenching data (Equation 8).

[g]Iodide K_{SV} is the Stern-Volmer quenching constant derived from the iodide quenching data (Equation 8).

Table 12. Comparison of the thermal denaturation parameters[a] of the two backgrounds in 30 mM MOPS at pH 7.0.

Protein	Wild-Type Background			Charge-Reversal Background		
	ΔH^0_M (kcal/mol)	T_M (ºC)	ΔT_M[b] (ºC)	ΔH^0_M (kcal/mol)	T_M (ºC)	ΔT_M[c] (ºC)
WT/D17R	95.0 ± 0.79	48.4 ± 0.02		86.3 ± 0.98	43.7 ± 0.03	
D1W	92.0 ± 0.77	47.8 ± 0.02	-0.6	83.4 ± 1.25	43.3 ± 0.04	-0.4
Y52W	71.4 ± 0.64	37.9 ± 0.03	-10.5	63.4 ± 0.77	32.3 ± 0.05	-11.4
Y55W	83.1 ± 0.80	41.0 ± 0.03	-7.4	73.9 ± 0.86	36.1 ± 0.04	-7.6
T76W	99.6 ± 1.00	50.5 ± 0.02	2.1	87.4 ± 1.19	46.5 ± 0.04	2.8
Y81W	90.9 ± 0.73	47.3 ± 0.02	-1.1	83.8 ± 0.94	43.0 ± 0.03	-0.7

[a]Equation 11 in the Materials and Methods section was used to fit the data.
[b]ΔT_M is compared to wild-type RNase Sa.
[c]ΔT_M is compared to RNase Sa D17R.

DISCUSSION

For the discussion, we will examine the data in the following order:

1. Peptides at pH 7.0
2. Proteins at pH 7.0
3. Proteins compared to peptides at pH 7.0
4. Proteins with the wild-type background compared to those with a charge-reversal background at pH 7.0.

The primary data can be found in the appendices, and a summary of the analyses can be found in the Results sections of the Dissertation.

Peptides, pH 7.0

Introduction

In an effort to better understand the fluorescent behavior of the tryptophan in proteins, we studied eight model compounds under the same conditions as the proteins. The model compounds were N-acetyl-tryptophan-amide (NATA), a tripeptide, Ala-Trp-Ala, and six pentapeptides. With the exception of Ala-Ala-Trp-Ala-Ala, the pentapeptides were based on the sequences around the tryptophan substitutions in RNase Sa. Those pentapeptides included (with the original tryptophan substitution in parentheses): Trp-Val-Ser-Gly-Thr (D1W), Gly-Tyr-Trp-His-Glu (Y52W), His-Glu-Trp-Thr-Val (Y55W), Glu-Ala-Trp-Gln-Glu (T76W), and Asp-Tyr-Trp-Thr-Gly (Y81W). With the exception of the D1W pentapeptide, all of the peptides were blocked at both the N- and C-terminus (N-acetyl; C-amide). The D1W pentapeptide was blocked only at the C-terminus to simulate the tryptophan substitution at the N-terminus of RNase Sa (D1W), where there is a positively charged α-amino group. To characterize the model

compounds, λ_{max}, spectral moment, fluorescence intensity at λ_{max} (I_F), Stern-Volmer quenching constants for iodide and acrylamide quenching, and anisotropy were determined in urea and guanidine hydrochloride at pH 7.0 and 3.0. Table 13, Figure 4, and Figure 5 summarize the data from the emission scans.

Spectral Moment and λ_{max}

The fluorescence intensity wavelength maxima, λ_{max}, for tryptophans range from 308 nm in the protein, Azurin, towards 350 nm for tryptophan in water (Eftink 1991; Vivian and Callis 2001). It is generally thought that as a tryptophan becomes more exposed to solvent, a red shift will occur. This generalization should be more valid with the peptides than with the proteins, as we will discuss later. Among the peptides, which we assume are structureless, we would expect the spectral moments and values of λ_{max} to be very similar, and that is what we observed. The spectral moments ranged from 361 to 364 nm in urea and guanidine hydrochloride, and λ_{max} ranged from 346 to 352 nm in urea and guanidine hydrochloride. It does appear that spectral moment and λ_{max} are greater for NATA than the peptides but the differences are small. This probably reflects the greater accessibility of the indole ring in NATA as compared to the peptides.

I_F

I_F is very dependent on the groups in the local environment, which are known to quench tryptophan fluorescence. These groups include amino acid side chains and peptide bonds. At least ten amino acid side chains have been determined to quench the fluorescence of tryptophan. With regard to peptide bonds, the distance between the indole ring and the carbonyl carbon has been correlated with fluorescence quenching (Chen et al. 1996; Sillen et al. 2000). It is not the intent of this research to fully explain

Table 13. Comparison of the fluorescence properties of the peptides in 8.5 M urea and 6 M guanidine hydrochloride, pH 7.0, and 25 °C.

Peptide	Trp	Charge	SM[a] (nm) Urea	SM (nm) GdnHCl	λ_{max}[b] (nm) Urea	λ_{max} (nm) GdnHCl	I_F at λ_{max}[c] Urea	I_F at λ_{max} GdnHCl	% Δ[d]	% Δ I_F from NATA Urea[e]	% Δ I_F from NATA GdnHCl[f]
NATA		0	363	364	352	351	49000	35500	28	0	0
AWA		0	362	362	349	346	24400	22100	9	50	38
AAWAA		0	362	362	350	350	28500	23100	19	42	35
WVSGT	1	+1	361	363	347	350	23900	22100	8	51	38
GYWHE	52	-0.5	361	361	347	347	24600	23100	6	50	35
HEWTV	55	-0.5	361	362	349	349	30800	25700	17	37	28
EAWQE	76	-2	361	362	347	348	32300	24900	23	34	30
DYWTG	81	-1	361	362	347	347	21500	18400	14	56	48

[a]Spectral Moment (SM) is the wavelength at which the total area under the emission spectrum is divided into two equal areas.
[b]λ_{max} is the wavelength of maximal intensity of the emission spectrum. We estimate the error to be ± 2 nm.
[c]I_F at λ_{max} is the fluorescence intensity at λ_{max}. We estimate the error to be 3%.

[d] $$\%\Delta = \left(\frac{I_{F,Urea} - I_{F,GdnHCl}}{I_{F,Urea}} \right) \times 100$$

[e] $$\%\Delta I_{F,Urea} = \left(\frac{I_{F,NATA} - I_{F,Peptide}}{I_{F,NATA}} \right) \times 100$$

[f] $$\%\Delta I_{F,GdnHCl} = \left(\frac{I_{F,NATA} - I_{F,Peptide}}{I_{F,NATA}} \right) \times 100$$

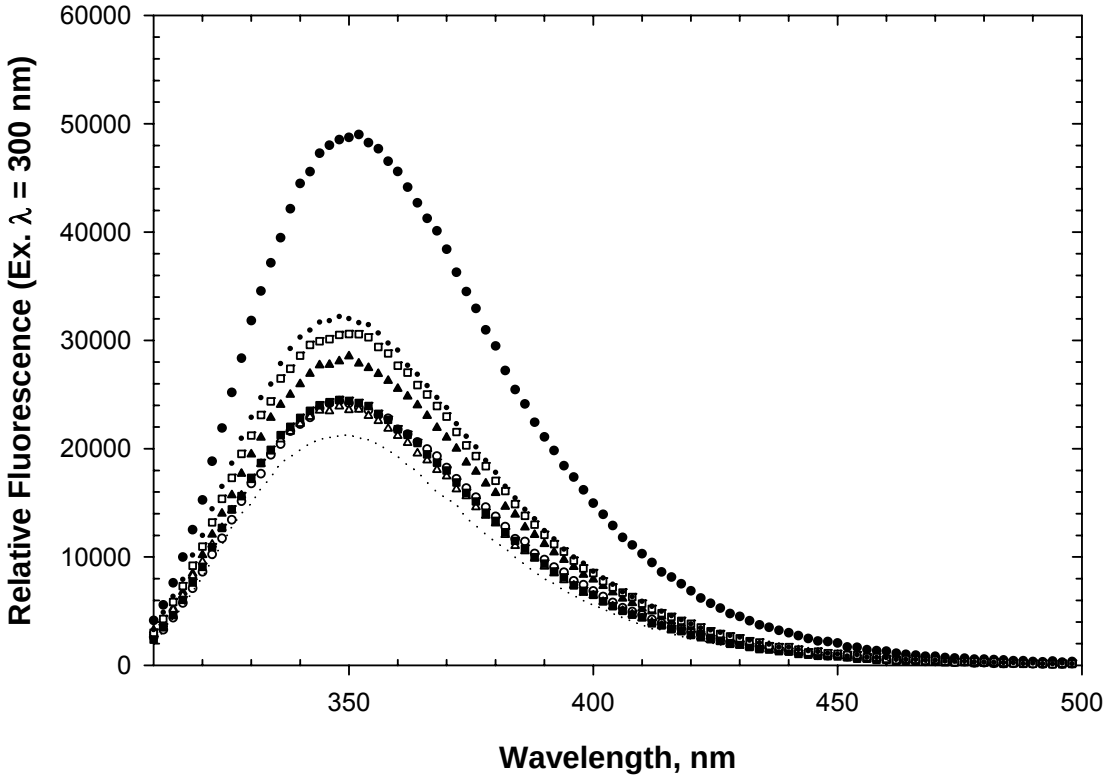

Figure 4. Fluorescence emission spectra (300 nm excitation) of all the peptides (10 μM) in 8.5 M urea, 10 mM TCEP, pH 7.0, and 25 °C. The scans represent the following model compounds: NATA (closed circles), AWA (open circles), AAWAA (closed triangles), WVSGT (D1W; open triangles), GYWHE (Y52W; closed squares), HEWTV (Y55W; open squares), EAWQE (T76W; dots), and DYWTG (Y81W; dashed line).

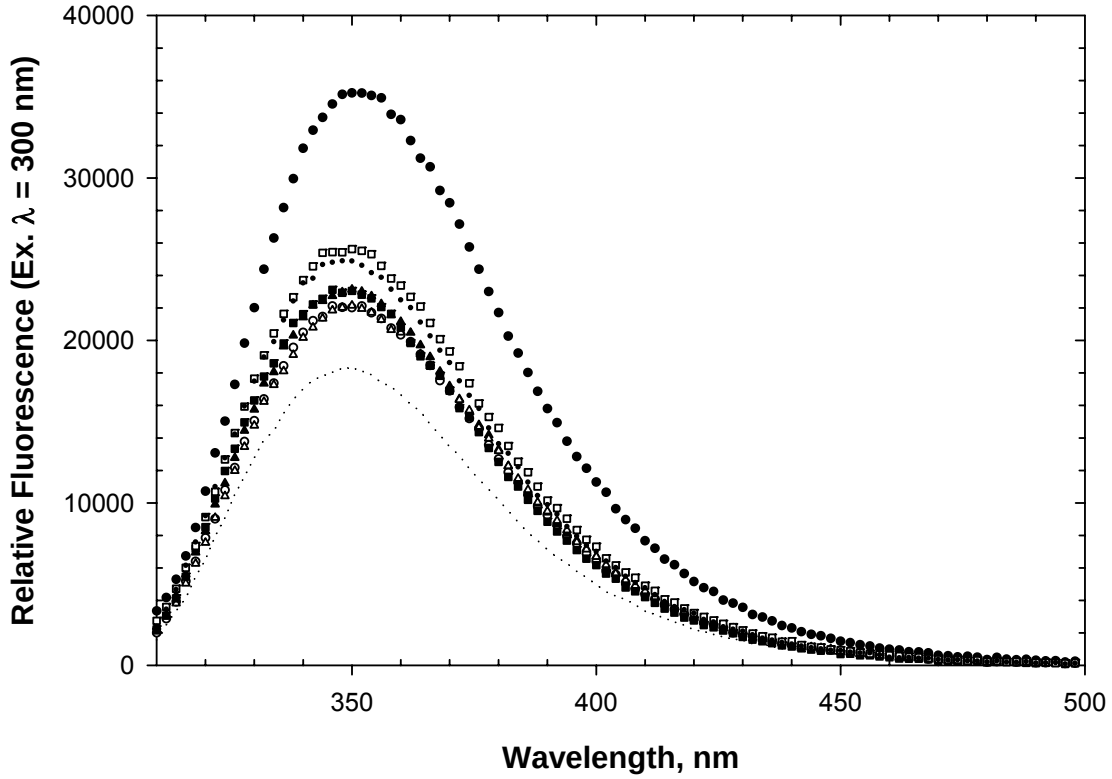

Figure 5. Fluorescence emission spectra (300 nm excitation) of all the peptides (10 μM) in 6 M guanidine hydrochloride, 10 mM TCEP, pH 7.0, and 25 °C. The scans represent the following model compounds: NATA (closed circles), AWA (open circles), AAWAA (closed triangles), WVSGT (D1W; open triangles), GYWHE (Y52W; closed squares), HEWTV (Y55W; open squares), EAWQE (T76W; dots), and DYWTG (Y81W; dashed line).

why tryptophans fluoresce more or less in certain conditions, but to describe the interesting differences we observed.

While both the spectral moment and λ_{max} did not differ significantly amongst the model compounds in urea or guanidine hydrochloride, there were significant differences in the fluorescence intensity at λ_{max}. This suggests that fluorescence intensity may be more sensitive to the immediate environment than λ_{max}. From the most to the least fluorescent at λ_{max} in urea were NATA > EAWQE (T76W) > HEWTV (Y55W) > AAWAA > GYWHE (Y52W) > AWA > WVSGT (D1W) > DYWTG (Y81W). In guanidine hydrochloride, the trend was generally the same. From the most fluorescent to the least fluorescent at λ_{max} in guanidine hydrochloride were NATA > EAWQE (T76W) > HEWTV (Y55W) > AAWAA > GYWHE (Y52W) > WVSGT (D1W) > AWA > DYWTG (Y81W). Fluorescence intensities at λ_{max} ranged from 49000 to 21500 in urea and from 35500 to 18400 in guanidine hydrochloride.

The fluorescence of the models was greater in urea than in guanidine hydrochloride. Therefore, the data suggest that guanidine hydrochloride is a better quencher of fluorescence than urea. Guanidine hydrochloride's ability to quench the fluorescence to a greater extent than urea may be due to its positive charge:

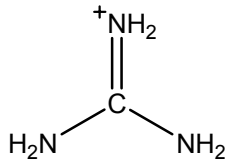

Guanidinium ion

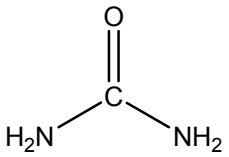

Urea

Figure 6. Chemical structures of the guanidinium ion and urea.

The percent change in fluorescence between urea and guanidine hydrochloride was greatest with NATA (28%) and the least with the Y52W peptide (6%). Also, the changes between NATA and the rest of the model compounds were lower in guanidine hydrochloride than in urea (Table 13), reinforcing the fact that guanidine hydrochloride is a strong quencher of fluorescence.

Guanidine hydrochloride's ability to quench the pentapeptides' fluorescence may be related to their net charges. Among the pentapeptides, the biggest difference between urea and guanidine hydrochloride was observed with the T76W peptide, with a 23% change in fluorescence intensity at λ_{max}. It also has the largest negative charge (-2). The positively charged guanidinium ion would be attracted to the negative charges of EAWQE, resulting in an increase in quenching. The Y55W peptide, HEWTV, had the next largest differences with a 17% change. Presumably, the negative charge next to the tryptophan and an overall net negative charge attracted the guanidinium ion to the tryptophan. The Y52W peptide, GYWHE, also has an overall net negative charge but guanidine hydrochloride's quenching effect was less than half that of the Y55W peptide. The difference may be that the Y52W peptide, GYWHE, has a positive charge next to the tryptophan. Perhaps, this is repelling the guanidinium ion enough to diminish the quenching effect. The D1W peptide, WVSGT, also had a small difference. This is not surprising since the positive charge is on the α-amino group of the tryptophan. While we feel that net charges and proximity of those charges may explain why guanidine hydrochloride quenched the pentapeptides to different degrees, it is not easy to understand the differences in the way it affected NATA (28%), AWA (9%), and AAWAA (19%). NATA may be explained by its greater accessibility, but obviously, the same argument would not work for AWA and AAWAA.

We will now consider the correlation between the environments of the tryptophans in the model compounds and the fluorescence intensity at λ_{max} in urea at 25 ^{o}C. In an effort to try to understand the fluorescence intensity at λ_{max}, we modeled all of the peptides in an extended conformation in Insight 2000. We realize that this conformation will not apply to the peptides in solution, but it shows how the adjacent side chains can partially shield the tryptophan side chain. Table 14 summarizes the characteristics of the microenvironment within seven angstroms of the geometric center of each tryptophan in the model compounds. Within the seven angstrom vicinity, our analysis includes the number of atoms, the number of peptide bonds, and the average distance between the CE3 atom of the tryptophan and the carbonyl carbon. We also considered the proximity of amino acid side chains, which could quench the fluorescence. However, according to Chen and Barkely, there is a significant difference among the side chains as to their quenching ability. For our peptides in urea at pH 7.0, it appears that the only two side chains which have a potential to quench are tyrosine and histidine. Finally, we calculated the percent burial based on a Gly-X-Gly model for each of the tryptophan side chains. While we cannot draw any concrete conclusions, we feel we can suggest some common trends. As previously stated, the most to the least fluorescent at λ_{max} in urea were NATA > EAWQE (T76W) > HEWTV (Y55W) > AAWAA > GYWHE (Y52W) > AWA > WVSGT (D1W) > DYWTG (Y81W). Kronman also found that, “the fluorescence of tryptophan residues incorporated into a peptide chain is in general quenched as compared to the free amino acid (Kronman and Holmes 1971).” Our data support this, since of all the model compounds, NATA has the greatest fluorescence intensity at λ_{max}. We will now consider the two smallest model compounds, NATA versus AWA.

Table 14. Characteristics of the environments[a] within seven angstroms of the geometric center[b] of each tryptophan in the model compounds.

Peptide	Trp	% Buried[c]	No of Atoms	No of Peptide Bonds	No of Potential Quenchers[d]
NATA		0.0	18	0	0
AWA		0.1	22	2	0
AAWAA		4.9	24	2	0
WVSGT	1	0.0	16	1	0
GYWHE	52	7.7	23	2	2
HEWTV	55	15.9	30	2	1
EAWQE	76	7.2	26	2	0
DYWTG	81	14.5	27	2	1

[a]The peptides were modeled using an extended conformation in Insight 2000. Hydrogens were omitted.
[b]The geometric center for the tryptophan is calculated by Equation 9 in Methods and Materials.
[c]Calculated using the algorithm of Lee and Richards based on a Gly-X-Gly model (Lee and Richards 1971).
[d]For this analysis, we only considered the quenchers, tyrosine and histidine.

In any of our fluorescence probes, we would expect the accessibility difference between NATA and any of the other model compounds to be a factor (Figure 7 through Figure 9). NATA has about twice the fluorescence intensity at λ_{max} compared to AWA. Neither model compound has any side chains which are known to quench tryptophan's fluorescence. NATA has four fewer atoms within the seven angstrom restraint. The remaining factor is the question of the peptide bonds. The current thought is that electron transfer from the indole ring to the carbonyl carbon of nearby peptide bonds is the primary mechanism of quenching of tryptophan fluorescence. If we consider a peptide bond as the bond between a carbonyl carbon and a nitrogen then NATA has two peptide bonds (both from the blocking groups) and AWA has three (two from the Ala to Trp bonds and one from a blocking group). Since the fluorescence intensity at λ_{max} for NATA is twice that of AWA, it does not seem reasonable that the peptide bonds derived from the blocking groups of NATA are equivalent to the bonds connecting the two alanines to the tryptophan. Therefore, the decrease in fluorescence intensity is more likely due to the electron transfer from the tryptophan side chains to the two peptide bonds of AWA.

Given the previous argument, one might expect the D1W peptide to have one of the largest fluorescence intensities at λ_{max}. It contains only one peptide bond and has no potential quenching side chains. However, it has one of the lowest fluorescence intensities. We feel like the D1W peptide is an exception. There are two possibilities for its fluorescence. First, perhaps the positive charge on the α-amino group quenches to lower the fluorescence. Secondly, there may be a correlation between percent burial and fluorescence intensity. The D1W peptide, as well as AWA, have increased accessibilities. One may expect that as accessibility goes up, fluorescence intensity

would go down. This could account for the decreased fluorescence intensities of D1W and AWA compared to the majority of the model compounds.

The Y81W peptide has the lowest fluorescence intensity, and the Y52W peptide has the third lowest (one above the D1W peptide) of all the model compounds. Both of these peptides have potential quenching groups adjacent to them. The Y52W peptide has a tyrosine on one side of the tryptophan and a histidine on the other side. The Y81W peptide has a tyrosine on one side of its tryptophan. These quenchers directly adjacent to the tryptophans are probably quenching the fluorescence.

AAWAA, the T76W (EAWQE) peptide, and the Y55W (HEWTV) peptide have the highest fluorescence intensities at λ_{max}. AAWAA and the T76W peptide have no quenching groups in their sequence. The Y55W peptide has one potentially quenching side chain, but it is one residue removed from the tryptophan. The absence of adjacent quenching groups may explain their increased fluorescence compared to the Y81W (DYWTG) and Y52W (GYWHE) peptides.

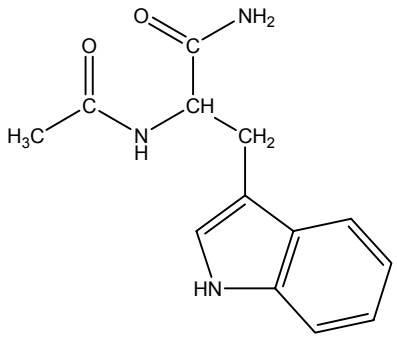

Figure 7. Structure of N-acetyl-Trp-amide (NATA).

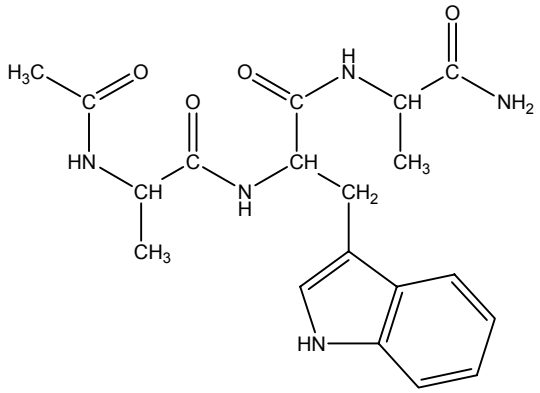

Figure 8. Structure of N-acetyl-Ala-Trp-Ala-amide (AWA).

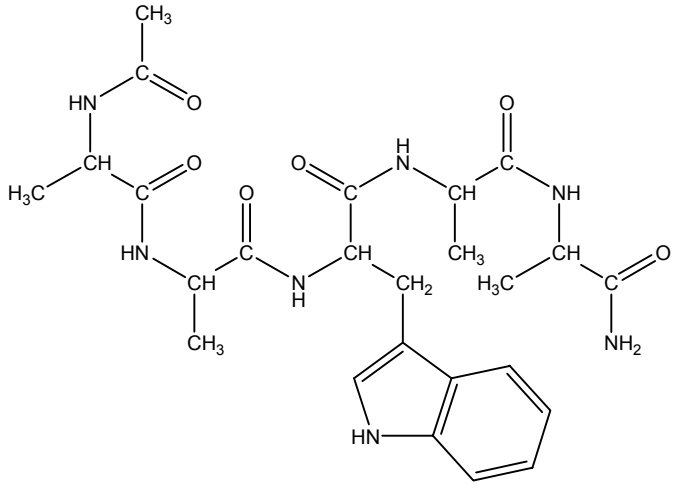

Figure 9. Structure of N-acetyl-Ala-Ala-Trp-Ala-Ala-amide (AAWAA).

Quenching

Fluorescence can be quenched by different mechanisms. In this section, we will focus primarily on quenching resulting from collisional encounters between the fluorophores and small molecule, extrinsic quenchers, specifically acrylamide and iodide. This quenching is referred to as collisional or dynamic quenching, because there must be contact between the fluorophore and the quencher. For collisional quenching to occur, the quencher must collide with the fluorophore during the lifetime of the excited state, causing the fluorophore to return to the ground state without emission of a photon. Studying this quenching yields insight into the accessibility of the fluorophores.

Table 15 and Figure 10 through Figure 13 summarize the iodide and acrylamide quenching data for the peptides. The rank order of the Stern-Volmer quenching constants from highest to lowest for the peptides were similar for acrylamide and iodide in urea and were in the same order for guanidine hydrochloride. This is expected since the peptides are all generally unstructured and the difference between the net charges of the peptides is not too great.

Table 15 shows the percent difference between acrylamide and iodide quenching for the peptides in urea and guanidine hydrochloride, pH 7.0, and 25 ^{o}C. In urea and guanidine hydrochloride, the Stern-Volmer quenching constants were always greater for acrylamide than iodide, showing that acrylamide is a better quencher of fluorescence than iodide. Acrylamide has been shown previously to quench 3-methylindole better than iodide. The rate constant for acrylamide quenching of 3-methylindole is 720 x 10^{7} M^{-1} s^{-1}, while the rate constant for iodide is 130 x 10^{7} M^{-1} s^{-1}, an 82% decrease in efficiency (Chen et al. 1996; Chen and Barkley 1998). The

Table 15. Acrylamide and Iodide Stern-Volmer quenching constants[a] (M^{-1}) for the peptides in 7.6 M urea and 3.8 M guanidine hydrochloride, pH 7.0, and 25 °C. The rank order from highest to lowest K_{SV} is given after each column for each dataset.

Peptide	Trp	Net Charge	% Buried[b]	Urea					GdnHCl				
				Acrylamide		Iodide		% Δ[d]	Acrylamide		Iodide		% Δ[e]
				K_{SV} (M^{-1})	Rank	K_{SV} (M^{-1})	Rank		K_{SV} (M^{-1})	Rank	K_{SV} (M^{-1})	Rank	
NATA		0	0.0	19.86	1	8.85	1	55	16.89	1	6.81	1	60
AWA		0	0.1	9.84	5	3.95	4	60	9.80	3	3.42	3	65
AAWAA		0	4.9	9.86	4	4.03	3	59	8.66	5	3.19	5	63
WVSGT	1	+1	0.0	12.81	2	7.73	2	40	10.52	2	5.35	2	49
GYWHE	52	-0.5	7.7	7.90	8	2.63	7	67	7.60	7	2.86	7	62
HEWTV	55	-0.5	15.9	10.06	3	3.72	5	63	8.85	4	3.39	4	62
EAWQE	76	-2	7.2	9.59	6	2.92	6	70	8.08	6	3.07	6	62
DYWTG	81	-1	14.5	8.39	7	2.49	8	70	7.20	8	2.36	8	67

[a]Equation 8 in the Methods and Materials section was used to calculate the Stern-Volmer quenching constants.
[b]Net charge of peptide.
[c]Calculated using the algorithm of Lee and Richards based on a Gly-X-Gly model (Lee and Richards 1971).

[d] $$\%\Delta_{A\rightarrow I,\,Urea} = \left(\frac{K_{SV,\,Acrylamide} - K_{SV,\,Iodide}}{K_{SV,\,Acrylamide}}\right)\times 100$$

[e] $$\%\Delta_{A\rightarrow I,\,GdnHCl} = \left(\frac{K_{SV,\,Acrylamide} - K_{SV,\,Iodide}}{K_{SV,\,Acrylamide}}\right)\times 100$$

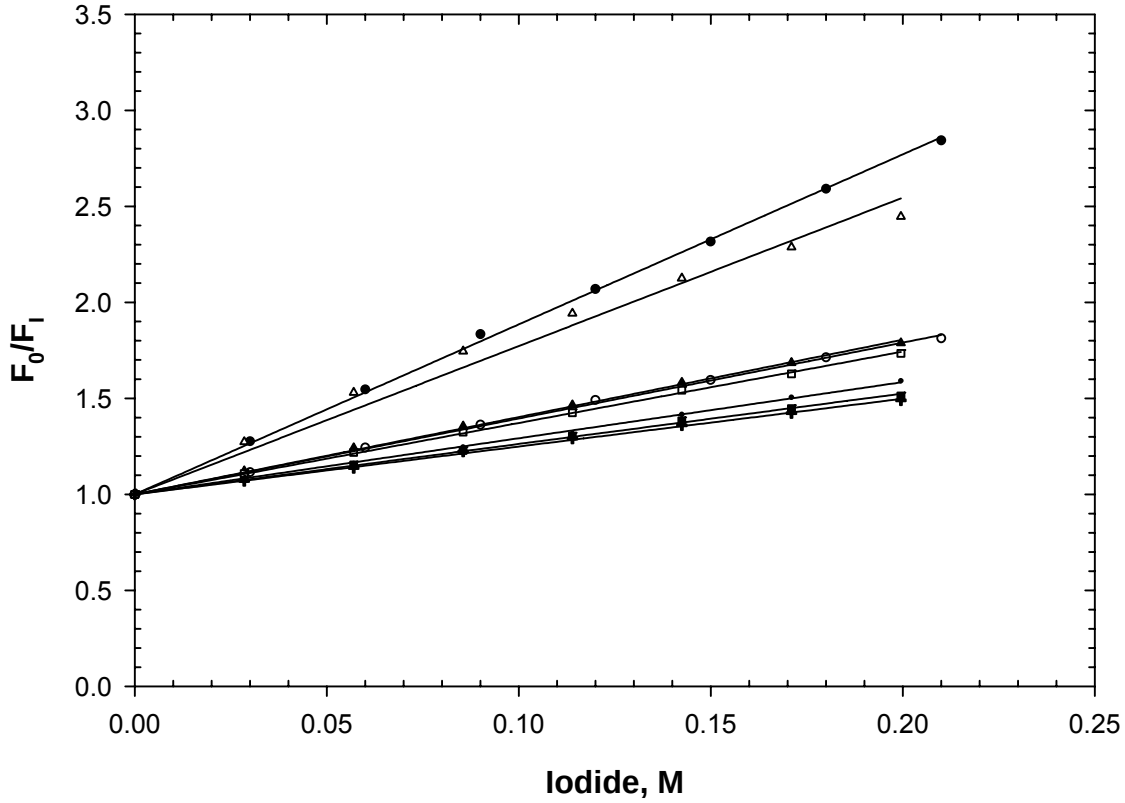

Figure 10. Fluorescence iodide quenching data (300 nm excitation, 350 nm emission) of all the peptides (10 μM) in 7.6 M urea, 10 mM TCEP, pH 7.0, and 25 °C. The scans represent the following variants: The scans represent the following conditions: NATA (closed circles), AWA (open circles), AAWAA (closed triangles), WVSGT (D1W; open triangles), GYWHE (Y52W; closed squares), HEWTV (Y55W; open squares), EAWQE (T76W; dots), and DYWTG (Y81W; plus symbols).

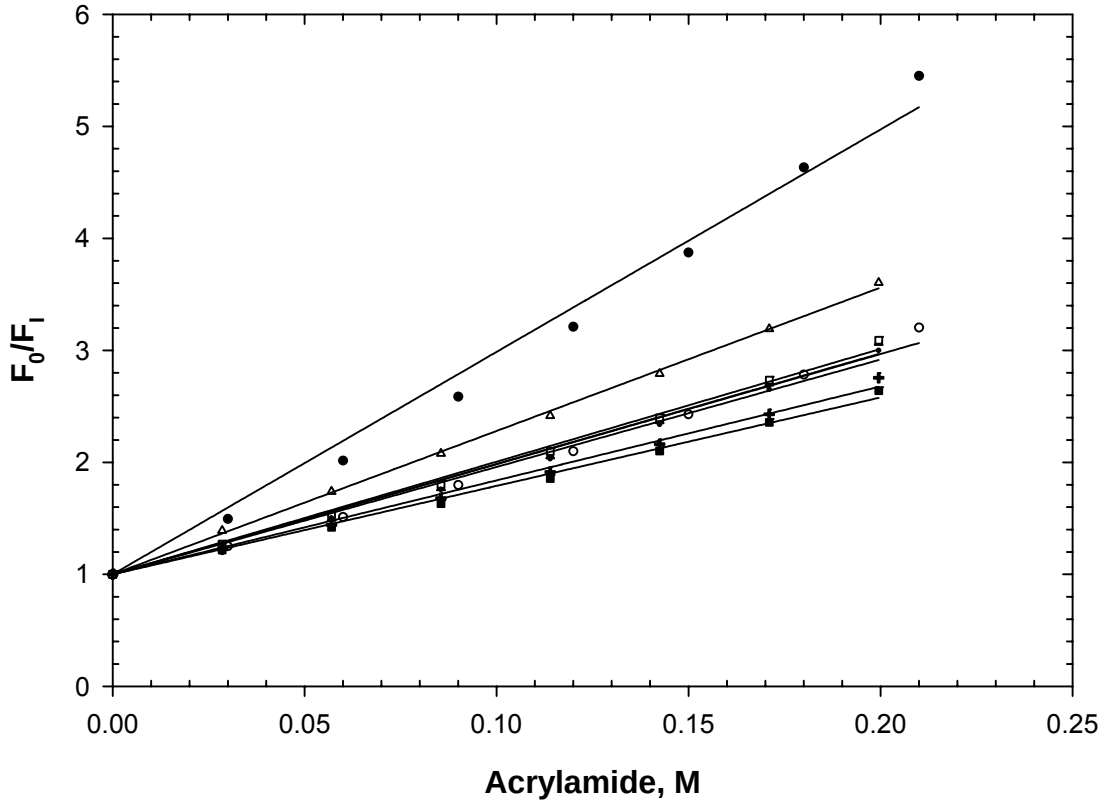

Figure 11. Fluorescence acrylamide quenching data (300 nm excitation, 350 nm emission) of all the peptides (10 μM) in 7.6 M urea, 10 mM TCEP, pH 7.0, and 25 °C. The scans represent the following variants: The scans represent the following conditions: NATA (closed circles), AWA (open circles), AAWAA (closed triangles), WVSGT (D1W; open triangles), GYWHE (Y52W; closed squares), HEWTV (Y55W; open squares), EAWQE (T76W; dots), and DYWTG (Y81W; plus symbols).

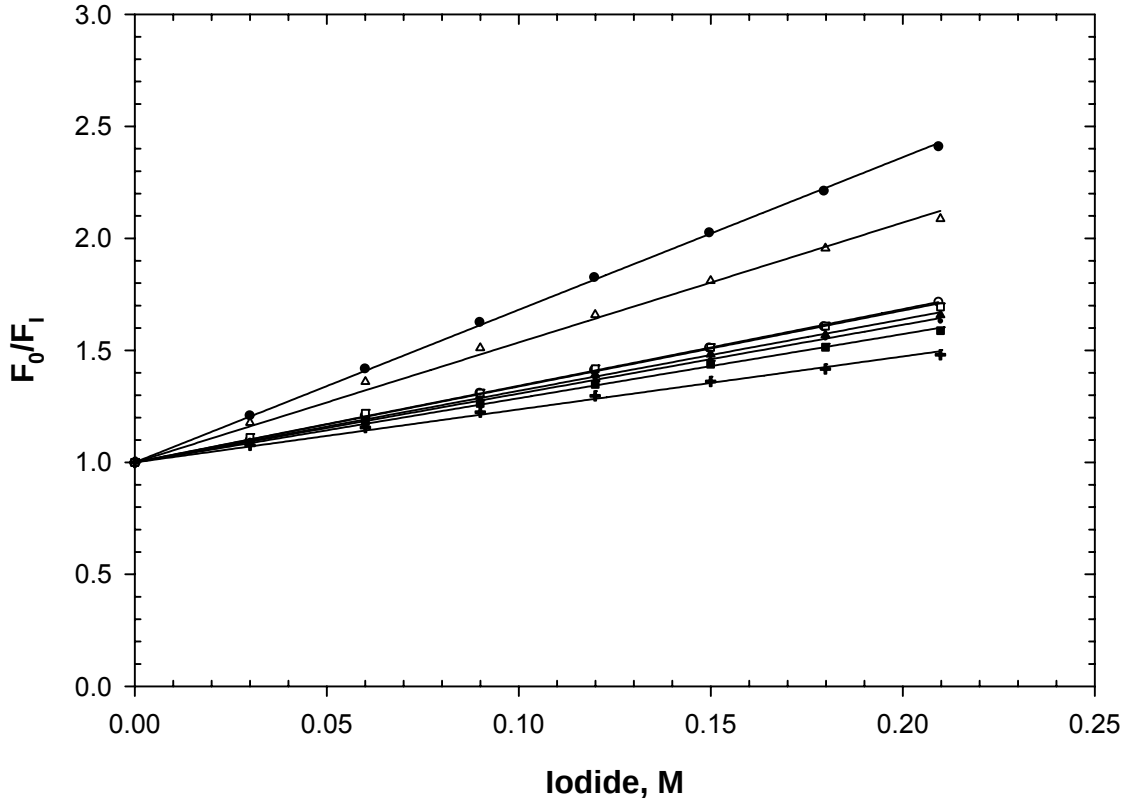

Figure 12. Fluorescence iodide quenching data (300 nm excitation, 350 nm emission) of all the peptides (10 μM) in 3.8 M GdnHCl, 10 mM TCEP, pH 7.0, and 25 ^{o}C. The scans represent the following variants: The scans represent the following conditions: NATA (closed circles), AWA (open circles), AAWAA (closed triangles), WVSGT (D1W; open triangles), GYWHE (Y52W; closed squares), HEWTV (Y55W; open squares), EAWQE (T76W; dots), and DYWTG (Y81W; plus symbols).

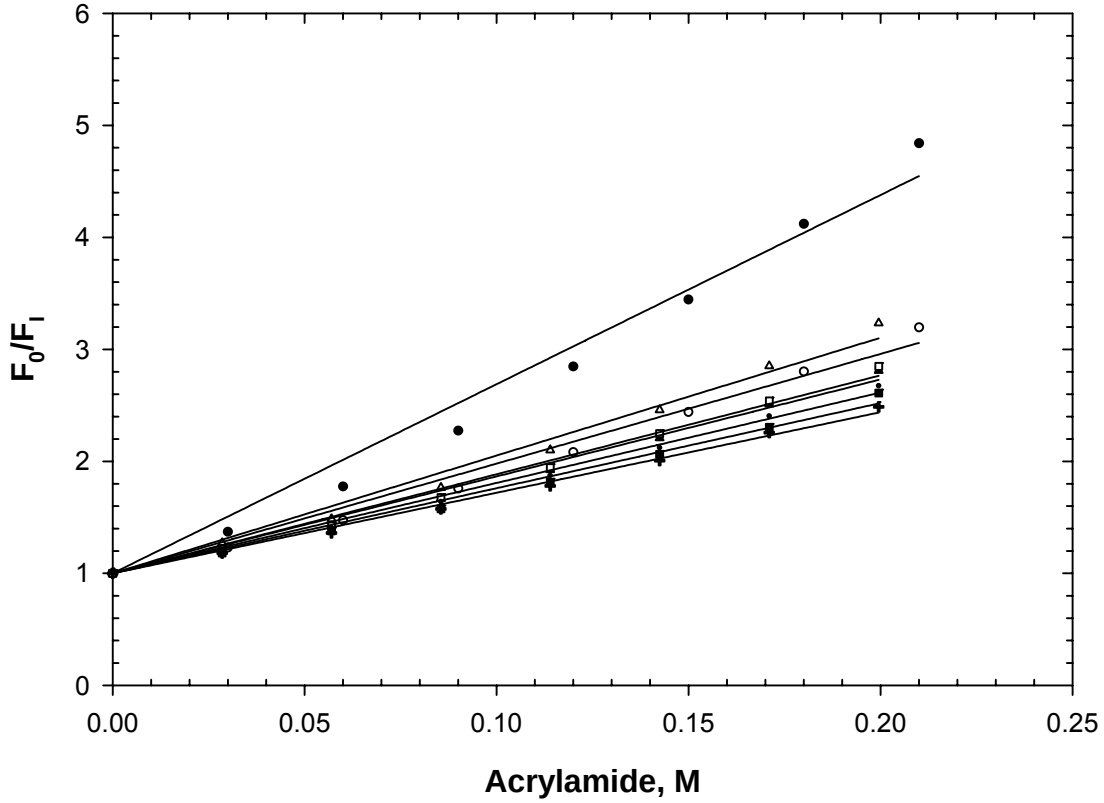

Figure 13. Fluorescence acrylamide quenching data (300 nm excitation, 350 nm emission) of all the peptides (10 μM) in 3.8 M GdnHCl, 10 mM TCEP, pH 7.0, and 25 ^{o}C. The scans represent the following variants: The scans represent the following conditions: NATA (closed circles), AWA (open circles), AAWAA (closed triangles), WVSGT (D1W; open triangles), GYWHE (Y52W; closed squares), HEWTV (Y55W; open squares), EAWQE (T76W; dots), and DYWTG (Y81W; plus symbols).

decrease in rate constant for iodide may be due to iodide's negative charge. Our data supports this. The greatest change we observed occurred with peptides with a net negative charge. Interestingly, the average percent differences between acrylamide and iodide quenching for all of the peptides were very similar for urea and guanidine hydrochloride (~61%). This suggests that, in general, the difference between acrylamide and iodide quenching of the same tryptophan is not dependent on denaturant.

The reason we observed a smaller difference in quenching between the peptides and 3-methylindole for iodide and acrylamide quenching is unclear. Either the efficiency of acrylamide quenching was decreased or the efficiency of the iodide quenching was increased or a combination of both. Certainly, peptides with net positive charges (e.g. the D1W peptide) could explain an increased efficiency for iodide quenching. Secondly, the extra groups on the peptides are providing some shielding effect, thereby lowering the quenching effect, and in turn, affecting the acrylamide more than the iodide quenching. The difference in the sizes of the two quenchers may also be a factor.

When comparing acrylamide quenching in urea to that in guanidine hydrochloride, the Stern-Volmer quenching constants were always higher in urea. One possibility is that the indole rings are more accessible in urea than in guanidine hydrochloride. This seems unlikely. Another possibility is the fact that guanidine hydrochloride quenches better than urea and is diminishing the quenching effect of acrylamide.

The main determinate in quenching by acrylamide is the degree of accessibility of the tryptophan side chains. We would expect that as a tryptophan becomes more

accessible then the degree of quenching would increase. Table 15 shows the percent buried for the tryptophans in each peptide. With one exception, the degree of quenching increased with increased accessibility. The exception is the Y55W peptide (HEWTV). If the percent burial calculation is correct (~16%), compared to the other peptides, it should be the most shielded tryptophan and consequently, should have the lowest Stern-Volmer quenching constant. However, its Stern-Volmer quenching constant is the third highest in urea and fourth highest in guanidine hydrochloride. It may be that the ion pair attraction between the histidine and glutamic acid are causing the increased accessibility of the tryptophan. Other than this exception, our results do generally correlate with accessibility as expected.

The main determinants in quenching by iodide are the degree of accessibility of the tryptophan side chain and the net charge of the peptide. The charge effects should be greater in urea than in guanidine hydrochloride. As we observed with urea, the correlation between the accessibility of the tryptophan and the degree of quenching correlates very well. However, HEWTV is still quenched more than expected, presumably from the ion pair. Otherwise, the data makes sense in terms of accessibility.

The iodide quenching data in urea suggests that quenching depends on the net charge on the peptide. As expected, a peptide with a net positive charge would attract the negative iodide ion, resulting in a higher Stern-Volmer quenching constant, and a peptide with a net negative charge would repel the negative iodide ion, resulting in lower Stern-Volmer quenching constants (Table 16).

Table 16. The Stern-Volmer quenching constants for iodide quenching in urea as a function of net charge.

Peptide	Trp	Net Charge	Iodide K_{SV} (M^{-1})
NATA		0	8.85
WVSGT	1	1	7.73
AAWAA		0	4.03
AWA		0	3.95
HEWTV	55	-0.5	3.72
EAWQE	76	-2	2.92
GYWHE	52	-0.5	2.63
DYWTG	81	-1	2.49

Proteins, pH 7.0

Introduction

In an effort to characterize the denatured ensemble of RNase Sa, five single-site tryptophan variants were made. The positions of four of the tryptophan variants (52, 55, 76, and 81) were based on where tryptophans are found in related microbial ribonucleases (Figure 1), and D1W introduced a substitution at a hyperexposed site. As previously stated, tryptophan fluorescence is a very complicated subject, and while it is not the intent of this research to fully explain the differences in λ_{max} and fluorescence intensity at λ_{max}, we find these differences among the tryptophan variants interesting and significant.

Spectral Moment and λ_{max}

The most blue shifted emission spectrum known in a single tryptophan protein is Azurin, which has a λ_{max} of 308 nm in its native conformation. It is suggested that the blue shift of Azurin results from the fact that the tryptophan is located in a very hydrophobic environment and forms no hydrogen bonds. However, this is not the case with denatured proteins. It is generally thought that as a tryptophan becomes more exposed to solvent then a red shift will occur. For example, when a protein unfolds, λ_{max} generally shifts toward a λ_{max} similar to that of tryptophan in water, 350 nm.

Table 17, Figure 14 and Figure 15 summarize the data from the fluorescence emission scans. We did not observe significant differences amongst the proteins in spectral moment and λ_{max}. The spectral moments ranged from 360 to 361 nm in urea and 360 to 363 nm in guanidine hydrochloride. λ_{max} ranged from 345 to 350 nm in urea and 346 to 351 in guanidine hydrochloride. The average value for λ_{max} in urea and

Table 17. Spectral Moment, λ_{max}, and fluorescence intensity at λ_{max} (I_F) of the reduced (10 mM TCEP) tryptophan variants in 8.5 M urea and 6 M guanidine hydrochloride, pH 7.0, and 25 °C.

Variant	Spectral Moment[a]		λ_{max}[b]		I_F at λ_{max}[c]		% Δ[d]
	Urea (nm)	GdnHCl (nm)	Urea (nm)	GdnHCl (nm)	Urea	GdnHCl	
D1W	361	363	345	351	25900	25000	3
Y52W	360	360	348	347	34600	30700	11
Y55W	360	361	350	346	41200	33800	18
T76W	360	361	346	346	40700	31100	24
Y81W	359	360	347	346	28700	26000	9

[a]Spectral Moment (SM) is the wavelength at which the total area under the emission spectrum is divided into two equal areas.

[b]λ_{max} is the wavelength of maximal intensity of the emission spectrum. We estimate the error to be ± 2 nm.

[c]I_F at λ_{max} is the fluorescence intensity at λ_{max}. We estimate the error to be 3%.

[d] $$\%\Delta = \left(\frac{I_{F,Urea} - I_{F,GdnHCl}}{I_{F,Urea}} \right) \times 100$$

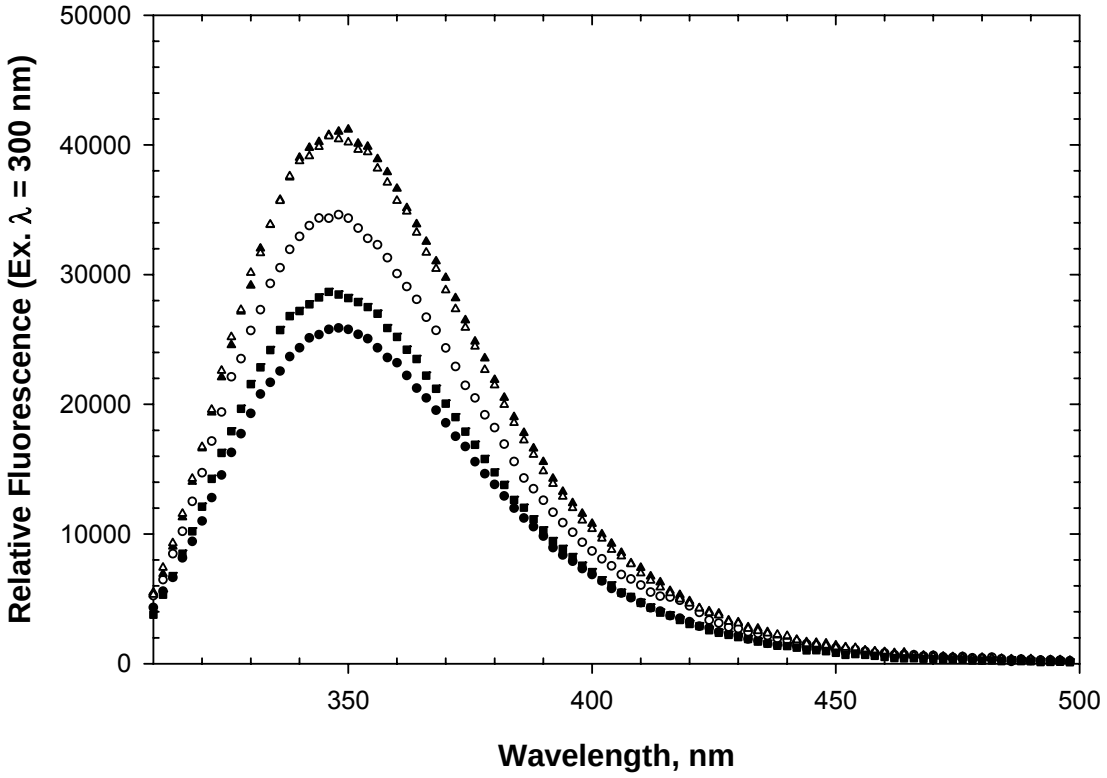

Figure 14. Fluorescence emission spectra (300 nm excitation) of all the reduced, denatured RNase Sa tryptophan variants (10 μM) in the wild-type background in 8.5 M urea, 10 mM TCEP, pH 7.0, and 25 °C. The scans represent the following variants: D1W (closed circles), Y52W (open circles), Y55W (closed triangles), T76W (open triangles), and Y81W (closed squares).

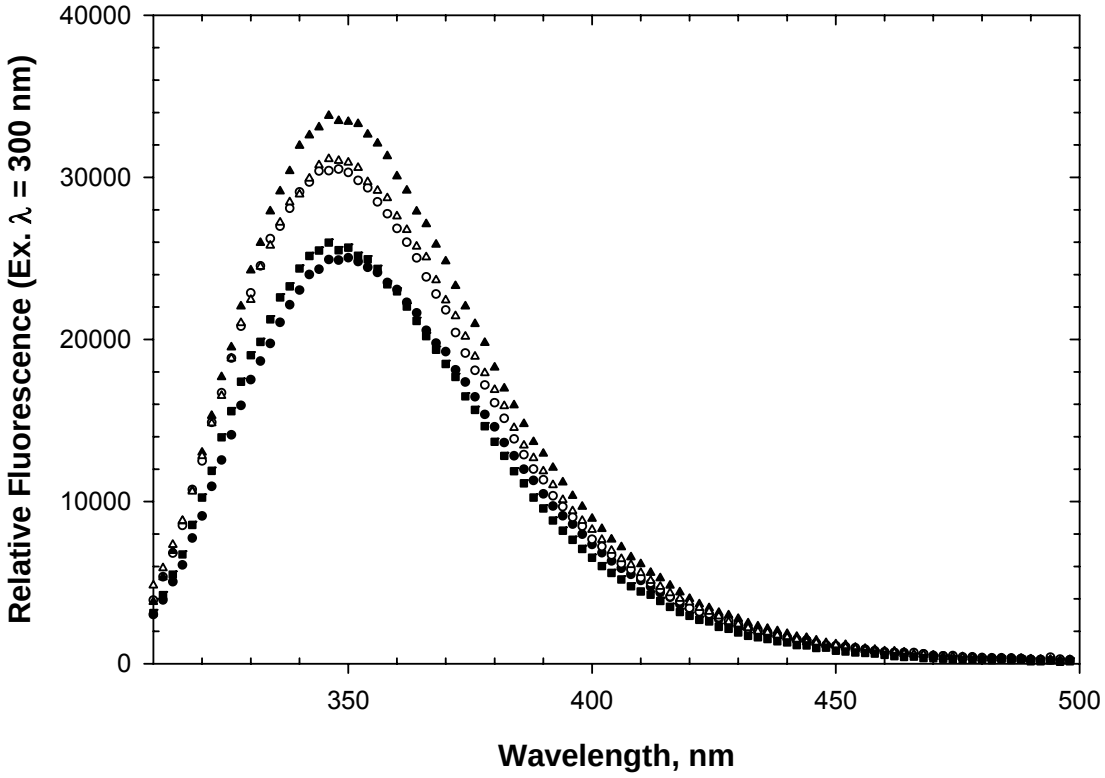

Figure 15. Fluorescence emission spectra (300 nm excitation) of all the reduced, denatured RNase Sa tryptophan variants (10 μM) in the wild-type background in 6 M guanidine hydrochloride, 10 mM TCEP, pH 7.0, and 25 °C. The scans represent the following variants: D1W (closed circles), Y52W (open circles), Y55W (closed triangles), T76W (open triangles), and Y81W (closed squares).

guanidine hydrochloride was 347 ± 2 nm; therefore, we do not feel that these differences are significant.

Others have observed that the emission λ_{max} for unfolded proteins is very close to 350 nm (Teale 1960; Kronman and Holmes 1971). Taking these data alone would suggest that the proteins were completely unfolded, because λ_{max} is approaching the λ_{max} of tryptophan in water. However, this conclusion is not consistent with our fluorescence intensity at λ_{max} or quenching data.

I_F

A decrease in fluorescence intensity at λ_{max} is generally observed when proteins unfold. However, this is not always the case. If a tryptophan was being quenched in the native state, as was observed in Y55W, one might see an increase in fluorescence intensity at λ_{max} upon unfolding. However, generally, fluorescence intensity at λ_{max} decreases upon unfolding. Furthermore, if the same protein with various single-site tryptophan substitutions were completely unfolded, one might expect the spectra to be coincident with one another.

While both the spectral moment and λ_{max} did not differ significantly amongst the tryptophan variants in urea or guanidine hydrochloride, there were differences in the fluorescence intensity at λ_{max}. This reinforces our previous suggestion that fluorescence intensity may be more sensitive to the immediate environment than λ_{max}. From the most to the least fluorescent at λ_{max} in urea were Y55W ≈ T76W > Y52W > Y81W > D1W. In guanidine hydrochloride, the trend was generally the same. From most to least fluorescent at λ_{max} in guanidine were Y55W > T76W > Y52W > Y81W ≈ D1W. Fluorescence intensities at λ_{max} ranged from 41200 to 26000 in urea and from 33800 to

25000 in guanidine hydrochloride. We feel that these differences are significant and interesting and suggest that they represent sensitivity to the presence of residual three dimensional structure persisting in the reduced, denatured state of the proteins. Since D1W is located at a hyperexposed site, it is not surprising that its fluorescence intensity at λ_{max} was the lowest.

The fluorescence intensity at λ_{max} was always lower for the tryptophan variants in guanidine hydrochloride than in urea, suggesting that guanidine hydrochloride is a better quencher of fluorescence than urea, perhaps due to guanidinium ion's positive charge. It has been shown that positive charges interact favorably with aromatic rings (Gallivan and Dougherty 1999). It has also been shown that guanidinium is very weakly hydrated, and this weak hydration strongly supports suggestions that a major contribution to the denaturant effect is the preferential interaction of the denaturant with the protein surface (Mason et al. 2003).

The change in fluorescence intensity at λ_{max} from urea to guanidine hydrochloride ranged from 23% to 3%, generally following the same trend of most to least fluorescence intensity at λ_{max} in the two denaturants. RNase T76W showed the greatest change, and D1W showed the least change. The percent changes are more than likely due to many factors. First, guanidine hydrochloride's quenching effect may be dependent upon the fluorescence intensity of the tryptophan in the absence of denaturant. Secondly, guanidine hydrochloride's quenching may be dependent on the charges surrounding the tryptophan. For example, D1W demonstrated the smallest percent difference in fluorescence intensity at λ_{max} between urea and guanidine hydrochloride. The positive charge on the α-amino group of D1W may be repelling the positive charge of the guanidinium ion. In contrast, T76W demonstrated the greatest

change. In the amino acid sequence, this is the only tryptophan with two negatively charged groups within ± two residues. Therefore, these groups might attract the guanidinium ion, thereby enhancing its quenching effect.

Quenching

Iodide and acrylamide quenching can give insight into the "accessibility" of the tryptophan side chains in proteins (Eftink and Ghiron 1976). Table 18 and Figure 16 through Figure 19 summarize the iodide and acrylamide quenching data for the proteins. The rank order of quenching was generally the same for acrylamide and iodide quenching in urea and guanidine hydrochloride. The general trend from highest to lowest K_{SV} was D1W > Y55W > T76W > Y52W > Y81W.

Regardless of denaturant or quencher, D1W always had the highest Stern-Volmer quenching constant, which is expected since the tryptophan is the N-terminal amino acid. Conversely, Y81W always had the lowest Stern-Volmer quenching constant. If there are pockets of residual structure which protect against quenching, this suggests that Y81W is more protected by residual structure than the other tryptophans.

In urea and guanidine hydrochloride, the Stern-Volmer quenching constants were always higher for acrylamide than iodide, suggesting the acrylamide is a better quencher of fluorescence. However, acrylamide's quenching efficiency decreased in guanidine hydrochloride. Perhaps, guanidine hydrochloride quenches better than urea and is diminishing the quenching effect of acrylamide.

As previously stated, acrylamide has been shown to quench 3-methylindole better than iodide. Iodide quenches 3-methylindole with 82% less efficiency than acrylamide. For all of the proteins in urea, we observed an average of 60% less efficiency for iodide quenching compared to acrylamide. In the proteins, the efficiency

Table 18. Stern-Volmer quenching constants for iodide and acrylamide quenching of the proteins in 7.6 M urea and 6 M guanidine hydrochloride, reduced (10 mM TCEP), pH 7.0, and 25 °C. The rank order from highest to lowest K_{SV} is given after each column for each dataset.

Variant	Acrylamide K_{SV}[a] (M^{-1})				Iodide K_{SV}[a] (M^{-1})			
	Urea	Rank	GdnHCl	Rank	Urea	Rank	GdnHCl	Rank
D1W	10.04	1	8.38	1	5.23	1	4.59	1
Y52W	7.20	4	6.87	4	2.77	4	3.06	3
Y55W	8.52	2	7.97	2	3.33	2	3.22	2
T76W	7.92	3	7.57	3	3.04	3	2.92	4
Y81W	6.15	5	5.96	5	1.87	5	2.47	5
Average	7.97 ± 1.46		7.35 ± 0.96		3.25 ± 1.24		3.25 ± 0.80	

[a]Equation 8 in the Methods and Materials section was used to calculate the Stern-Volmer quenching constants.

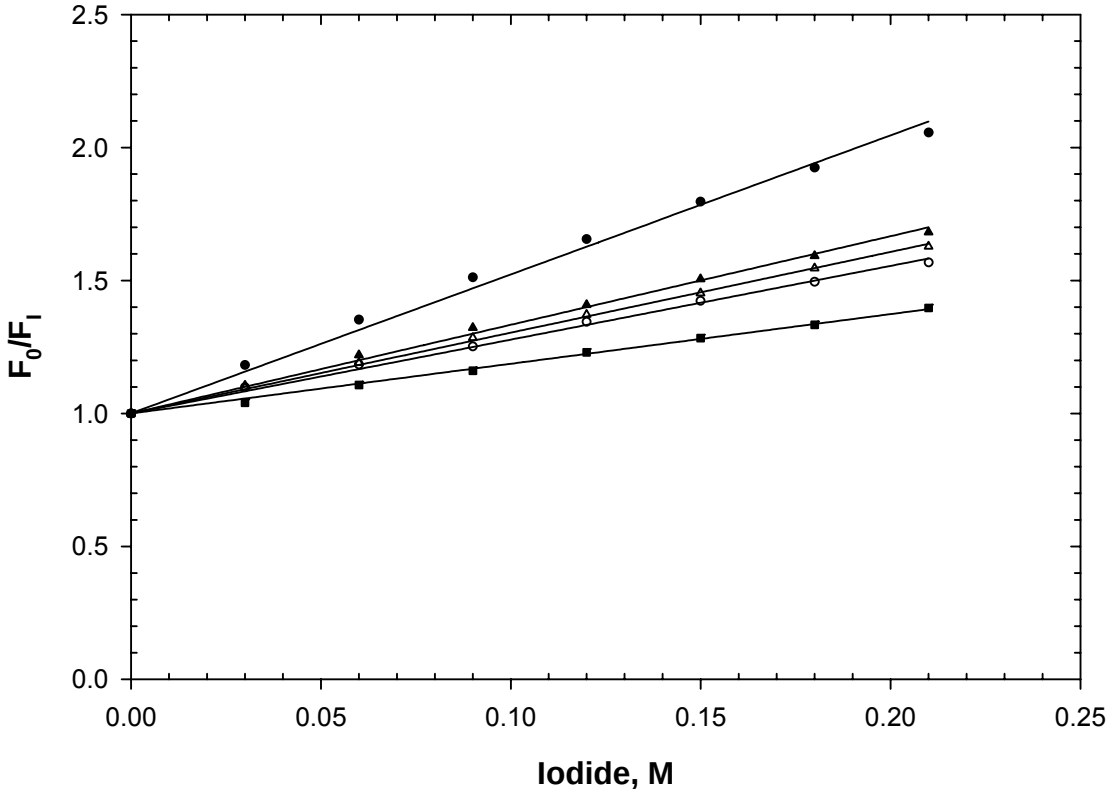

Figure 16. Iodide quenching of fluorescence (300 nm excitation, 350 nm emission) of the reduced, denatured RNase Sa tryptophan variants (10 μM) in the wild-type background in 7.6 M urea, 10 mM TCEP, pH 7.0, and 25 °C. The data represent the following variants: D1W (closed circles), Y52W (open circles), Y55W (closed triangles), T76W (open triangles), and Y81W (closed squares).

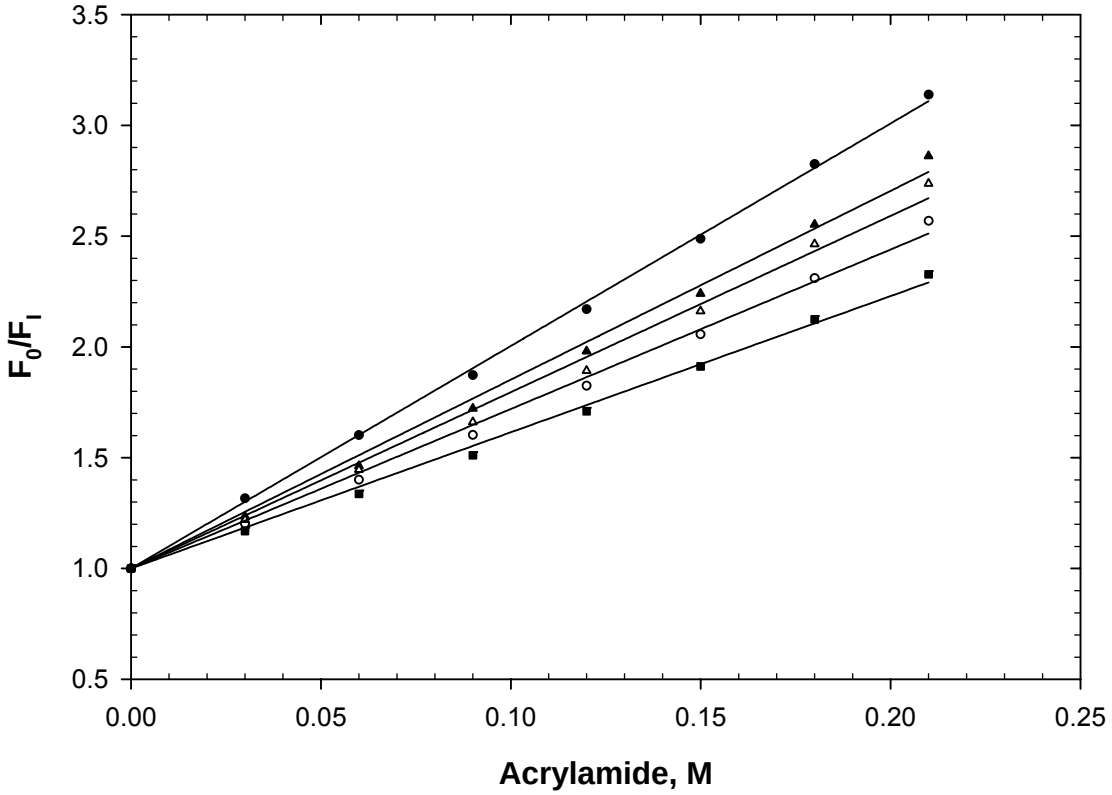

Figure 17. Acrylamide quenching of fluorescence (300 nm excitation, 350 nm emission) of the reduced, denatured RNase Sa tryptophan variants (10 μM) in the wild-type background in 7.6 M urea, 10 mM TCEP, pH 7.0, and 25 °C. The data represent the following variants: D1W (closed circles), Y52W (open circles), Y55W (closed triangles), T76W (open triangles), and Y81W (closed squares).

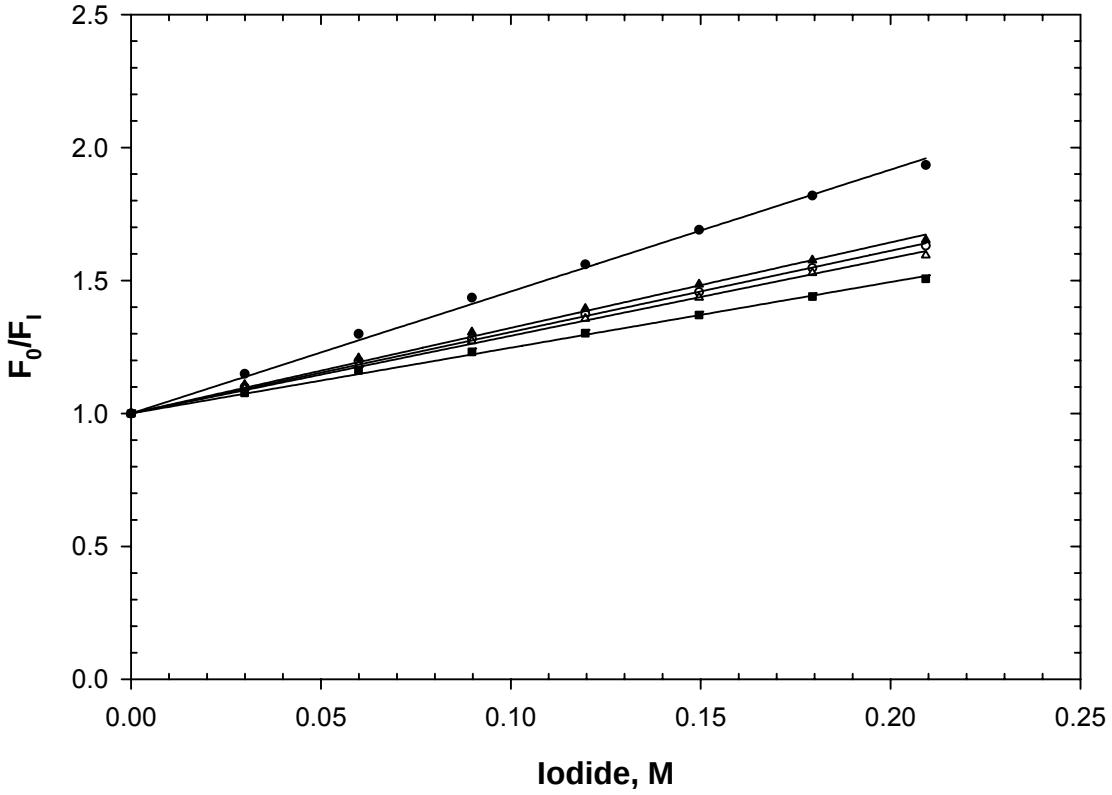

Figure 18. Iodide quenching of fluorescence (300 nm excitation, 350 nm emission) of the reduced, denatured RNase Sa tryptophan variants (10 μM) in the wild-type background in 3.8 M guanidine hydrochloride, 10 mM TCEP, pH 7.0, and 25 °C. The data represent the following variants: D1W (closed circles), Y52W (open circles), Y55W (closed triangles), T76W (open triangles), and Y81W (closed squares).

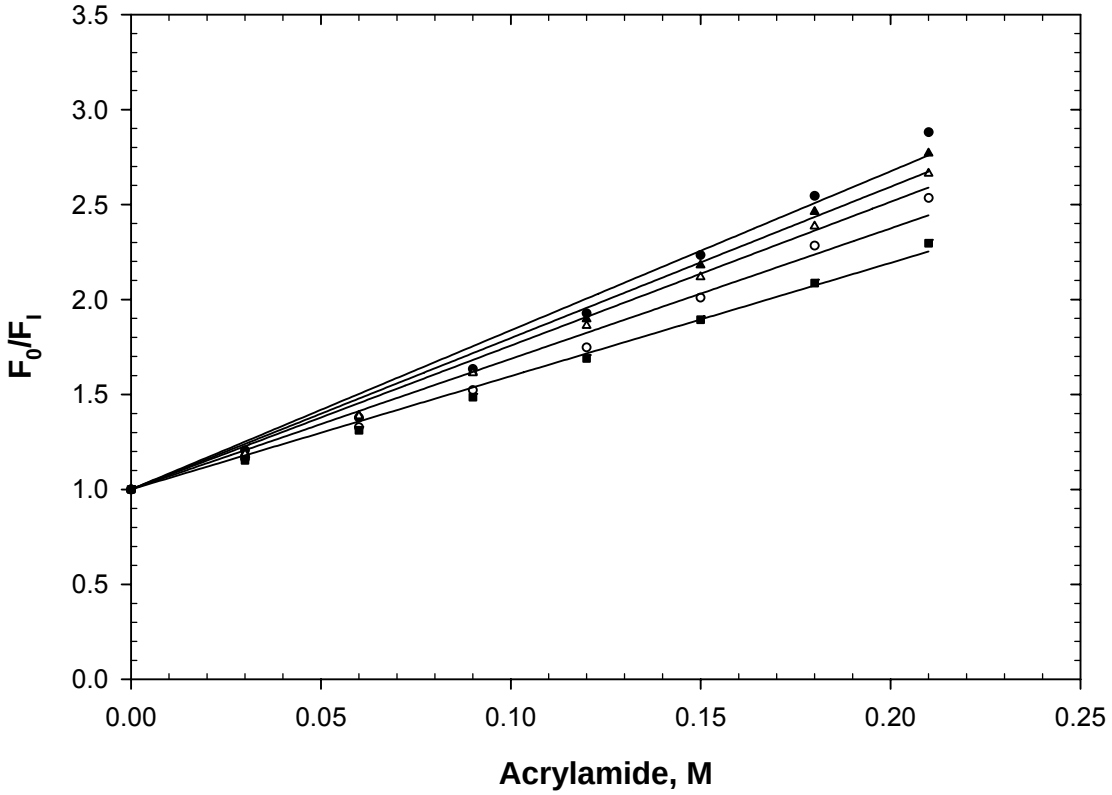

Figure 19. Acrylamide quenching of fluorescence (300 nm excitation, 350 nm emission) of the reduced, denatured RNase Sa tryptophan variants (10 μM) in the wild-type background in 3.8 M guanidine hydrochloride, 10 mM TCEP, pH 7.0, and 25 °C. The data represent the following variants: D1W (closed circles), Y52W (open circles), Y55W (closed triangles), T76W (open triangles), and Y81W (closed squares).

of iodide may be diminished by additional negative charges in the vicinity of the tryptophans. At pH 7.0, the net charge on RNase Sa should be about -7. Acrylamide's efficiency would have been reduced, too.

For acrylamide quenching, the main factor determining the degree of quenching is the accessibility of the tryptophan. The Stern-Volmer quenching constants ranged from 6.15 to 10.04 M^{-1} in urea and from 5.96 to 8.38 M^{-1} in guanidine hydrochloride. As was observed with the fluorescence intensity at λ_{max}, these differences are significant and provide further evidence that residual structure exists in the denatured state. Additional insight will be gained later when the proteins are compared to the model compounds.

For iodide quenching, there are two factors that determine the degree of quenching, accessibility of the tryptophan and charges in its vicinity. The Stern-Volmer quenching constants ranged from 1.87 to 5.23 M^{-1} in urea and from 2.47 to 4.59 M^{-1} in guanidine hydrochloride.

RNase Sa Y52W and Y81W had higher Stern-Volmer quenching constants for iodide quenching in guanidine hydrochloride than in urea. Both of these residues have charged residues nearby in the sequence. RNase Sa Y52W has a histidine residue adjacent to the tryptophan, and Y81W has an aspartic acid one residue away. It is conceivable that the guanidine hydrochloride disrupted electrostatic interactions near the environments of Y52W and Y81W, causing the change in the trend when comparing iodide quenching in urea versus iodide quenching in guanidine hydrochloride.

If a low Stern-Volmer quenching constant corresponds to a protected ("buried") tryptophan, and a high fluorescence intensity value at λ_{max} corresponds to a protected ("buried") tryptophan then the quenching of RNase D1W, Y52W, and T76W correspond

fairly well with the emission scan data (Table 19). It may be that a fluorescence emission scan is a more “global” event, whereas quenching data is a more “local” event. This idea will be discussed further in the comparison between the peptides and the proteins. Obviously, the lack of complete agreement suggests that there are other factors affecting the fluorescence of the tryptophans.

Table 19. Comparison of rank order of emission scans, iodide and acrylamide quenching data. Emission scans are ranked from lowest to highest fluorescence intensity at λ_{max}, and iodide and acrylamide quenching are ranked from highest to lowest Stern-Volmer quenching constants, pH 7.0, and 25 ^{o}C.

	Urea			GdnHCl		
	I_F at λ_{max}	Iodide K_{SV}	Acrylamide K_{SV}	I_F at λ_{max}	Iodide K_{SV}	Acrylamide K_{SV}
D1W	1	1	1	1	1	1
Y52W	3	4	4	3	3	4
Y55W	4	2	2	5	2	2
T76W	5	3	3	4	4	3
Y81W	2	5	5	2	5	5

Influence of the Disulfide Bond on Fluorescence

RNase Sa has one disulfide bond, from residue 7 to 96, and all of our experiments were performed on the oxidized and reduced states of the proteins. With a disulfide bond intact, one would expect a more compact denatured state, which might stabilize pockets of structure. With the disulfide bond cleaved, one would expect a more expanded denatured state. In addition, -SH groups are the most potent fluorescence quenchers of the protein side chains (Chen and Barkley 1998). Furthermore, since cysteine residues can quench tryptophan fluorescence, one might expect the differences between the oxidized and reduced states of the proteins to be greater in the fluorescence intensities at λ_{max} and to have no effect in the quenching

data. Table 20 and Table 21 summarize the oxidized versus reduced data for the proteins in urea and guanidine hydrochloride at pH 7.0, and 25 ^{o}C.

We observed no difference in spectral moment or λ_{max} between the oxidized and reduced states of the proteins. Based on previous results in this study, this was not surprising. Additionally, we observed small differences in fluorescence intensity at λ_{max} between the oxidized and reduced states of the proteins in urea. These small differences suggest that no -SH quenching is occurring. If -SH quenching had occurred, it should have been the most pronounced for D1W, since it is the closest tryptophan variant to an -SH group. Interestingly, we did observe a difference between the oxidized and reduced states of D1W in guanidine hydrochloride, with the oxidized state having a greater fluorescence at λ_{max} than the reduced state. This is a puzzling result. However, generally, the differences in fluorescence intensity at λ_{max} for all the proteins were negligible and within experimental error. These results were in agreement with other work. Kronman and Holmes also observed that, “cleavage of disulfide bonds appears to have little effect on narrowing the range of values that the tryptophan quantum yields can take on (Kronman and Holmes 1971).”

For the quenching data, if the disulfide bond was contributing to a more compact denatured state then we would expect a higher Stern-Volmer quenching constant for the reduced state of the proteins, and with the exception of D1W, this is what we see for the proteins in guanidine hydrochloride. This trend was not observed with urea. The changes that were observed in urea were negligible and probably all within experimental error. RNase D1W demonstrated opposite effects in the two denaturants. In urea, the reduced state had a higher Stern-Volmer quenching constant as expected. In guanidine hydrochloride, the oxidized state had a higher Stern-Volmer quenching

constant. Why the proteins did not show the same difference in urea as they did in guanidine hydrochloride and why there are differences in D1W in the two denaturants are puzzling.

Table 20. Comparison of oxidized and reduced (10 mM TCEP) fluorescence emission data for the proteins in urea and guanidine hydrochloride, pH 7, and 25 °C.

Variant		Urea[a]				GdnHCl[b]			
		SM[c] (nm)	λ_{max}[d] (nm)	I_F at λ_{max}[e]	% Δ[f]	SM (nm)	λ_{max} (nm)	I_F at λ_{max}	% Δ[g]
D1W	Red	361	345	25900		363	351	25000	
	Ox	360	347	25300	2	363	351	28000	-12
Y52W	Red	360	348	34600		360	347	30700	
	Ox	360	348	35600	-3	360	349	31500	-3
Y55W	Red	360	350	41200		361	346	33800	
	Ox	360	347	42400	-3	361	346	35000	-4
T76W	Red	360	346	40700		361	346	31100	
	Ox	359	346	42400	-4	361	347	31500	-1
Y81W	Red	359	347	28700		360	346	26000	
	Ox	358	346	30800	-7	360	345	27100	-4

[a]The concentration of urea used was 8.5 M.
[b]The concentration of guanidine hydrochloride used was 6 M.
[c]Spectral Moment (SM) is the wavelength at which the total area under the emission spectrum is divided into two equal areas.
[d]λ_{max} is the wavelength of maximal intensity of the emission spectrum. We estimate the error to be ± 2 nm.
[e]I_F at λ_{max} is the fluorescence intensity at λ_{max}. We estimate the error to be 3%.

[f] $$\%\Delta_{Urea} = \left(\frac{I_{F,\mathrm{Red}} - I_{F,\mathrm{Ox}}}{I_{F,\mathrm{Red}}} \right) \times 100$$

[g] $$\%\Delta_{GdnHCl} = \left(\frac{I_{F,\mathrm{Red}} - I_{F,\mathrm{Ox}}}{I_{F,\mathrm{Red}}} \right) \times 100$$

Table 21. Comparison of oxidized and reduced fluorescence acrylamide quenching data for the proteins in urea and guanidine hydrochloride, pH 7, and 25 °C.

Variant		Urea[a]		GdnHCl[b]	
		Acrylamide K_{SV}[c] (M^{-1})	% Δ[d]	Acrylamide K_{SV}[c] (M^{-1})	% Δ[d]
D1W	Red	10.04		8.38	
	Ox	9.17	9	9.05	-8
Y52W	Red	7.20		6.87	
	Ox	7.44	-3	6.13	11
Y55W	Red	8.52		7.97	
	Ox	8.65	-2	6.82	14
T76W	Red	7.92		7.57	
	Ox	8.26	-4	6.23	18
Y81W	Red	6.15		5.96	
	Ox	6.53	-6	5.30	11

[a]The concentrations of urea used were 8.5 M for oxidized and 7.6 M for reduced.
[b]The concentrations of guanidine hydrochloride used were 6 M for oxidized and 3.8 M for reduced.
[c]Equation 8 in the Methods and Materials section was used to calculate the Stern-Volmer quenching constants.

[d] $$\%\Delta_{Urea} = \left(\frac{K_{SV,\,\mathrm{Red}} - K_{SV,\,\mathrm{Ox}}}{K_{SV,\,\mathrm{Red}}} \right) \times 100$$

[e] $$\%\Delta_{GdnHCl} = \left(\frac{K_{SV,\,\mathrm{Red}} - K_{SV,\,\mathrm{Ox}}}{K_{SV,\,\mathrm{Red}}} \right) \times 100$$

Comparison of Denatured Proteins to Peptides, pH 7.0

Introduction

Fluorescence data have been compared by others to study the denatured state (Amir et al. 1992; Navon et al. 2001; Tew and Bottomley 2001; Crowhurst et al. 2002; Chattopadhyay et al. 2003). We now consider the question, "What makes a good model for the denatured state ensemble?" For example, the fluorescence data of proteins has been compared to the behavior of NATA under the same denaturing conditions to provide evidence of residual structure in the denatured state (Chattopadhyay et al. 2003). We have taken this a step further by providing what should be better models of the unfolded state. Five pentapeptides, whose sequences are based on the original tryptophan substitutions in the proteins, were studied under the same denaturing conditions as the proteins. With the exception of the D1W pentapeptide, all of the pentapeptides are blocked at the N and C termini. To mimic the D1W substitution in the protein, the D1W pentapeptide is blocked only at the C-terminus. If our best model represents a completely unfolded protein then we should expect to see at least three common trends in our data. First, λ_{max} of the proteins should red shift to the same degree as our model. Secondly, the emission intensity of our model and protein should be coincident, and thirdly, the Stern-Volmer quenching constants should be the same for our model and proteins.

Spectral Moment and λ_{max}

If there is a correlation between λ_{max}, spectral moment and protein unfolding under denaturing conditions then one might expect a difference in λ_{max} and spectral moment between the model compounds and a protein if residual structure existed in the denatured ensemble. However, this was not observed. The average spectral moment

for all of the model compounds and proteins in urea and guanidine hydrochloride was 361 ± 1 and 362 ± 1 nm, respectively. The average λ_{max} for all of the model compounds and proteins in urea and guanidine hydrochloride was 348 ± 2 nm. However, the spectral moment and λ_{max} for NATA were generally shifted to slightly longer wavelengths compared to the other model compounds and proteins. This has been observed by others (Kronman and Holmes 1971). We will now consider the fluorescent behavior of NATA, AWA and AAWAA under the same denaturing conditions as the proteins.

NATA, AWA, and AAWAA

When comparing the fluorescence intensity at λ_{max} from greatest to least, the trend was NATA > AAWAA > AWA. As stated previously, peptide bonds can quench the fluorescence of tryptophan. Therefore, the increased I_F of NATA compared to AWA seems to be derived from the “peptide bonds” of NATA not being equivalent to those of AWA. Furthermore, since the tryptophan side chain of NATA is the most accessible side chain of our models, it was expected to have the largest Stern-Volmer quenching constant, and that was observed. Conversely, we would expect the tryptophan side chain in AWA to be somewhat more shielded than the tryptophan side chain in NATA.

An increase in fluorescence intensity at λ_{max} was observed for AAWAA compared to AWA. Since AWA and AAWAA have no potential groups in their sequences to quench the fluorescence of the tryptophans, presumably, the additional alanines in AAWAA are influencing the fluorescence intensity at λ_{max} to a small degree. Additionally, the tryptophan side chain in AWA should be somewhat more accessible than the tryptophan side chain in AAWAA. However, the difference will probably not be

overwhelmingly substantial. This small difference in accessibility could account for the comparable Stern-Volmer quenching constants observed between AWA and AAWAA.

AAWAA Compared to the Corresponding Pentapeptides

The tryptophan in AAWAA should be more exposed than that in any of the pentapeptides, because alanine is smaller than any of the other side chains except glycine. If fluorescence intensity at λ_{max} were solely dependent on the accessibility of the side chain on the tryptophan then one would expect AAWAA to be the least fluorescent. However, this was not observed. AAWAA had a greater I_F than the Y81W (DYWTG), the D1W (WVSGT), and the Y52W (GYWHE) peptides. As previously discussed, all of these tryptophans have potential quenching groups adjacent to them or in the case of the D1W peptide, a positive charge on the α-amino group, which could diminish their fluorescence.

The main determinate in quenching by acrylamide is the degree of accessibility of the tryptophan side chains. We would expect that as a tryptophan becomes more accessible then the degree of quenching would increase. Since AAWAA should have the most exposed tryptophan of the pentapeptides, one might suppose that the Stern-Volmer quenching constant for AAWAA would be the highest among the pentapeptides. However, this was not observed. The D1W (WVSGT) and Y55W (HEWTV) peptides actually had higher Stern-Volmer quenching constants than AAWAA. With one exception, the Y55W peptide (HEWTV), the degree of quenching increased with increased accessibility. We proposed that the ion pair attraction between the histidine and glutamic acid of HEWTV may be causing the increased accessibility of the tryptophan. However, other than this exception, our results do generally correlate with accessibility as expected.

The Pentapeptides as Models for the Denatured State

We will first examine how the pentapeptides did as a group. Table 22, Table 23, and Figure 20 through Figure 23 summarize the data comparing the pentapeptides to their corresponding proteins. Without exception in urea or guanidine hydrochloride, the fluorescence intensities at λ_{max} for the pentapeptides were always less than for their corresponding proteins. This strongly suggests that structure beyond the local sequence is important for fluorescence intensity at λ_{max}. Furthermore, for acrylamide quenching in urea and guanidine hydrochloride, the Stern-Volmer quenching constants were always greater for the pentapeptides than for their corresponding proteins, suggesting again, that structure beyond the local sequence is important.

Figure 24 and Figure 25 show the correlation between the Stern-Volmer quenching constants of the pentapeptides to the Stern-Volmer quenching constants of their corresponding proteins in urea and guanidine hydrochloride. The correlation plots may suggest at least two things. A slope of one would indicate that the pentapeptides perfectly modeled the proteins. The observed slopes equaling less than one shows that the tryptophans are quenched less in the proteins than in the pentapeptides and reinforces our belief that structure beyond the local level is important.

If we now consider how the pentapeptides did individually, the least percent difference in fluorescence intensity at λ_{max} between a protein and its corresponding pentapeptide occurred with D1W. As discussed previously, I_F is very dependent on groups that can potentially quench the fluorescence of tryptophan. It may be that the positively charged α-amino group of the tryptophan in the protein and pentapeptide is the most influential quencher of the fluorescence of these two tryptophans. Since the tryptophan is at the N-terminus and there are no other quenching groups in the

Table 22. Comparison of the fluorescence emission scan data of the reduced proteins with the model compounds and their corresponding pentapeptides in urea and guanidine hydrochloride at pH 7.0 and 25 °C.

	Spectral Moment[a]		λ_{max}[b]		I_F at λ_{max}[c]			
	Urea (nm)	GdnHCl (nm)	Urea (nm)	GdnHCl (nm)	Urea	%Δ[d]	GdnHCl	%Δ[d]
NATA	363	364	352	351	49000		35500	
AWA	362	362	349	346	24400		22100	
AAWAA	362	362	350	350	28500		23100	
WVSGT	361	363	347	350	23900		22100	
D1W	361	363	345	351	25900	8	25000	12
GYWHE	361	361	347	347	24600		23100	
Y52W	360	360	348	347	34600	29	30700	25
HEWTV	361	362	349	349	30800		25700	
Y55W	360	361	350	346	41200	25	33800	24
EAWQE	361	362	347	348	32300		24900	
T76W	360	361	346	346	40700	21	31100	20
DYWTG	361	362	347	347	21500		18400	
Y81W	359	360	347	346	28700	25	26000	29

[a]Spectral Moment is the wavelength at which the total area under the emission spectrum is divided into two equal areas.

[b]λ_{max} is the wavelength of maximal intensity of the emission spectrum. We estimate the error to be ± 2 nm.

[c]I_F at λ_{max} is the fluorescence intensity at λ_{max}. We estimate the error to be 3%.

[d] $$\%\Delta = \left(\frac{I_{F,\,\text{Protein}} - I_{F,\,\text{Model}}}{I_{F,\,\text{Protein}}} \right) \times 100$$

Table 23. Comparison of the acrylamide and iodide Stern-Volmer quenching constants (M^{-1}) of the reduced proteins with the model compounds and their corresponding pentapeptides in urea and guanidine hydrochloride at pH 7.0 and 25 °C.

	Acrylamide K_{SV}[a] (M^{-1})				Iodide K_{SV}[a] (M^{-1})			
	Urea	%Δ[b]	GdnHCl	%Δ[b]	Urea	%Δ[b]	GdnHCl	%Δ[b]
NATA	19.86		16.89		8.85		6.81	
AWA	9.84		9.80		3.95		3.42	
AAWAA	9.86		8.66		4.03		3.19	
WVSGT	12.81		10.52		7.73		5.35	
D1W	10.04	-28	8.38	-26	5.23	-48	4.59	-17
GYWHE	7.90		7.60		2.63		2.86	
Y52W	7.20	-10	6.87	-11	2.77	5	3.06	7
HEWTV	10.06		8.85		3.72		3.39	
Y55W	8.52	-18	7.97	-11	3.33	-12	3.22	-5
EAWQE	9.59		8.08		2.92		3.07	
T76W	7.92	-21	7.57	-7	3.04	4	2.92	-5
DYWTG	8.39		7.20		2.49		2.36	
Y81W	6.15	-36	5.96	-21	1.87	-33	2.47	4

[a]Equation 8 in the Methods and Materials section was used to calculate the Stern-Volmer quenching constants.

[b] $\%\Delta = \left(\frac{I_{F,\,\text{Protein}} - I_{F,\,\text{Model}}}{I_{F,\,\text{Protein}}} \right) \times 100$

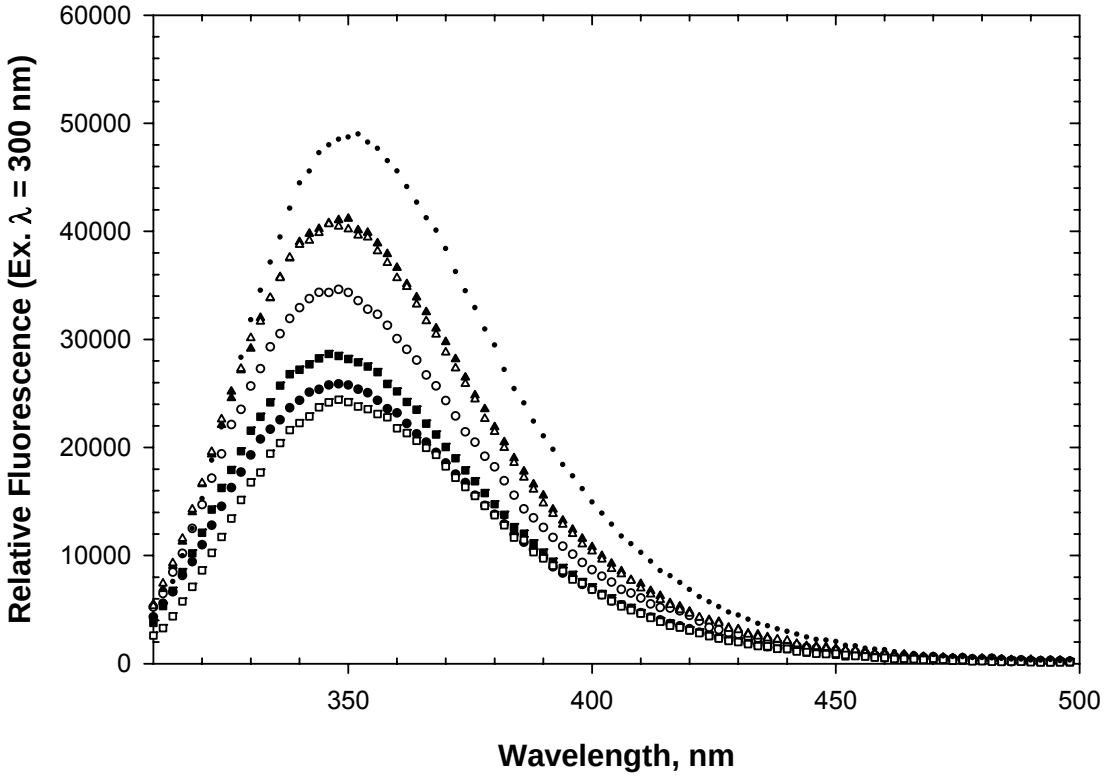

Figure 20. Denatured, reduced fluorescence emission spectra (300 nm excitation) of all the wild-type background RNase Sa tryptophan variants (10 μM) compared to AWA and NATA (10 μM) in 8.5 M urea, 10 mM TCEP, pH 7.0, and 25 °C. The scans represent the following variants: D1W (closed circles), Y52W (open circles), Y55W (closed triangles), T76W (open triangles), Y81W (closed squares), AWA (open squares), and NATA (dots).

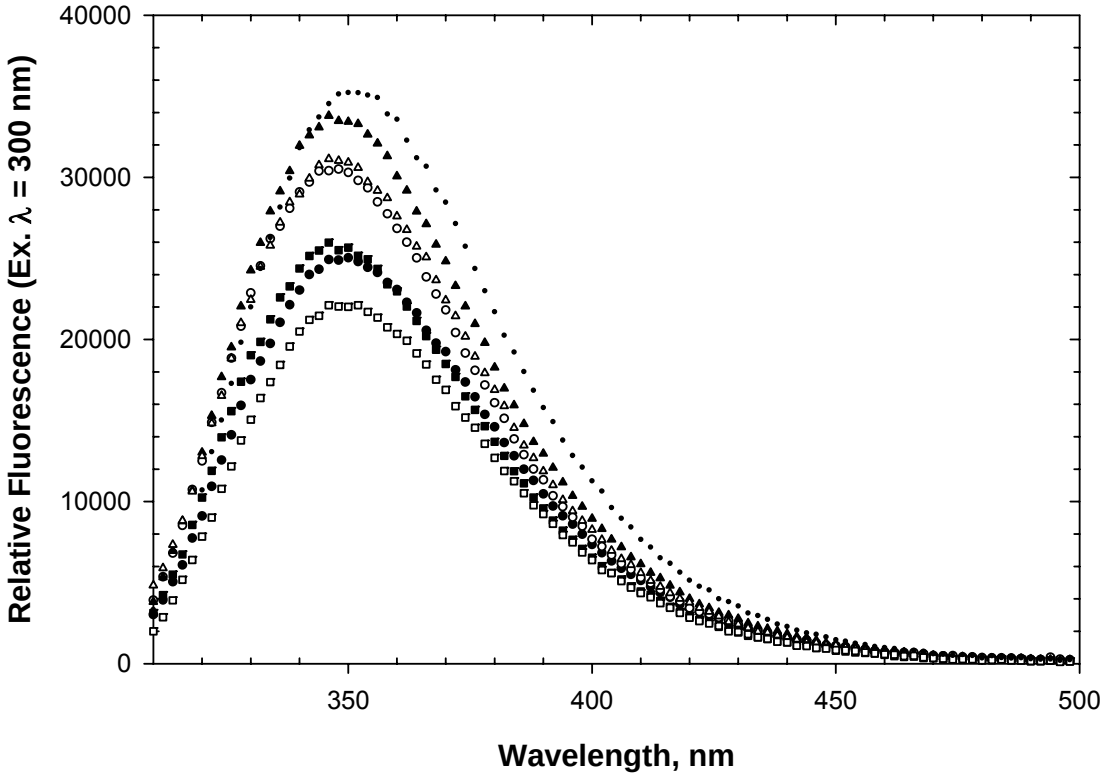

Figure 21. Denatured, reduced fluorescence emission spectra (300 nm excitation) of all the wild-type background RNase Sa tryptophan variants (10 μM) compared to AWA and NATA (10 μM) in 6.0 M urea, 10 mM TCEP, pH 7.0, and 25 °C. The scans represent the following variants: D1W (closed circles), Y52W (open circles), Y55W (closed triangles), T76W (open triangles), Y81W (closed squares), AWA (open squares), and NATA (dots).

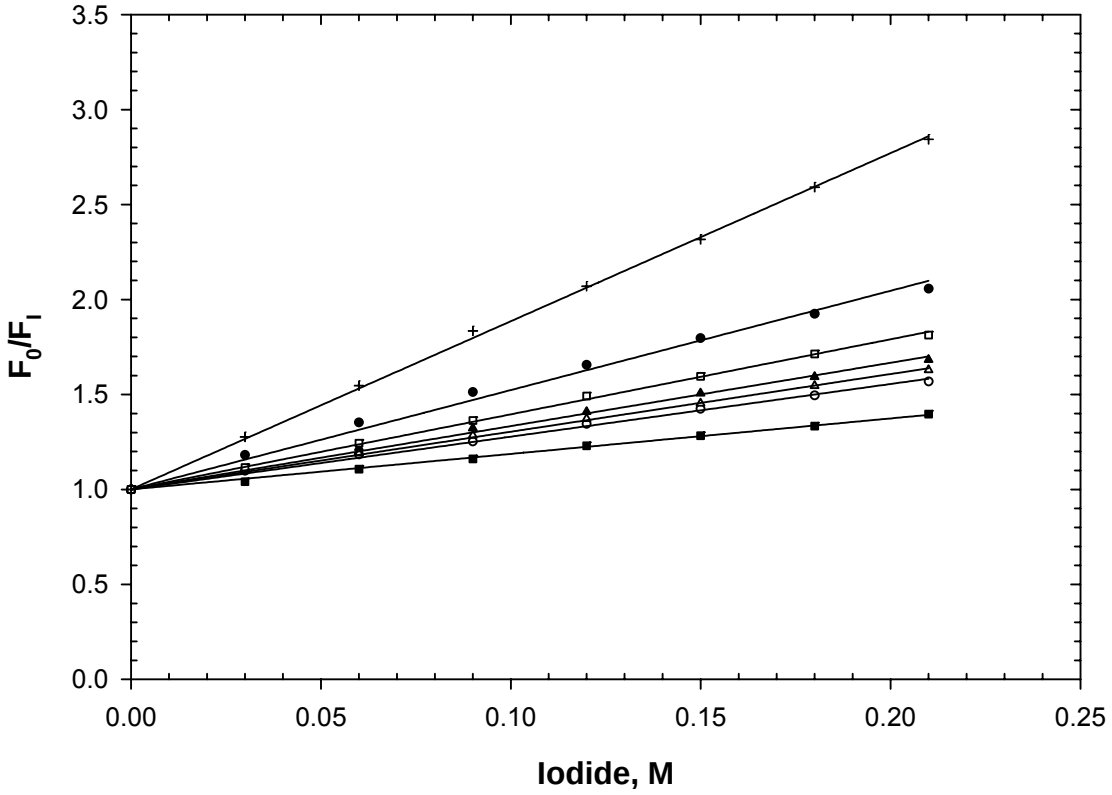

Figure 22. Denatured, reduced fluorescence iodide quenching data (300 nm excitation, 350 nm emission) of all the wild-type background RNase Sa tryptophan variants, NATA, and AWA (10 μM) in 7.6 M urea, 10 mM TCEP, pH 7.0, and 25 °C. The scans represent the following variants: D1W (closed circles), Y52W, Y55W (closed triangles), T76W (open triangles), Y81W (closed squares), NATA (plus symbols), and AWA (open squares).

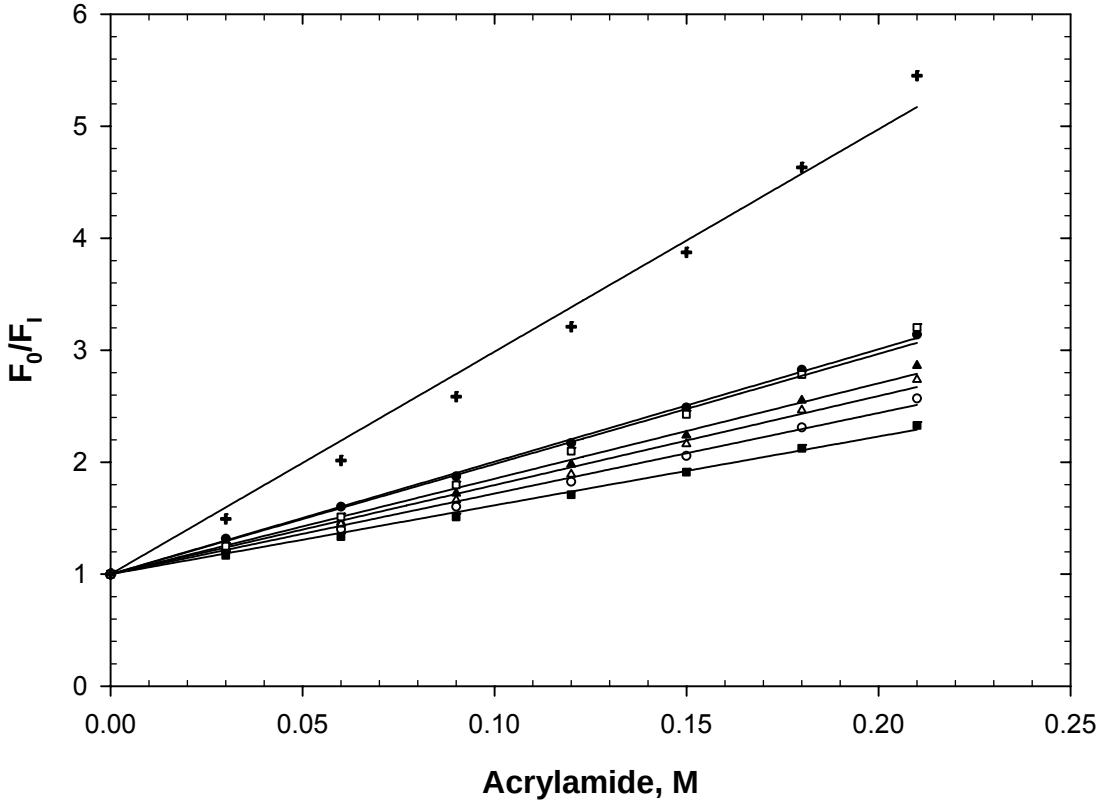

Figure 23. Denatured, reduced fluorescence acrylamide quenching data (300 nm excitation, 350 nm emission) of all the wild-type background RNase Sa tryptophan variants, NATA, and AWA (10 μM) in 7.6 M urea, 10 mM TCEP, pH 7.0, and 25 °C. The scans represent the following variants: D1W (closed circles), Y52W, Y55W (closed triangles), T76W (open triangles), Y81W (closed squares), NATA (plus symbols), and AWA (open squares).

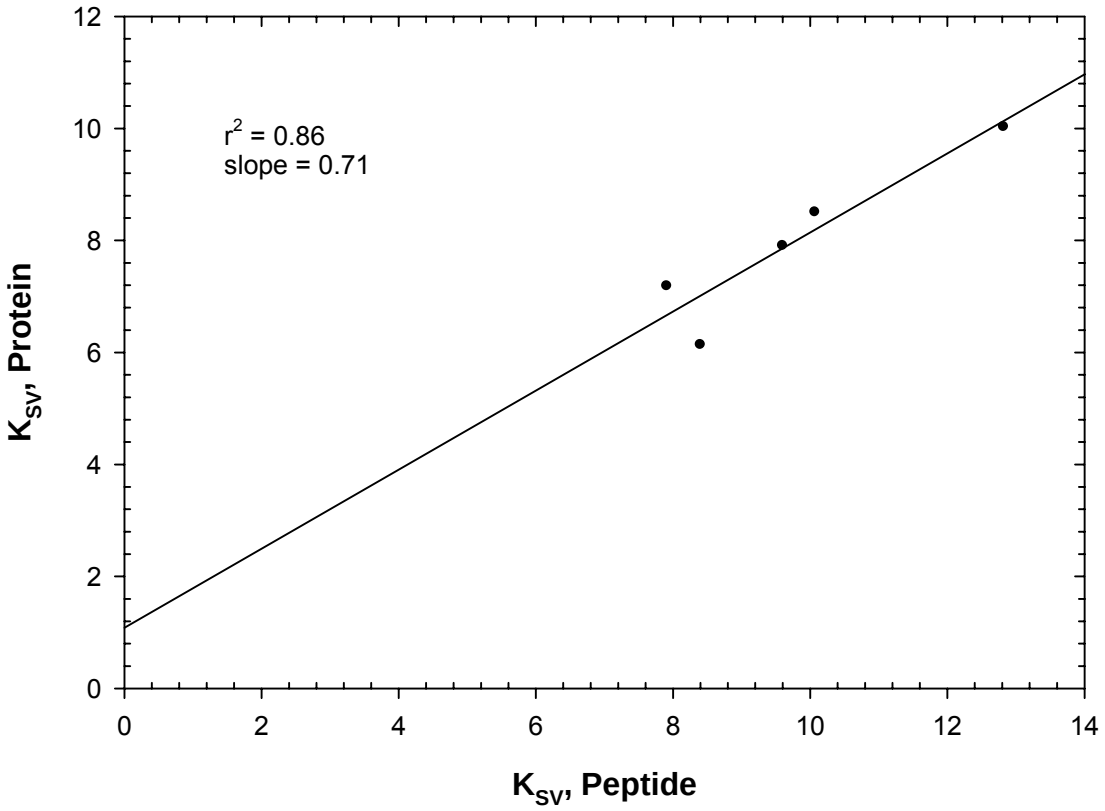

Figure 24. Correlation plot of the Stern-Volmer quenching constants from acrylamide quenching of the proteins versus their corresponding pentapeptides in urea, pH 7.0, and 25 ^{o}C.

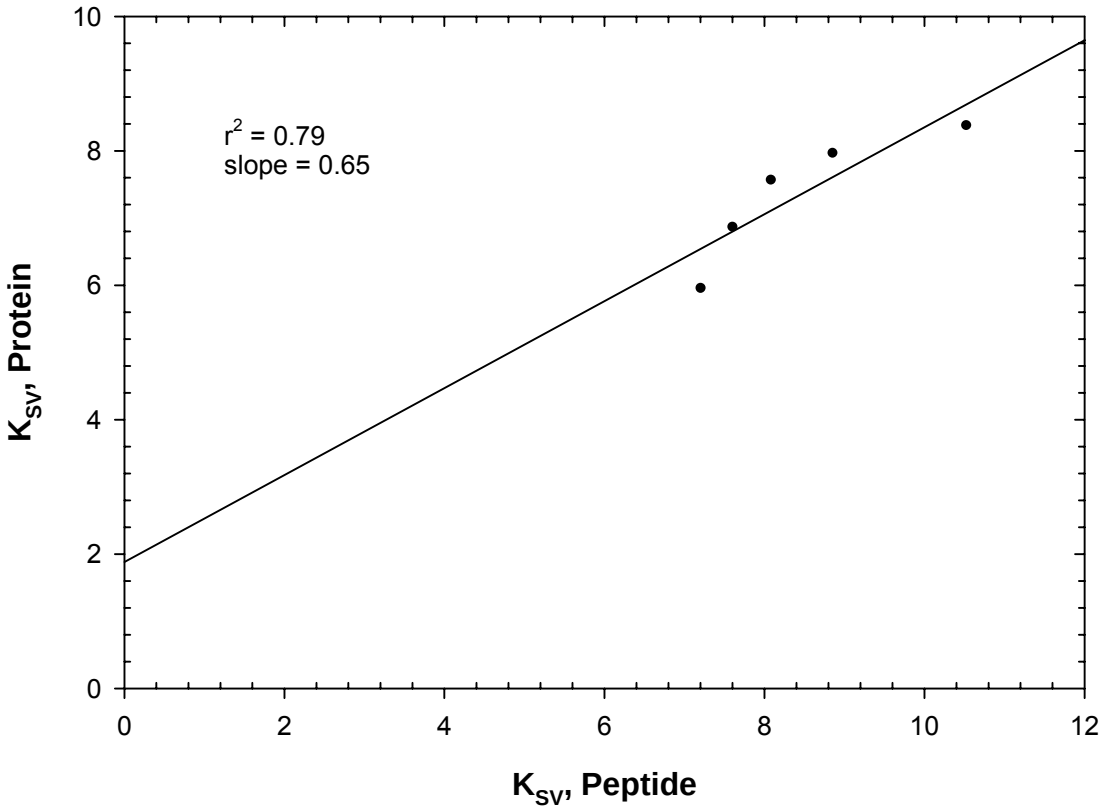

Figure 25. Correlation plot of the Stern-Volmer quenching constants from acrylamide quenching of the proteins versus their corresponding pentapeptides in guanidine hydrochloride, pH 7.0, and 25 ^{o}C.

immediate sequence, it might make sense that these two have the smallest percent difference in I_F.

Interestingly, the percent differences between each protein and its corresponding pentapeptide were very close in urea and guanidine hydrochloride. This suggests that guanidine hydrochloride affected the fluorescence of the tryptophan in the protein and corresponding pentapeptide about the same.

Y52W and its corresponding pentapeptide had among the lowest percent differences for the iodide and acrylamide quenching experiments. All the corresponding pentapeptides have at least one charged residue, and we would expect the charge-charge interactions to be a greater factor in urea than in guanidine hydrochloride. The overall net charge of the Y52W (GYWHE) peptide is -0.5. Because we have already observed that quenching is dependent on more than just the local sequence, it may be reasonable to expect to observe the smallest percent difference in acrylamide or iodide quenching between a protein and its corresponding pentapeptide if there were no charged residues in the immediate sequence. Since the Y52W peptide has one of the lowest net charges, perhaps this is the reason we observe smaller differences.

For iodide quenching, the results are much more variable, suggesting again that charge-charge interactions can be important in quenching. D1W and its corresponding pentapeptide had the largest percent difference for iodide quenching in urea. Because of the positively charged α-amino groups on the two tryptophans, one might expect that the two tryptophans would give very similar Stern-Volmer quenching constants. However, this was not the case. Additionally, there were two cases where the protein and corresponding pentapeptide actually switched which had the higher Stern-Volmer quenching constant in urea and guanidine hydrochloride. In urea, the T76W (EAWQE)

peptide had a higher Stern-Volmer quenching constant than its corresponding protein and the Y81 (DYWTG) peptide had a lower Stern-Volmer quenching constant than its corresponding proteins. However, in guanidine hydrochloride, those trends were reversed. All of these results again strongly suggest that there is more influencing the tryptophan in the proteins than can be mimicked by the pentapeptides.

Summary

We come back to our original question about what makes a good model and also ask, how well did our models do? In other words, how well did the models do at mimicking the proteins? Considering our models, the pentapeptides should do the best job mimicking the denatured state of the proteins. After comparing our pentapeptides to their corresponding proteins, we observed significant differences. Therefore, the behavior of the models was significantly different than the proteins. However, this is quite interesting, because it is suggesting that there is some shielding of the tryptophans beyond what is observed in the pentapeptides. This demonstrates that the protein is exerting an effect even beyond what you see with a very good model, the pentapeptides. Given this, it is not surprising that the models get worse as they become less realistic, and it is quite surprising that NATA is such a bad model given how often it is used.

Comparison of Denatured Proteins with the Wild-type Background to the Charge-reversal Background, pH 7.0

Ribonuclease Sa is an acidic protein with a pI of 3.5, a net charge of ≈ -7 at pH 7.0, that contains no lysines. To change the charge of RNase Sa, four single-site charge-reversal variants were made (D17K, D25K, E41K, and E76K). The residues replaced are relatively solvent exposed and form no intramolecular hydrogen bonds.

We measured the stability of the variants and compared them to wild type. The $\Delta(\Delta G)$ values showed that some of the variants had increased stability and some decreased stability. To understand these observations, we used Coulomb's Law ($E = q_1q_2 / Dr$) to predict the changes in stability expected if only electrostatic interactions in the folded state were important. (Coulomb's Law gives the energy required to bring two unit charges, q_1 and q_2, from infinity to a distance r apart in a medium of dielectric constant, D.) For all of the charge-reversal variants, Coulomb's Law predicted an increase in stability (Appendix A, Table 28). However, the increases observed were considerably smaller than predicted by the Coulomb's Law calculation, and in some cases (D17K and E41K), a charge reversal on the surface lead to a decrease in stability when an increase was predicted. We concluded that for the variants with decreased stability, the electrostatic interactions were more favorable in the denatured state than for wild-type RNase Sa. Two other observations supported this conclusion, *m*-values and salt screening.

One goal of the present study was to see if we could use fluorescence to observe differences in the denatured state ensemble of D17R compared to wild type. (Note that D17R gives the same stability result as D17K.) Thus, we compared the single-site tryptophan variants in the "wild-type" background to those with the D17R substitution, the "charge-reversal" background. For example, we compared Y52W with Y52W/D17R. Table 24 and Table 25 summarize the data from the reduced, wild-type proteins compared to the reduced, charge-reversal proteins.

In the most simple view, if our hypothesis is correct and the electrostatics are more favorable for the charge-reversal background compared to the wild-type background, we would expect to see a greater fluorescence intensity at λ_{max} for the

tryptophans in the charge-reversal background. However, that is not what we observed. Generally, no significant differences were seen in fluorescence intensity at λ_{max} between a tryptophan in the wild-type background and the same tryptophan in the charge-reversal background. RNase Y55W did show a small change in the fluorescence emission data (Figure 27). While we cannot explain these differences, it is promising that we can observe the subtle changes in the denatured state ensemble with fluorescence.

With quenching, if the charge-reversal background has more favorable electrostatics, then we would expect to see smaller Stern-Volmer quenching constants for the tryptophans in the charge-reversal background than in the wild-type background. Taking the most straightforward quenching data, acrylamide in urea, D1W showed the greatest change (19% or 1.95 M^{-1}) between its tryptophan in the wild-type background versus the charge-reversal background (Figure 28). It makes sense that D1W was the most likely affected by the charge-reversal background, since it is the closest to D17R. However, the tryptophan in the charge-reversal background had a higher Stern-Volmer quenching constant (i.e. more accessible) than the tryptophan in the wild-type background. Figure 26 shows the sequence alignment of the charged residues for D1W in the two backgrounds.

WT	**W1**	E14	**D17**	D25	D33
	+	-	**-**	-	-
CR	**W1**	E14	**R17**	D25	D33
	+	-	**+**	-	-

Figure 26. Sequence alignment of the charged residues for D1W in the wild-type (WT) background and charge-reversal (CR) backgrounds.

Table 24. Comparison of the fluorescence emission scan data of the reduced, wild-type (WT) proteins with the reduced, charge-reversal (CR) proteins in urea and guanidine hydrochloride at pH 7.0 and 25 °C.

Variant		Urea				GdnHCl			
		SM[a] (nm)	λ_{max}[b] (nm)	I_F at λ_{max}[c]	% Δ[d]	SM[a] (nm)	λ_{max}[b] (nm)	I_F at λ_{max}[c]	% Δ[e]
D1W	WT	361	345	25900		363	351	25000	
	CR	362	348	26200	-1	363	350	24400	2
Y52W	WT	360	348	34600		360	347	30700	
	CR	360	345	34400	1	360	346	30200	2
Y55W	WT	360	350	41200		361	346	33800	
	CR	361	350	38700	6	361	348	32100	5
T76W	WT	360	346	40700		361	346	31100	
	CR	360	348	41400	-2	361	347	32100	-3
Y81W	WT	359	347	28700		360	346	26000	
	CR	360	349	29300	-2	361	347	26400	-2

[a]Spectral Moment (SM) is the wavelength at which the total area under the emission spectrum is divided into two equal areas.

[b]λ_{max} is the wavelength of maximal intensity of the emission spectrum. We estimate the error to be ± 2 nm.

[c]I_F at λ_{max} is the fluorescence intensity at λ_{max}. We estimate the error to be 3%.

[d] $$\%\Delta_{Urea} = \left(\frac{I_{F,\mathrm{WT}} - I_{F,\mathrm{CR}}}{I_{F,\mathrm{WT}}} \right) \times 100$$

[e] $$\%\Delta_{GdnHCl} = \left(\frac{I_{F,\mathrm{WT}} - I_{F,\mathrm{CR}}}{I_{F,\mathrm{WT}}} \right) \times 100$$

Table 25. Comparison of the fluorescence quenching data of the reduced, wild-type (WT) proteins with the reduced, charge-reversal (CR) proteins in urea and guanidine hydrochloride at pH 7.0 and 25 °C.

Variant		Urea				GdnHCl			
		Acrylamide		Iodide		Acrylamide		Iodide	
		K_{SV}[a] (M^{-1})	% Δ[b]	K_{SV}[a] (M^{-1})	% Δ[c]	K_{SV}[a] (M^{-1})	% Δ[b]	K_{SV}[a] (M^{-1})	% Δ[c]
D1W	WT	10.04		5.23		8.38		4.59	
	CR	11.99	-19	5.83	-11	9.45	-13	4.70	-2
Y52W	WT	7.20		2.77		6.87		3.06	
	CR	7.03	2	2.63	5	6.85	0	3.02	1
Y55W	WT	8.52		3.33		7.97		3.22	
	CR	8.32	2	3.41	-2	7.62	4	3.31	-3
T76W	WT	7.92		3.04		7.57		2.92	
	CR	7.41	6	2.70	11	6.97	8	2.92	0
Y81W	WT	6.15		1.87		5.96		2.47	
	CR	6.37	-4	2.09	-12	6.15	-3	2.49	-1

[a]Equation 8 in the Methods and Materials section was used to calculate the Stern-Volmer quenching constants.

[b] $$\%\Delta_{Acrylamide} = \left(\frac{K_{SV,\,\mathrm{WT}} - K_{SV,\,\mathrm{CR}}}{K_{SV,\,\mathrm{WT}}} \right) \times 100$$

[c] $$\%\Delta_{Iodide} = \left(\frac{K_{SV,\,\mathrm{WT}} - K_{SV,\,\mathrm{CR}}}{K_{SV,\,\mathrm{WT}}} \right) \times 100$$

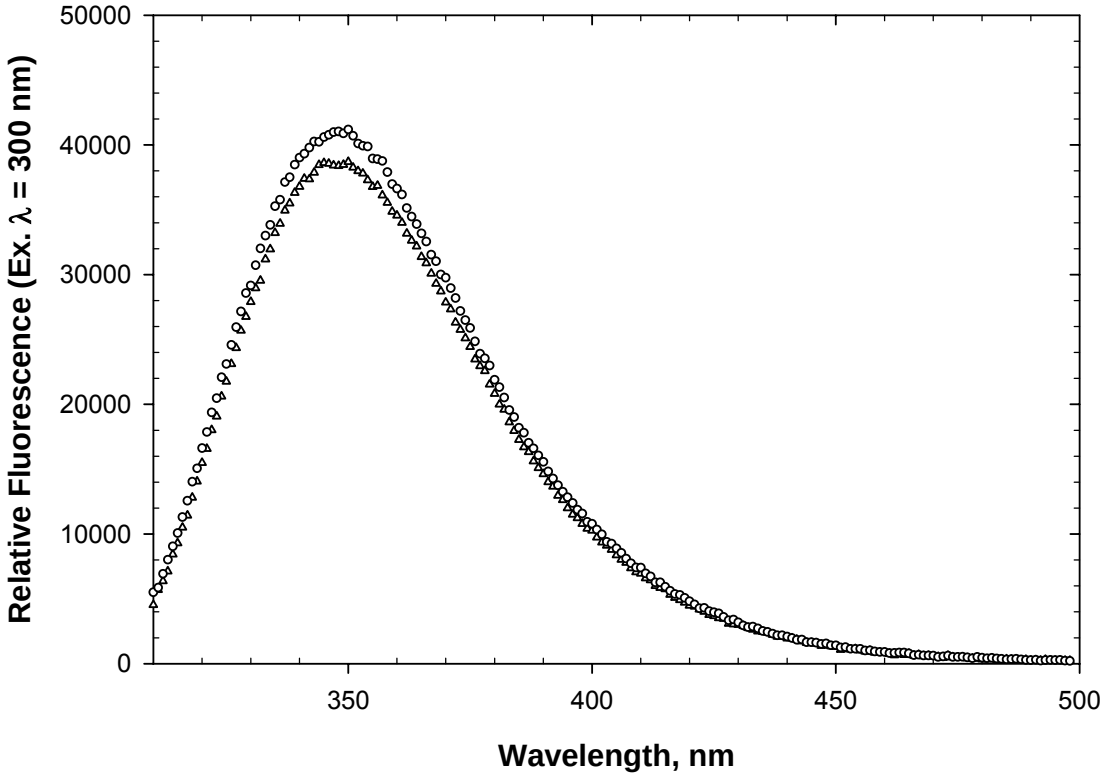

Figure 27. Comparison of the reduced, wild-type and reduced, charge-reversal backgrounds' denatured fluorescence emission spectra (300 nm excitation) of RNase Sa Y55W (10 μM) in 8.5 M urea, pH 7.0, and 25 °C. The scans represent the following conditions: reduced, wild-type background (open circles) and reduced, charge-reversal background (open triangles).

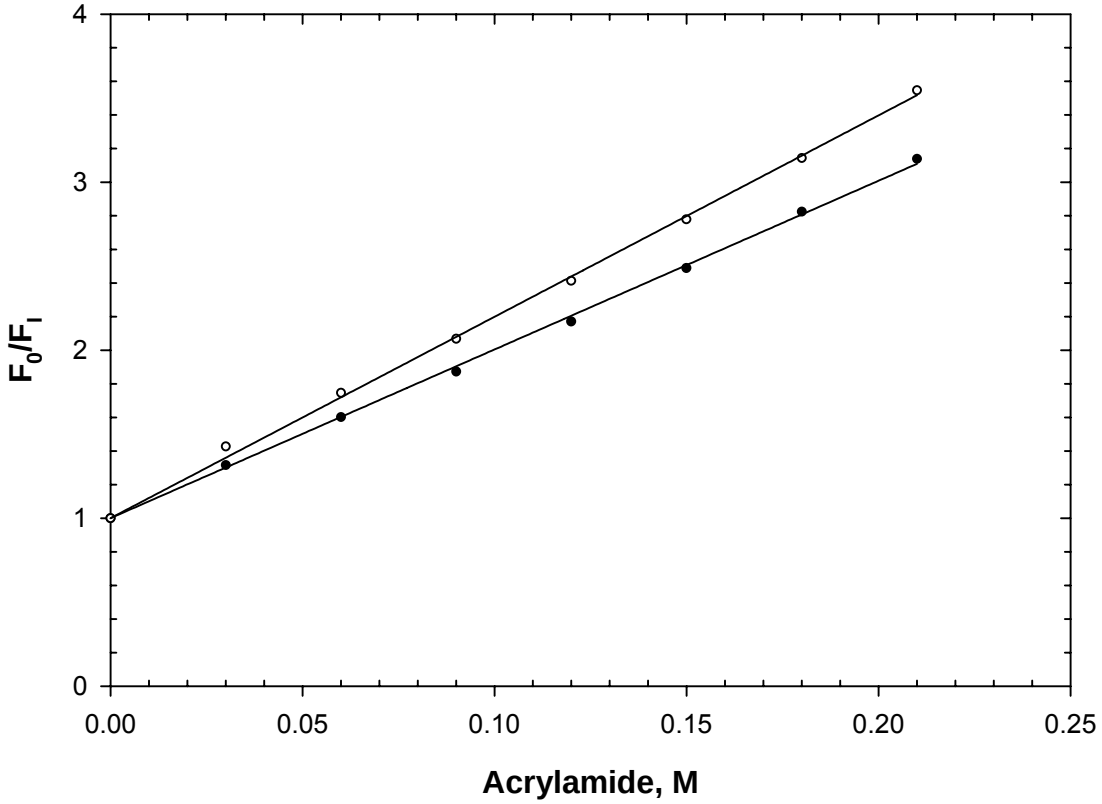

Figure 28. Comparison of the reduced, wild-type and reduced, charge-reversal backgrounds' acrylamide quenching data of RNase Sa D1W (10 μM) in 7.6 M urea, pH 7.0, and 25 °C. The scans represent the following conditions: reduced, wild-type background (closed circles) and reduced, charge-reversal background (open circles).

In the D1W wild-type background, there is a majority of negative charges through Arg40, where the next positive charge occurs in the sequence. D1W, with a positively charged α-amino group, should be able to make favorable electrostatic interactions with the negative charges in the wild-type sequence. In the charge-reversal background, W1 and R17 are both positively charged. It is reasonable to conclude that in the charge-reversal background, the two positive charges could be repelling one another, resulting in a more accessible tryptophan side chain and higher Stern-Volmer quenching constant. While the trend is opposite of what we might have expected, presumably due to the positive charge on the α-amino group of the tryptophan, it may still lend evidence to the electrostatic interactions being more favorable in the charge-reversal background and support our hypothesis.

Because only a small difference was seen between the oxidized and reduced states of the proteins, it is not surprising that we do not see significant differences between the two backgrounds in more of the tryptophans. However, because of the D1W and Y55W data and the fact that we cannot differentiate between the oxidized and reduced states of the proteins, we do not feel that our original hypothesis is wrong, but that the sensitivity of the experiments performed to date surpassed the ability to detect the subtle changes in the denatured state ensemble.

SUMMARY

The research presented here has lead to certain conclusions. When a protein unfolds, generally, the wavelength of maximum intensity (λ_{max}) shifts to the red, approaching the wavelength of N-acetyl-tryptophan-amide (NATA) in water, and this was observed in our research. However, regardless of the denaturant, λ_{max} differed very little among the proteins or model compounds, 349.3 ± 1.2 nm. However, significant differences were observed in the fluorescence intensity at λ_{max} (I_F). Therefore, I_F is more sensitive to the immediate environment than λ_{max}.

To understand the behavior of the proteins in their denatured state, we also studied eight model compounds under the same conditions. These model compounds included: N-acetyl-tryptophan-amide (NATA), N-acetyl-Ala-Trp-Ala-amide (AWA), N-acetyl-Ala-Ala-Trp-Ala-Ala-amide (AAWAA), and five pentapeptides based on the sequence around the original tryptophan substitutions in RNase Sa. With the exception of the pentapeptide based on D1W, all of the pentapeptides were blocked at both the N- and C-termini. The D1W pentapeptide was only blocked at the C-terminus to mimic the positive charge on the α-amino group of the N-terminus of Ribonuclease Sa (RNase Sa). One would expect NATA to have the most solvent exposed tryptophan side chain of the model compounds. Without exception, NATA always had a greater I_F than the other model compounds or the proteins. It has been proposed that an important mechanism for tryptophan quenching is the electron transfer to the carbonyl carbon of a neighboring peptide group. We suggest that the increased I_F of NATA is derived from the fact that NATA has fewer carbonyl carbons than the other model compounds (or proteins). This fact would suggest that NATA is not a good model for mimicking

tryptophans in proteins in their denatured states, an important result considering how often NATA is used as a model.

I_F for the model compounds and proteins was always less in urea than in guanidine hydrochloride, suggesting that the guanidinium ion is a better quencher of fluorescence than urea. One reason may be that aromatic rings are known to interact favorably with cations. The ability of the guanidinium ion to quench the tryptophan fluorescence of the peptides and proteins may be depend in part on the net charge of the peptide or protein.

I_F is also very dependent on the groups in the local environment, which are known to quench tryptophan fluorescence. These groups include amino acid side chains, and at least ten amino acid side chains have been determined to quench the fluorescence of tryptophan. For the pentapeptides, generally, those with no quenching groups or those with no adjacent quenching groups had a higher I_F than those with adjacent quenching groups. The exception was the pentapeptide based on D1W. We propose that its quenching is due to the positively charged α-amino group on the tryptophan.

Small molecule extrinsic quenching experiments were performed using acrylamide and iodide, and the Stern-Volmer quenching constants were measured. The Stern-Volmer quenching constants for acrylamide quenching were always greater than those derived from iodide quenching, and generally, the Stern-Volmer quenching constants in urea were greater than those measured in guanidine hydrochloride. To understand the data, the peptides were modeled in an extended conformation and percent accessibility was calculated. For acrylamide quenching, the Stern-Volmer quenching constants generally correlated with tryptophan accessibility. For iodide

quenching, the Stern-Volmer quenching constants generally correlated with tryptophan accessibility and the net charge on the peptide.

One exception in both quenching experiments was the peptide based on Y55W, which has a lower percent accessibility but a relatively higher Stern-Volmer quenching constant. The peptide contains an adjacent His and Glu, and we propose that this ion pair may be causing the tryptophan to be more exposed than the solvent accessibility estimate predicts.

The proteins showed significant differences in I_F and the Stern-Volmer quenching constants. We propose that these differences represent residual structure in the denatured state, and to address this, we compared our pentapeptides to their corresponding proteins. Significant differences were observed in I_F between the pentapeptides and their corresponding proteins, ranging from 8% to 29%, and the I_F of the proteins was always greater than their corresponding pentapeptides. Additionally, significant differences were observed between the proteins and the corresponding pentapeptides in the fluorescence quenching experiments. The differences in the Stern-Volmer quenching constants ranged from 10% to 36% for acrylamide quenching in urea, and the Stern-Volmer quenching constant was always less in the protein than its corresponding pentapeptides. These observations lead to two important conclusions. First, the tryptophan fluorescence properties and quenching in the proteins are not mimicked by the pentapeptides. Secondly, this shows that non-local structure in the unfolded state influences tryptophan fluorescence and accessibility.

Finally, a recent paper from our lab made several acidic to basic mutations at solvent exposed sites in order to change the pI of RNase Sa. We observed that some mutations increased stability and some decreased stability. However, Coulomb's Law

predicted an increase in stability for all of the variants. It was proposed that the electrostatic interactions were more favorable in the denatured state for the destabilizing variants than for the stabilizing variants. In an effort to see if we could observe this phenomenon with fluorescence, we compared tryptophans in a charge-reversal, D17R, background to tryptophans in the wild-type background.

We observed interesting differences in some of our variants. The most interesting was D1W, which showed a difference in acrylamide quenching in urea between the two backgrounds. If the electrostatic interactions are more favorable for the charge-reversal background then we would expect a lower Stern-Volmer quenching constant for the charge-reversal background. However, the opposite was observed, indicating the tryptophan in the charge-reversal background is more accessible. We believe we can explain this result. In the D1W variant, there will be a positive charge on the α-amino group of the tryptophan. In the wild-type background, the closest charged residues are E14, D17, and D25, all negatively charged. In this background, there is a potential for attraction between D1W and the negative charges. In the charge-reversal background, D17 will be replaced with R17, a positively charged residue. Therefore, in the charge-reversal background, there should be less attraction, resulting in a more exposed tryptophan side chain. The differences observed between the wild-type and charge-reversal backgrounds suggest that reversing a charge in a protein is capable of perturbing the denatured state ensemble enough so that it can be observed using fluorescence quenching of the tryptophan residues.

REFERENCES

Adams, P.D., Chen, Y., Ma, K., Zagorski, M.G., Sonnichsen, F.D., McLaughlin, M.L., and Barkley, M.D. 2002. Intramolecular quenching of tryptophan fluorescence by the peptide bond in cyclic hexapeptides. *JACS* **124:** 9278-9286.

Alston, R.W. 1999. *Characterization of four single-site tryptophan variants of ribonuclease Sa*. M.S. Thesis Texas A&M University, College Station, pp. 77.

Amir, D., Krausz, S., and Haas, E. 1992. Detection of local structures in reduced unfolded bovine pancreatic trypsin inhibitor. *Proteins* **13:** 162-173.

Auer, H.E., and Doty, P. 1966. The conformational stability of alpha-helical nonpolar polypeptides in solution. *Biochemistry* **5:** 1716-1725.

Axe, D.D., Foster, N.W., and Fersht, A.R. 1999. An irregular beta-bulge common to a group of bacterial RNases is an important determinant of stability and function in barnase. *JMB* **286:** 1471-1485.

Axelsen, P.H., and Prendergast, F.G. 1989. Molecular dynamics of tryptophan in ribonuclease-T1. II. Correlations with fluorescence. *Biophys J* **56:** 43-66.

Bacova, M., Zelinkova, E., and Zelinka, J. 1971. Exocellular ribonuclease from *Streptomyces aureofaciens* I. Isolation and purification. *Biochim Biophys Acta* **235:** 335-342.

Baldwin, R.L. 2002. A new perspective on unfolded proteins. *Adv Protein Chem* **62:** 361-367.

Beechem, J.M., and Brand, L. 1985. Time-resolved fluorescence of proteins. *Annu Rev Biochem* **54:** 43-71.

Bond, C.J., Wong, K.B., Clarke, J., Fersht, A.R., and Daggett, V. 1997. Characterization of residual structure in the thermally denatured state of barnase by simulation

and experiment: description of the folding pathway. *Proc Natl Acad Sci USA* **94:** 13409-13413.

Burstein, E.A., Abornev, S.M., and Reshetnyak, Y.K. 2001. Decomposition of protein tryptophan fluorescence spectra into log-normal components. I. Decomposition algorithms. *Biophys J* **81:** 1699-1709.

Burstein, E.A., Vedenkina, N.S., and Ivkova, M.N. 1973. Fluorescence and the location of tryptophan residues in protein molecules. *Photochem Photobiol* **18:** 263-279.

Calhoun, D.B., Vanderkooi, J.M., Holtom, G.R., and Englander, S.W. 1986. Protein fluorescence quenching by small molecules: protein penetration versus solvent exposure. *Proteins* **1:** 109-115.

Calhoun, D.B., Vanderkooi, J.M., Woodrow, G.V., 3rd, and Englander, S.W. 1983. Penetration of dioxygen into proteins studied by quenching of phosphorescence and fluorescence. *Biochemistry* **22:** 1526-1532.

Callis, P.R. 1997. 1La and 1Lb transitions of tryptophan: applications of theory and experimental observations to fluorescence of proteins. *Methods Enzymol* **278:** 113-150.

Callis, P.R., and Burgess, B.K. 1997. Tryptophan fluorescence shifts in proteins from hybrid simulations: an electrostatic approach. *J Phys Chem B* **101:** 9429-9432.

Callis, P.R., and Vivian, J.T. 2003. Understanding the variable fluorescence quantum yield of tryptophan in proteins using QM-MM simulations. Quenching by charge transfer to the peptide backbone. *Chem Phys Lett* **369:** 409-414.

Chattopadhyay, A., Rawat, S.S., Kelkar, D.A., Ray, S., and Chakrabarti, A. 2003. Organization and dynamics of tryptophan residues in erythroid spectrin: novel

structural features of denatured spectrin revealed by the wavelength-selective fluorescence approach. *Protein Sci* **12:** 2389-2403.

Chen, Y., and Barkley, M.D. 1998. Toward understanding tryptophan fluorescence in proteins. *Biochemistry* **37:** 9976-9982.

Chen, Y., Liu, B., Yu, H.T., and Barkley, M.D. 1996. The peptide bond quenches indole fluorescence. *JACS* **118:** 9271-9278.

Clark, P.L., Liu, Z.P., Zhang, J., and Gierasch, L.M. 1996. Intrinsic tryptophans of CRABPI as probes of structure and folding. *Protein Sci* **5:** 1108-1117.

Cowgill, R.W. 1967. Fluorescence and protein structure. X. Reappraisal of solvent and structural effects. *Biochim Biophys Acta* **133:** 6-18.

Crowhurst, K.A., Tollinger, M., and Forman-Kay, J.D. 2002. Cooperative interactions and a non-native buried Trp in the unfolded state of an SH3 domain. *JMB* **322:** 163-178.

Dill, K.A., and Shortle, D. 1991. Denatured states of proteins. *Annu Rev Biochem* **60:** 795-825.

Eftink, M.R. 1991. Fluorescence techniques for studying protein structure. *Methods Biochem Anal* **35:** 127-205.

Eftink, M.R., and Ghiron, C.A. 1976. Exposure of tryptophanyl residues in proteins. Quantitative determination by fluorescence quenching studies. *Biochemistry* **15:** 672-680.

Eftink, M.R., and Ghiron, C.A. 1977. Exposure of tryptophanyl residues and protein dynamics. *Biochemistry* **16:** 5546-5551.

Eftink, M.R., and Ghiron, C.A. 1981. Fluorescence quenching studies with proteins. *Anal Biochem* **114:** 199-227.

Engelborghs, Y. 2003. Correlating protein structure and protein fluorescence. *J Fluoresc* **13:** 9-16.

Fauchere, J.L., and Pliska, V.E. 1983. Hydrophobic parameters of amino-acid side-chains from the partitioning of N-acetyl-amino-acid amides. *Eur J Med Chem* **18:** 369-375.

Gallivan, J.P., and Dougherty, D.A. 1999. Cation-pi interactions in structural biology. *Proc Natl Acad Sci USA* **96:** 9459-9464.

Garcia, P., Merola, F., Receveur, V., Blandin, P., Minard, P., and Desmadril, M. 1998. Steady state and time-resolved fluorescence study of residual structures in an unfolded form of yeast phosphoglycerate kinase. *Biochemistry* **37:** 7444-7455.

Giletto, A., and Pace, C.N. 1999. Buried, charged, non-ion-paired aspartic acid 76 contributes favorably to the conformational stability of ribonuclease T1. *Biochemistry* **38:** 13379-13384.

Gratton, E., Jameson, D.M., Weber, G., and Alpert, B. 1984. A model of dynamic quenching of fluorescence in globular proteins. *Biophys J* **45:** 789-794.

Grimsley, G.R., Shaw, K.L., Fee, L.R., Alston, R.W., Huyghues-Despointes, B.M., Thurlkill, R.L., Scholtz, J.M., and Pace, C.N. 1999. Increasing protein stability by altering long-range coulombic interactions. *Protein Sci* **8:** 1843-1849.

Gryczynski, I., Wiczk, W., Johnson, M.L., and Lakowicz, J.R. 1988. Lifetime distributions and anisotropy decays of indole fluorescence in cyclohexane/ethanol mixtures by frequency-domain fluorometry. *Biophys. Chem.* **32:** 173-185.

Gurd, F.R., and Rothgeb, T.M. 1979. Motions in proteins. *Adv Protein Chem* **33:** 73-165.

Hagel, P., Gerding, J., Fieggen, W., and Bloemendal, H. 1971. Cyanate formation in solutions of urea. I. calculation of cyanate concentrations at different temperature and pH. *Biochim Biophys Acta* **243:** 366-373.

Harpaz, Y., Gerstein, M., and Chothia, C. 1994. Volume changes in protein folding. *Structure* **2:** 641-649.

Hartley, R.W. 1980. Homology between prokaryotic and eukaryotic ribonucleases. *J Mol Evol* **15:** 355-358.

Hartley, R.W., Jucovic, M., Sevcik, J., Nazarov, V., Both, V., Hebert, E.J., and Pace, C.N. 1996. Expression of extracellular ribonuclease from recombinant genes of four Streptomyces strains with the aid of the barstar gene. *Protein Peptide Lett* **3:** 225-231.

Hebert, E.J. 1997. *Conformational stability of ribonuclease Sa from Streptomyces aureofaciens*. Ph.D. Dissertation Texas A&M University, College Station, pp. 61.

Hebert, E.J., Grimsley, G.R., Hartley, R.W., Horn, G., Schell, D., Garcia, S., Both, V., Sevcik, J., and Pace, C.N. 1997. Purification of ribonucleases Sa, Sa2, and Sa3 after expression in *Escherichia coli*. *Protein Expr Purif* **11:** 162-168.

Hill, C.P., Dodson, G.G., Heinemann, U., Saenger, W., Mitsui, Y., Nakamura, K.T., Borisov, S., Tischenko, G., Polyakov, K.M., and Pavlovsky, S. 1983. The structural and sequence homology of a family of microbial ribonucleases. *Trends in Biochem Sci* **8:** 364-369.

Ho, S.N., Hunt, H.D., Horton, R.M., Pullen, J.K., and Pease, L.R. 1989. Site-directed mutagenesis by overlap extension using the polymerase chain reaction. *Gene* **77:** 51-59.

Huyghues-Despointes, B.M., Thurlkill, R.L., Daily, M.D., Schell, D., Briggs, J.M., Antosiewicz, J.M., Pace, C.N., and Scholtz, J.M. 2003. pK values of histidine residues in ribonuclease Sa: effect of salt and net charge. *JMB* **325:** 1093-1105.

Karplus, M., and McCammon, J.A. 1981. The internal dynamics of globular proteins. *CRC Crit Rev Biochem* **9:** 293-349.

Kawahara, K., and Tanford, C. 1966. Viscosity and density of aqueous solutions of urea and guanidine hydrochloride. *JBC* **241:** 3228-3232.

Kemmink, J., van Mierlo, C.P., Scheek, R.M., and Creighton, T.E. 1993. Local structure due to an aromatic-amide interaction observed by 1H- nuclear magnetic resonance spectroscopy in peptides related to the N terminus of bovine pancreatic trypsin inhibitor. *JMB* **230:** 312-322.

Killick, T.R., Freund, S.M., and Fersht, A.R. 1998. Real-time NMR studies on folding of mutants of barnase and chymotrypsin inhibitor 2. *FEBS Lett* **423:** 110-112.

Komath, S.S., and Swamy, M.J. 1999. Fluorescence quenching, time-resolved fluorescence and chemical modification studies on the tryptophan residues of snake gourd (Trichosanthes anguina) seed lectin. *J Photoch Photobio B* **50:** 108-118.

Konev, S.V. 1967. *Fluorescence and phosphorescence of proteins and nucleic acids*. Plenum Press, New York.

Kraulis, P.J. 1991. MOLSCRIPT: a program to produce both detailed and schematic plots of protein structures. *J Appl Crystallogr* **24:** 946-950.

Kronman, M.J., and Holmes, L.G. 1971. Fluorescence of native, denatured, and reduced-denatured proteins. *Photochem Photobiol* **14:** 113-134.

Lakowicz, J.R. 1983. *Principles of fluorescence spectroscopy*. Plenum Press, New York.

Lakowicz, J.R. 1999. *Principles of fluorescence spectroscopy*, 2nd ed. Kluwer Academic/Plenum Publishers, New York.

Lakowicz, J.R., and Weber, G. 1973a. Quenching of fluorescence by oxygen. A probe for structural fluctuations in macromolecules. *Biochemistry* **12:** 4161-4170.

Lakowicz, J.R., and Weber, G. 1973b. Quenching of protein fluorescence by oxygen. Detection of structural fluctuations in proteins on the nanosecond time scale. *Biochemistry* **12:** 4171-4179.

Laurents, D., Perez-Canadillas, J.M., Santoro, J., Rico, M., Schell, D., Pace, C.N., and Bruix, M. 2001. Solution structure and dynamics of ribonuclease Sa. *Proteins* **44:** 200-211.

Laurents, D.V., Huyghues-Despointes, B.M., Bruix, M., Thurlkill, R.L., Schell, D., Newsom, S., Grimsley, G.R., Shaw, K.L., Trevino, S., Rico, M., et al. 2003. Charge-charge interactions are key determinants of the pK values of ionizable groups in ribonuclease Sa (pI=3.5) and a basic variant (pI=10.2). *JMB* **325:** 1077-1092.

Lee, B., and Richards, F.M. 1971. The interpretation of protein structures: estimation of static accessibility. *JMB* **55:** 379-400.

Lehrer, S.S. 1971. Solute perturbation of protein fluorescence. The quenching of the tryptophyl fluorescence of model compounds and of lysozyme by iodide ion. *Biochemistry* **10:** 3254-3263.

Lesser, G.J., and Rose, G.D. 1990. Hydrophobicity of amino acid subgroups in proteins. *Proteins* **8:** 6-13.

Longworth, J.W. 1971. The luminescence of the aromatic amino acids. In *Excited states of proteins and nucleic acids*. (eds. R.F. Steiner, and I. Weinryb), pp. 319-484. Plenum Press, New York.

Lumb, K.J., and Kim, P.S. 1994. Formation of a hydrophobic cluster in denatured bovine pancreatic trypsin inhibitor. *JMB* **236:** 412-420.

Maity, H., Lim, W.K., Rumbley, J.N., and Englander, S.W. 2003. Protein hydrogen exchange mechanism: local fluctuations. *Protein Sci* **12:** 153-160.

Martinez-Oyanedel, J., Choe, H.-W., Heinemann, U., and Saenger, W. 1991. Ribonuclease T1 with free recognition and catalytic site: crystal structure analysis at 1.5 Å resolution. *JMB* **222:** 335-352.

Mason, P.E., Neilson, G.W., Dempsey, C.E., Barnes, A.C., and Cruickshank, J.M. 2003. The hydration structure of guanidinium and thiocyanate ions: implications for protein stability in aqueous solution. *Proc Natl Acad Sci USA* **100:** 4557-4561.

McCaldon, P., and Argos, P. 1988. Oligopeptide biases in protein sequences and their use in predicting protein coding regions in nucleotide sequences. *Proteins* **4:** 99-122.

Meagher, J.L., Beechem, J.M., Olson, S.T., and Gettins, P.G. 1998. Deconvolution of the fluorescence emission spectrum of human antithrombin and identification of the tryptophan residues that are responsive to heparin binding. *JBC* **273:** 23283-23289.

Miranker, A.D., and Dobson, C.M. 1996. Collapse and cooperativity in protein folding. *Curr Opin Struct Biol* **6:** 31-42.

Mullins, L.S., Pace, C.N., and Raushel, F.M. 1997. Conformational stability of ribonuclease T1 determined by hydrogen- deuterium exchange. *Protein Sci* **6:** 1387-1395.

Myers, J.K., Pace, C.N., and Scholtz, J.M. 1997. Helix propensities are identical in proteins and peptides. *Biochemistry* **36:** 10923-10929.

Navon, A., Ittah, V., Laity, J.H., Scheraga, H.A., Haas, E., and Gussakovsky, E.E. 2001. Local and long-range interactions in the thermal unfolding transition of bovine pancreatic ribonuclease A. *Biochemistry* **40:** 93-104.

Neri, D., Billeter, M., Gerhard, W., and Wuthrich, K. 1992. NMR determination of residual structure in a urea-denatured protein, the 434-repressor. *Science* **257:** 1559-1563.

Neu, H.C., and Heppel, L.A. 1965. The release of enzymes from *Escherichia coli* by osmotic shock and during the formation of spheroplasts. *JBC* **240:** 3685-3692.

Nozaki, Y. 1972. The preparation of guanidine hydrochloride. *Methods Enzymol* **26 PtC:** 43-50.

Nozaki, Y., and Tanford, C. 1967. Proteins as random coils. II. Hydrogen ion titration curve of ribonuclease in 6 M guanidine hydrochloride. *JACS* **89:** 742-749.

Pace, C.N. 1990. Conformational stability of globular proteins. *Trends Biochem Sci* **15:** 14-17.

Pace, C.N. 2001. Polar group burial contributes more to protein stability than nonpolar group burial. *Biochemistry* **40:** 310-313.

Pace, C.N., Alston, R.W., and Shaw, K.L. 2000. Charge-charge interactions influence the denatured state ensemble and contribute to protein stability. *Protein Sci* **9:** 1395-1398.

Pace, C.N., Hebert, E.J., Shaw, K.L., Schell, D., Both, V., Krajcikova, D., Sevcik, J., Wilson, K.S., Dauter, Z., Hartley, R.W., et al. 1998. Conformational stability and thermodynamics of folding of ribonucleases Sa, Sa2 and Sa3. *JMB* **279:** 271-286.

Pace, C.N., Vajdos, F., Fee, L., Grimsley, G., and Gray, T. 1995. How to measure and predict the molar absorption coefficient of a protein. *Protein Sci* **4:** 2411-2423.

Reshetnyak, Y.K., and Burstein, E.A. 2001. Decomposition of protein tryptophan fluorescence spectra into log-normal components. II. The statistical proof of discreteness of tryptophan classes in proteins. *Biophys J* **81:** 1710-1734.

Reshetnyak, Y.K., Koshevnik, Y., and Burstein, E.A. 2001. Decomposition of protein tryptophan fluorescence spectra into log-normal components. III. Correlation between fluorescence and microenvironment parameters of individual tryptophan residues. *Biophys J* **81:** 1735-1758.

Ross, J.B., Szabo, A.G., and Hogue, C.W. 1997. Enhancement of protein spectra with tryptophan analogs: fluorescence spectroscopy of protein-protein and protein-nucleic acid interactions. *Methods Enzymol* **278:** 151-190.

Sage, H.J., and Fasman, G.D. 1966. Conformational studies on poly-L-glutamic acid and copolymers of L- glutamic acid and L-phenylalanine. *Biochemistry* **5:** 286-296.

Sambrook, J., Fritsch, E.F., and Maniatis, T. 1989. *Molecular cloning: a laboratory manual*, 2nd ed. Cold Spring Harbor Laboratory Press, New York.

Santoro, M.M., and Bolen, D.W. 1988. Unfolding free energy changes determined by the linear extrapolation method. 1. Unfolding of phenylmethanesulfonyl α-chymotrypsin using different denaturants. *Biochemistry* **27:** 8063-8068.

Schein, C.H. 1997. From housekeeper to microsurgeon: the diagnostic and therapeutic potential of ribonucleases. *Nat Biotechnol* **15:** 529-536.

Schmid, F.X. 1997. Optical spectroscopy to characterize protein conformation and conformational changes. In *Protein structure: a practical approach*. (ed. T.E. Creighton), pp. 261-297. Oxford University Press, New York.

Schwalbe, H., Fiebig, K.M., Buck, M., Jones, J.A., Grimshaw, S.B., Spencer, A., Glaser, S.J., Smith, L.J., and Dobson, C.M. 1997. Structural and dynamical properties of a denatured protein. Heteronuclear 3D NMR experiments and theoretical simulations of lysozyme in 8 M urea. *Biochemistry* **36:** 8977-8991.

Sendak, R.A., Rothwarf, D.M., Wedemeyer, W.J., Houry, W.A., and Scheraga, H.A. 1996. Kinetic and thermodynamic studies of the folding/unfolding of a tryptophan-containing mutant of ribonuclease A. *Biochemistry* **35:** 12978-12992.

Sevcik, J., Dauter, Z., Lamzin, V.S., and Wilson, K.S. 1996. Ribonuclease from *Streptomyces aureofaciens* at atomic resolution. *Acta Crystallogr D* **52:** 327-344.

Sevcik, J., Dodson, E.J., and Dodson, G.G. 1991. Determination and restrained least-squares refinement of the structures of ribonuclease Sa and its complex with 3'-guanylic acid at 1.8 Å resolution. *Acta Crystallogr B* **47:** 240-253.

Sevcik, J., Lamzin, V.S., Dauter, Z., and Wilson, K.S. 2002. Atomic resolution data reveal flexibility in the structure of RNase Sa. *Acta Crystallogr D Biol Crystallogr* **58:** 1307-1313.

Shortle, D. 1993. Denatured states of proteins and their roles in folding and stability. *Curr Opin Struct Biol* **3:** 66-74.

Shortle, D. 1996. The denatured state (the other half of the folding equation) and its role in protein stability. *FASEB J* **10:** 27-34.

Sillen, A., Diaz, J.F., and Engelborghs, Y. 2000. A step toward the prediction of the fluorescence lifetimes of tryptophan residues in proteins based on structural and spectral data. *Protein Sci* **9:** 158-169.

Smith, L.J., Fiebig, K.M., Schwalbe, H., and Dobson, C.M. 1996. The concept of a random coil. Residual structure in peptides and denatured proteins. *Fold Des* **1:** R95-106.

Soler-Gonzalez, A.S., and Fersht, A.R. 1997. Helix stability in barstar peptides. *Eur J Biochem* **249:** 724-732.

Takano, K., Scholtz, J.M., Sacchettini, J.C., and Pace, C.N. 2003. The contribution of polar group burial to protein stability is strongly context-dependent. *JBC* **278:** 31790-31795.

Tanford, C. 1968. Protein denaturation. *Adv Protein Chem* **23:** 121-282.

Tanford, C., Kawahara, K., Lapanje, S., Hooker, T.M., Jr., Zarlengo, M.H., Salahuddin, A., Aune, K.C., and Takagi, T. 1967. Proteins as random coils. 3. Optical rotatory dispersion in 6 M guanidine hydrochloride. *JACS* **89:** 5023-5029.

Teale, F.W. 1960. The ultraviolet fluorescence of proteins in neutral solution. *Biochem J* **76:** 381-388.

Tew, D.J., and Bottomley, S.P. 2001. Probing the equilibrium denaturation of the serpin alpha(1)-antitrypsin with single tryptophan mutants; evidence for structure in the urea unfolded state. *JMB* **313:** 1161-1169.

Turoverov, K.K., and Kuznetsova, I.M. 2003. Intrinsic Fluorescence of Actin. *J Fluoresc* **13:** 41-57.

Uchida, T., and Egami, F. 1967. Ribonuclease T1 from Taka-Diastase. *Methods Enzymol* **30:** 229-239.

Vivian, J.T., and Callis, P.R. 2001. Mechanisms of tryptophan fluorescence shifts in proteins. *Biophys J* **80:** 2093-2109.

Warren, J.R., and Gordon, J.A. 1966. On the refractive indices of aqueous solutions of urea. *J Phys Chem* **70:** 297-300.

Weinryb, I., and Steiner, R.F. 1971. The luminescence of the aromatic amino acids. In *Excited states of proteins and nucleic acids*. (eds. R.F. Steiner, and I. Weinryb), pp. 277-318. Plenum Press, New York.

Willaert, K., Loewenthal, R., Sancho, J., Froeyen, M., Fersht, A., and Engelborghs, Y. 1992. Determination of the excited-state lifetimes of the tryptophan residues in barnase, via multifrequency phase fluorometry of tryptophan mutants. *Biochemistry* **31:** 711-716.

Woody, R.W. 1994. Contributions of tryptophan side chains to the far-ultraviolet circular dichroism of proteins. *Eur Biophys J* **23:** 253-262.

Yu, Y., Makhatadze, G.I., Pace, C.N., and Privalov, P.L. 1994. Energetics of ribonuclease T1 structure. *Biochemistry* **33:** 3312-3319.

APPENDIX A

PREVIOUS RESEARCH

Table 26. Parameters characterizing the urea unfolding curves of wild-type RNase Sa and four single Trp containing variants.[a]

Protein	Probe	$[Urea]_{1/2}$ (M)	*m*-value (cal mol^{-1} M^{-1})	ΔG^0 (kcal mol^{-1})	$\Delta(\Delta G^0)^b$ (kcal mol^{-1})
WT	Fluorescence				
	CD	6.52 ± .01	899 ± 9	5.86	
Y52W	Fluorescence	3.47 ± .03	971 ± 36	3.37	
	CD	3.48 ± .01	992 ± 10	3.45	-2.90
Y55W	Fluorescence	4.51 ± .03	1198 ± 62	5.41	
	CD	4.44 ± .01	1088 ± 19	4.83	-2.21
T76W	Fluorescence				
	CD	7.30 ± .01	920 ± 14	6.72	+0.71
Y81W	Fluorescence	6.00 ± .03	944 ± 40	5.69	
	CD	6.10 ± .01	1046 ± 14	6.39	-0.40

[a] The urea denaturation curves were determined at 25°C, pH = 7, in 30 mM MOPS buffer, and analyzed using Equation 10 as described in Methods. Urea denaturation curves could not be determined using fluorescence measurements for RNase Sa and the T76W variant.

[b] $\Delta(\Delta G)$ values were calculated As follows: (average *m*-value) * ($[Urea]_{1/2,\ variant}$ - $[Urea]_{1/2,\ wt}$). A positive values denotes an increase in stability over wild type.

Table 27. The emission λ_{max} and the fluorescence intensities at λ_{max} for the native[a] state of the four RNase Sa variants and the wild-type protein on which the variants are based. Similar data for NATA is also given.

Variant		% Buried		λ_{max}, nm		I_F at λ_{max}	
Y52W	(Ba)	98%	(98%)	309	(332)[b]	30900	(n/a)
Y55W	(T1)	89%	(100%)	310[c]	(318)	8150	(82800)
T76W	(Sa3)	10%	(0%)	335	(337)	30100	(21200)
Y81W	(Sa2)	89%	(94%)	319	(320)	40200	(62700)
NATA				351		4180	

[a]30 mM MOPS buffer, pH 7, 25°C

[b]Data from Willaert et al. for barnase with a single tryptophan at residue 71 (Willaert et al. 1992).

[c]If a wavelength of 296 nm is used for the excitation instead of 280 nm, λ_{max} = 322 nm.

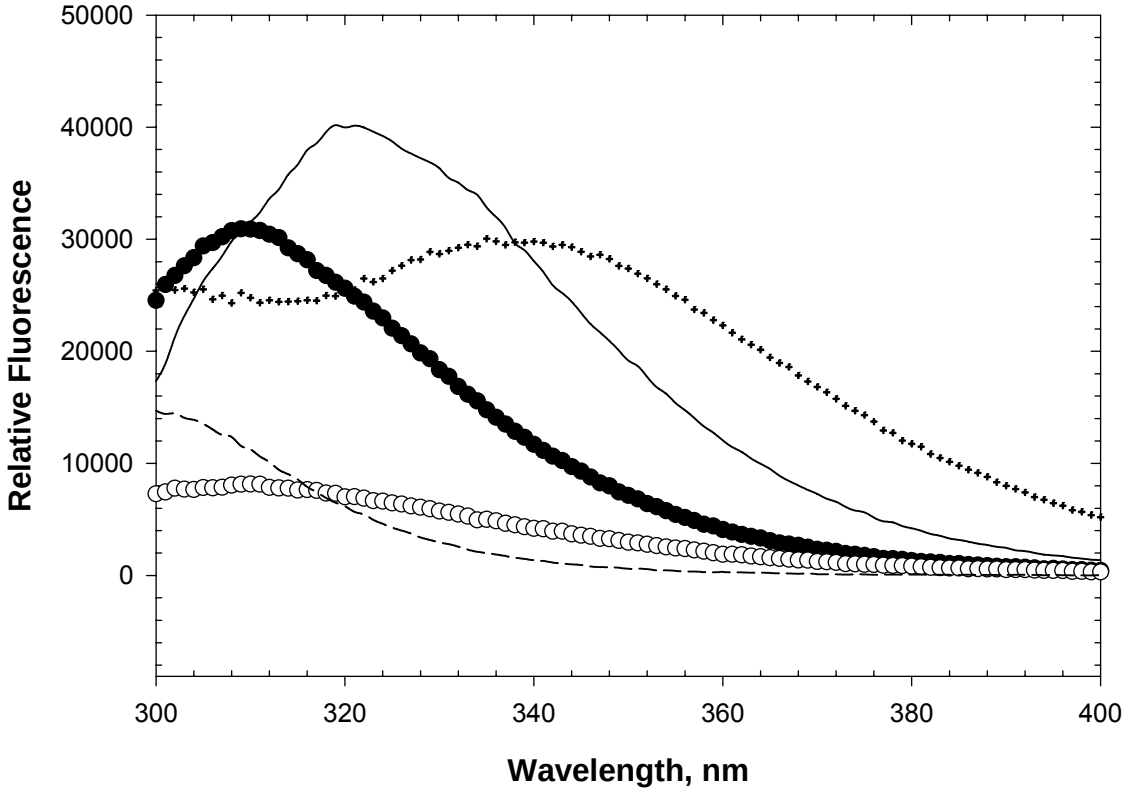

Figure 29. Native fluorescence emission spectra (278 nm excitation) of all the RNase Sa tryptophan variants as compared to wild-type RNase Sa (~0.94 μM) in 30 mM MOPS, pH 7.0, 25 ^{o}C, and using a 2 nm emission bandpass. The scans represent the following variants: Y81W (solid line), Y52W (closed circles), T76W (+ symbols), Wild type (dashed line), and Y55W (open circles).

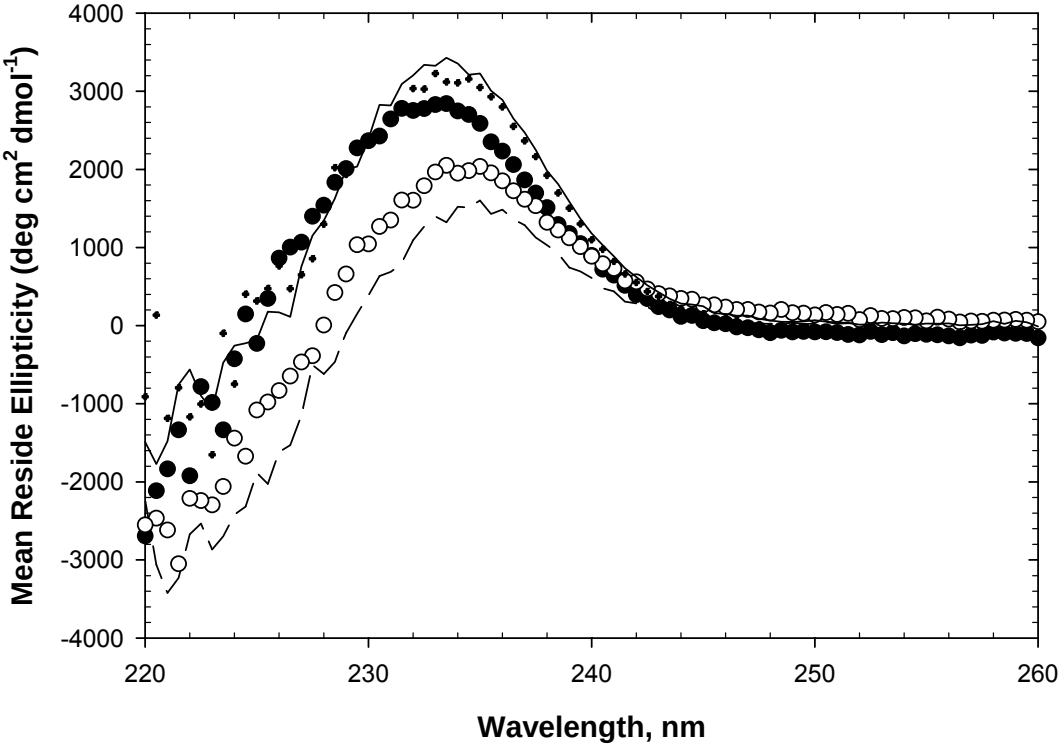

Figure 30. Far UV CD spectra of wild-type RNase Sa and the four tryptophan variants (~ 200 μM) in 30 mM MOPS, pH 7.0 and 25 °C. The scans represent the following variants: wild-type (dashed line), Y81W (solid line), Y52W (closed circles), T76W (+ symbols), and Y55W (open circles).

Table 28. Effect of charge reversal variants on protein stability[a].

Variant	Accessibility[b]	Nearest Charges[c]		Coulomb's Law[d]	$\Delta(\Delta G)$[e]
	%	- (Å)	+ (Å)	(kcal/mol)	(kcal/mol)
D17K	66	6.1	12.6	1.6 + ≈ 1.6 = 3.2	-1.1
D25K	92	10.7	9.9	1.2 + ≈ 1.2 = 2.4	+0.9
E41K	71	12.4	10.0	0.6 + ≈ 0.6 = 1.2	-1.2
E74K	63	8.4	6.6	1.1 + ≈ 1.1 = 2.2	+1.1

[a](Grimsley et al. 1999; Pace et al. 2000)

[b]Accessibilities were calculated as described by Lee and Richards (Lee and Richards 1971). For the RNases, the side-chain accessibility in the wild-type protein is given (1RGG).

[c]Nearest charges gives the distance from the charge on the designated side chain to the nearest negative (-) and positive (+) charges in the wild-type protein. The charge was placed on the following groups: α-amino, N; α-carboxyl, C; Asp, Cγ; Glu, Cδ; His, Cε1; Lys, Nζ; and Arg, Nζ.

[d]Coulomb's Law ($E = q_1q_2 / Dr$) with a dielectric constant, D, of 80 was used to calculate the first number by summing the interactions of the charge on the designated side chain of the wild-type protein with all of the other charges on the proteins. The second calculation could not be done because the variant structures are not available. Consequently, we just doubled the first number given.

[e]The last column gives the observed $\Delta(\Delta G)$ value for the charge-reversal variants. $\Delta(\Delta G) = \Delta G(\text{variant}) - \Delta G(\text{wild type})$ so that a positive $\Delta(\Delta G)$ indicated that the variant protein is more stable than the wild-type protein. The $\Delta(\Delta G)$ values were measured at pH 7 in the presence of 30 mM MOPS.

APPENDIX B

PEPTIDES AT pH 7.0

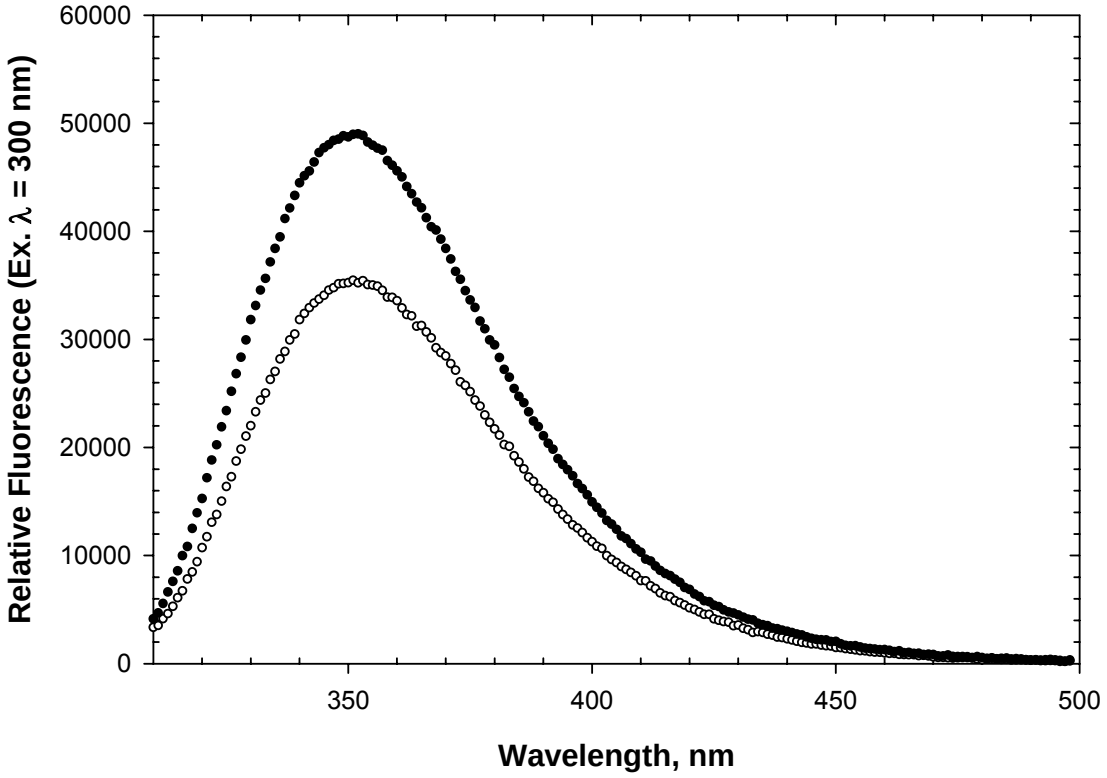

Figure 31. Fluorescence emission spectra (300 nm excitation) of NATA (10 μM) in 10 mM TCEP, pH 7.0, 25 °C with 8.5 M urea (closed circles) and 6 M GdnHCl (open circles).

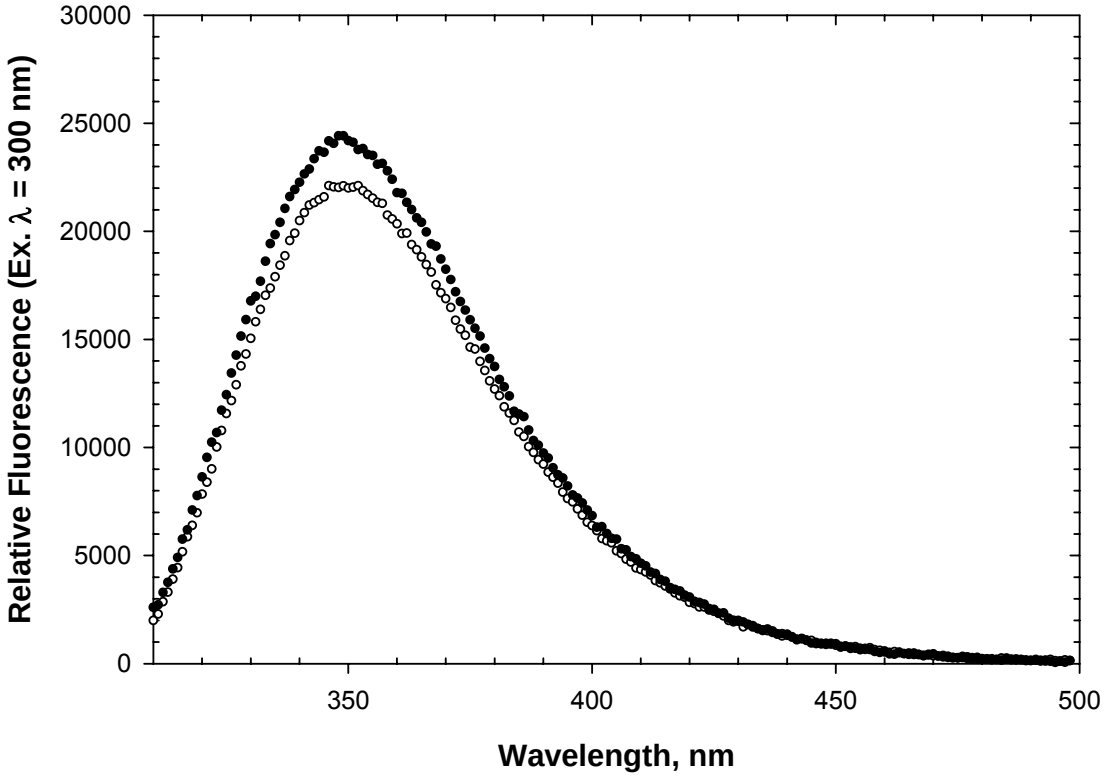

Figure 32. Fluorescence emission spectra (300 nm excitation) of AWA (10 μM) in 10 mM TCEP, pH 7.0, 25 °C with 8.5 M urea (closed circles) and 6 M GdnHCl (open circles).

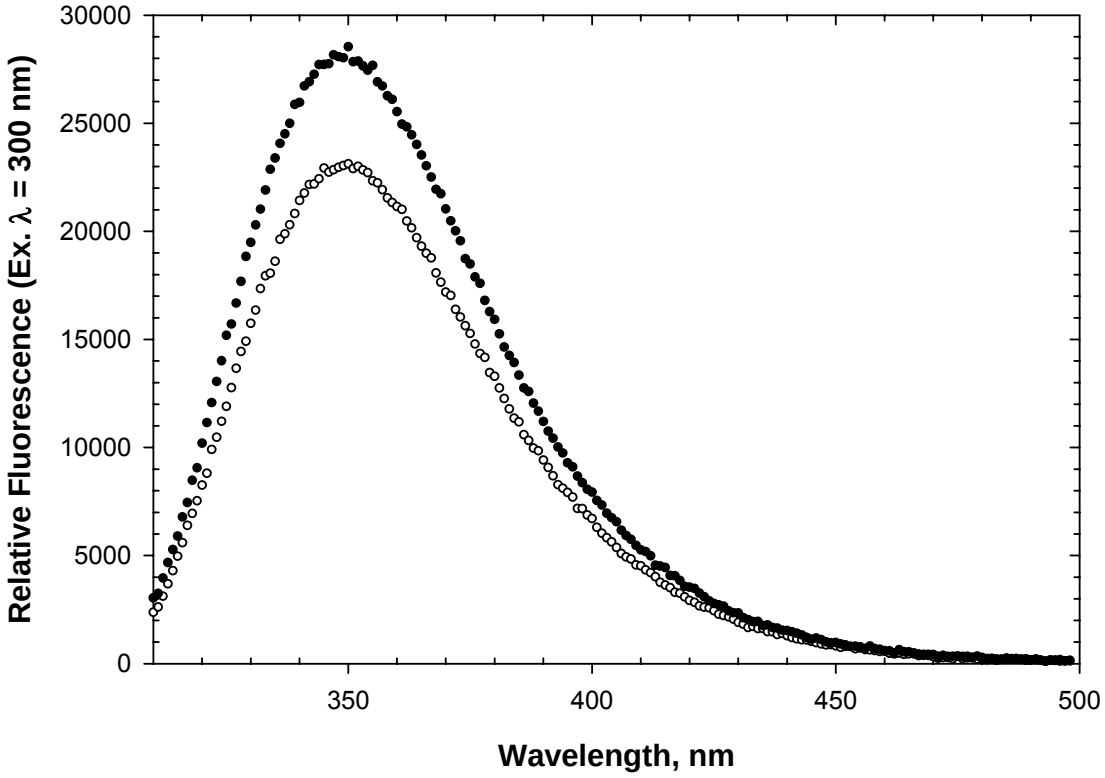

Figure 33. Fluorescence emission spectra (300 nm excitation) of AAWAA (10 μM) in 10 mM TCEP, pH 7.0, 25 ^{o}C with 8.5 M urea (closed circles) and 6 M GdnHCl (open circles).

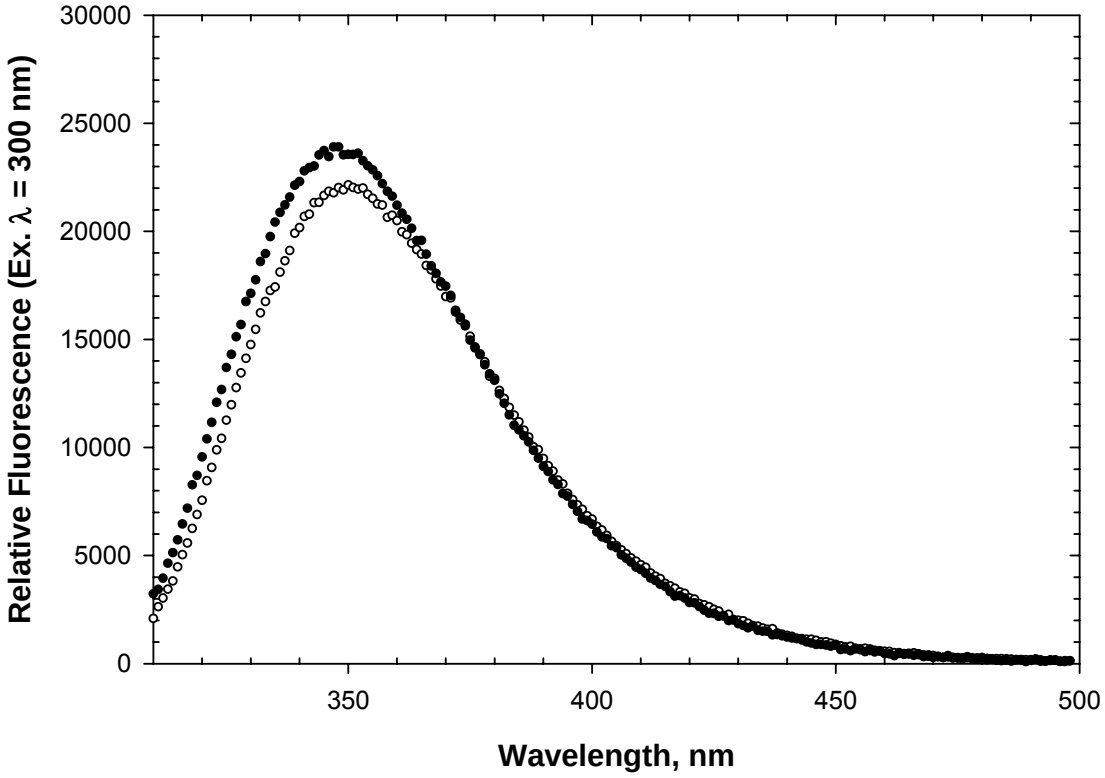

Figure 34. Fluorescence emission spectra (300 nm excitation) of WVSGT (D1W) (10 μM) in 10 mM TCEP, pH 7.0, 25 ^{o}C with 8.5 M urea (closed circles) and 6 M GdnHCl (open circles).

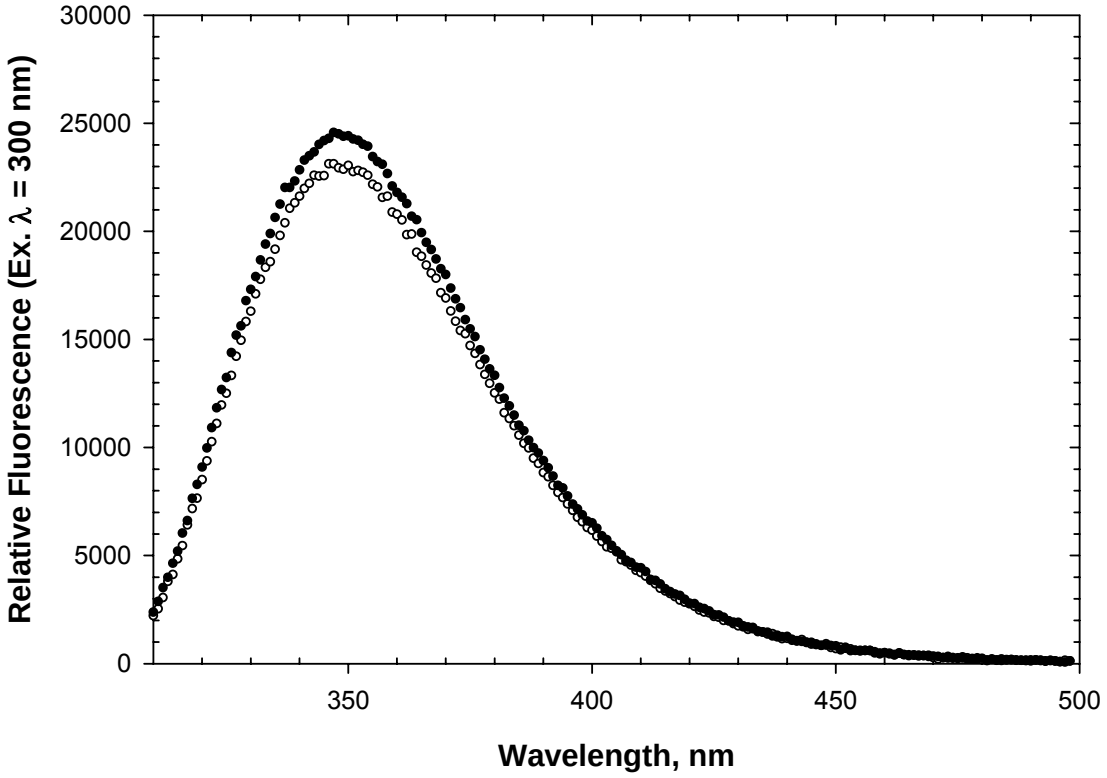

Figure 35. Fluorescence emission spectra (300 nm excitation) of GYWHE (Y52W) (10 μM) in 10 mM TCEP, pH 7.0, 25 ^{o}C with 8.5 M urea (closed circles) and 6 M GdnHCl (open circles).

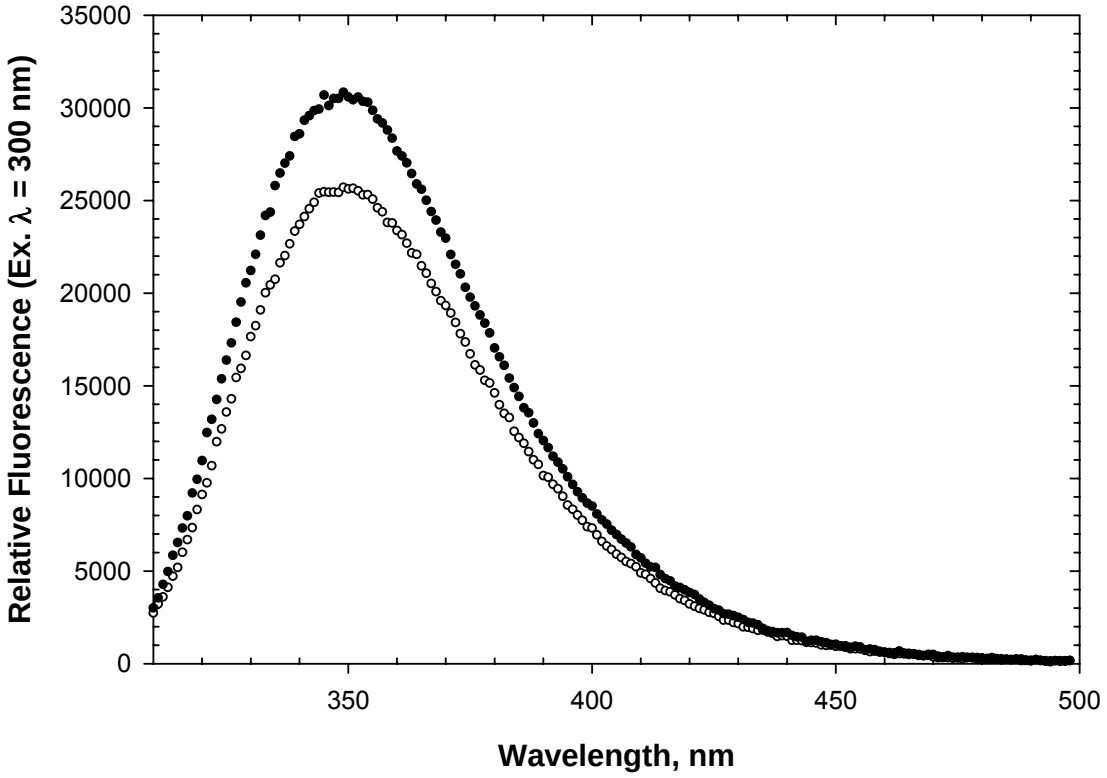

Figure 36. Fluorescence emission spectra (300 nm excitation) of HEWTV (Y55W) (10 μM) in 10 mM TCEP, pH 7.0, 25 ^{o}C with 8.5 M urea (closed circles) and 6 M GdnHCl (open circles).

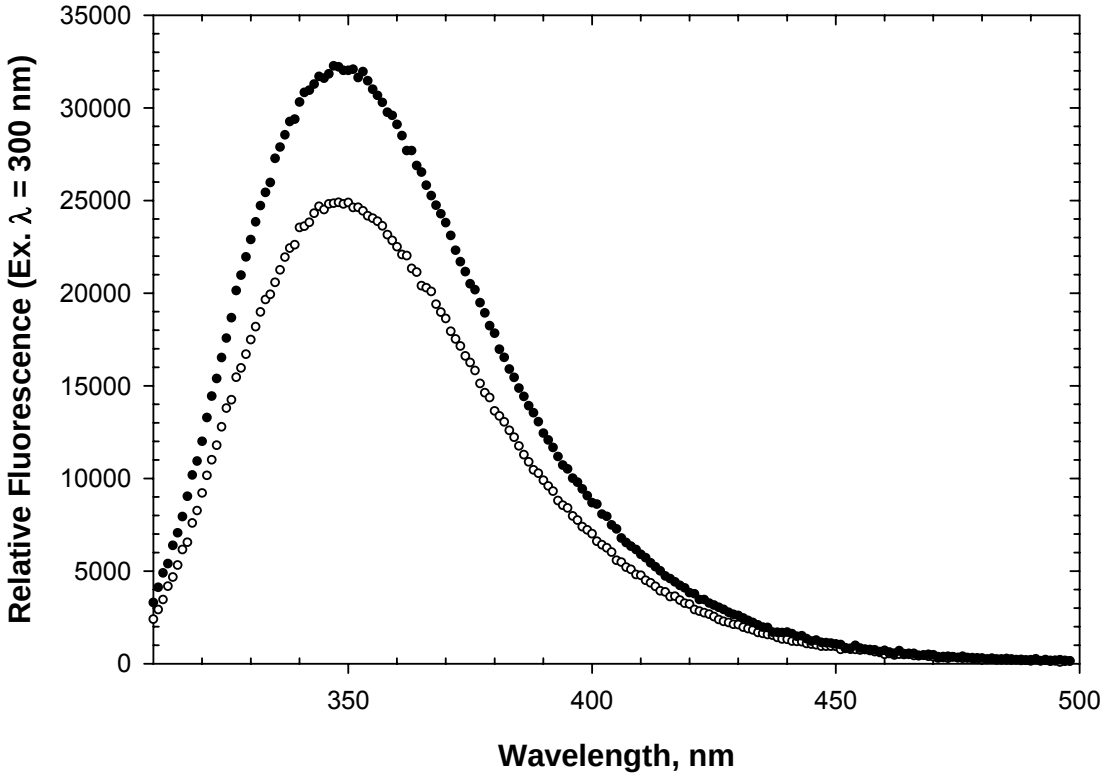

Figure 37. Fluorescence emission spectra (300 nm excitation) of EAWQE (T76W) (10 μM) in 10 mM TCEP, pH 7.0, 25 ^{o}C with 8.5 M urea (closed circles) and 6 M GdnHCl (open circles).

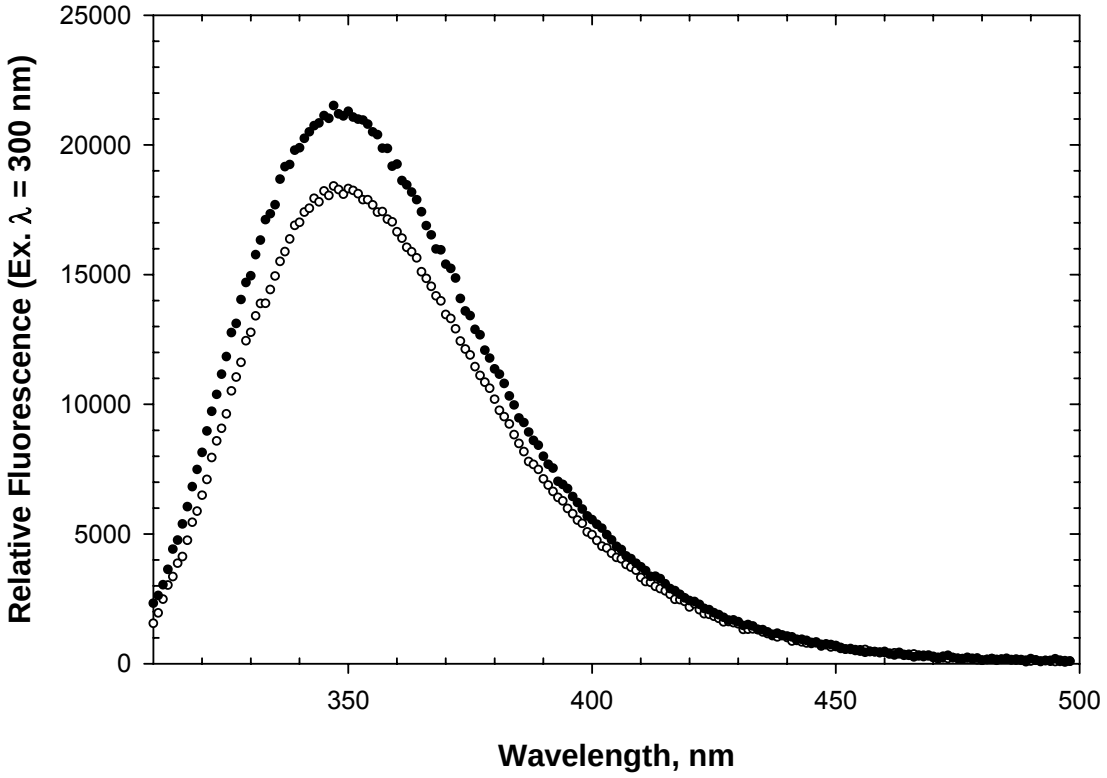

Figure 38. Fluorescence emission spectra (300 nm excitation) of DYWTG (Y81W) (10 μM) in 10 mM TCEP, pH 7.0, 25 ^{o}C with 8.5 M urea (closed circles) and 6 M GdnHCl (open circles).

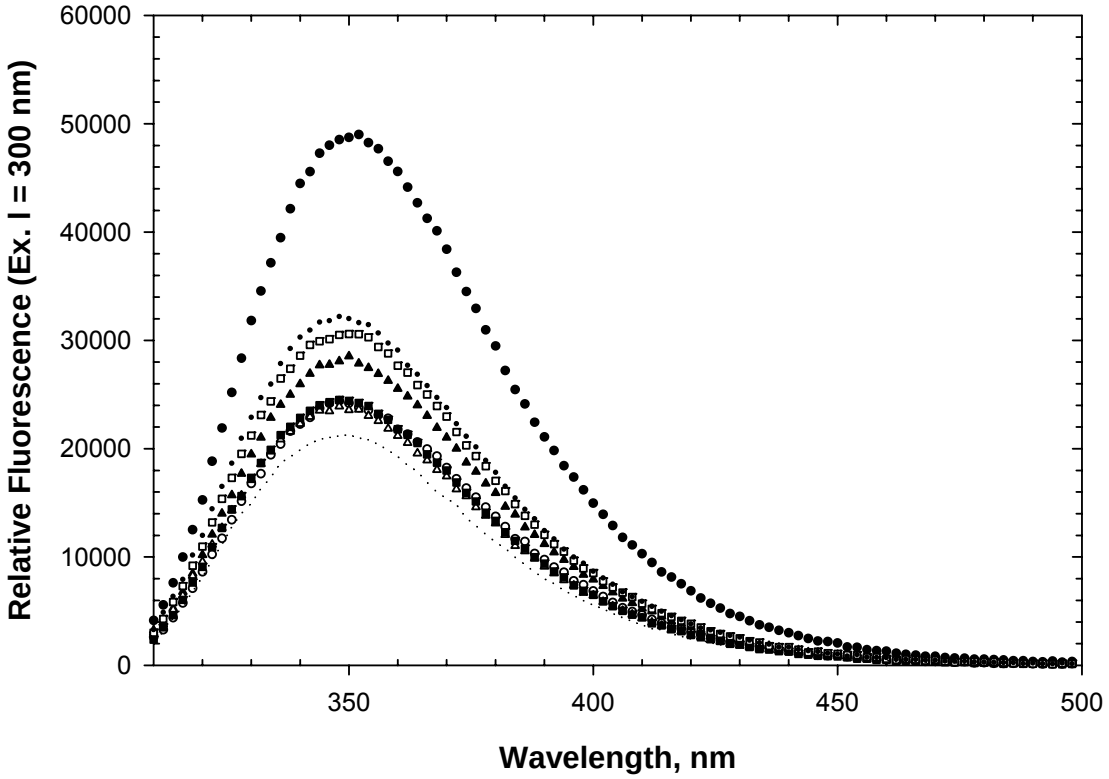

Figure 39. Fluorescence emission spectra (300 nm excitation) of the peptides (10 μM) in 8.5 M urea, 10 mM TCEP, pH 7.0, and 25 °C. The scans represent the following peptides: NATA (closed circles), AWA (open circles), AAWAA (closed triangles), WVSGT (D1W; open triangles), GYWHE (Y52W; closed squares), HEWTV (Y55W; open squares), EAWQE (T76W; dots), and DYWTG (Y81W; dashed line).

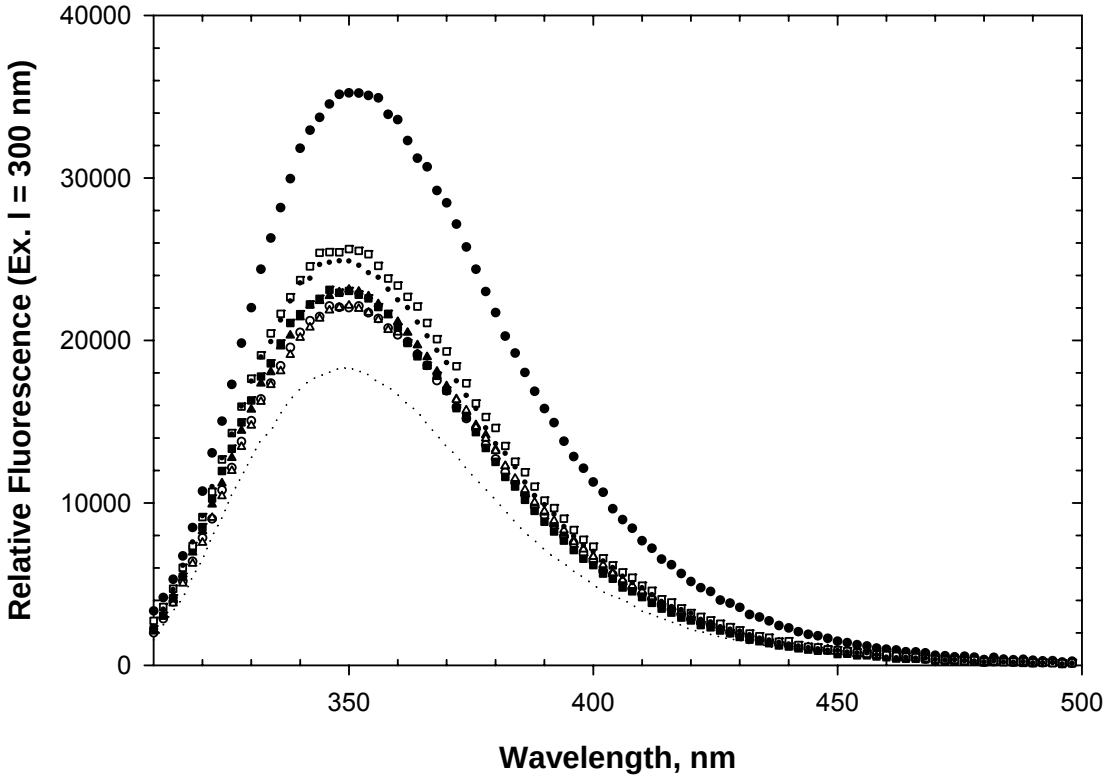

Figure 40. Fluorescence emission spectra (300 nm excitation) of the peptides (10 μM) in 6 M GdnHCl, 10 mM TCEP, pH 7.0, and 25 °C. The scans represent the following peptides: NATA (closed circles), AWA (open circles), AAWAA (closed triangles), WVSGT (D1W; open triangles), GYWHE (Y52W; closed squares), HEWTV (Y55W; open squares), EAWQE (T76W; dots), and DYWTG (Y81W; dashed line).

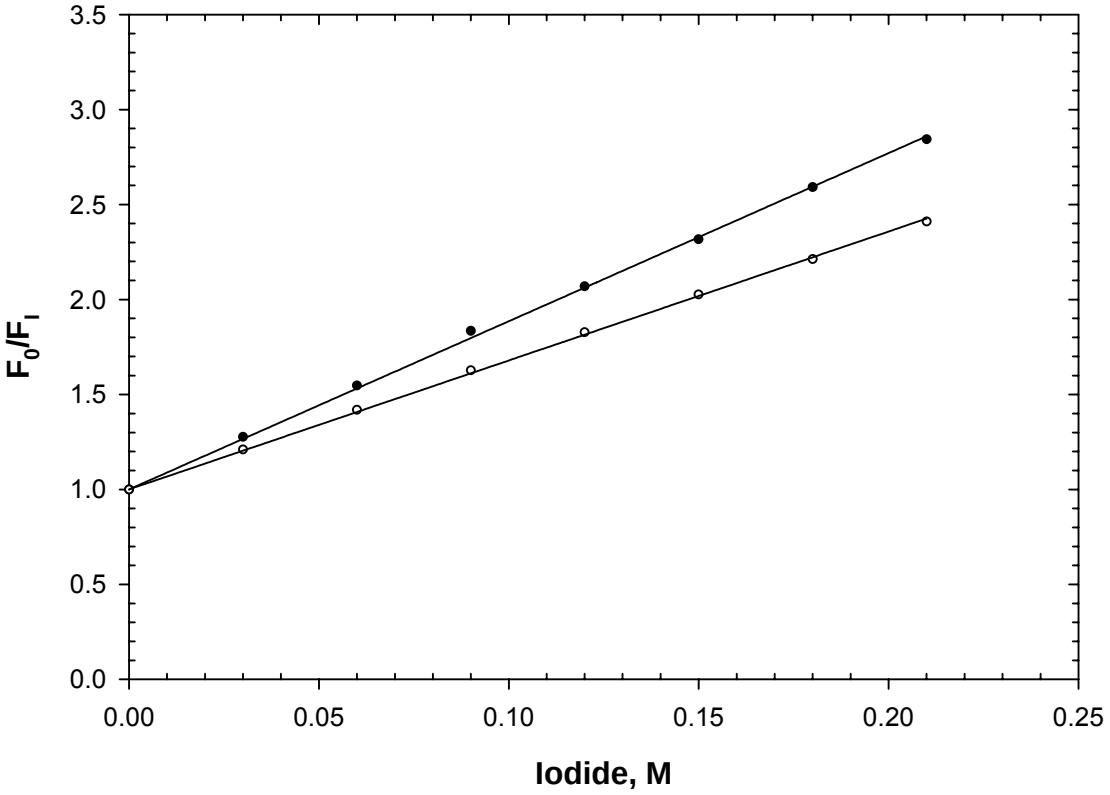

Figure 41. Iodide quenching of fluorescence (300 nm excitation, 350 nm emission) of NATA (10 μM) in 10 mM TCEP, pH 7.0, and 25 ^{o}C. The data were determined under the following conditions: peptide in 7.6 M urea (closed circles) and peptide in 3.8 M guanidine hydrochloride (open circles).

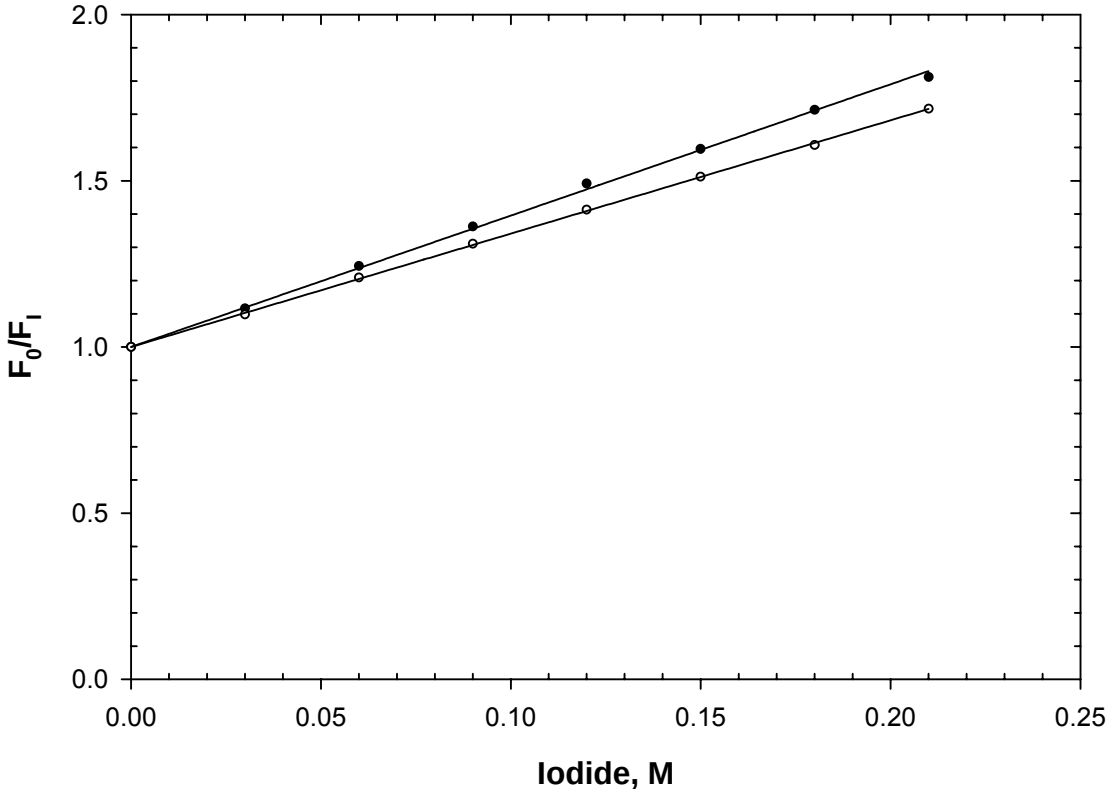

Figure 42. Iodide quenching of fluorescence (300 nm excitation, 350 nm emission) of AWA (10 μM) in 10 mM TCEP, pH 7.0, and 25 °C. The data were determined under the following conditions: peptide in 7.6 M urea (closed circles) and peptide in 3.8 M guanidine hydrochloride (open circles).

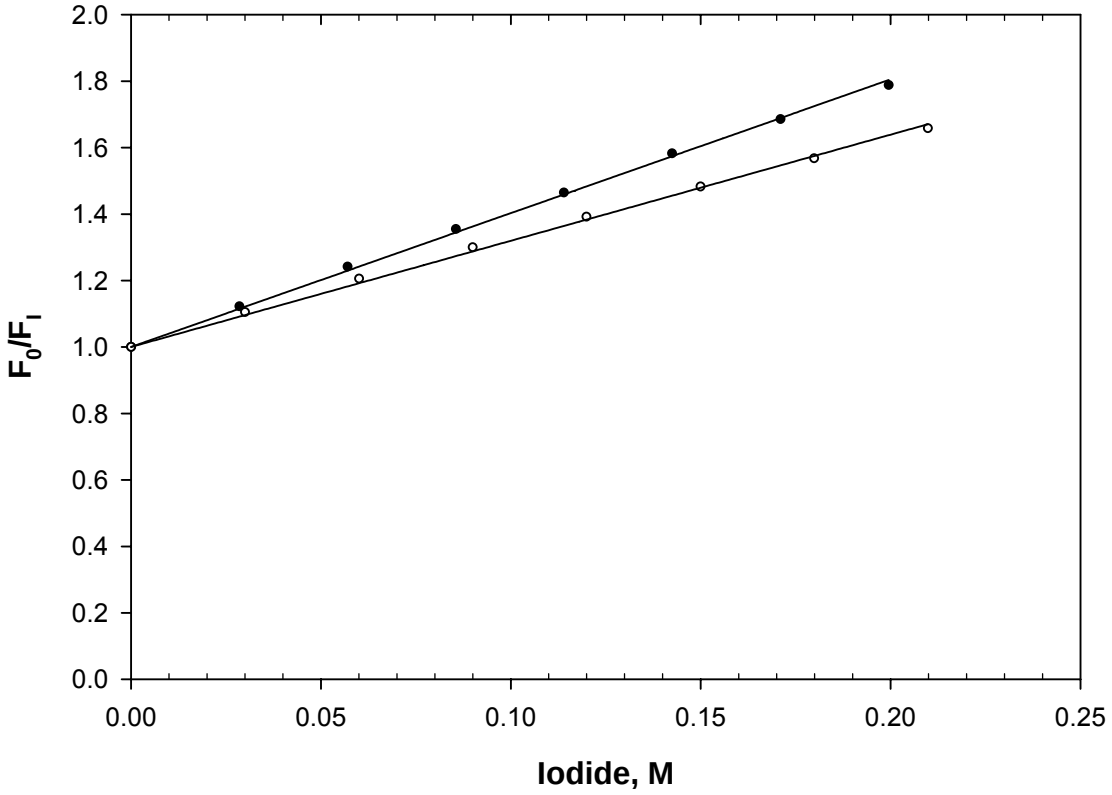

Figure 43. Iodide quenching of fluorescence (300 nm excitation, 350 nm emission) of AAWAA (10 μM) in 10 mM TCEP, pH 7.0, and 25 °C. The data were determined under the following conditions: peptide in 7.6 M urea (closed circles) and peptide in 3.8 M guanidine hydrochloride (open circles).

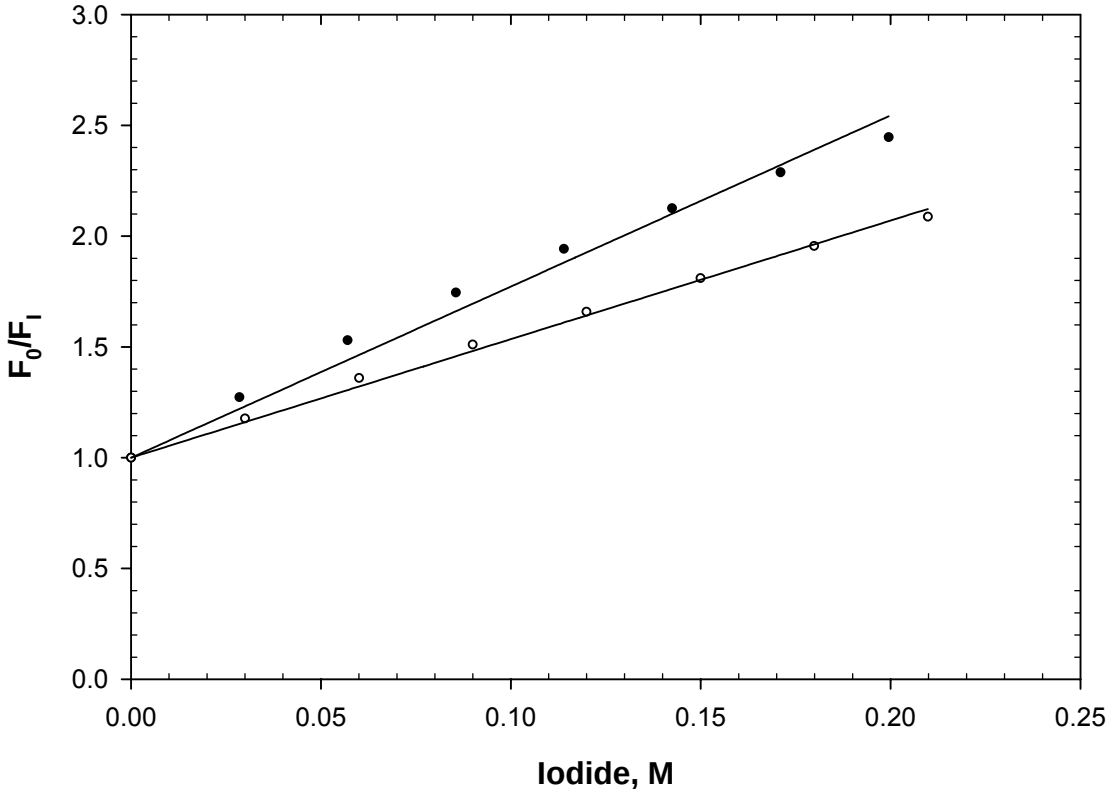

Figure 44. Iodide quenching of fluorescence (300 nm excitation, 350 nm emission) of WVSGT (D1W;10 μM) in 10 mM TCEP, pH 7.0, and 25 °C. The data were determined under the following conditions: peptide in 7.6 M urea (closed circles) and peptide in 3.8 M guanidine hydrochloride (open circles).

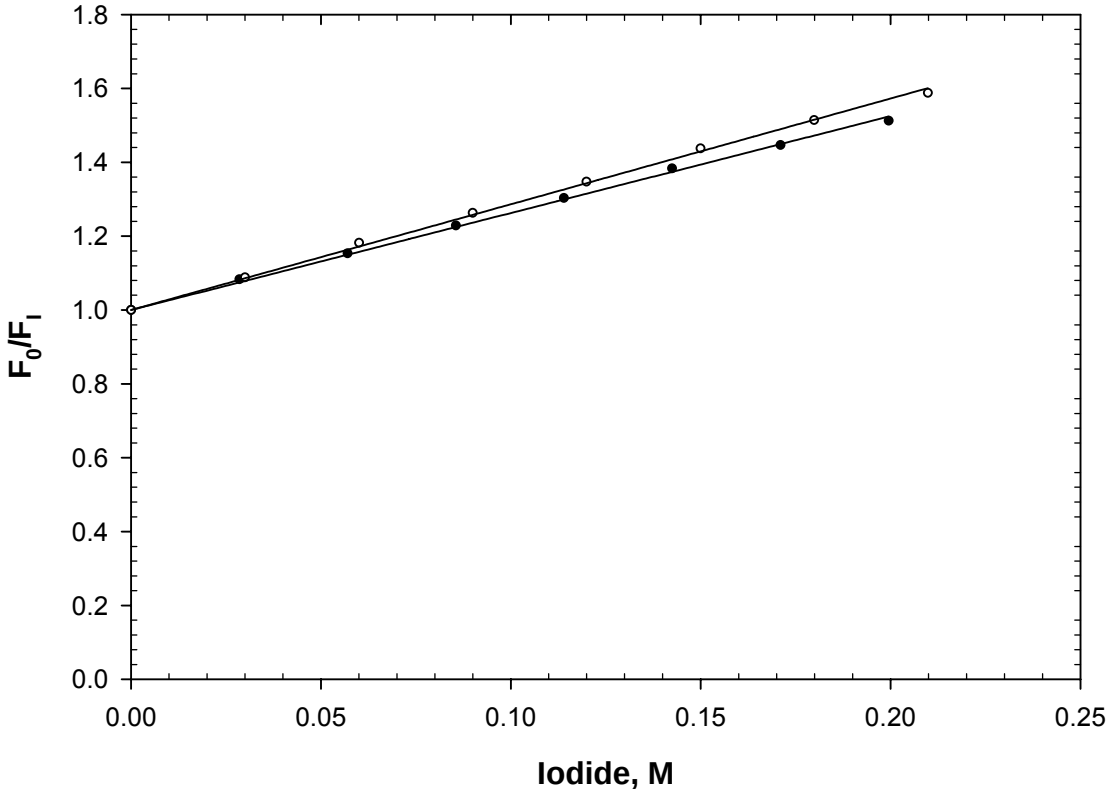

Figure 45. Iodide quenching of fluorescence (300 nm excitation, 350 nm emission) of GYWHE (Y52W; 10 μM) in 10 mM TCEP, pH 7.0, and 25 °C. The data were determined under the following conditions: peptide in 7.6 M urea (closed circles) and peptide in 3.8 M guanidine hydrochloride (open circles).

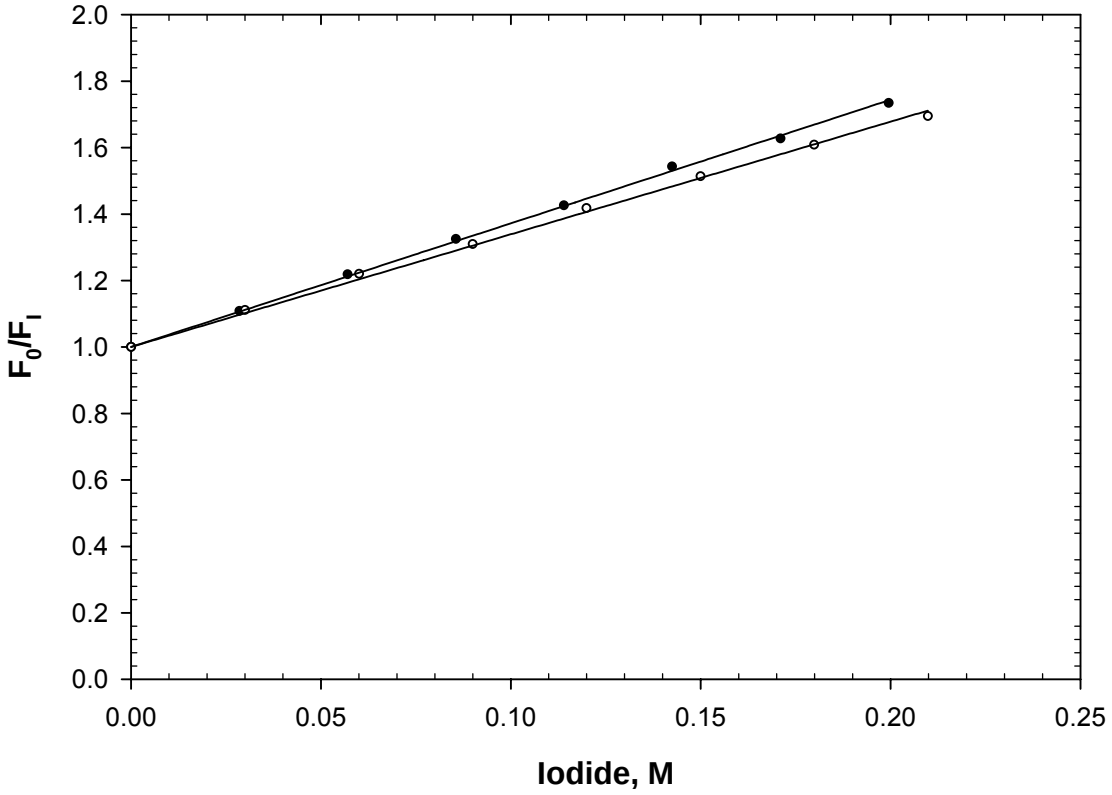

Figure 46. Iodide quenching of fluorescence (300 nm excitation, 350 nm emission) of HEWTV (Y55W; 10 μM) in 10 mM TCEP, pH 7.0, and 25 °C. The data were determined under the following conditions: peptide in 7.6 M urea (closed circles) and peptide in 3.8 M guanidine hydrochloride (open circles).

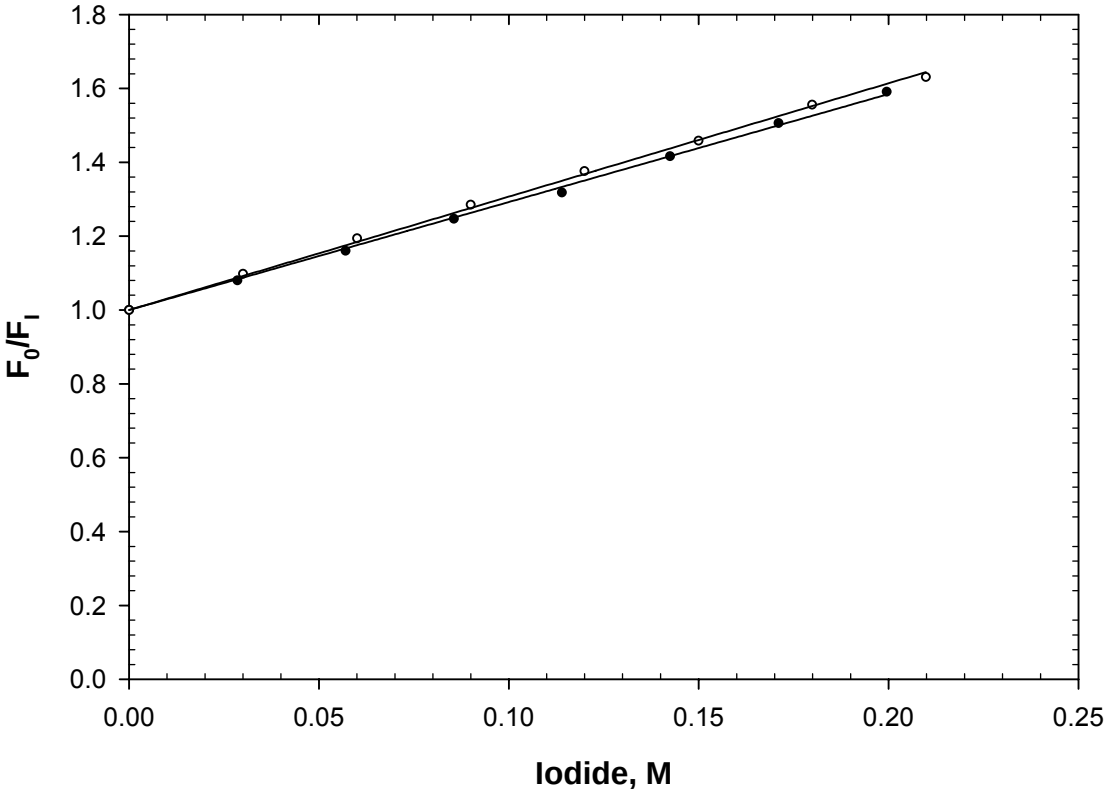

Figure 47. Iodide quenching of fluorescence (300 nm excitation, 350 nm emission) of EAWQE (T76W; 10 μM) in 10 mM TCEP, pH 7.0, and 25 °C. The data were determined under the following conditions: peptide in 7.6 M urea (closed circles) and peptide in 3.8 M guanidine hydrochloride (open circles).

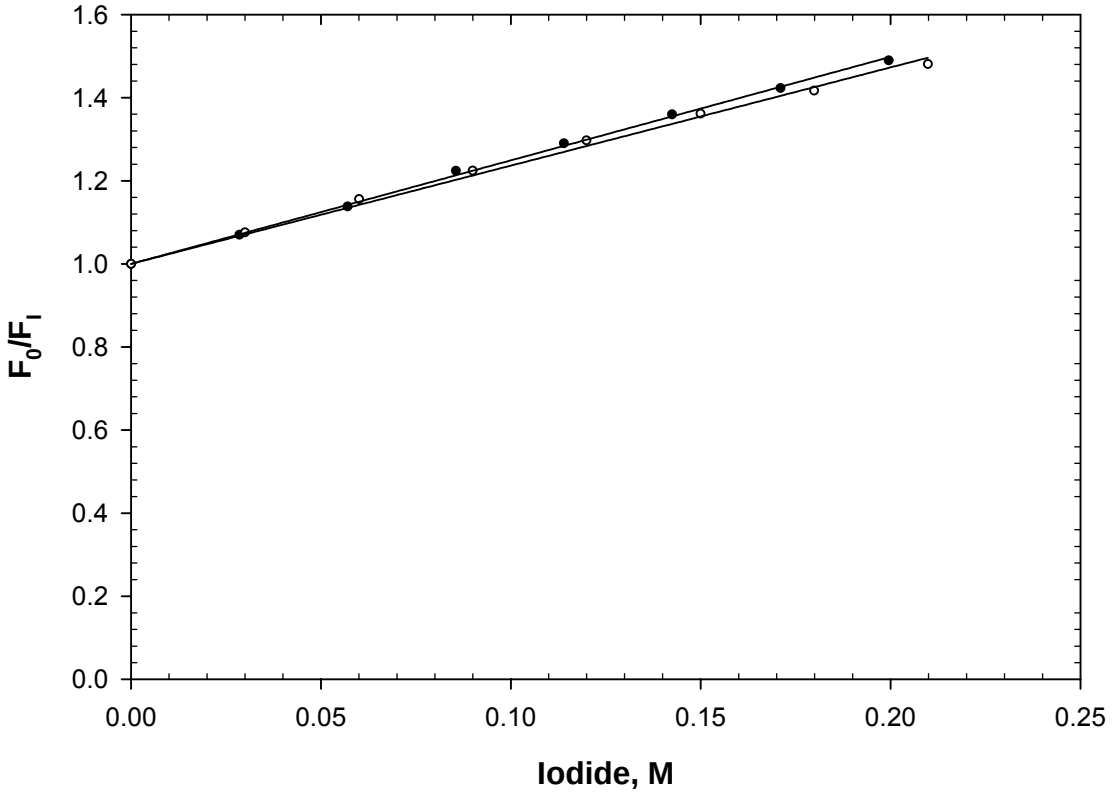

Figure 48. Iodide quenching of fluorescence (300 nm excitation, 350 nm emission) of DYWTG (Y81W; 10 μM) in 10 mM TCEP, pH 7.0, and 25 °C. The data were determined under the following conditions: peptide in 7.6 M urea (closed circles) and peptide in 3.8 M guanidine hydrochloride (open circles).

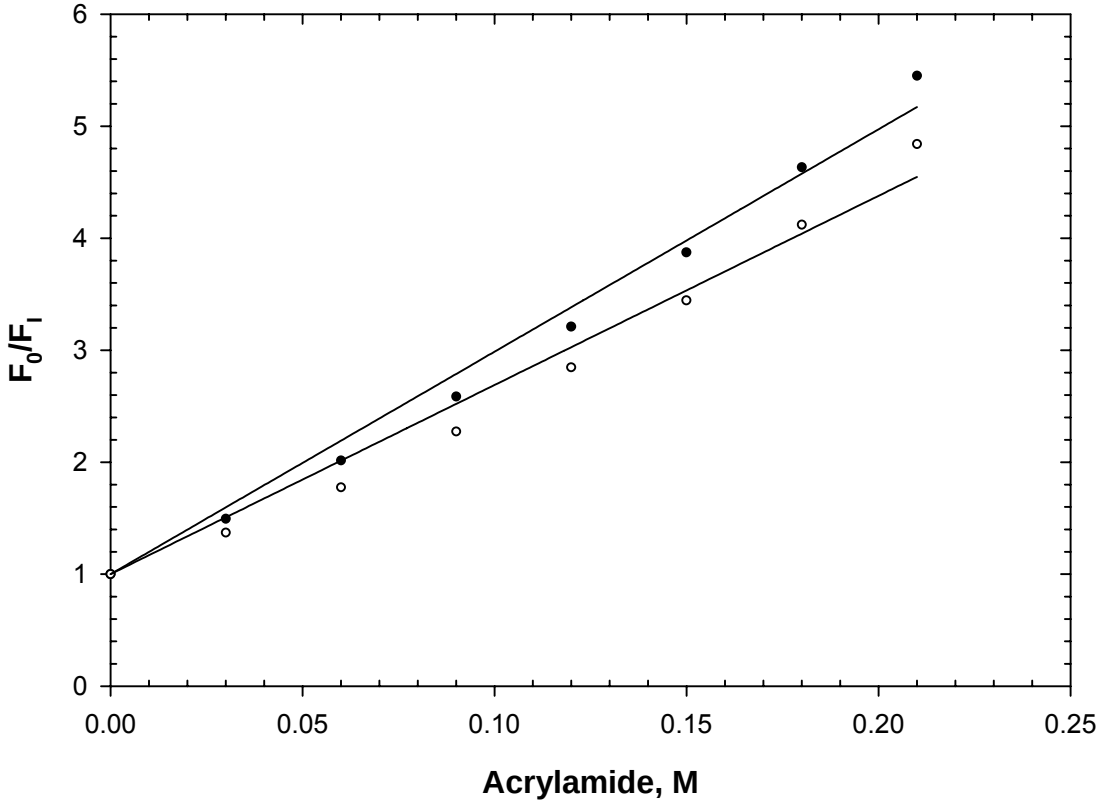

Figure 49. Acrylamide quenching of fluorescence (300 nm excitation, 350 nm emission) of NATA (10 μM) in 10 mM TCEP, pH 7.0, and 25 °C. The data were determined under the following conditions: peptide in 7.6 M urea (closed circles) and peptide in 3.8 M guanidine hydrochloride (open circles).

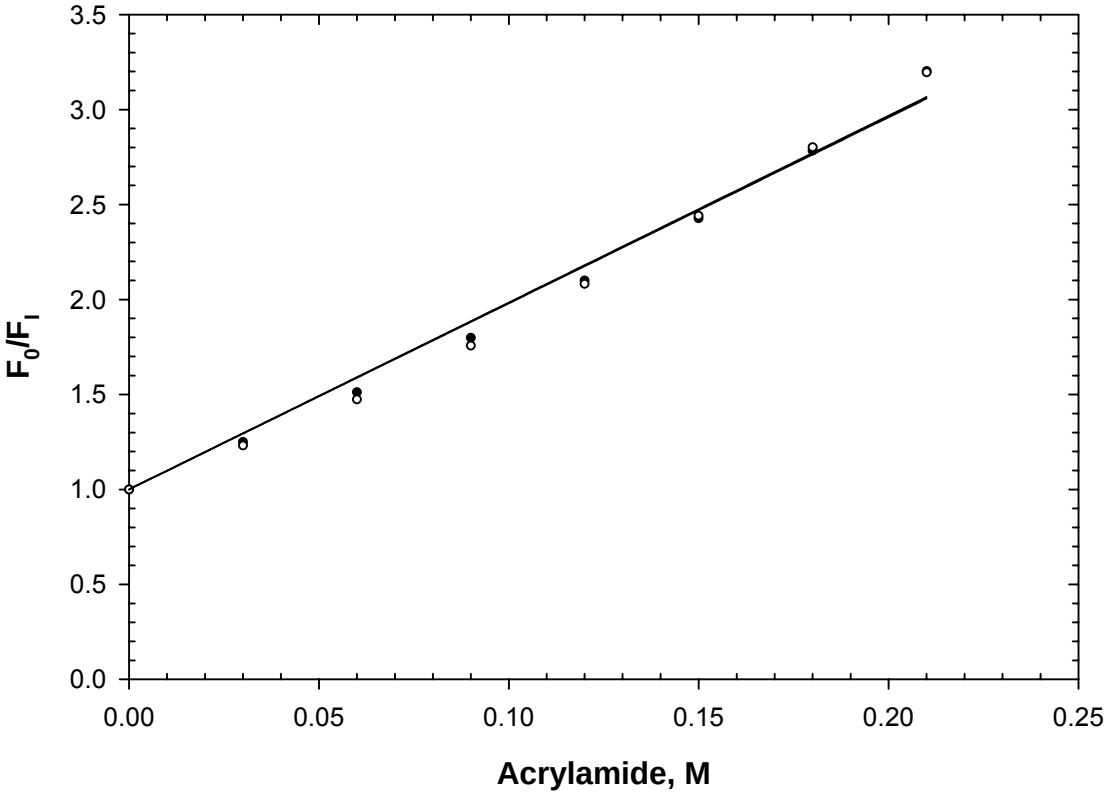

Figure 50. Acrylamide quenching of fluorescence (300 nm excitation, 350 nm emission) of AWA (10 μM) in 10 mM TCEP, pH 7.0, and 25 °C. The data were determined under the following conditions: peptide in 7.6 M urea (closed circles) and peptide in 3.8 M guanidine hydrochloride (open circles).

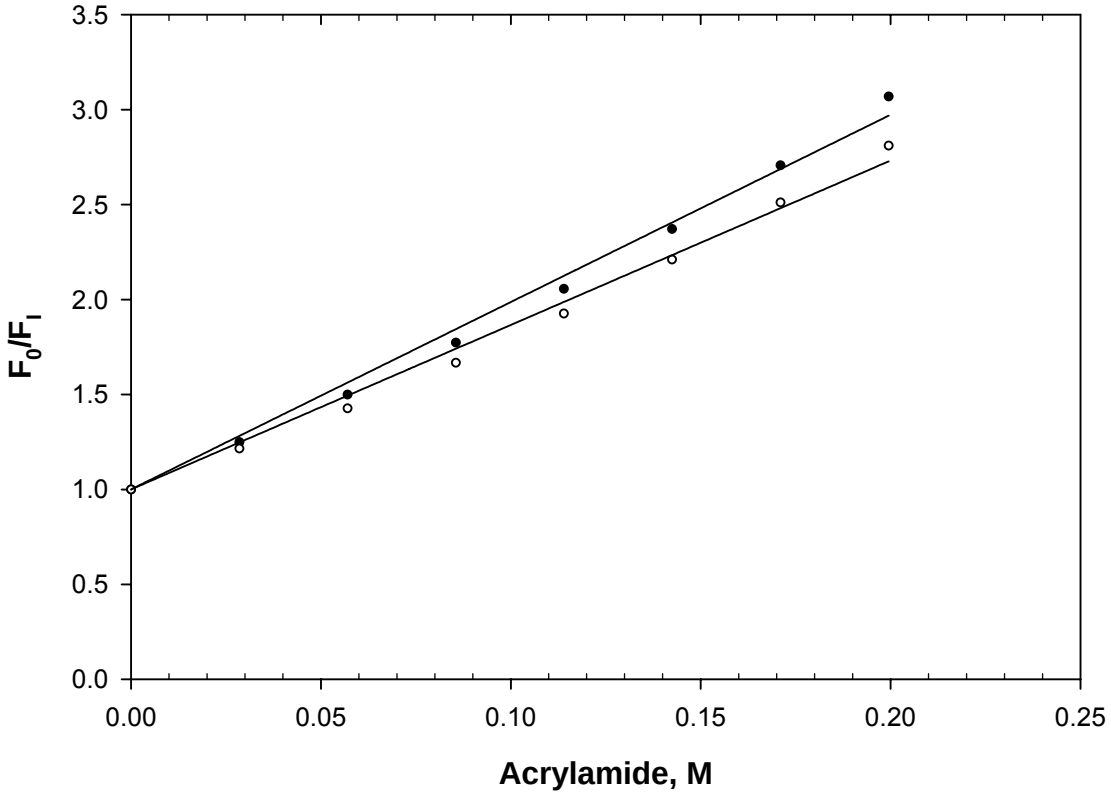

Figure 51. Acrylamide quenching of fluorescence (300 nm excitation, 350 nm emission) of AAWAA (10 μM) in 10 mM TCEP, pH 7.0, and 25 °C. The data were determined under following conditions: peptide in 7.6 M urea (closed circles) and peptide in 3.8 M guanidine hydrochloride (open circles).

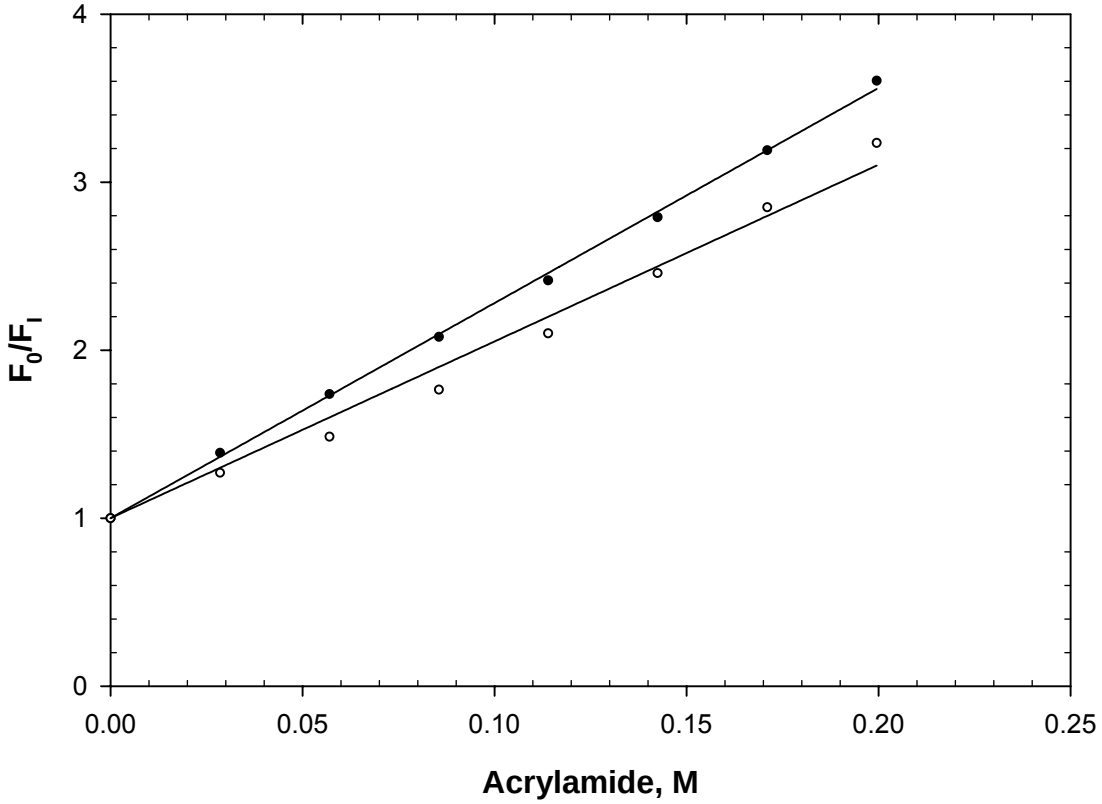

Figure 52. Acrylamide quenching of fluorescence (300 nm excitation, 350 nm emission) of WVSGT (D1W;10 μM) in 10 mM TCEP, pH 7.0, and 25 ^{o}C. The data were determined under the following conditions: peptide in 7.6 M urea (closed circles) and peptide in 3.8 M guanidine hydrochloride (open circles).

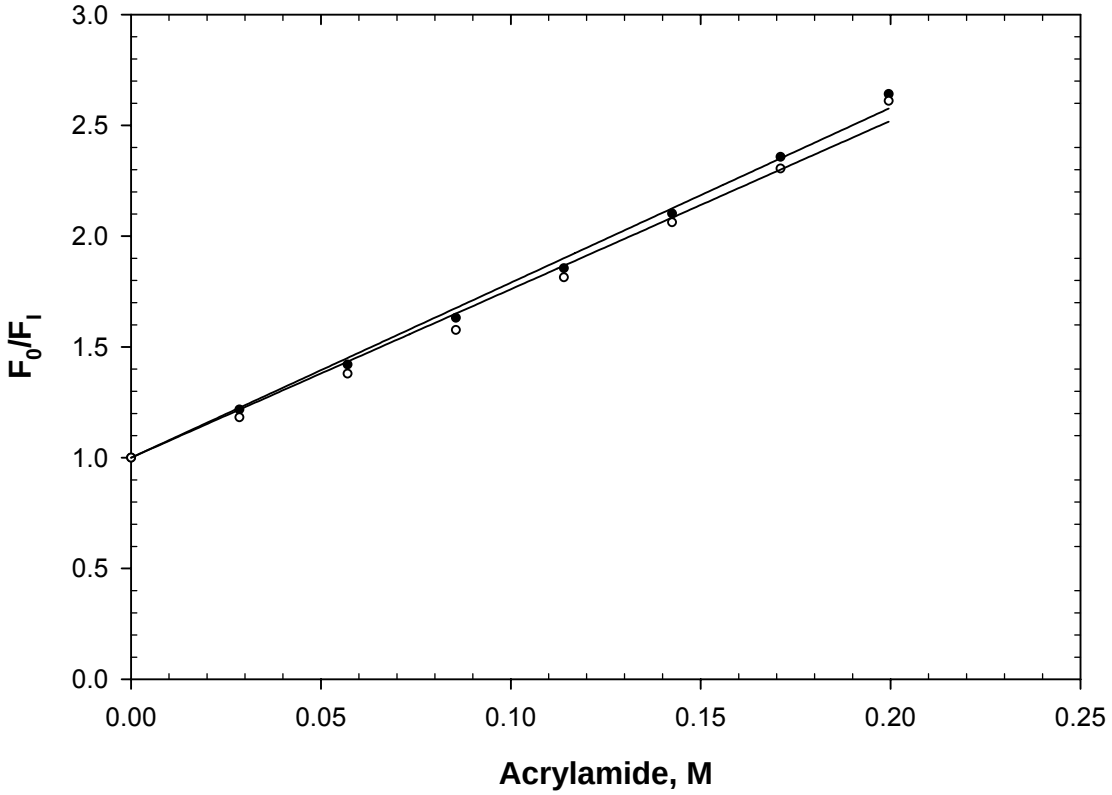

Figure 53. Acrylamide quenching of fluorescence (300 nm excitation, 350 nm emission) of GYWHE (Y52W; 10 μM) in 10 mM TCEP, pH 7.0, and 25 °C. The data were determined under the following conditions: peptide in 7.6 M urea (closed circles) and peptide in 3.8 M guanidine hydrochloride (open circles).

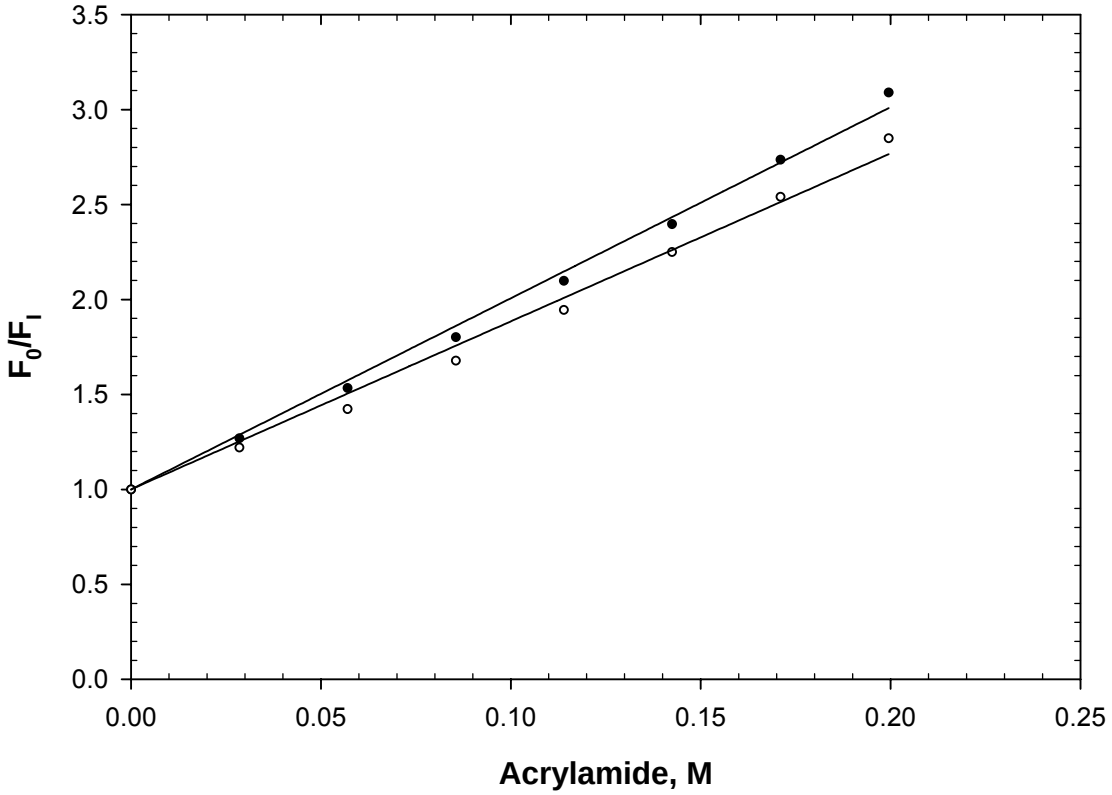

Figure 54. Acrylamide quenching of fluorescence (300 nm excitation, 350 nm emission) of HEWTV (Y55W; 10 μM) in 10 mM TCEP, pH 7.0, and 25 °C. The data were determined under the following conditions: peptide in 7.6 M urea (closed circles) and peptide in 3.8 M guanidine hydrochloride (open circles).

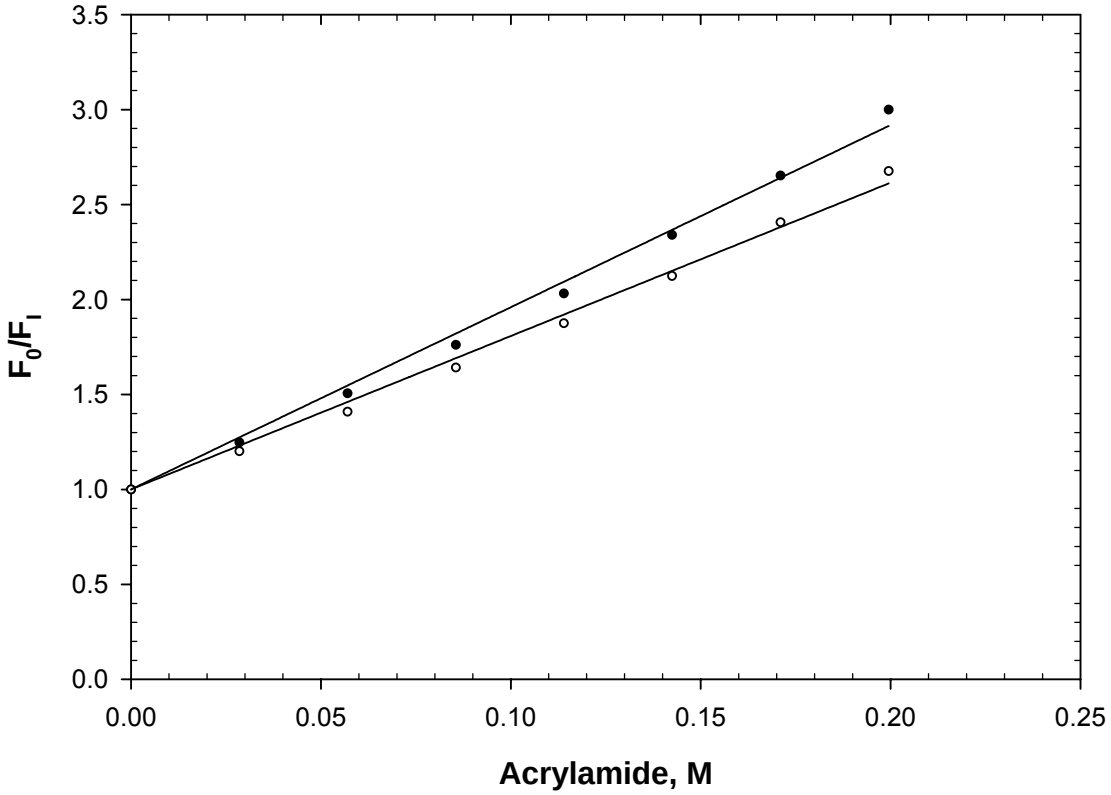

Figure 55. Acrylamide quenching of fluorescence (300 nm excitation, 350 nm emission) of EAWQE (T76W; 10 μM) in 10 mM TCEP, pH 7.0, and 25 ^{o}C. The data were determined under the following conditions: peptide in 7.6 M urea (closed circles) and peptide in 3.8 M guanidine hydrochloride (open circles).

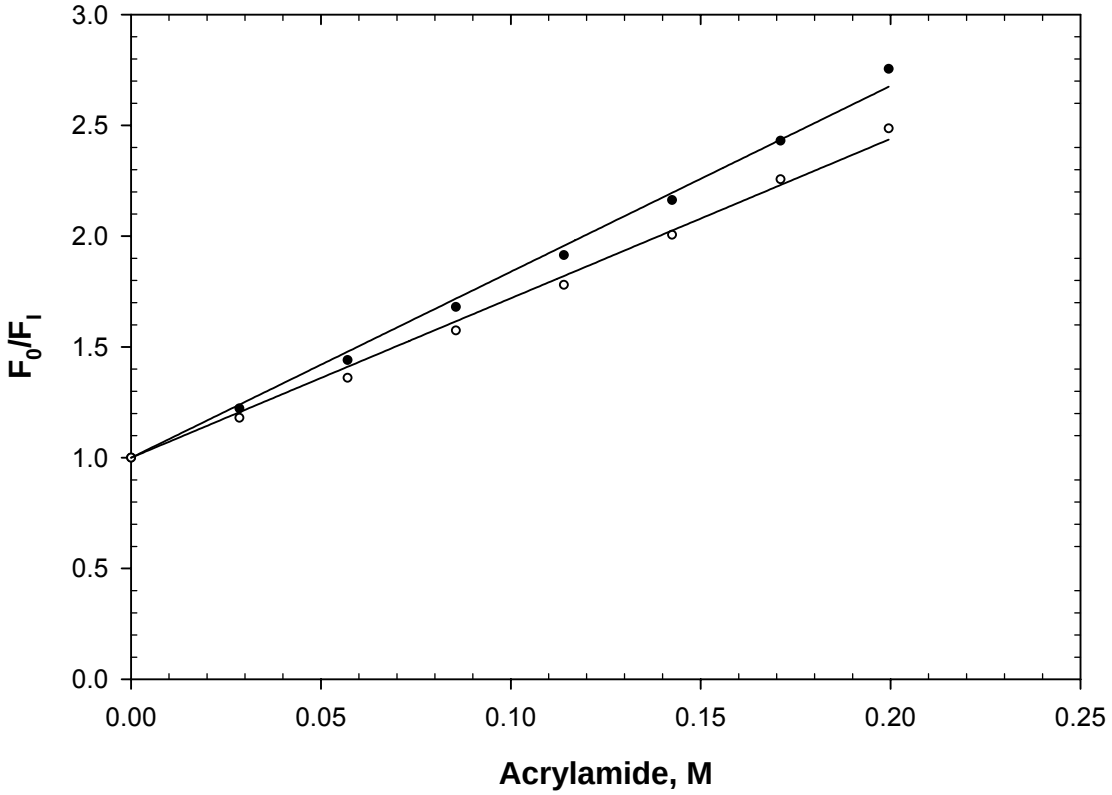

Figure 56. Acrylamide quenching of fluorescence (300 nm excitation, 350 nm emission) of DYWTG (Y81W; 10 μM) in 10 mM TCEP, pH 7.0, and 25 °C. The data were determined under the following conditions: peptide in 7.6 M urea (closed circles) and peptide in 3.8 M guanidine hydrochloride (open circles).

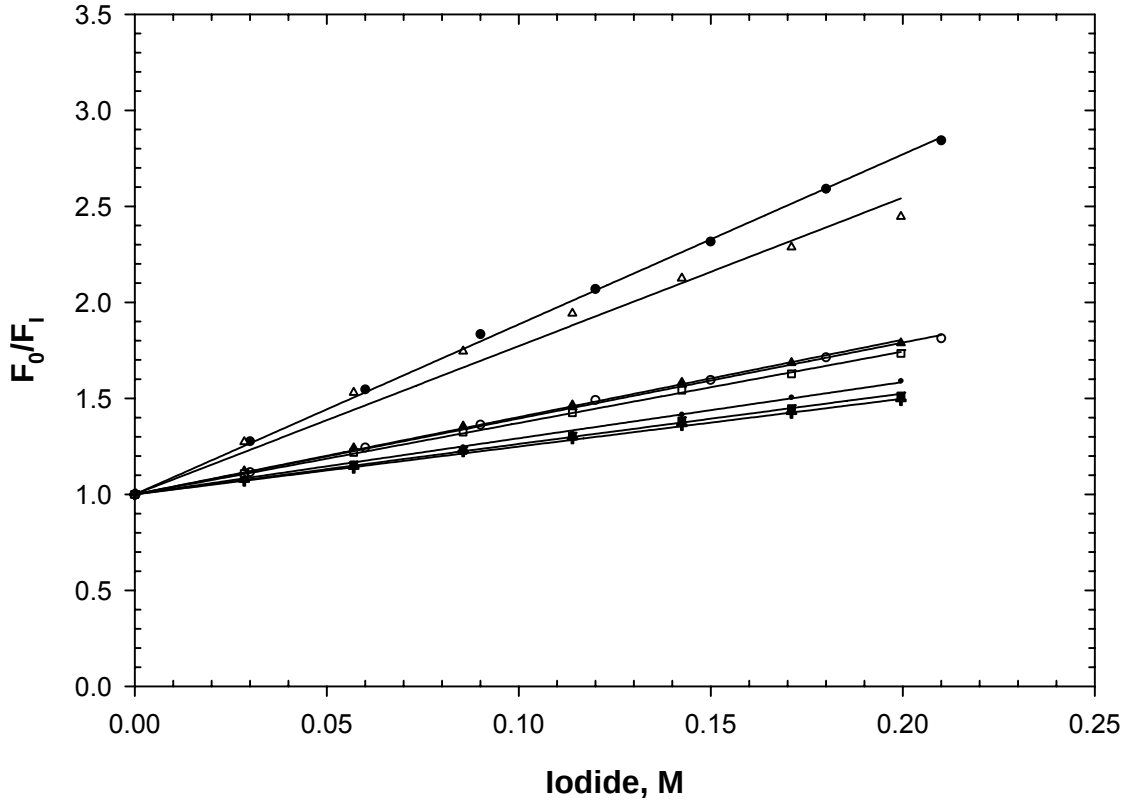

Figure 57. Iodide quenching of fluorescence (300 nm excitation, 350 nm emission) of the peptides (10 μM) in 7.6 M urea, 10 mM TCEP, pH 7.0, and 25 °C. The data represent the following peptides: NATA (closed circles), AWA (open circles), AAWAA (closed triangles), WVSGT (D1W; open triangles), GYWHE (Y52W; closed squares), HEWTV (Y55W; open squares), EAWQE (T76W; dots), and DYWTG (Y81W; plus symbols).

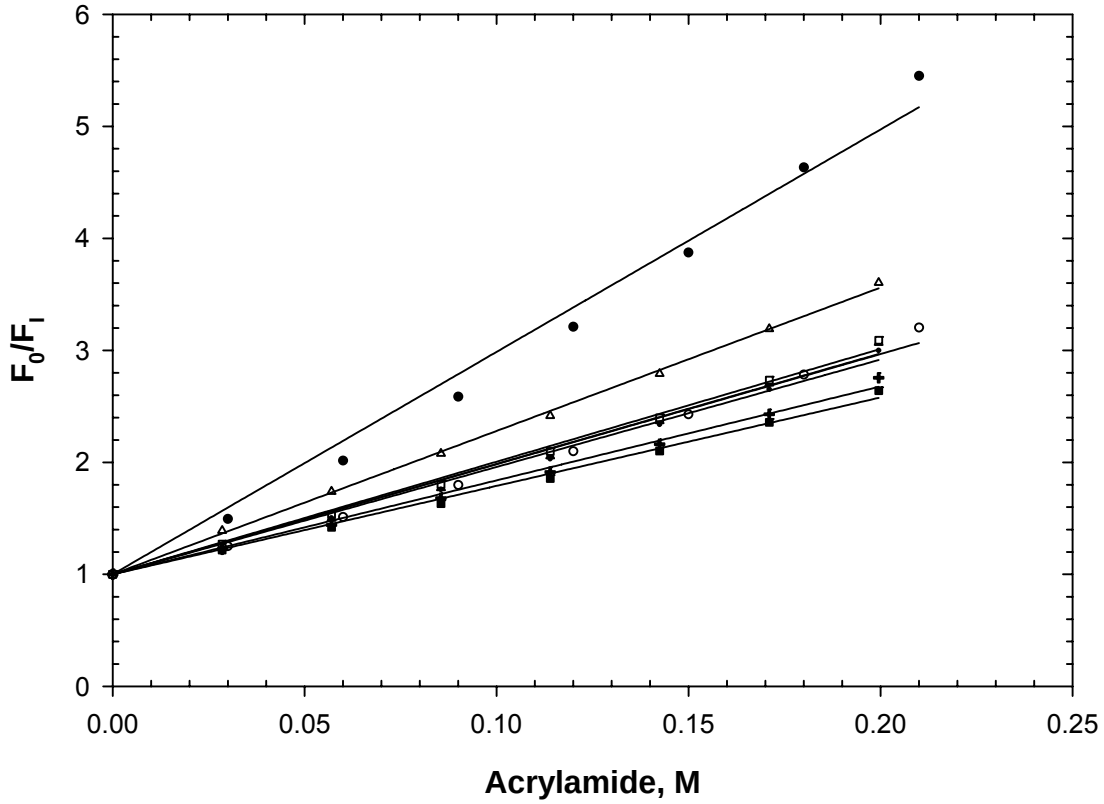

Figure 58. Acrylamide quenching of fluorescence (300 nm excitation, 350 nm emission) of the peptides (10 μM) in 7.6 M urea, 10 mM TCEP, pH 7.0, and 25 °C. The data represent the following peptides: NATA (closed circles), AWA (open circles), AAWAA (closed triangles), WVSGT (D1W; open triangles), GYWHE (Y52W; closed squares), HEWTV (Y55W; open squares), EAWQE (T76W; dots), and DYWTG (Y81W; plus symbols).

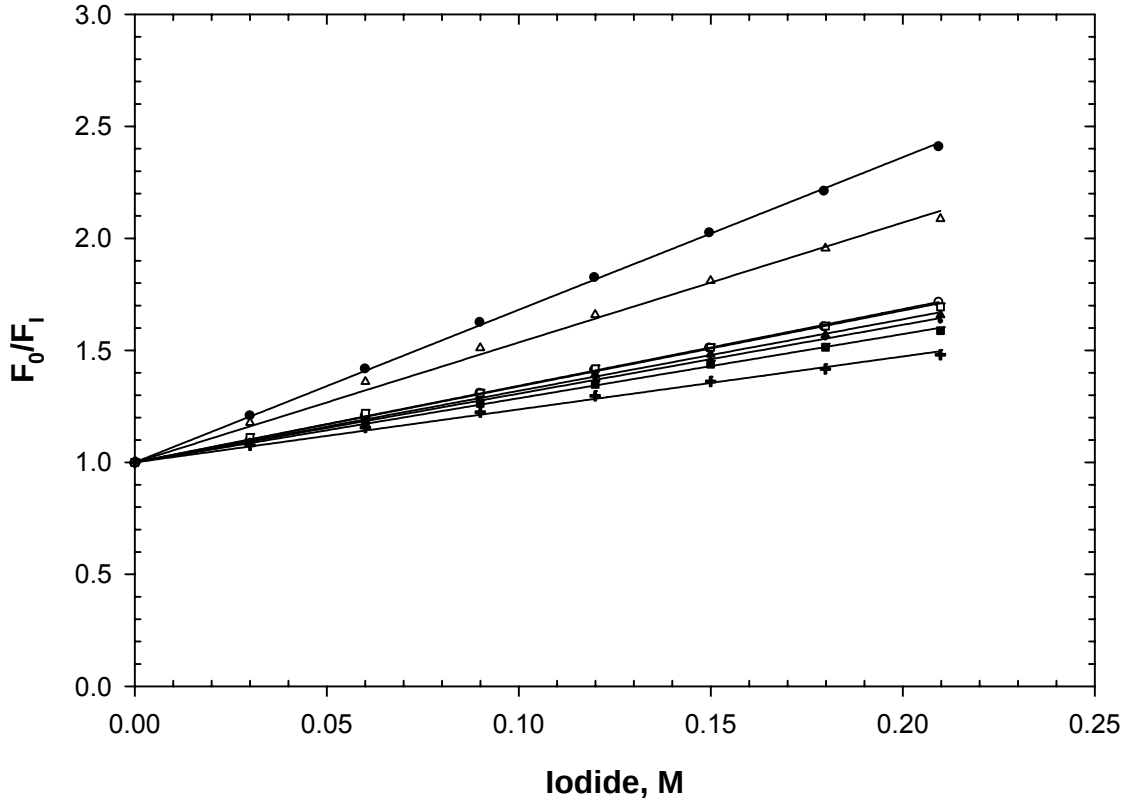

Figure 59. Iodide quenching of fluorescence (300 nm excitation, 350 nm emission) of the peptides (10 μM) in 3.8 M GdnHCl, 10 mM TCEP, pH 7.0, and 25 °C. The data represent the following peptides: NATA (closed circles), AWA (open circles), AAWAA (closed triangles), WVSGT (D1W; open triangles), GYWHE (Y52W; closed squares), HEWTV (Y55W; open squares), EAWQE (T76W; dots), and DYWTG (Y81W; plus symbols).

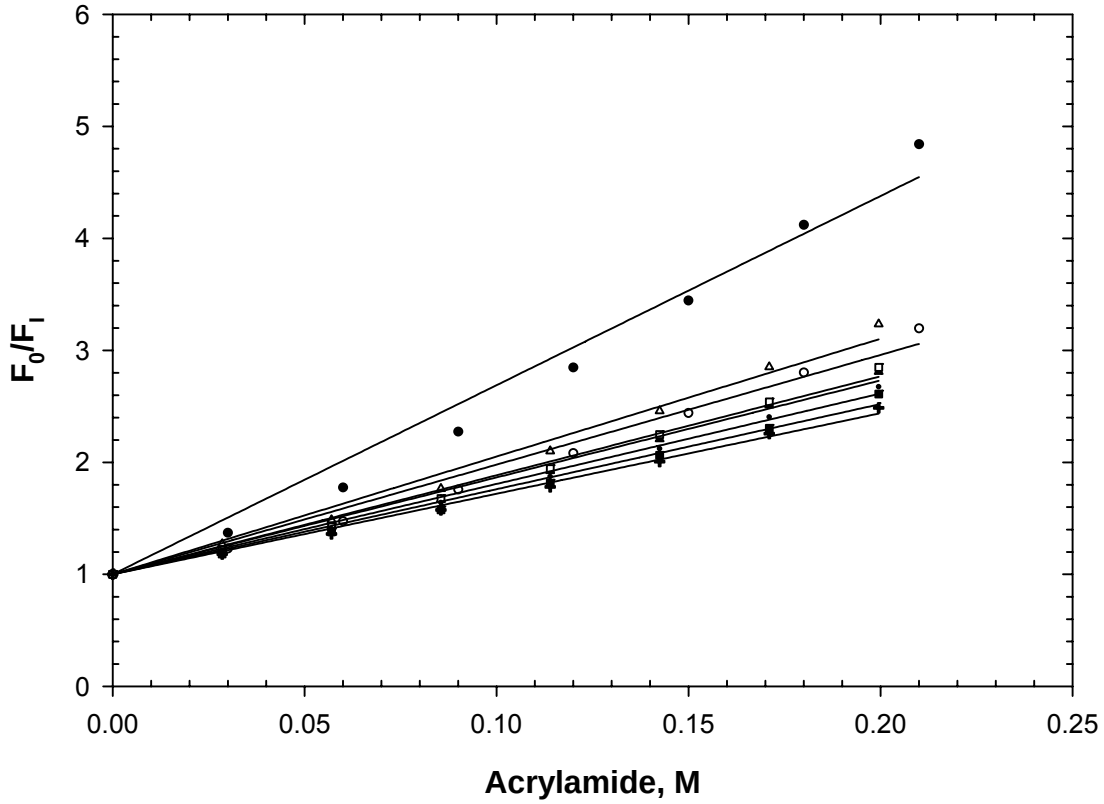

Figure 60. Acrylamide quenching of fluorescence (300 nm excitation, 350 nm emission) of the peptides (10 μM) in 3.8 M GdnHCl, 10 mM TCEP, pH 7.0, and 25 °C. The data represent the following peptides: NATA (closed circles), AWA (open circles), AAWAA (closed triangles), WVSGT (D1W; open triangles), GYWHE (Y52W; closed squares), HEWTV (Y55W; open squares), EAWQE (T76W; dots), and DYWTG (Y81W; plus symbols).

APPENDIX C

PROTEIN DENATURED STATES, pH 7.0

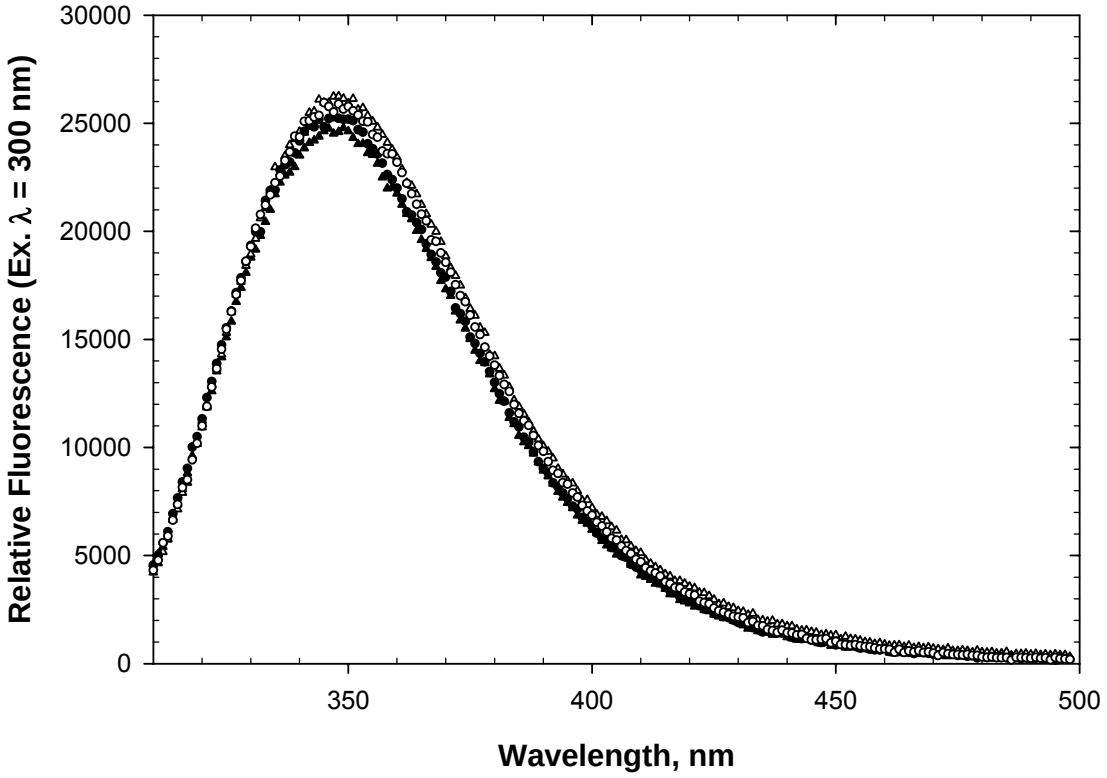

Figure 61. Fluorescence emission spectra (300 nm excitation) of denatured RNase Sa D1W (10 mM) in 8.5 M urea, pH 7.0, and 25 °C. The scans represent the following conditions: reduced, wild-type background (open circles), oxidized wild-type background (closed circles), reduced charge-reversal background (open triangles), and oxidized charge-reversal background (open triangles).

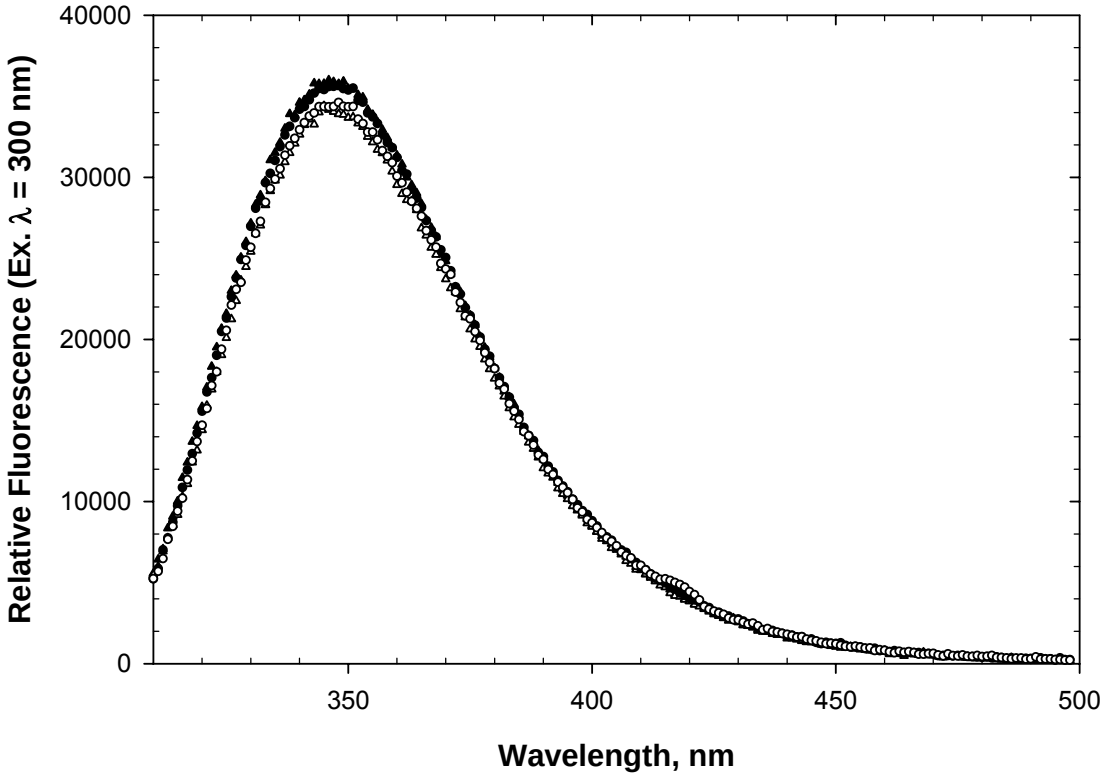

Figure 62. Fluorescence emission spectra (300 nm excitation) of denatured RNase Sa Y52W (10 μM) in 8.5 M urea, pH 7.0, and 25 °C. The scans represent the following conditions: reduced, wild-type background (open circles), oxidized wild-type background (closed circles), reduced charge-reversal background (open triangles), and oxidized charge-reversal background (open triangles).

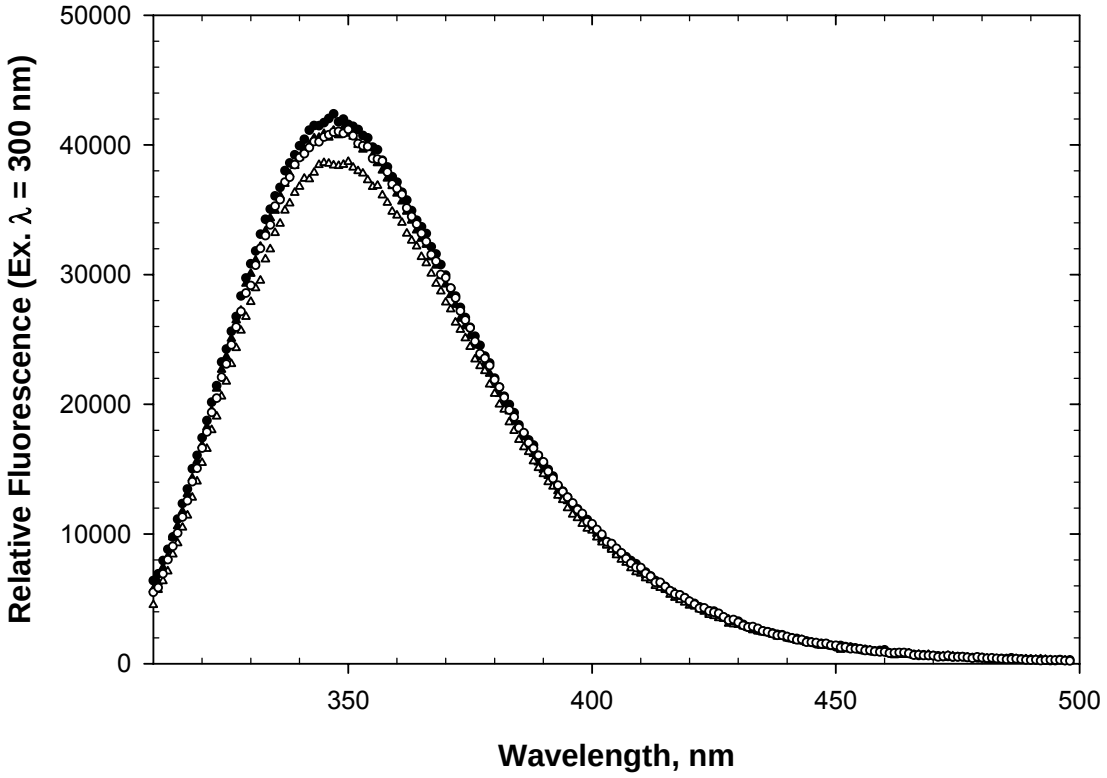

Figure 63. Fluorescence emission spectra (300 nm excitation) of denatured RNase Sa Y55W (10 μM) in 8.5 M urea, pH 7.0, and 25 °C. The scans represent the following conditions: reduced, wild-type background (open circles), oxidized wild-type background (closed circles), reduced charge-reversal background (open triangles), and oxidized charge-reversal background (open triangles).

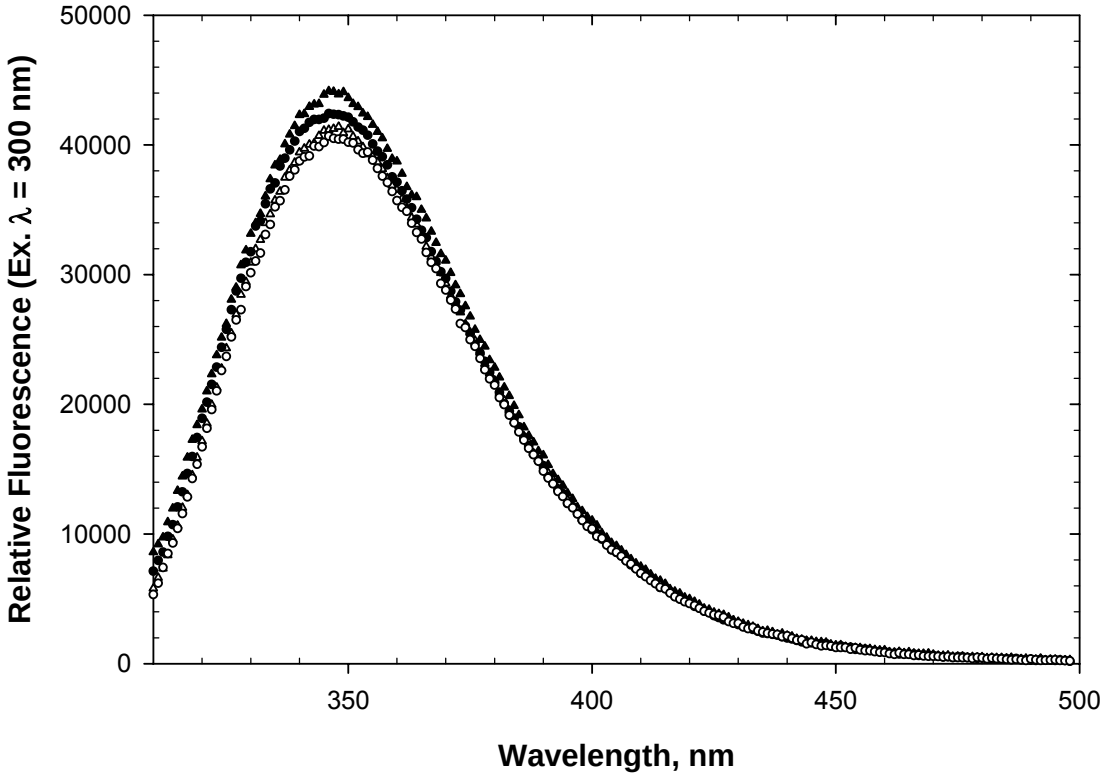

Figure 64. Fluorescence emission spectra (300 nm excitation) of denatured RNase Sa T76W (10 μM) in 8.5 M urea, pH 7.0, and 25 °C. The scans represent the following conditions: reduced, wild-type background (open circles), oxidized wild-type background (closed circles), reduced charge-reversal background (open triangles), and oxidized charge-reversal background (open triangles).

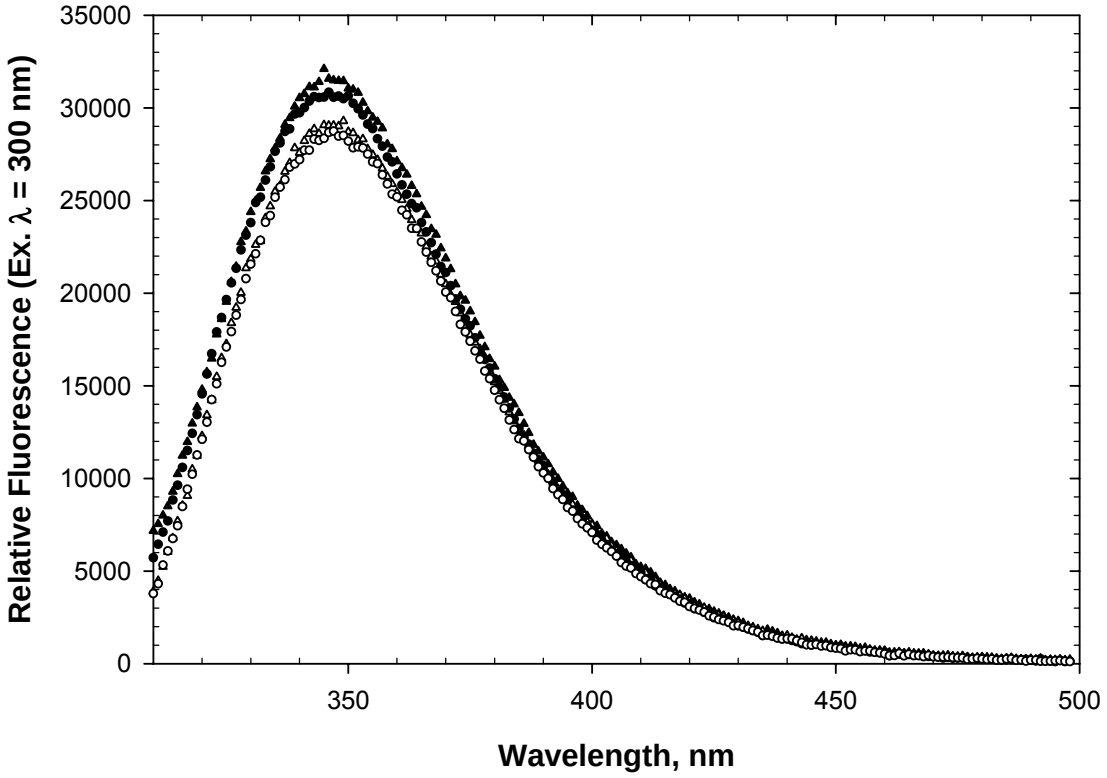

Figure 65. Fluorescence emission spectra (300 nm excitation) of denatured RNase Sa Y81W (10 μM) in 8.5 M urea, pH 7.0, and 25 °C. The scans represent the following conditions: reduced, wild-type background (open circles), oxidized wild-type background (closed circles), reduced charge-reversal background (open triangles), and oxidized charge-reversal background (open triangles).

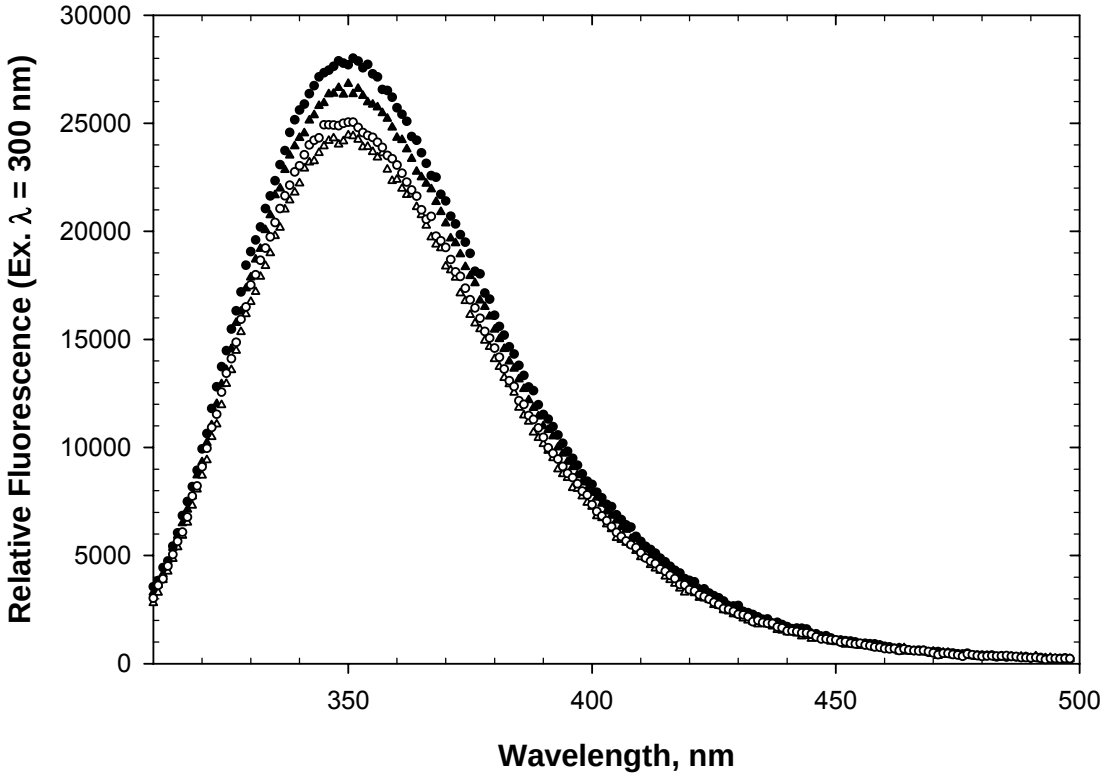

Figure 66. Fluorescence emission spectra (300 nm excitation) of denatured RNase Sa D1W (10 μM) in 6 M guanidine hydrochloride, pH 7.0, and 25 °C. The scans represent the following conditions: reduced, wild-type background (open circles), oxidized wild-type background (closed circles), reduced charge-reversal background (open triangles), and oxidized charge-reversal background (open triangles).

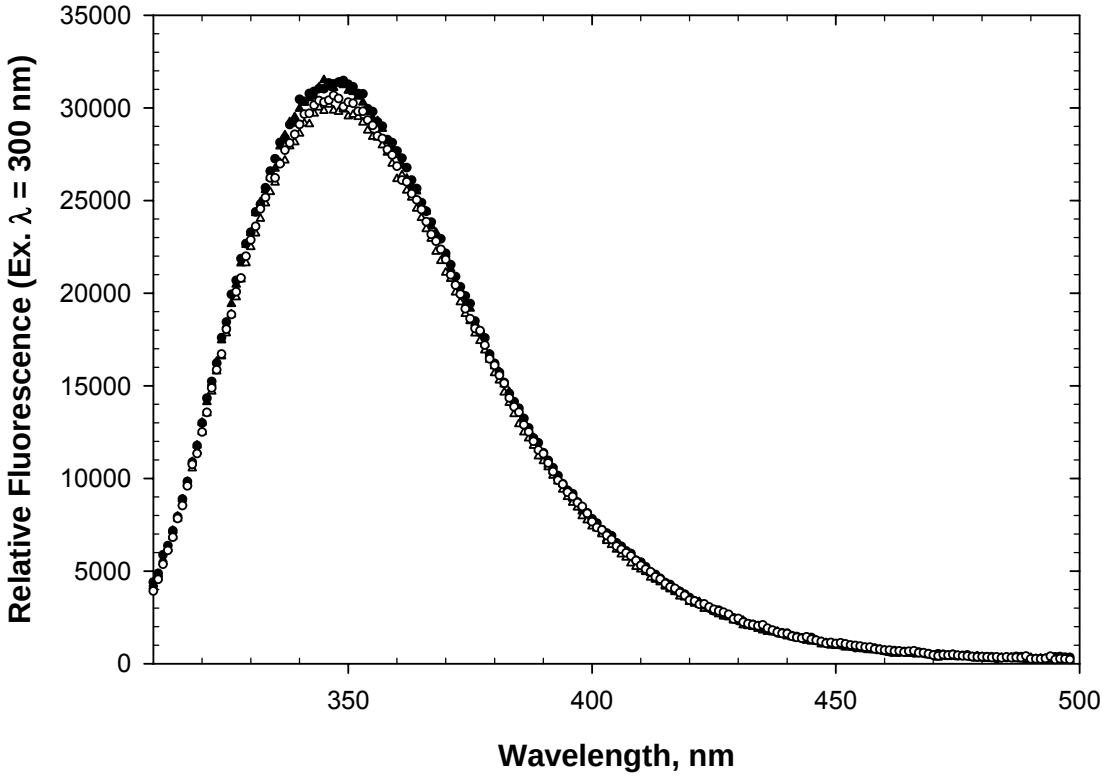

Figure 67. Fluorescence emission spectra (300 nm excitation) of denatured RNase Sa Y52W (10 μM) in 6 M guanidine hydrochloride, pH 7.0, and 25 °C. The scans represent the following conditions: reduced, wild-type background (open circles), oxidized wild-type background (closed circles), reduced charge-reversal background (open triangles), and oxidized charge-reversal background (open triangles).

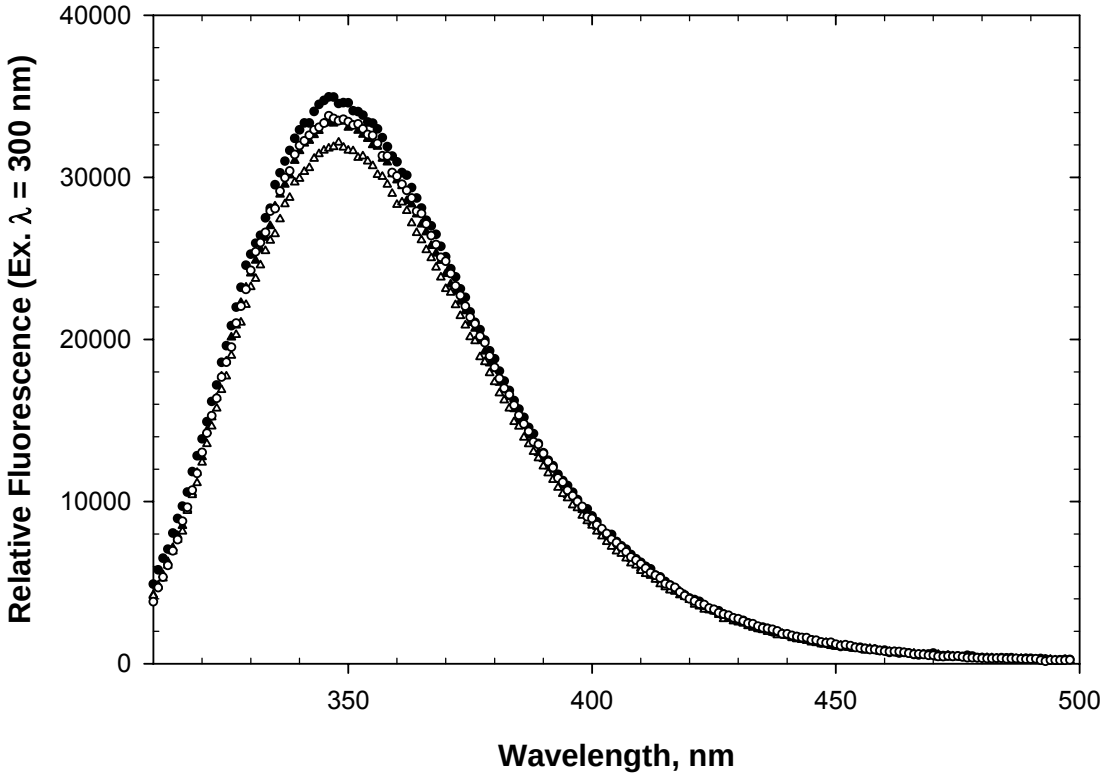

Figure 68. Fluorescence emission spectra (300 nm excitation) of denatured RNase Sa Y55W (10 μM) in 6 M guanidine hydrochloride, pH 7.0, and 25 °C. The scans represent the following conditions: reduced, wild-type background (open circles), oxidized wild-type background (closed circles), reduced charge-reversal background (open triangles), and oxidized charge-reversal background (open triangles).

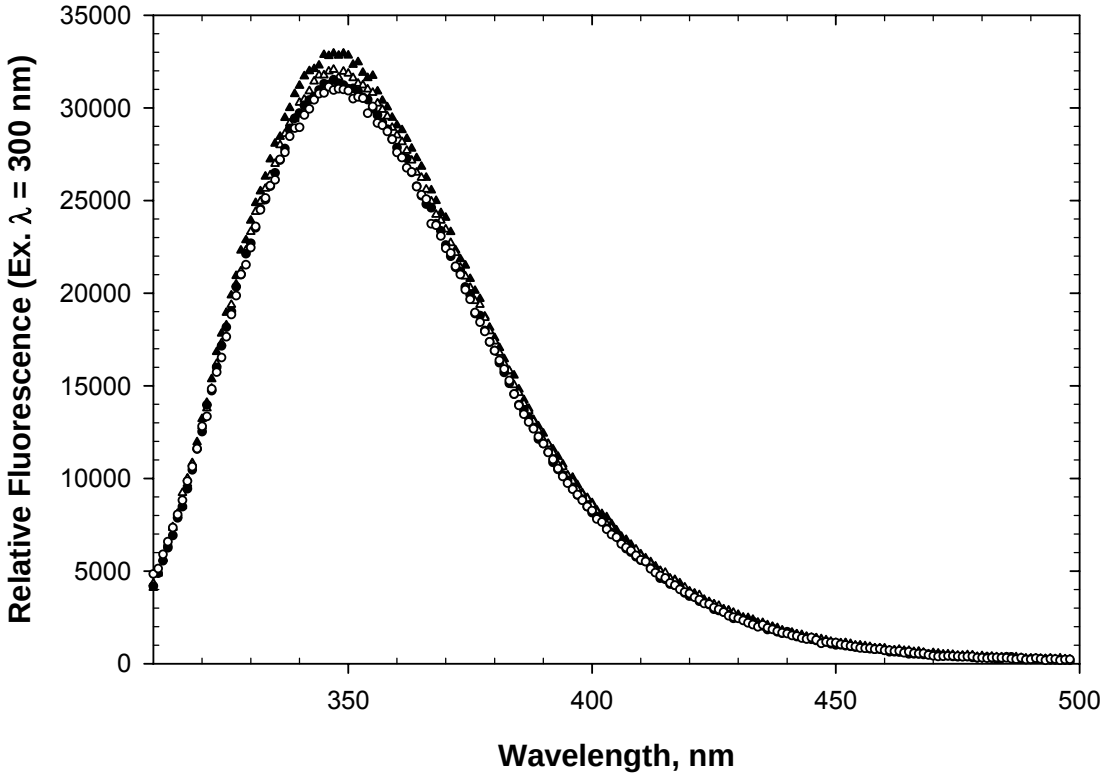

Figure 69. Fluorescence emission spectra (300 nm excitation) of denatured RNase Sa T76W (10 μM) in 6 M guanidine hydrochloride, pH 7.0, and 25 °C. The scans represent the following conditions: reduced, wild-type background (open circles), oxidized wild-type background (closed circles), reduced charge-reversal background (open triangles), and oxidized charge-reversal background (open triangles).

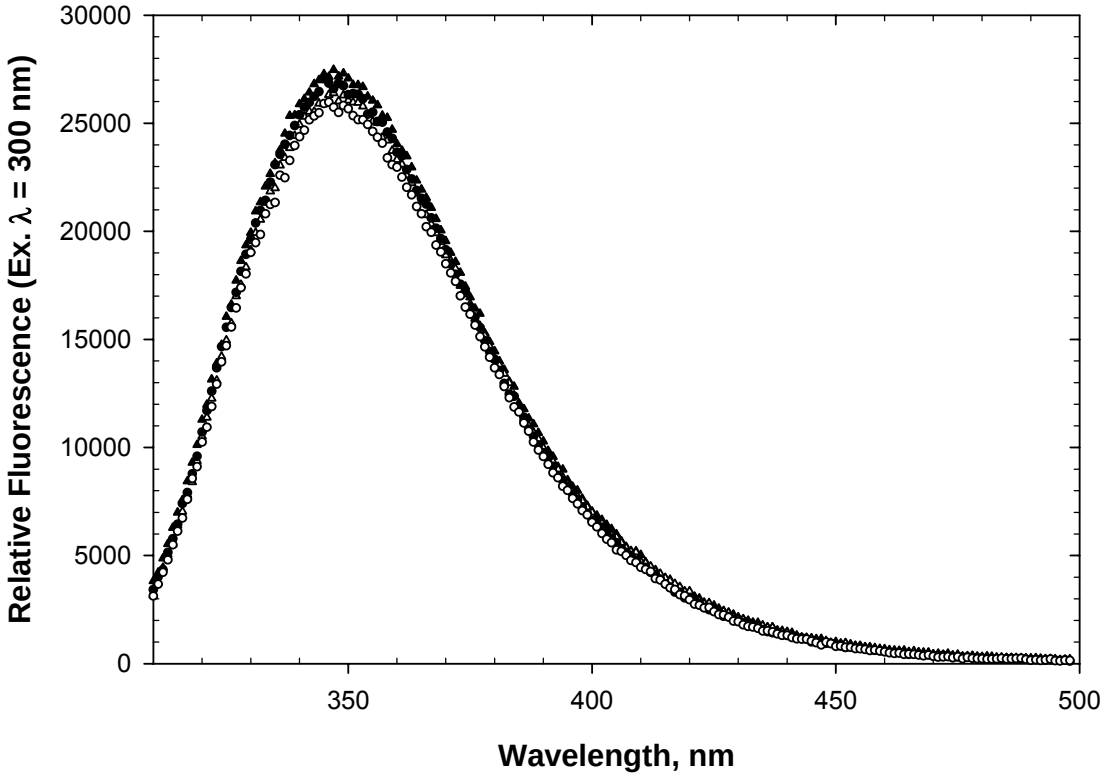

Figure 70. Fluorescence emission spectra (300 nm excitation) of denatured RNase Sa Y81W (10 μM) in 6 M guanidine hydrochloride, pH 7.0, and 25 °C. The scans represent the following conditions: reduced, wild-type background (open circles), oxidized wild-type background (closed circles), reduced charge-reversal background (open triangles), and oxidized charge-reversal background (open triangles).

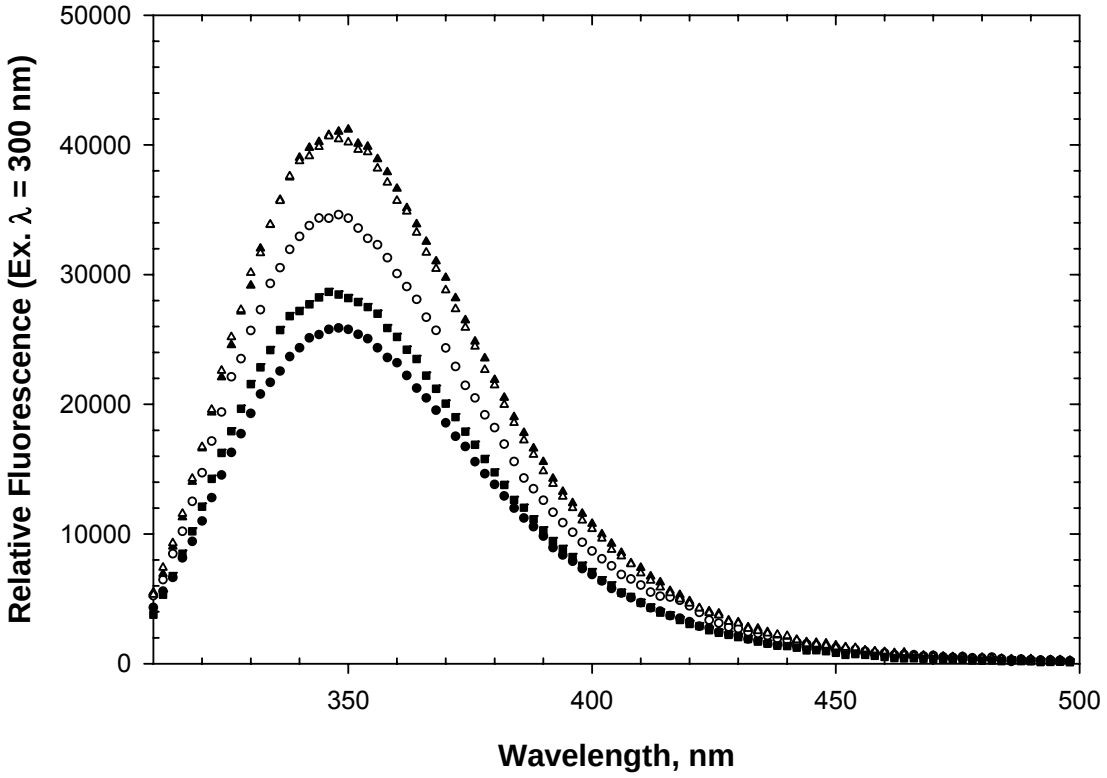

Figure 71. Fluorescence emission spectra (300 nm excitation) of all the reduced, denatured RNase Sa tryptophan variants (10 μM) in the wild-type background in 8.5 M urea, 10 mM TCEP, pH 7.0, and 25 ^{o}C. The scans represent the following variants: D1W (closed circles), Y52W (open circles), Y55W (closed triangles), T76W (open triangles), and Y81W (closed squares).

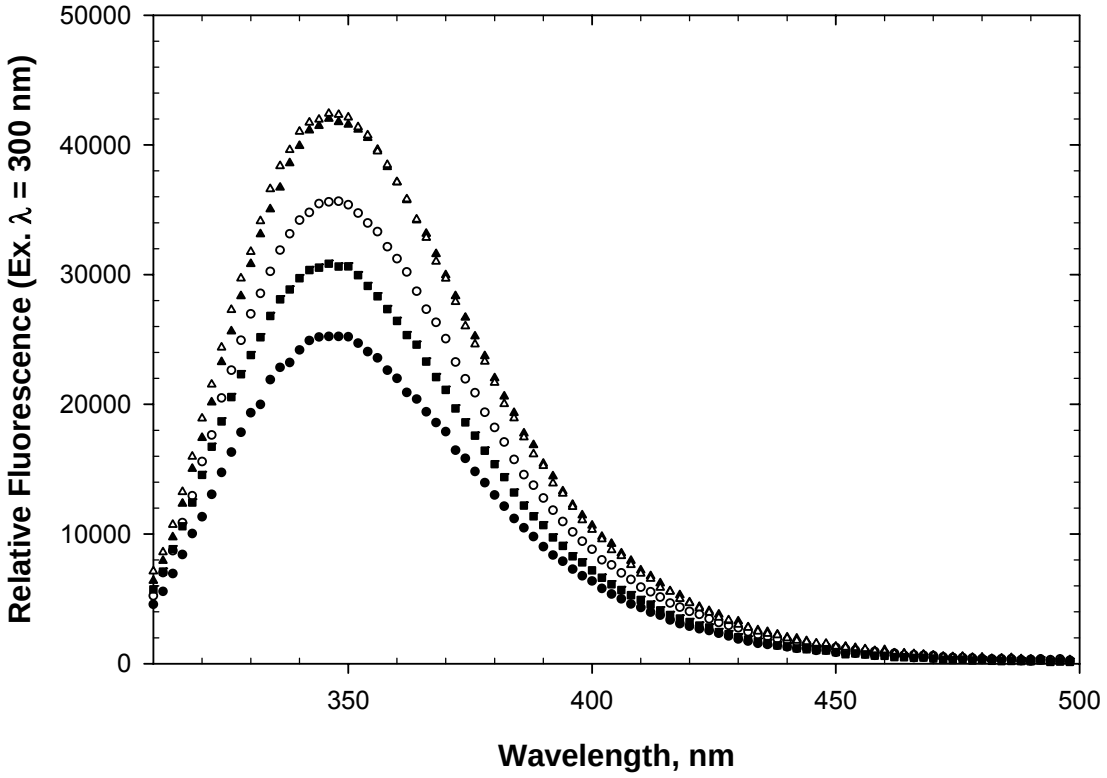

Figure 72. Fluorescence emission spectra (300 nm excitation) of all the oxidized, denatured RNase Sa tryptophan variants (10 μM) in the wild-type background in 8.5 M urea, pH 7.0, and 25 °C. The scans represent the following variants: D1W (closed circles), Y52W (open circles), Y55W (closed triangles), T76W (open triangles), and Y81W (closed squares).

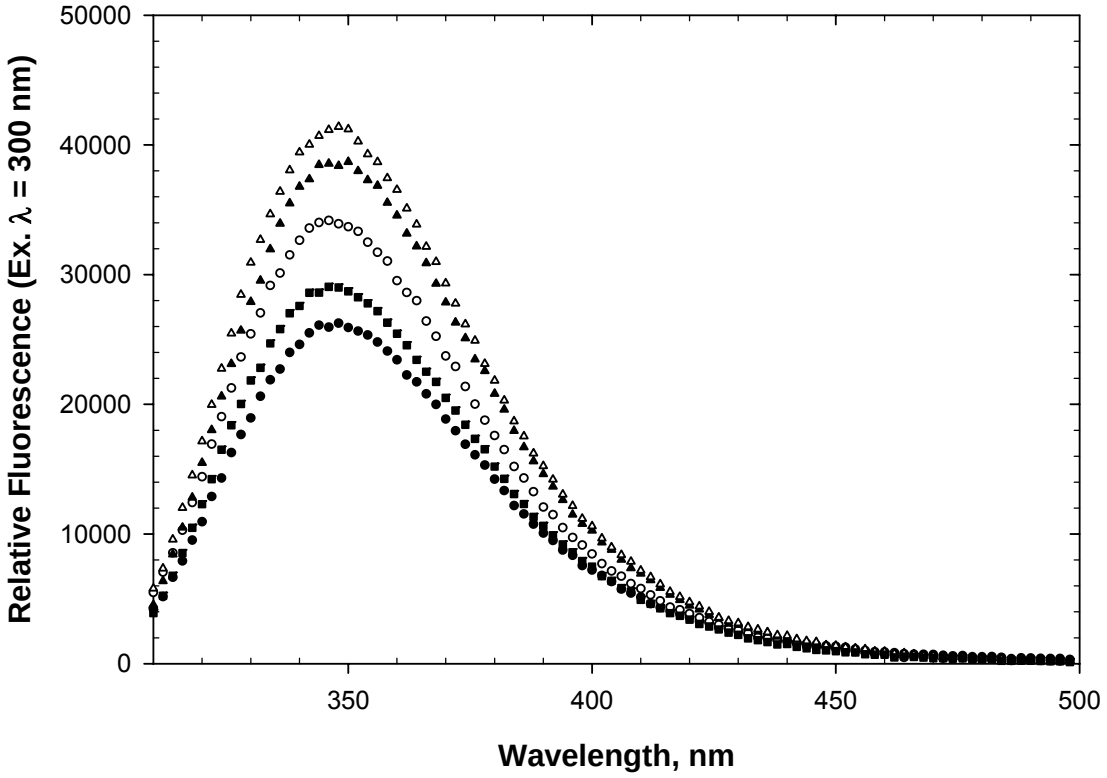

Figure 73. Fluorescence emission spectra (300 nm excitation) of all the reduced, denatured RNase Sa tryptophan variants (10 μM) in the charge-reversal background in 8.5 M urea, 10 mM TCEP, pH 7.0, and 25 °C. The scans represent the following variants: D1W (closed circles), Y52W (open circles), Y55W (closed triangles), T76W (open triangles), and Y81W (closed squares).

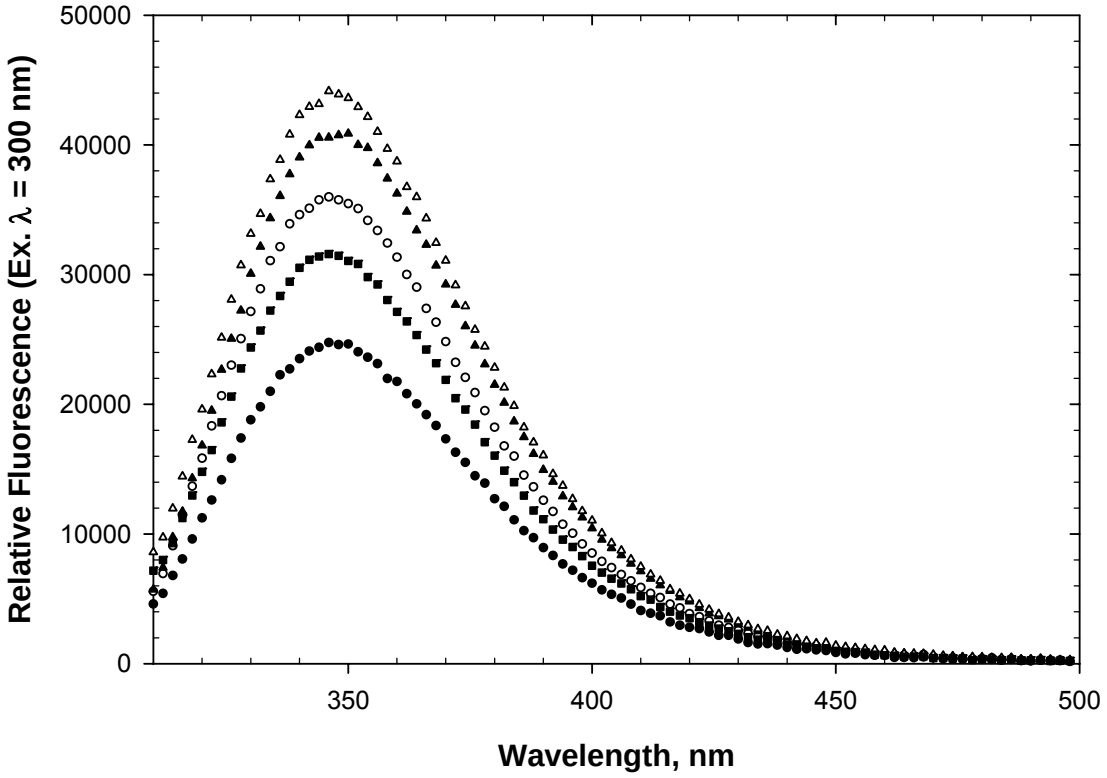

Figure 74. Fluorescence emission spectra (300 nm excitation) of all the oxidized, denatured RNase Sa tryptophan variants (10 μM) in the charge-reversal background in 8.5 M urea, pH 7.0, and 25 ^{o}C. The scans represent the following variants: D1W (closed circles), Y52W (open circles), Y55W (closed triangles), T76W (open triangles), and Y81W (closed squares).

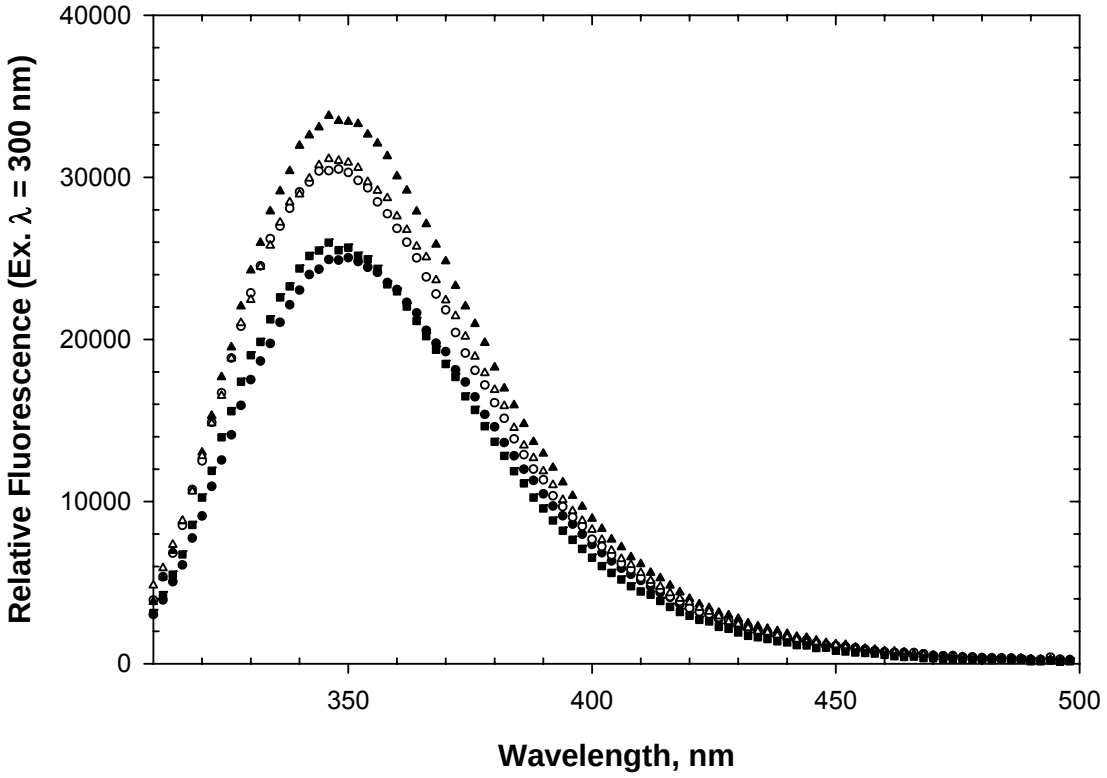

Figure 75. Fluorescence emission spectra (300 nm excitation) of all the reduced, denatured RNase Sa tryptophan variants (10 μM) in the wild-type background in 6 M guanidine hydrochloride, 10 mM TCEP, pH 7.0, and 25 °C. The scans represent the following variants: D1W (closed circles), Y52W (open circles), Y55W (closed triangles), T76W (open triangles), and Y81W (closed squares).

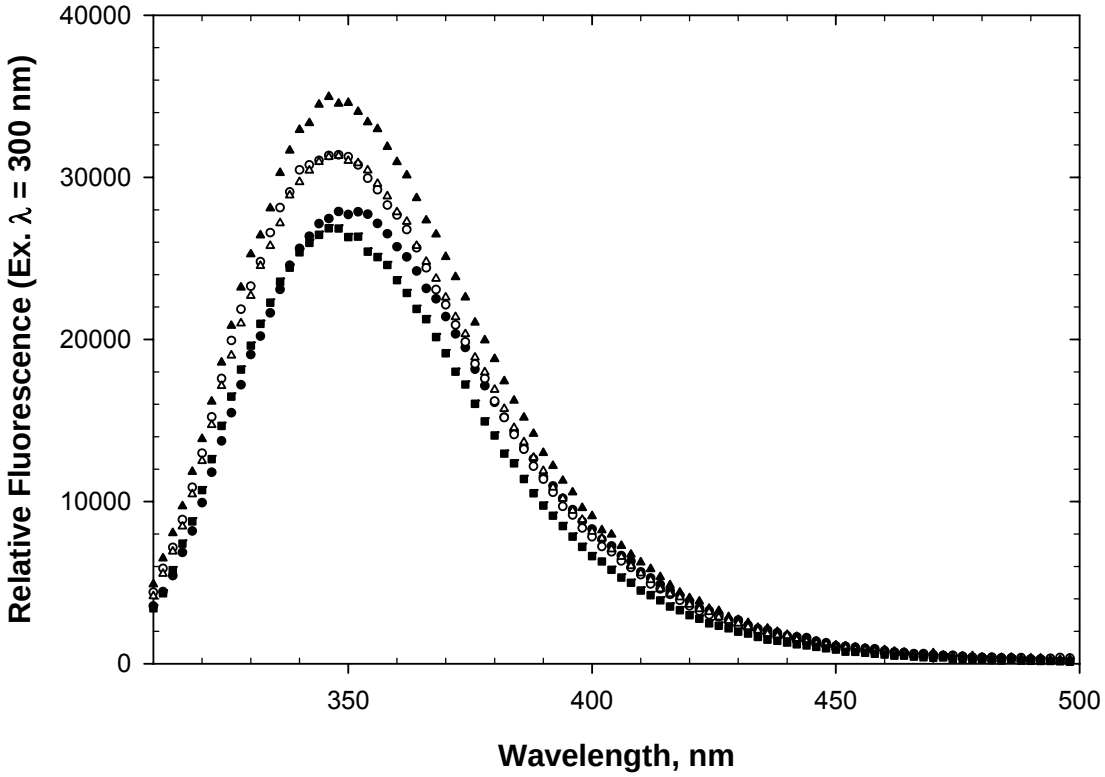

Figure 76. Fluorescence emission spectra (300 nm excitation) of all the oxidized, denatured RNase Sa tryptophan variants (10 μM) in the wild-type background in 6 M guanidine hydrochloride, pH 7.0, and 25 °C. The scans represent the following variants: D1W (closed circles), Y52W (open circles), Y55W (closed triangles), T76W (open triangles), and Y81W (closed squares).

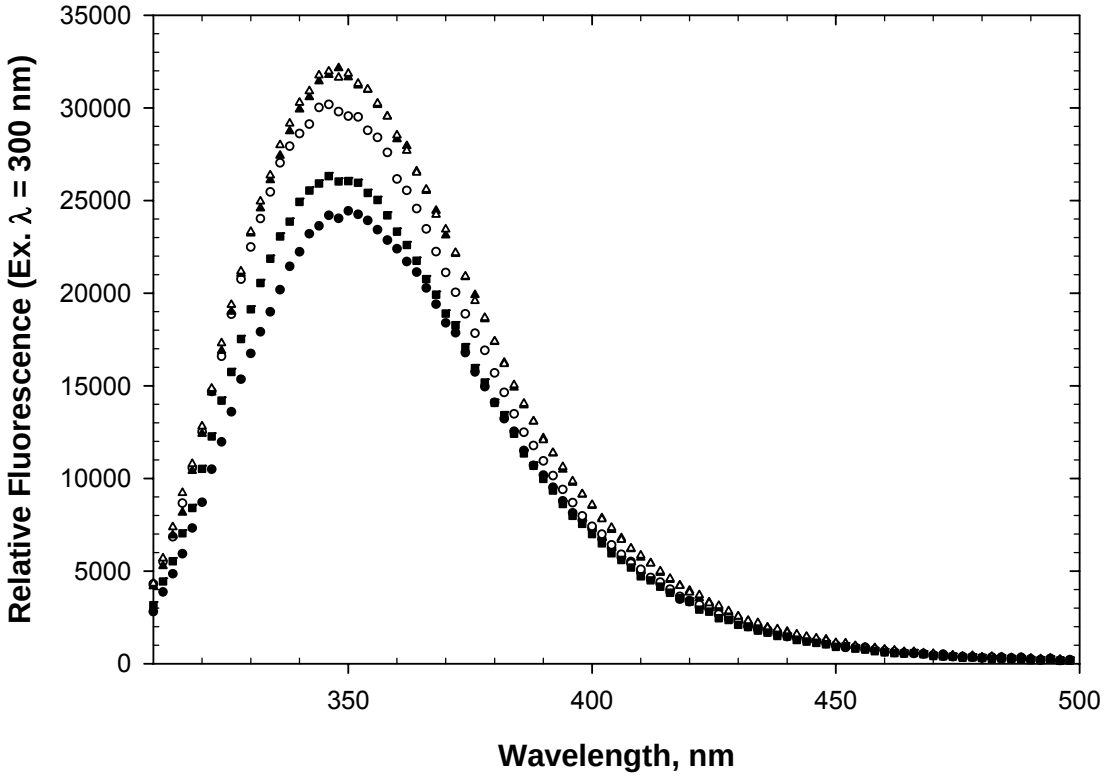

Figure 77. Fluorescence emission spectra (300 nm excitation) of all the reduced, denatured RNase Sa tryptophan variants (10 μM) in the charge-reversal background in 6 M guanidine hydrochloride, 10 mM TCEP, pH 7.0, and 25 ^{o}C. The scans represent the following variants: D1W (closed circles), Y52W (open circles), Y55W (closed triangles), T76W (open triangles), and Y81W (closed squares).

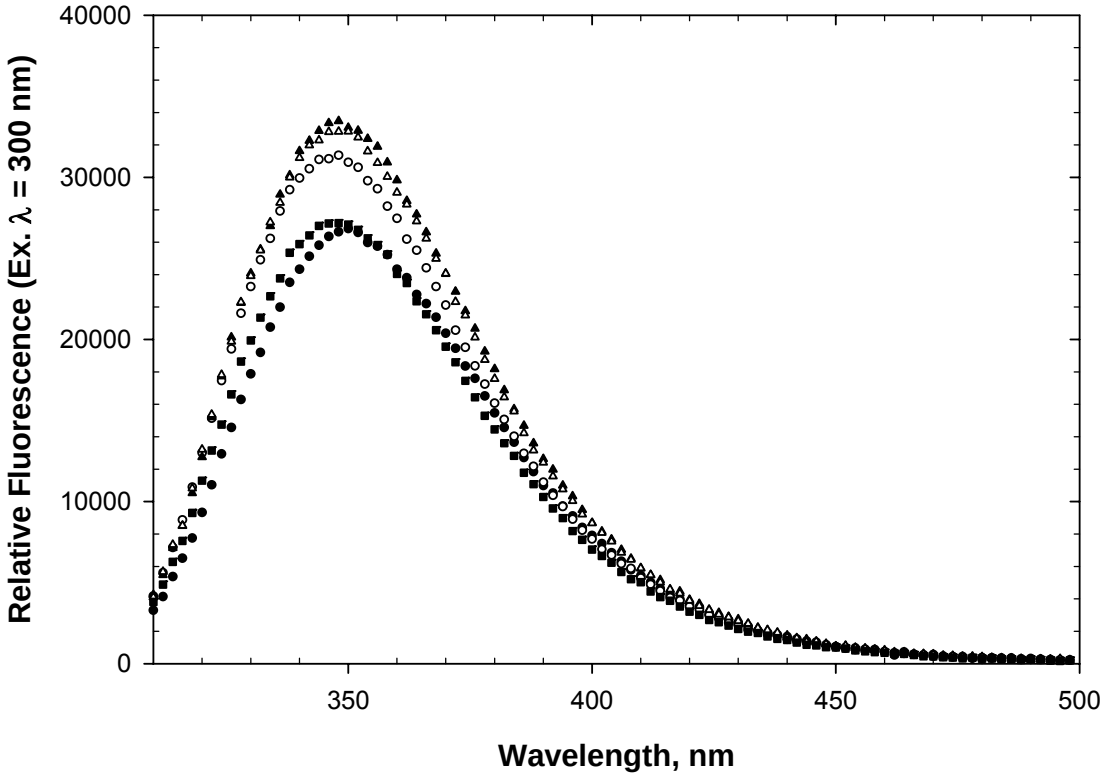

Figure 78. Fluorescence emission spectra (300 nm excitation) of all the oxidized, denatured RNase Sa tryptophan variants (10 μM) in the charge-reversal background in 6 M guanidine hydrochloride, pH 7.0, and 25 ^{o}C. The scans represent the following variants: D1W (closed circles), Y52W (open circles), Y55W (closed triangles), T76W (open triangles), and Y81W (closed squares).

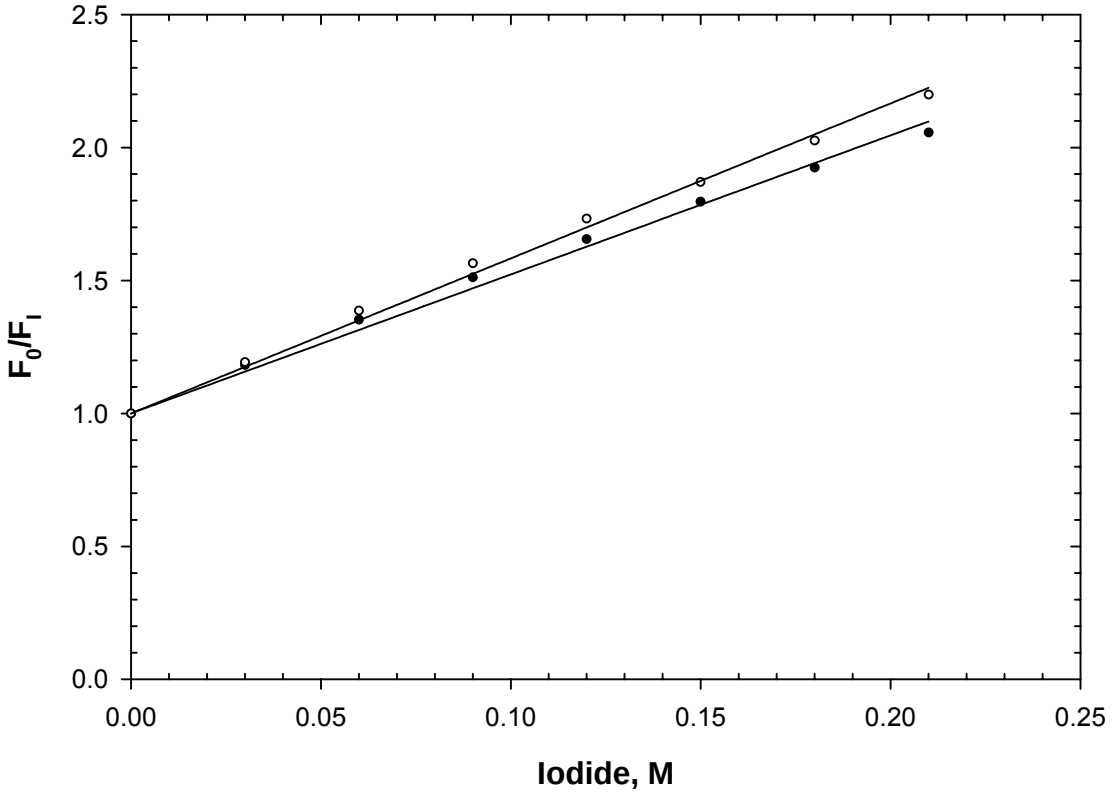

Figure 79. Iodide quenching of fluorescence (300 nm excitation, 350 nm emission) of reduced, denatured RNase Sa D1W (10 μM) in 7.6 M urea, 10 mM TCEP, pH 7.0, and 25 °C. The data represent the following variants: Wild-type background (closed circles) and charge-reversal background (open circles).

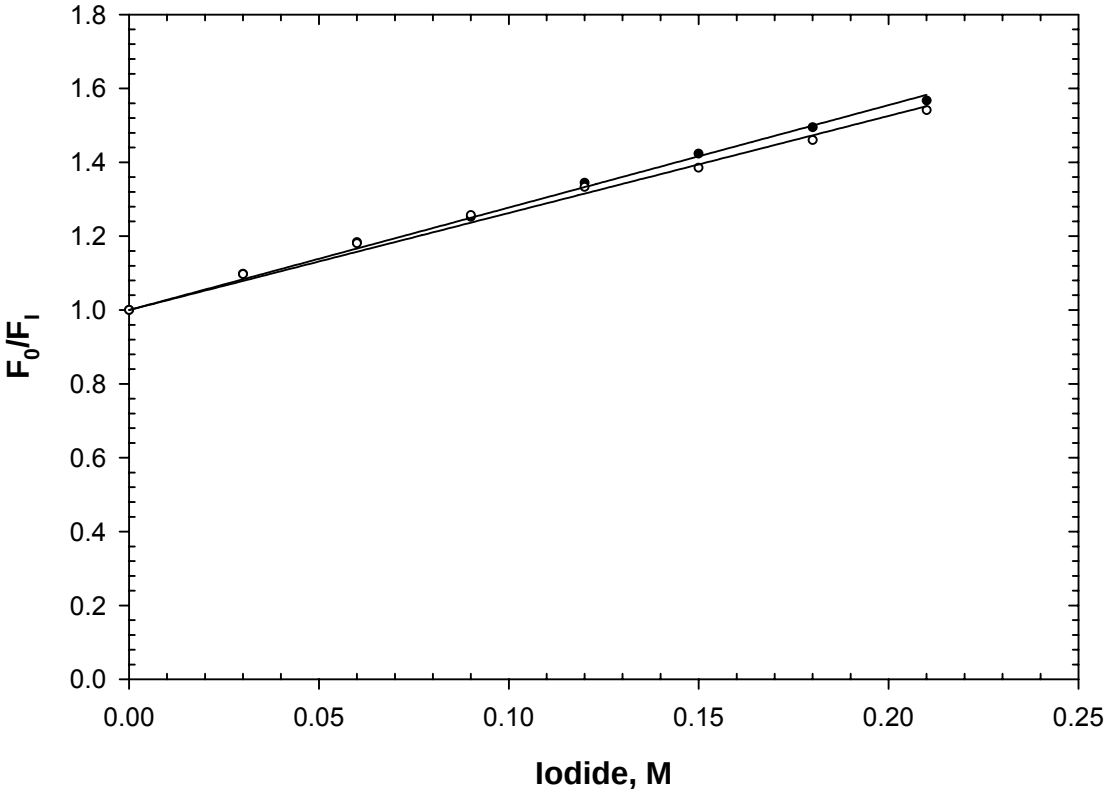

Figure 80. Iodide quenching of fluorescence (300 nm excitation, 350 nm emission) of reduced, denatured RNase Sa Y52W (10 μM) in 7.6 M urea, 10 mM TCEP, pH 7.0, and 25 ^{o}C. The data represent the following variants: Wild-type background (closed circles) and charge-reversal background (open circles).

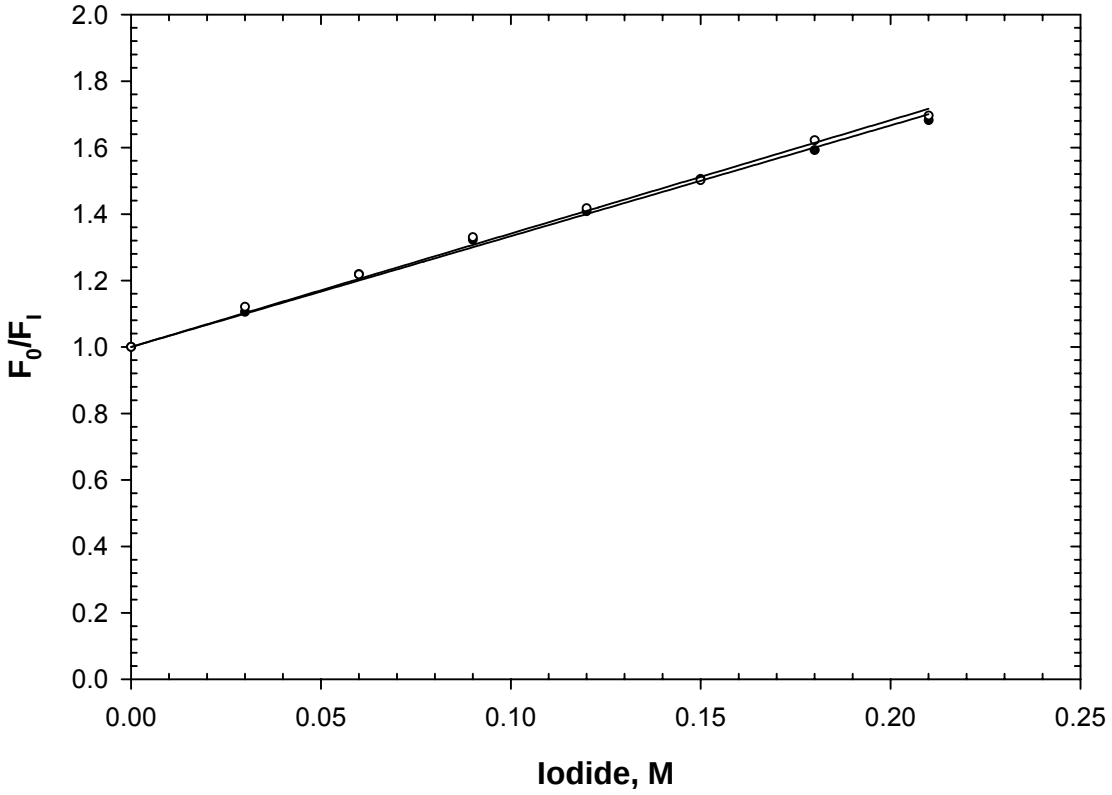

Figure 81. Iodide quenching of fluorescence (300 nm excitation, 350 nm emission) of reduced, denatured RNase Sa Y55W (10 μM) in 7.6 M urea, 10 mM TCEP, pH 7.0, and 25 ^{o}C. The data represent the following variants: Wild-type background (closed circles) and charge-reversal background (open circles).

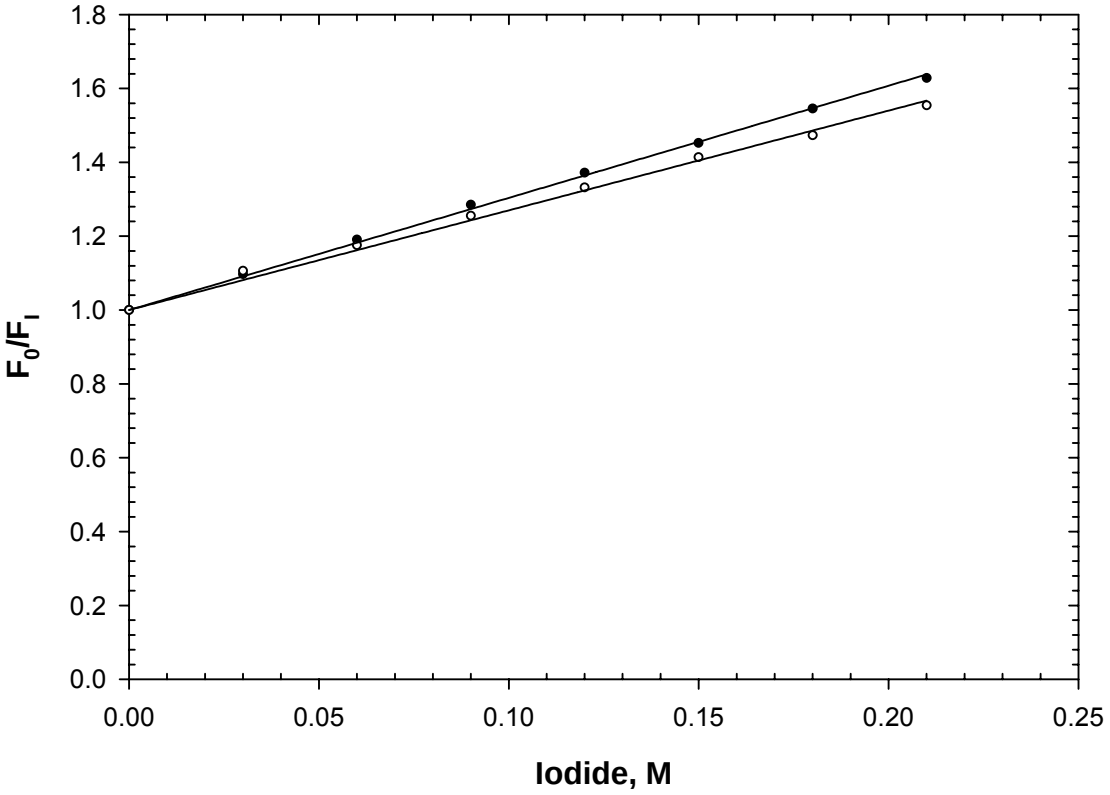

Figure 82. Iodide quenching of fluorescence (300 nm excitation, 350 nm emission) of reduced, denatured RNase Sa T76W (10 μM) in 7.6 M urea, 10 mM TCEP, pH 7.0, and 25 ^{o}C. The data represent the following variants: Wild-type background (closed circles) and charge-reversal background (open circles).

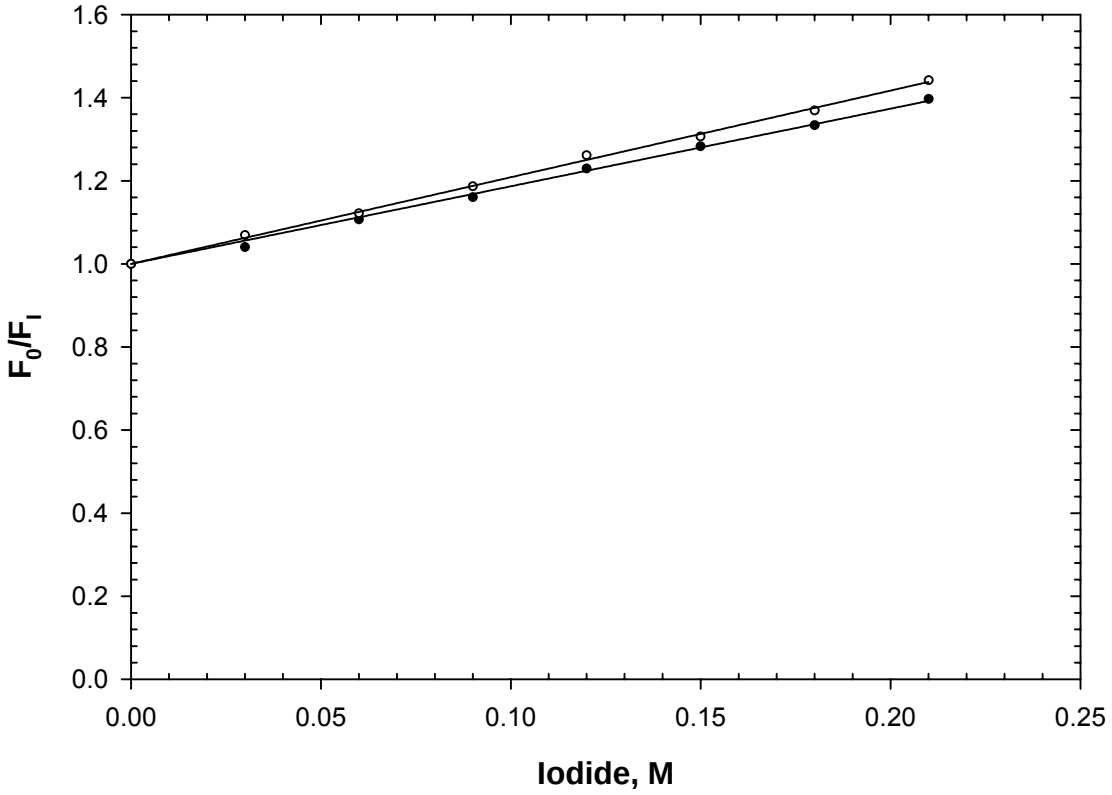

Figure 83. Iodide quenching of fluorescence (300 nm excitation, 350 nm emission) of reduced, denatured RNase Sa Y81W (10 μM) in 7.6 M urea, 10 mM TCEP, pH 7.0, and 25 °C. The data represent the following variants: Wild-type background (closed circles) and charge-reversal background (open circles).

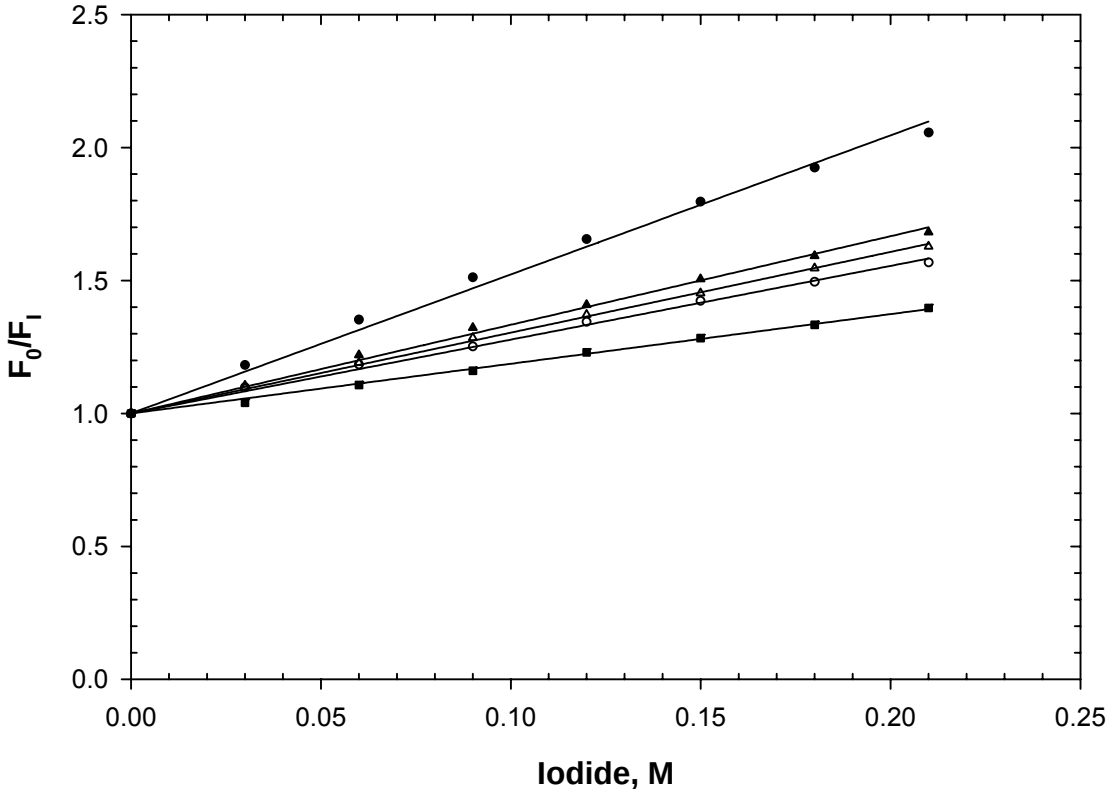

Figure 84. Iodide quenching of fluorescence (300 nm excitation, 350 nm emission) of the reduced, denatured RNase Sa tryptophan variants (10 μM) in the wild-type background in 7.6 M urea, 10 mM TCEP, pH 7.0, and 25 °C. The data represent the following variants: D1W (closed circles), Y52W (open circles), Y55W (closed triangles), T76W (open triangles), and Y81W (closed squares).

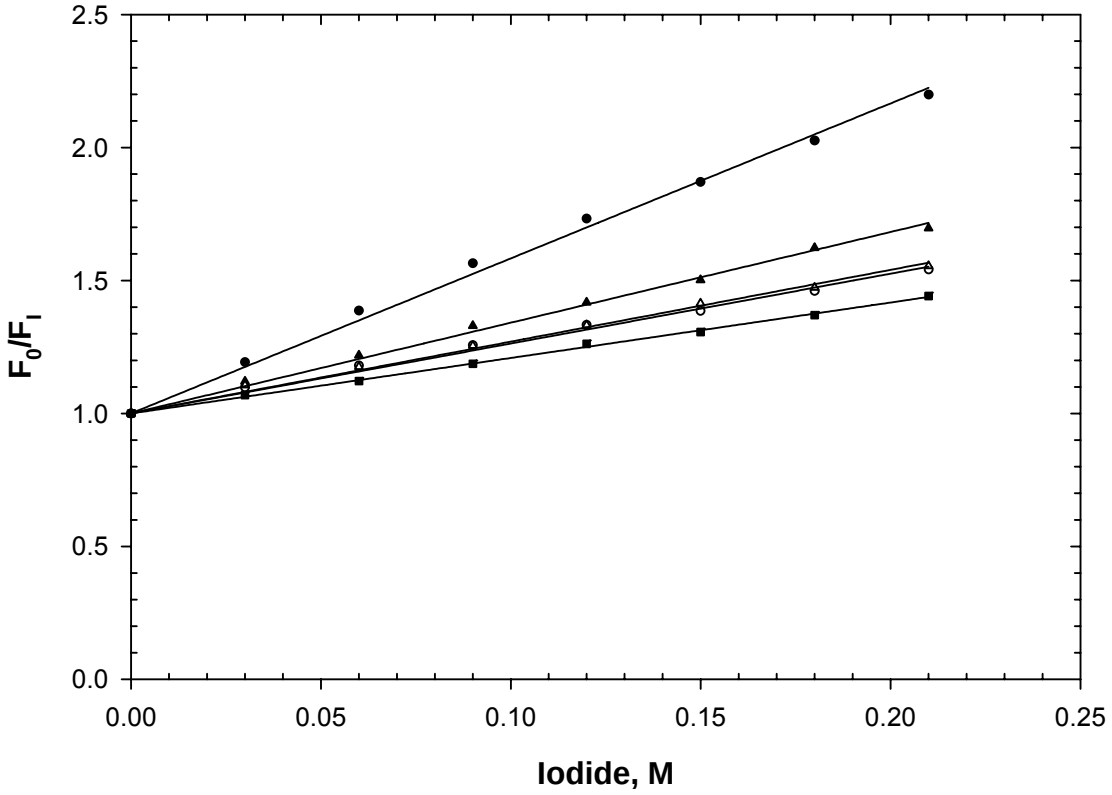

Figure 85. Iodide quenching of fluorescence (300 nm excitation, 350 nm emission) of the reduced, denatured RNase Sa tryptophan variants (10 μM) in the charge-reversal background in 7.6 M urea, 10 mM TCEP, pH 7.0, and 25 °C. The data represent the following variants: D1W (closed circles), Y52W (open circles), Y55W (closed triangles), T76W (open triangles), and Y81W (closed squares).

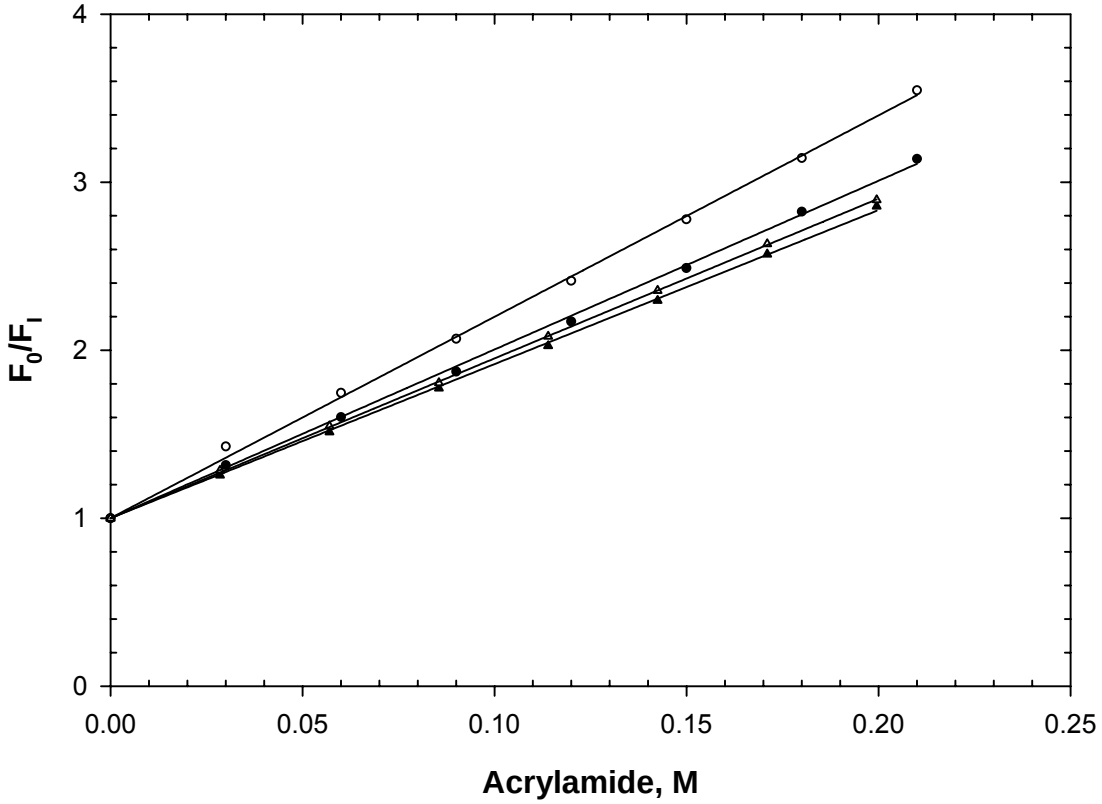

Figure 86. Acrylamide quenching of fluorescence (300 nm excitation, 350 nm emission) of denatured RNase Sa D1W (10 μM) in 7.6 M (reduced) or 8.5 M (oxidized) urea, pH 7.0, and 25 °C. The data represent the following variants: Wild-type background, reduced (closed circles), charge-reversal background, reduced (open circles), wild-type background, oxidized (closed triangles), and charge-reversal background, oxidized (open triangles).

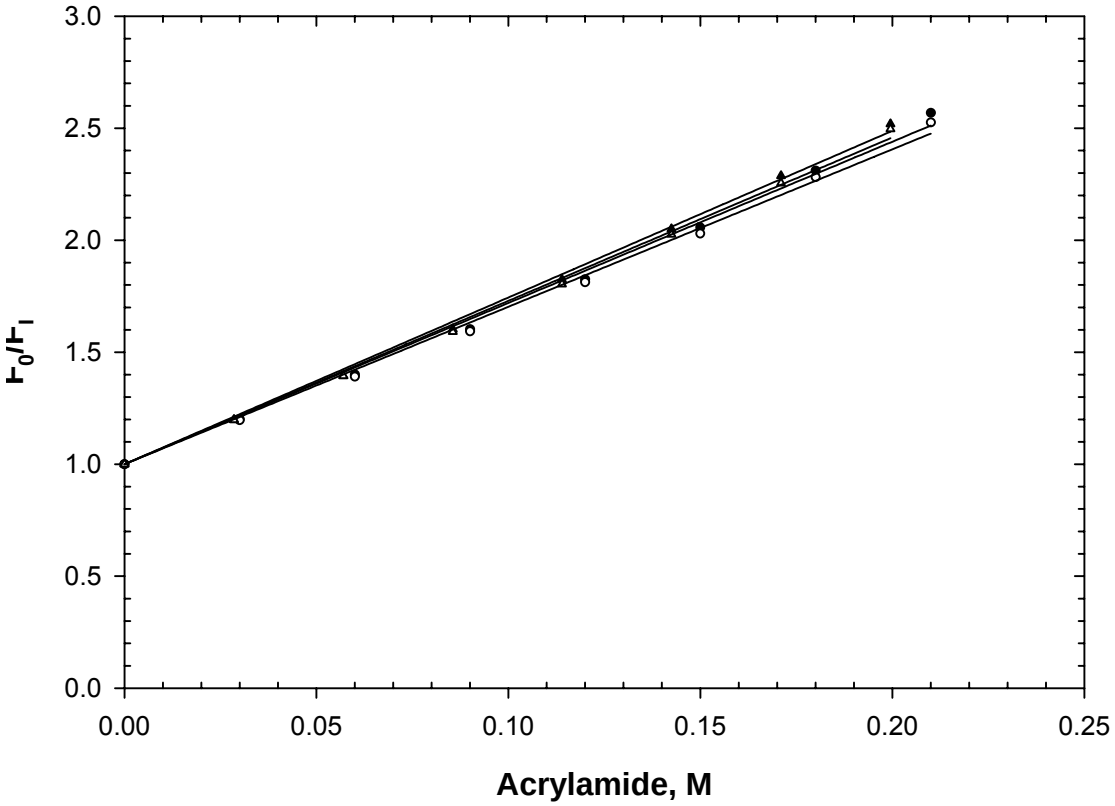

Figure 87. Acrylamide quenching of fluorescence (300 nm excitation, 350 nm emission) of denatured RNase Sa Y52W (10 μM) in 7.6 M (reduced) or 8.5 M (oxidized) urea, pH 7.0, and 25 °C. The data represent the following variants: Wild-type background, reduced (closed circles), charge-reversal background, reduced (open circles), wild-type background, oxidized (closed triangles), and charge-reversal background, oxidized (open triangles).

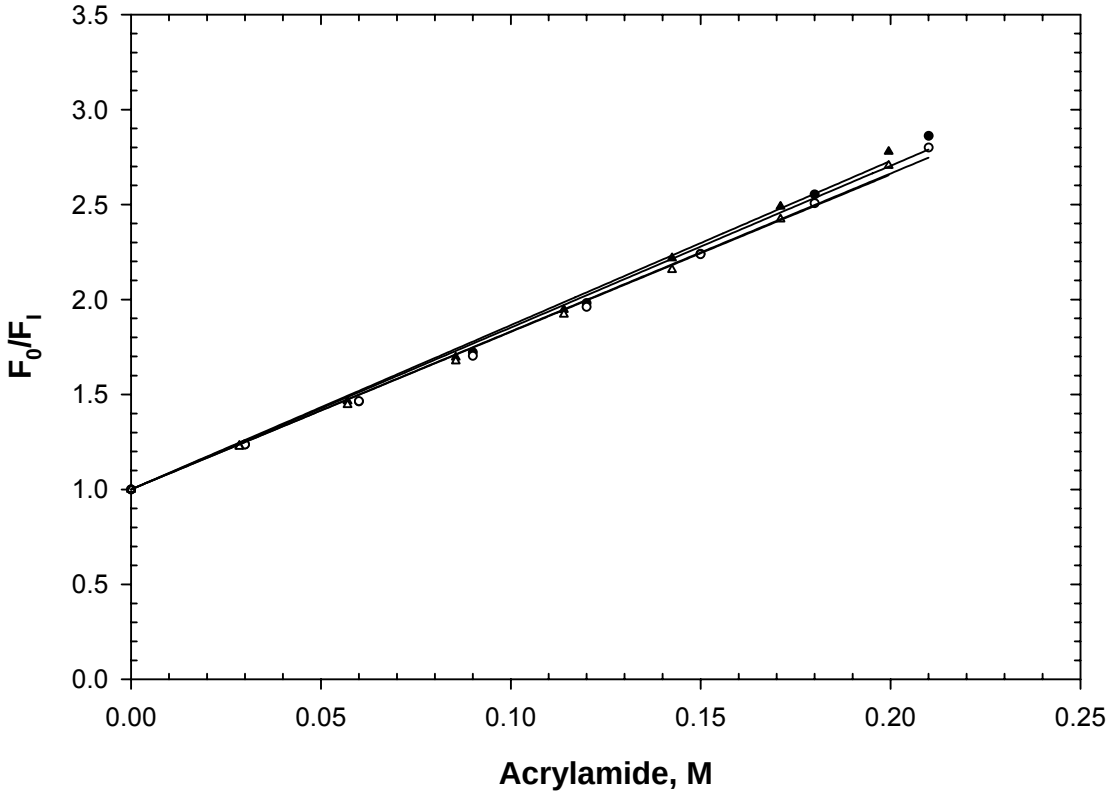

Figure 88. Acrylamide quenching of fluorescence (300 nm excitation, 350 nm emission) of denatured RNase Sa Y55W (10 μM) in 7.6 M (reduced) or 8.5 M (oxidized) urea, pH 7.0, and 25 °C. The data represent the following variants: Wild-type background, reduced (closed circles), charge-reversal background, reduced (open circles), wild-type background, oxidized (closed triangles), and charge-reversal background, oxidized (open triangles).

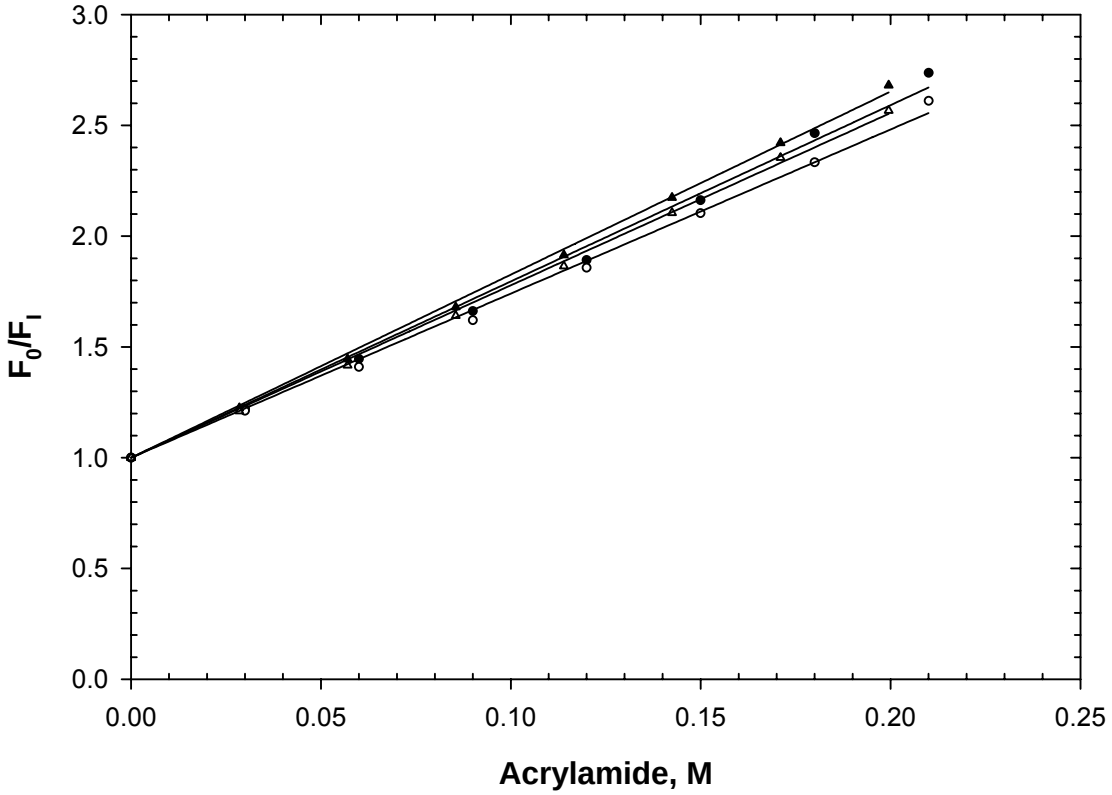

Figure 89. Acrylamide quenching of fluorescence (300 nm excitation, 350 nm emission) of denatured RNase Sa T76W (10 μM) in 7.6 M (reduced) or 8.5 M (oxidized) urea, pH 7.0, and 25 °C. The data represent the following variants: Wild-type background, reduced (closed circles), charge-reversal background, reduced (open circles), wild-type background, oxidized (closed triangles), and charge-reversal background, oxidized (open triangles).

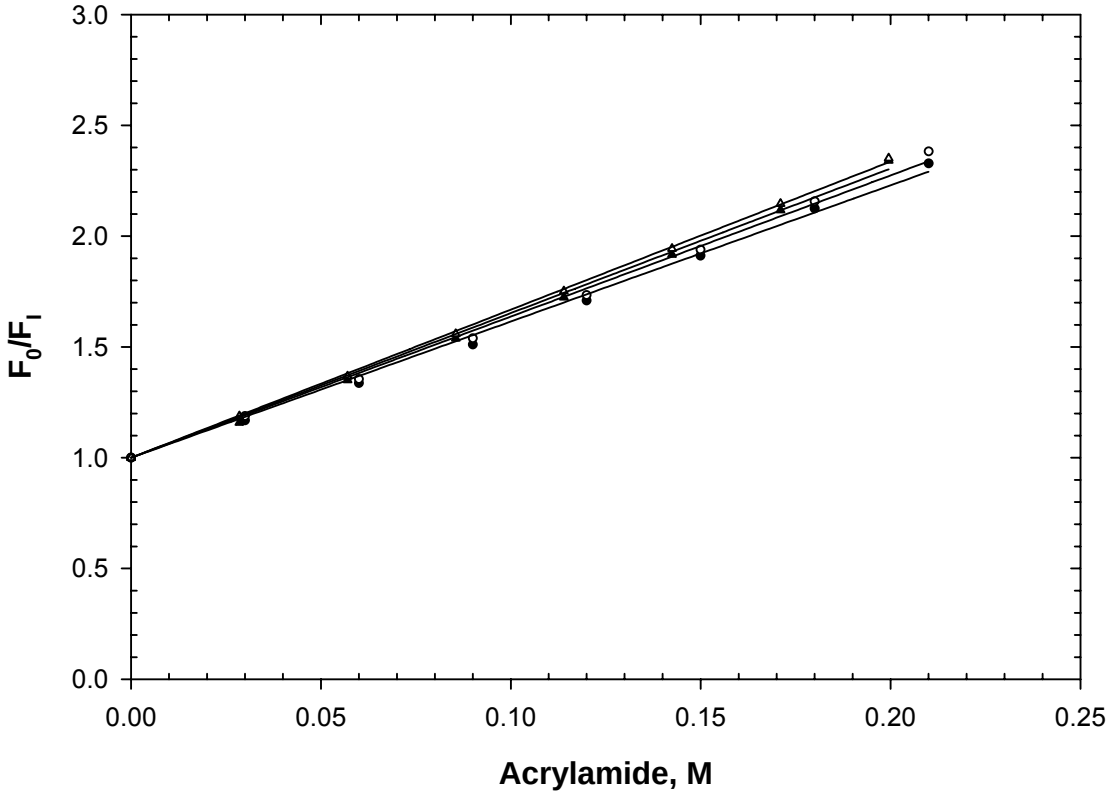

Figure 90. Acrylamide quenching of fluorescence (300 nm excitation, 350 nm emission) of denatured RNase Sa Y81W (10 μM) in 7.6 M (reduced) or 8.5 M (oxidized) urea, pH 7.0, and 25 °C. The data represent the following variants: Wild-type background, reduced (closed circles), charge-reversal background, reduced (open circles), wild-type background, oxidized (closed triangles), and charge-reversal background, oxidized (open triangles).

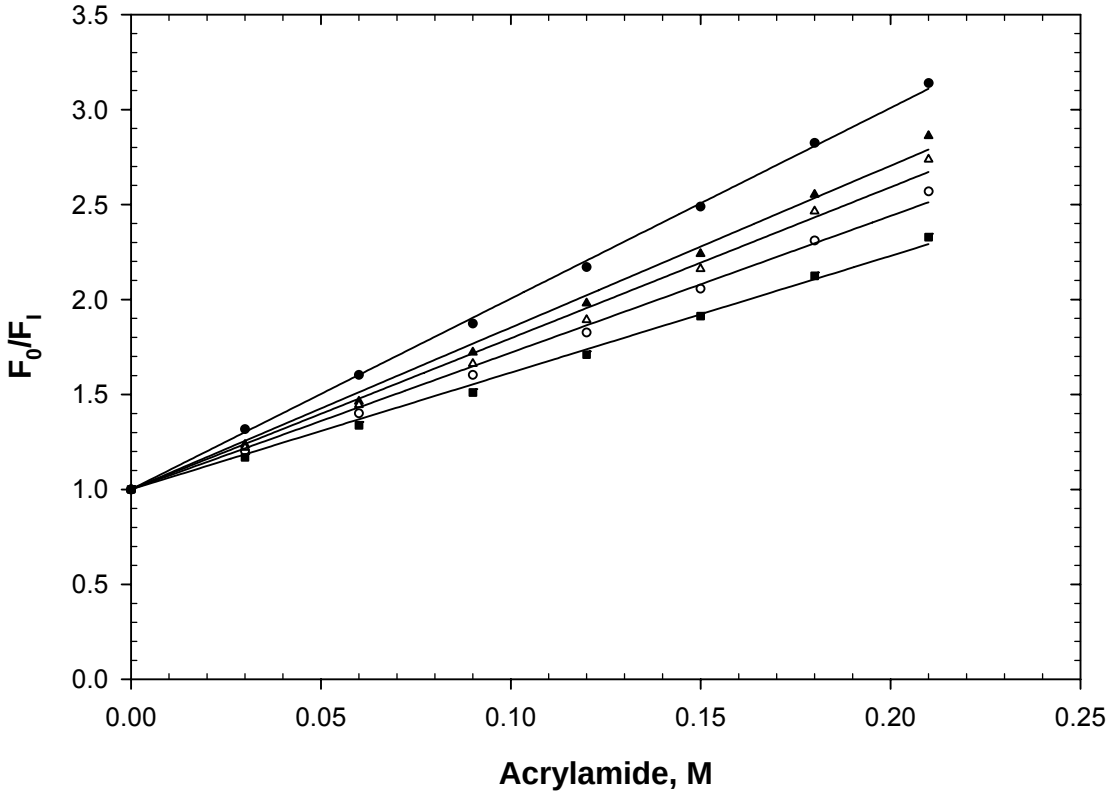

Figure 91. Acrylamide quenching of fluorescence (300 nm excitation, 350 nm emission) of the reduced, denatured RNase Sa tryptophan variants (10 μM) in the wild-type background in 7.6 M urea, 10 mM TCEP, pH 7.0, and 25 °C. The data represent the following variants: D1W (closed circles), Y52W (open circles), Y55W (closed triangles), T76W (open triangles), and Y81W (closed squares).

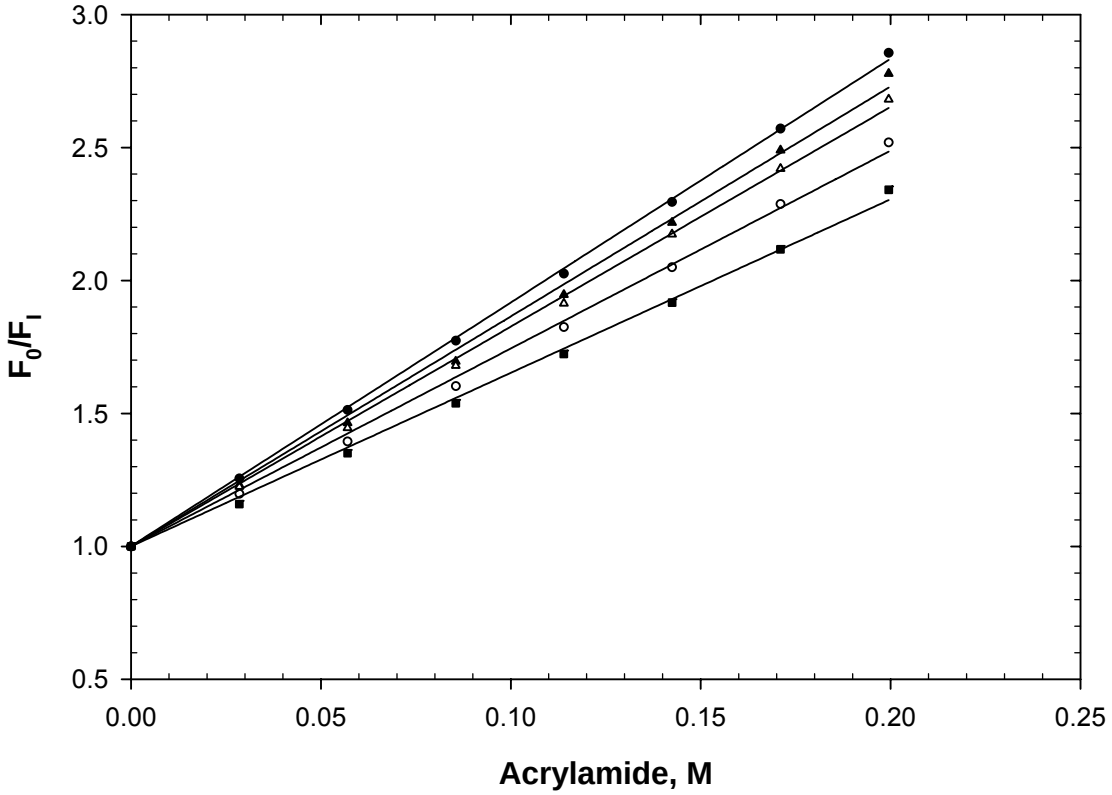

Figure 92. Acrylamide quenching of fluorescence (300 nm excitation, 350 nm emission) of the oxidized, denatured RNase Sa tryptophan variants (10 μM) in the wild-type background in 8.5 M urea, pH 7.0, and 25 °C. The data represent the following variants: D1W (closed circles), Y52W (open circles), Y55W (closed triangles), T76W (open triangles), and Y81W (closed squares).

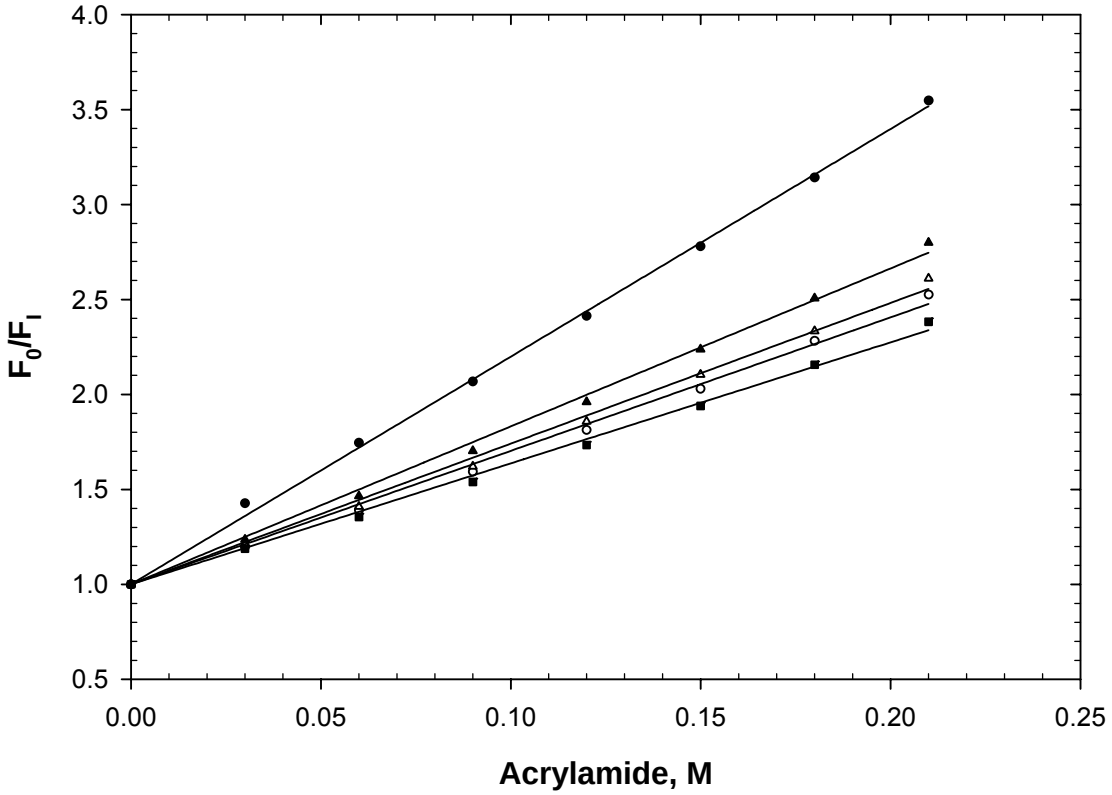

Figure 93. Acrylamide quenching of fluorescence (300 nm excitation, 350 nm emission) of the reduced, denatured RNase Sa tryptophan variants (10 μM) in the charge-reversal background in 7.6 M urea, 10 mM TCEP, pH 7.0, and 25 °C. The data represent the following variants: D1W (closed circles), Y52W (open circles), Y55W (closed triangles), T76W (open triangles), and Y81W (closed squares).

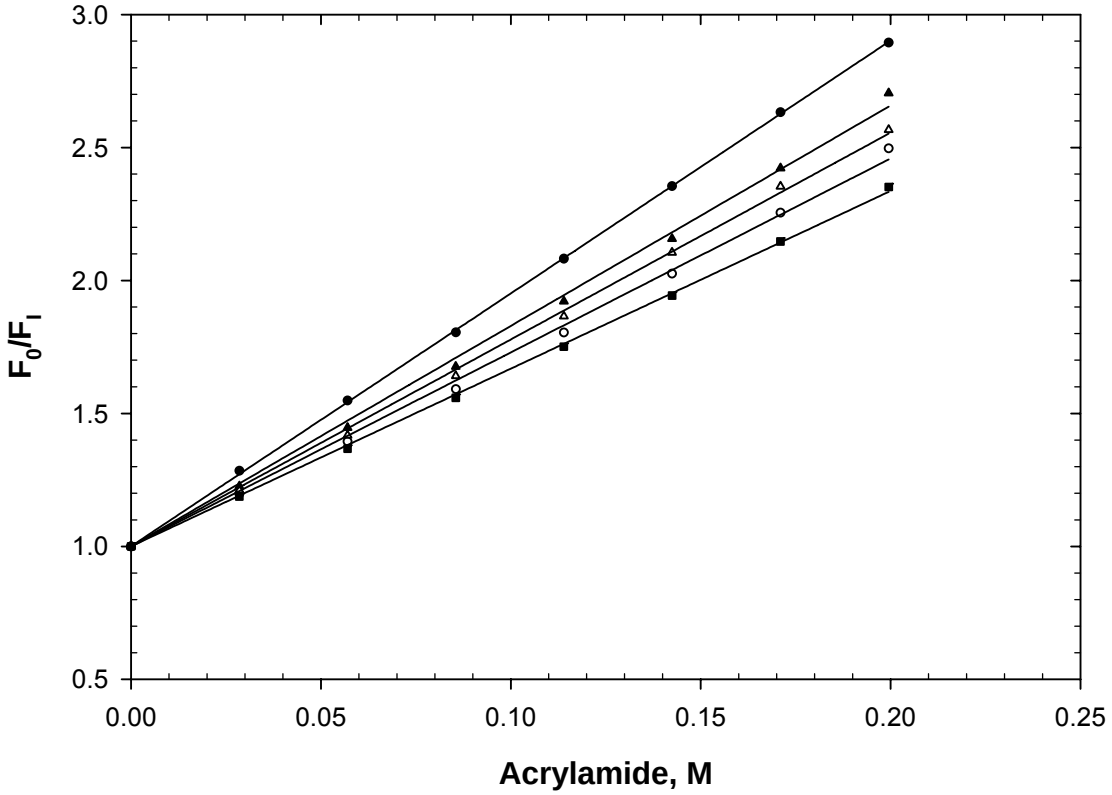

Figure 94. Acrylamide quenching of fluorescence (300 nm excitation, 350 nm emission) of the oxidized, denatured RNase Sa tryptophan variants (10 μM) in the charge-reversal background in 8.5 M urea, pH 7.0, and 25 °C. The data represent the following variants: D1W (closed circles), Y52W (open circles), Y55W (closed triangles), T76W (open triangles), and Y81W (closed squares).

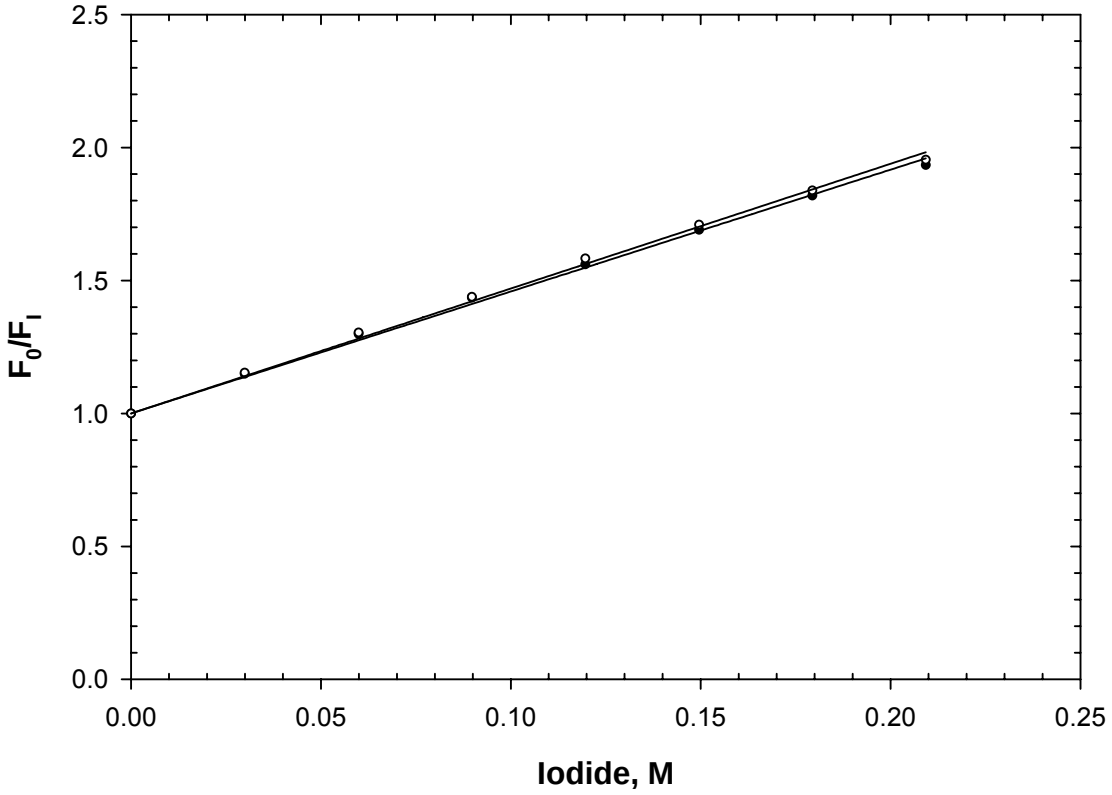

Figure 95. Iodide quenching of fluorescence (300 nm excitation, 350 nm emission) of reduced, denatured RNase Sa D1W (10 μM) in 3.8 M guanidine hydrochloride, 10 mM TCEP, pH 7.0, and 25 °C. The data represent the following variants: Wild-type background (closed circles) and charge-reversal background (open circles).

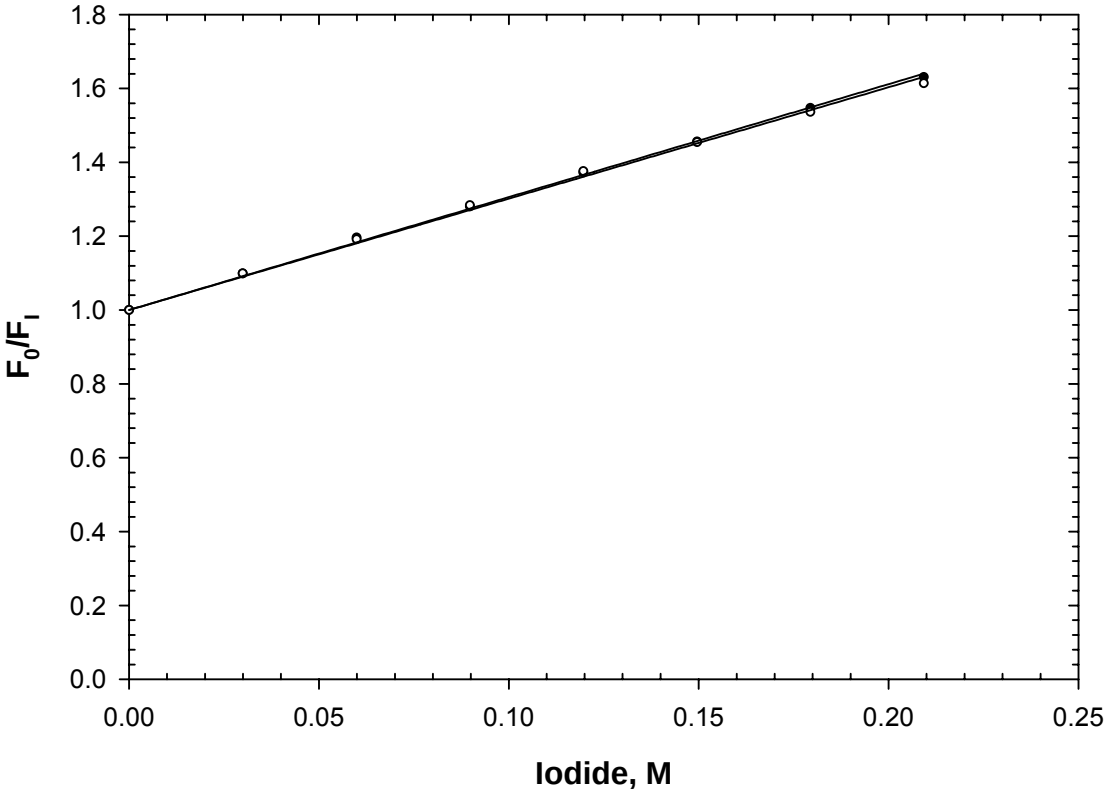

Figure 96. Iodide quenching of fluorescence (300 nm excitation, 350 nm emission) of reduced, denatured RNase Sa Y52W (10 μM) in 3.8 M guanidine hydrochloride, 10 mM TCEP, pH 7.0, and 25 °C. The data represent the following variants: Wild-type background (closed circles) and charge-reversal background (open circles).

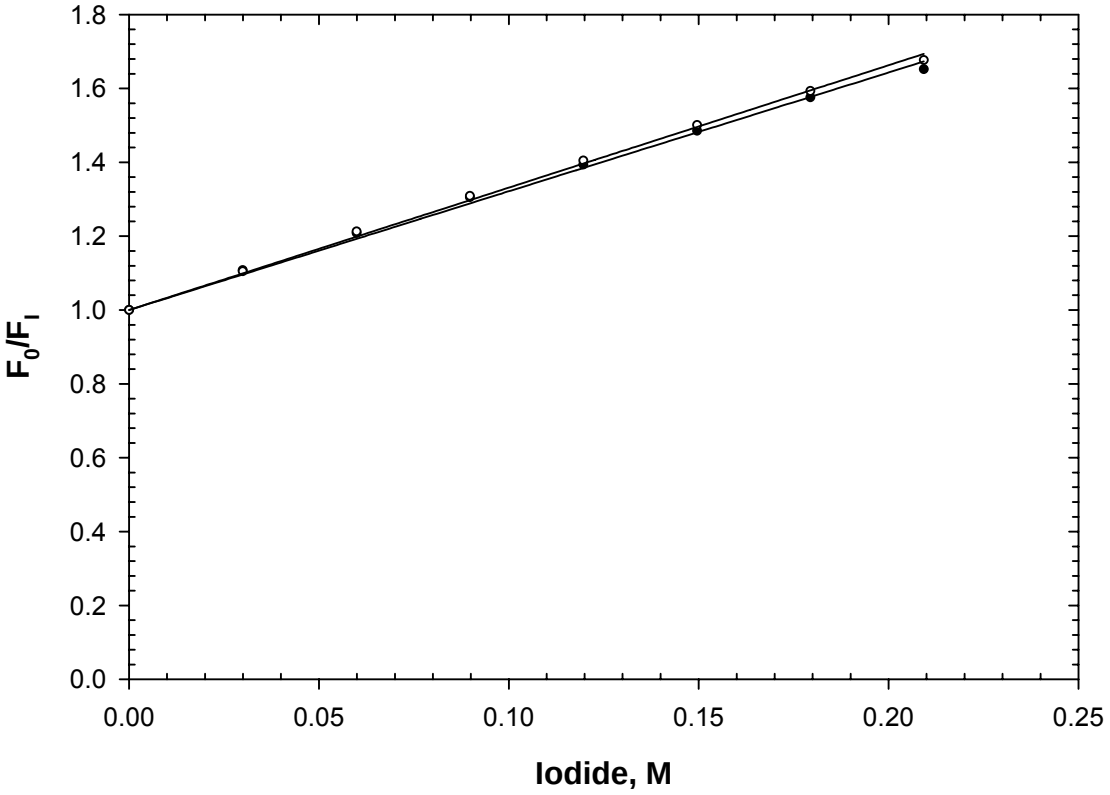

Figure 97. Iodide quenching of fluorescence (300 nm excitation, 350 nm emission) of reduced, denatured RNase Sa Y55W (10 μM) in 3.8 M guanidine hydrochloride, 10 mM TCEP, pH 7.0, and 25 °C. The data represent the following variants: Wild-type background (closed circles) and charge-reversal background (open circles).

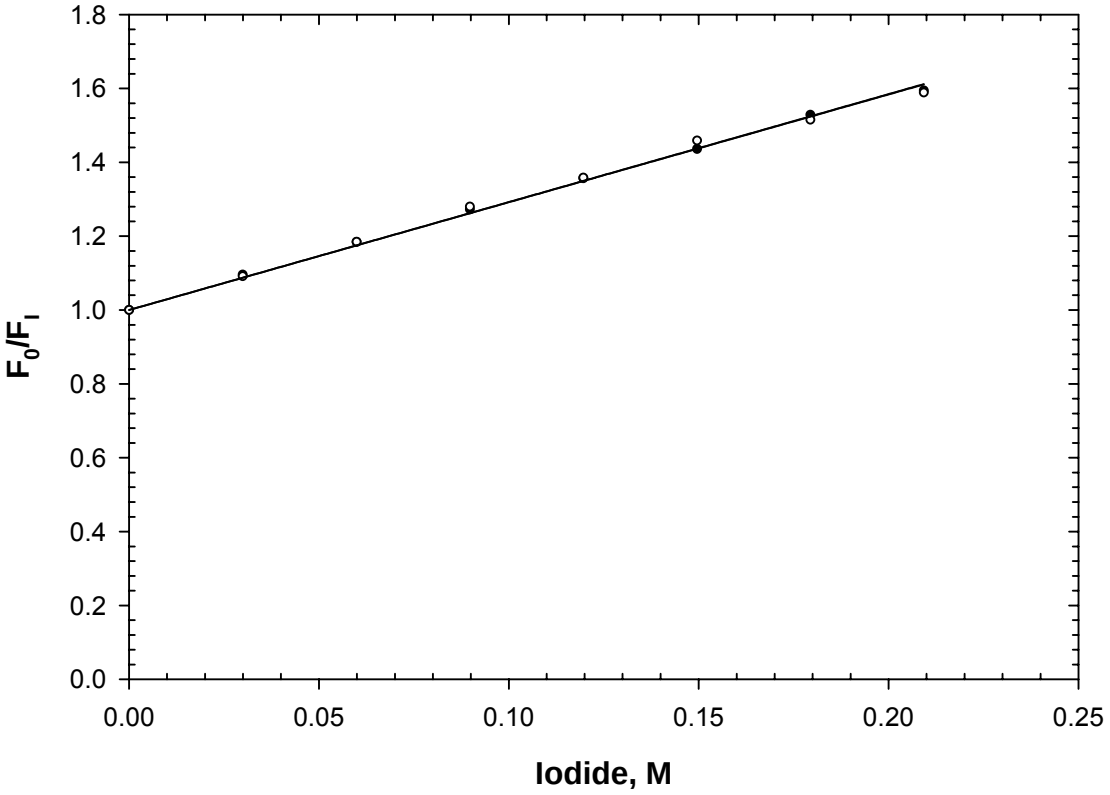

Figure 98. Iodide quenching of fluorescence (300 nm excitation, 350 nm emission) of reduced, denatured RNase Sa T76W (10 μM) in 3.8 M guanidine hydrochloride, 10 mM TCEP, pH 7.0, and 25 °C. The data represent the following variants: Wild-type background (closed circles) and charge-reversal background (open circles).

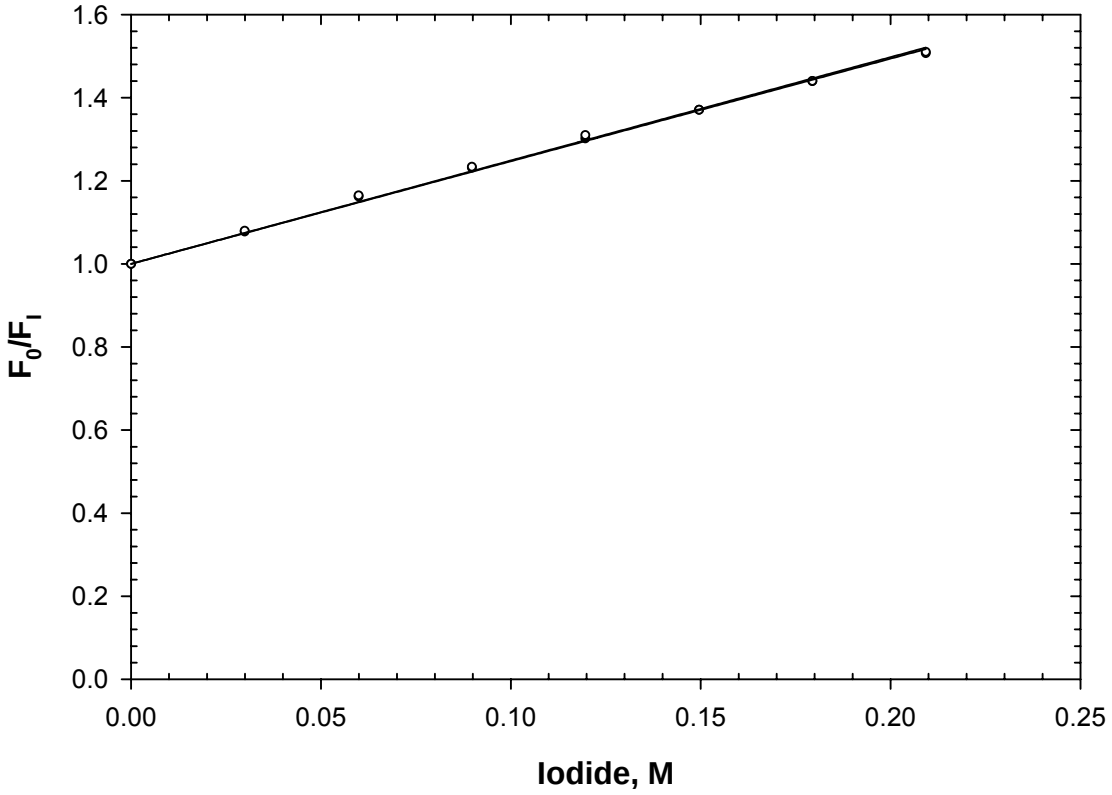

Figure 99. Iodide quenching of fluorescence (300 nm excitation, 350 nm emission) of reduced, denatured RNase Sa Y81W (10 μM) in 3.8 M guanidine hydrochloride, 10 mM TCEP, pH 7.0, and 25 °C. The data represent the following variants: Wild-type background (closed circles) and charge-reversal background (open circles).

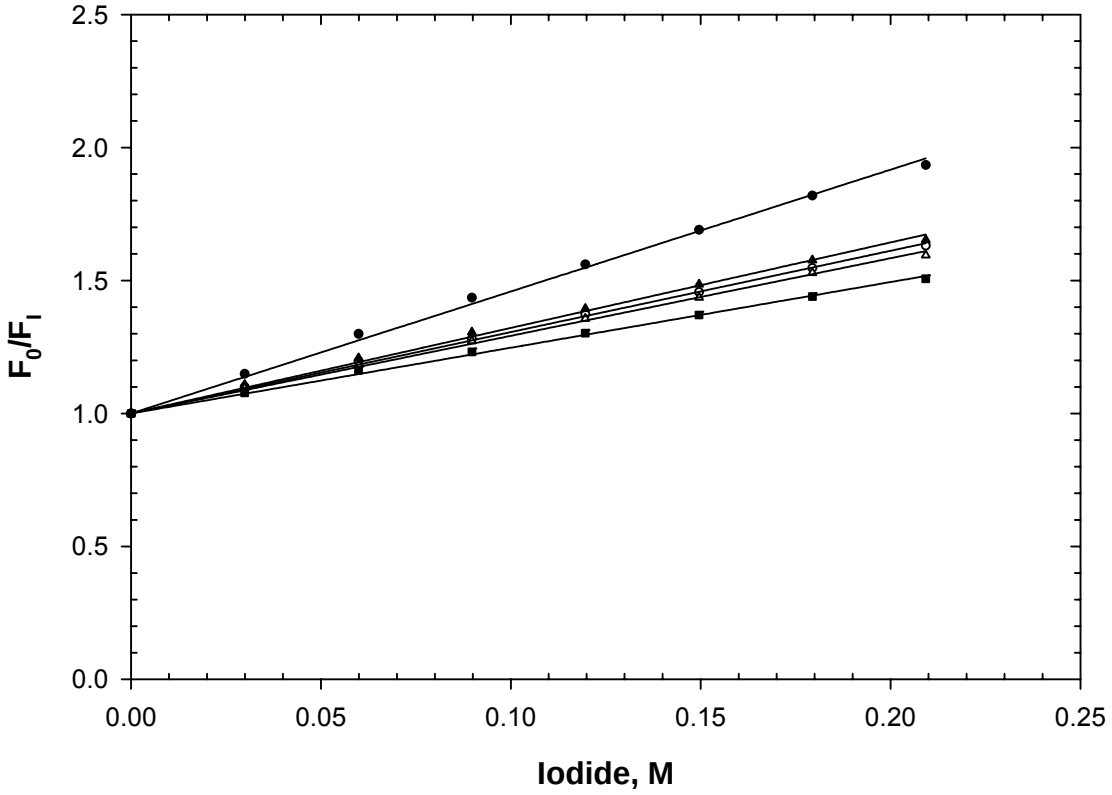

Figure 100. Iodide quenching of fluorescence (300 nm excitation, 350 nm emission) of the reduced, denatured RNase Sa tryptophan variants (10 μM) in the wild-type background in 3.8 M guanidine hydrochloride, 10 mM TCEP, pH 7.0, and 25 °C. The data represent the following variants: D1W (closed circles), Y52W (open circles), Y55W (closed triangles), T76W (open triangles), and Y81W (closed squares).

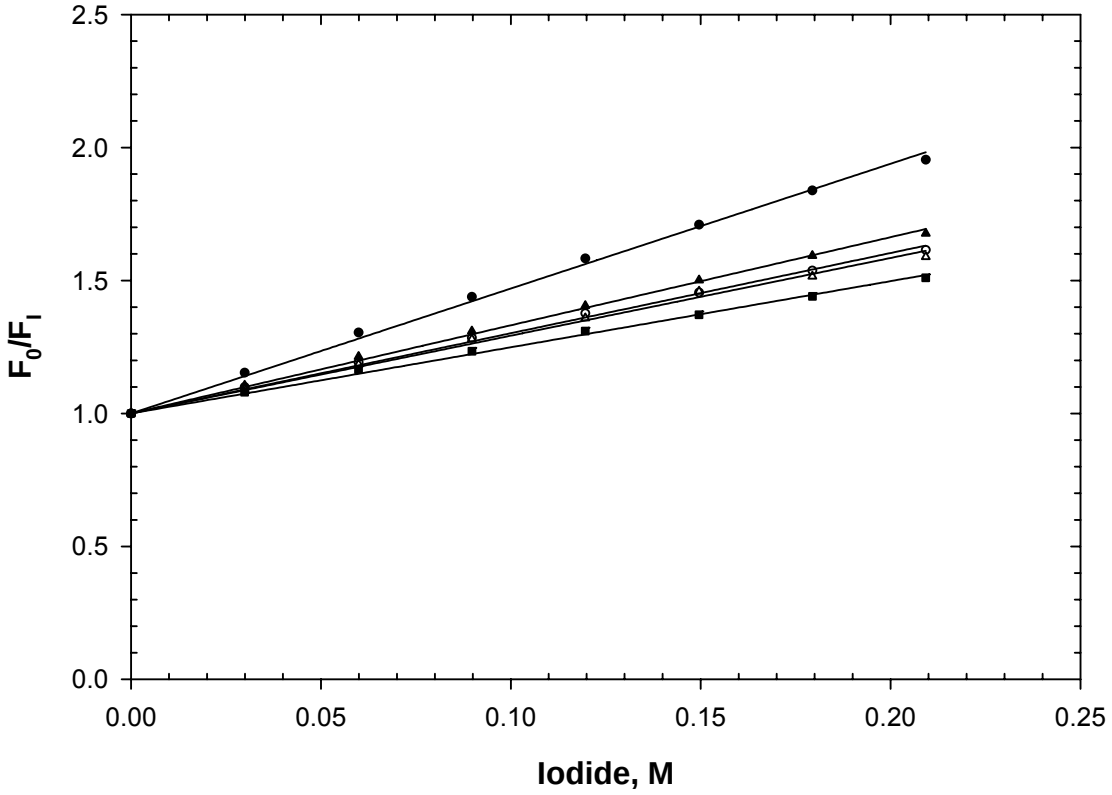

Figure 101. Iodide quenching of fluorescence (300 nm excitation, 350 nm emission) of the reduced, denatured RNase Sa tryptophan variants (10 μM) in the charge-reversal background in 3.8 M guanidine hydrochloride, 10 mM TCEP, pH 7.0, and 25 °C. The data represent the following variants: D1W (closed circles), Y52W (open circles), Y55W (closed triangles), T76W (open triangles), and Y81W (closed squares).

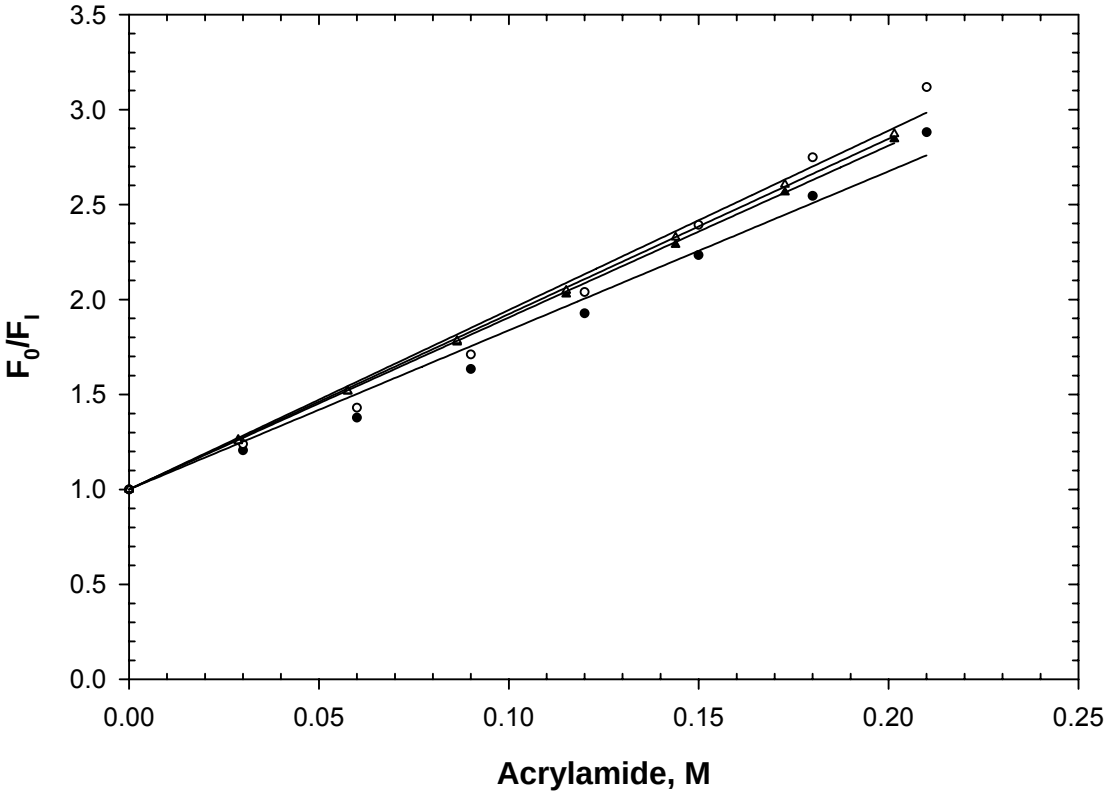

Figure 102. Acrylamide quenching of fluorescence (300 nm excitation, 350 nm emission) of denatured RNase Sa D1W (10 μM) in 3.8 M (reduced) or 6 M (oxidized) guanidine hydrochloride , pH 7.0, and 25 ^{o}C. The data represent the following variants: Wild-type background, reduced (closed circles), charge-reversal background, reduced (open circles), wild-type background, oxidized (closed triangles), and charge-reversal background, oxidized (open triangles).

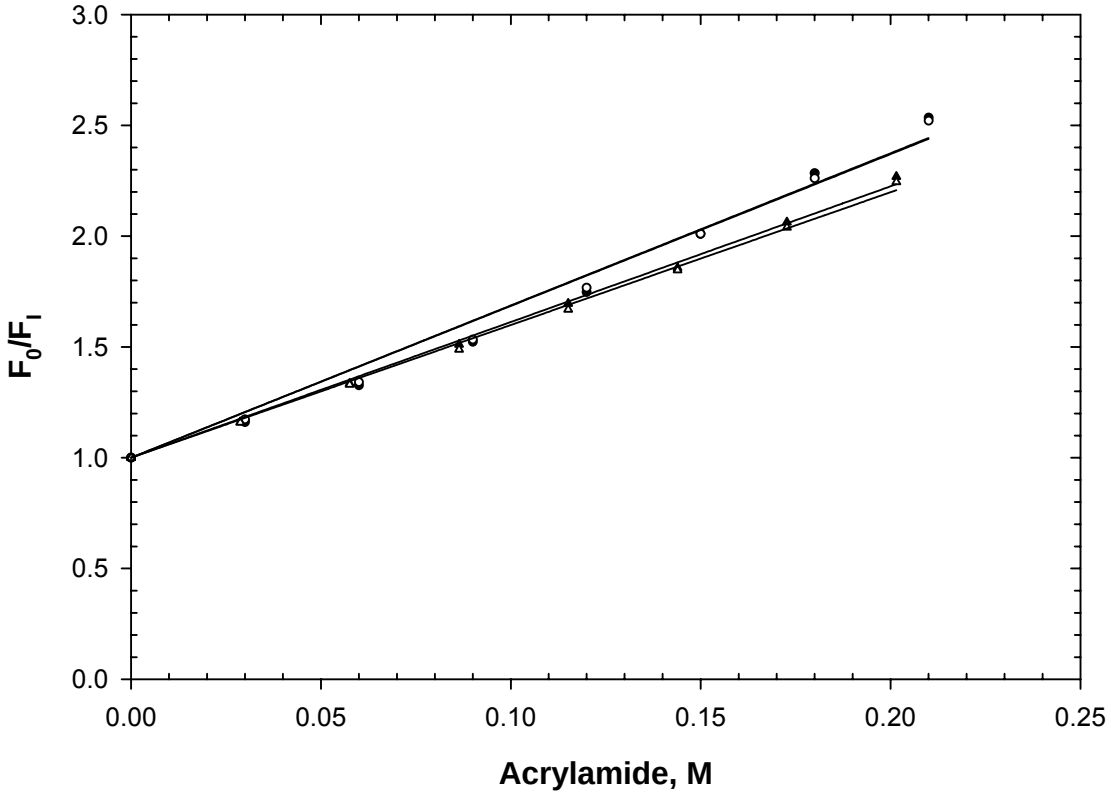

Figure 103. Acrylamide quenching of fluorescence (300 nm excitation, 350 nm emission) of denatured RNase Sa Y52W (10 μM) in 3.8 M (reduced) or 6 M (oxidized) guanidine hydrochloride, pH 7.0, and 25 °C. The data represent the following variants: Wild-type background, reduced (closed circles), charge-reversal background, reduced (open circles), wild-type background, oxidized (closed triangles), and charge-reversal background, oxidized (open triangles).

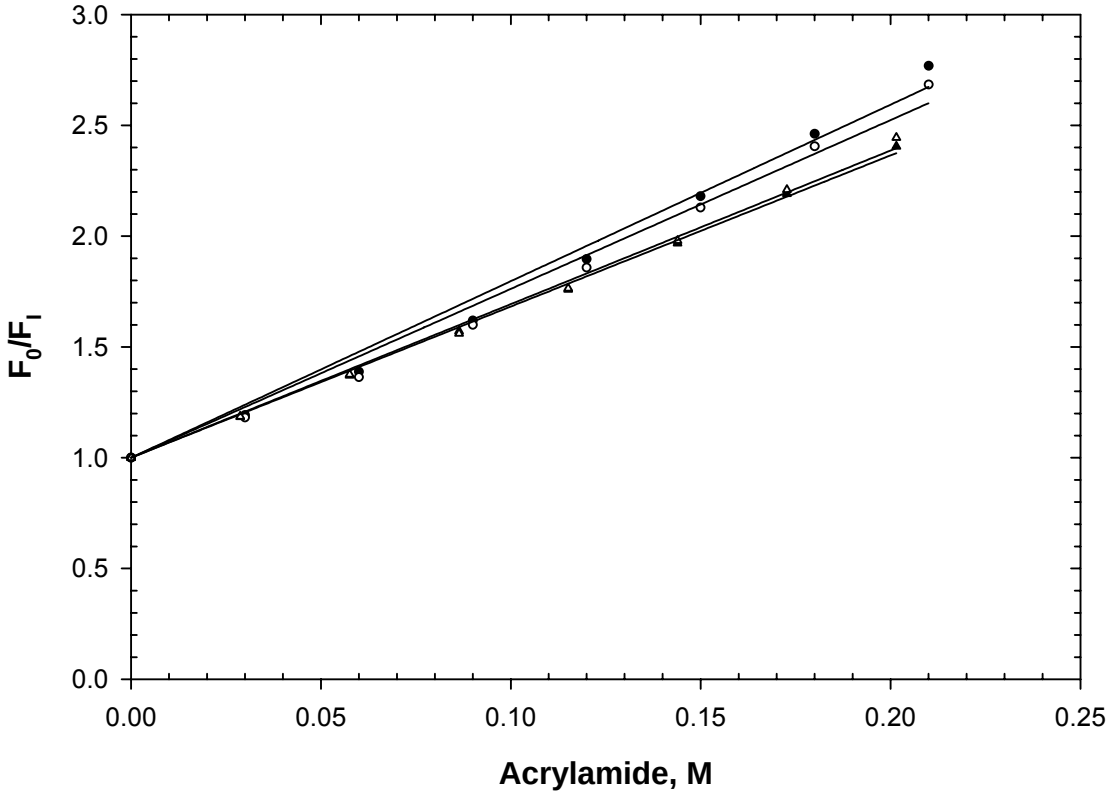

Figure 104. Acrylamide quenching of fluorescence (300 nm excitation, 350 nm emission) of denatured RNase Sa Y55W (10 μM) in 3.8 M (reduced) or 6 M (oxidized) guanidine hydrochloride, pH 7.0, and 25 °C. The data represent the following variants: Wild-type background, reduced (closed circles), charge-reversal background, reduced (open circles), wild-type background, oxidized (closed triangles), and charge-reversal background, oxidized (open triangles).

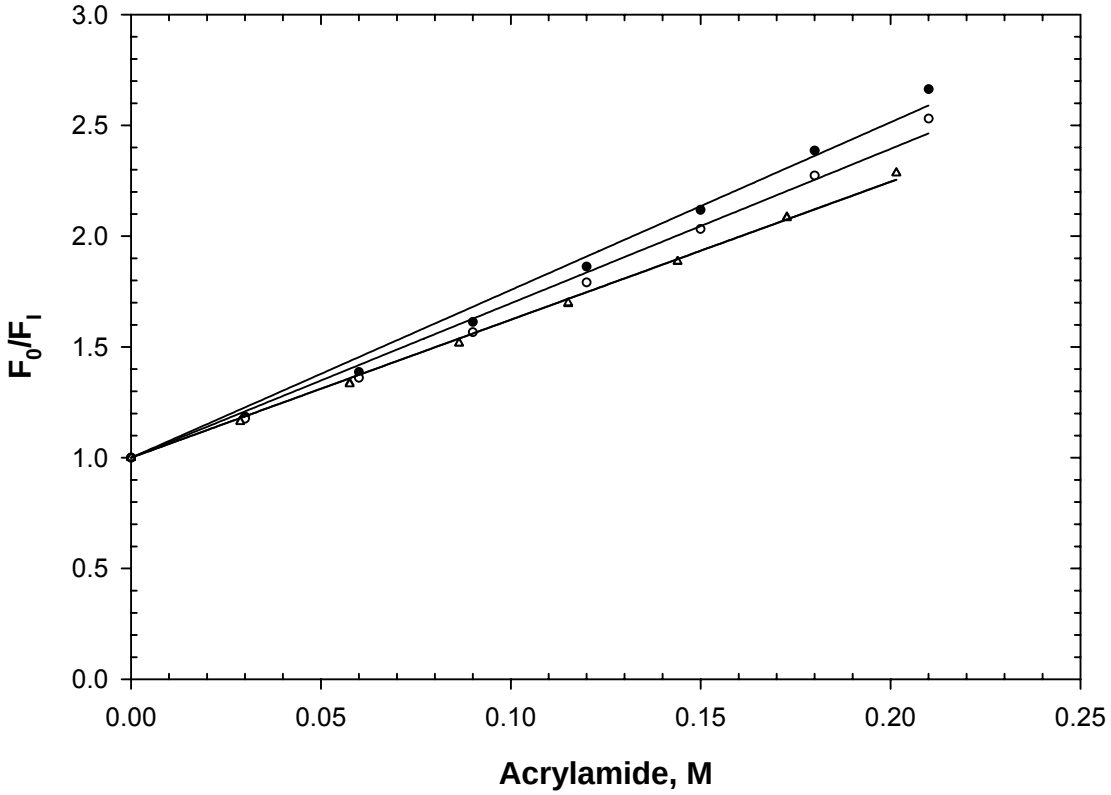

Figure 105. Acrylamide quenching of fluorescence (300 nm excitation, 350 nm emission) of denatured RNase Sa T76W (10 μM) in 3.8 M (reduced) or 6 M (oxidized) guanidine hydrochloride, pH 7.0, and 25 °C. The data represent the following variants: Wild-type background, reduced (closed circles), charge-reversal background, reduced (open circles), wild-type background, oxidized (closed triangles), and charge-reversal background, oxidized (open triangles).

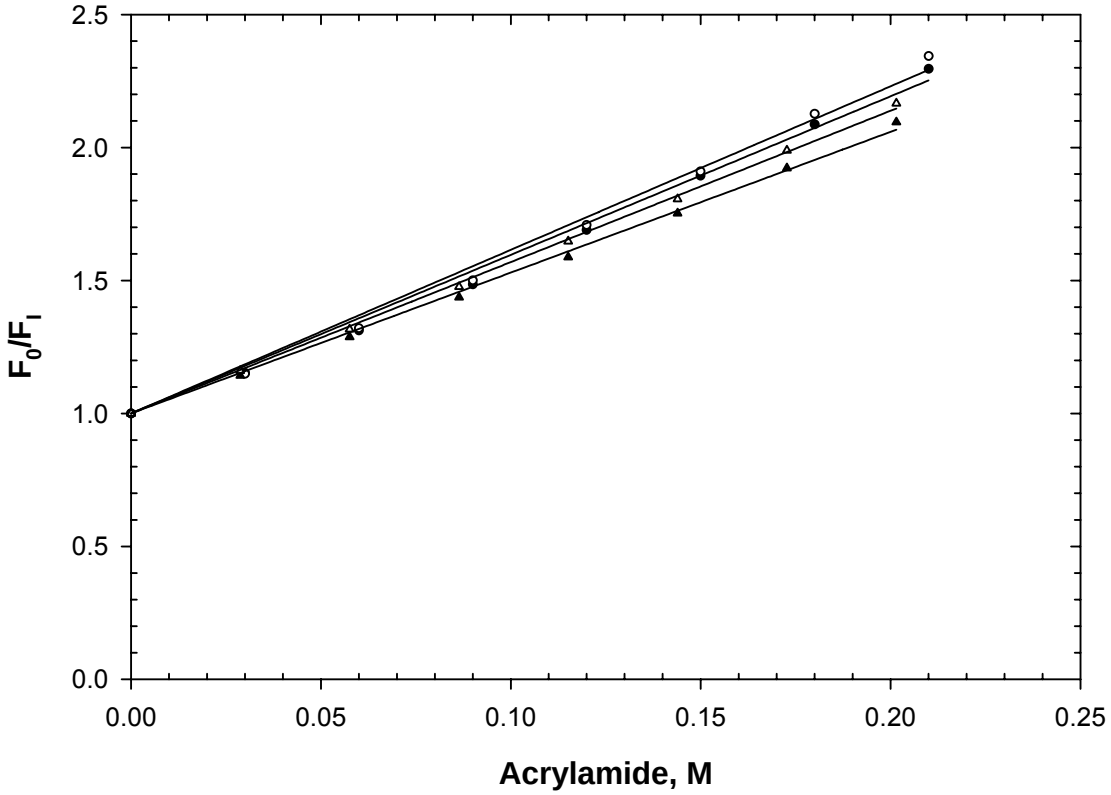

Figure 106. Acrylamide quenching of fluorescence (300 nm excitation, 350 nm emission) of denatured RNase Sa Y81W (10 μM) in 3.8 M (reduced) or 6 M (oxidized) guanidine hydrochloride, pH 7.0, and 25 °C. The data represent the following variants: Wild-type background, reduced (closed circles), charge-reversal background, reduced (open circles), wild-type background, oxidized (closed triangles), and charge-reversal background, oxidized (open triangles).

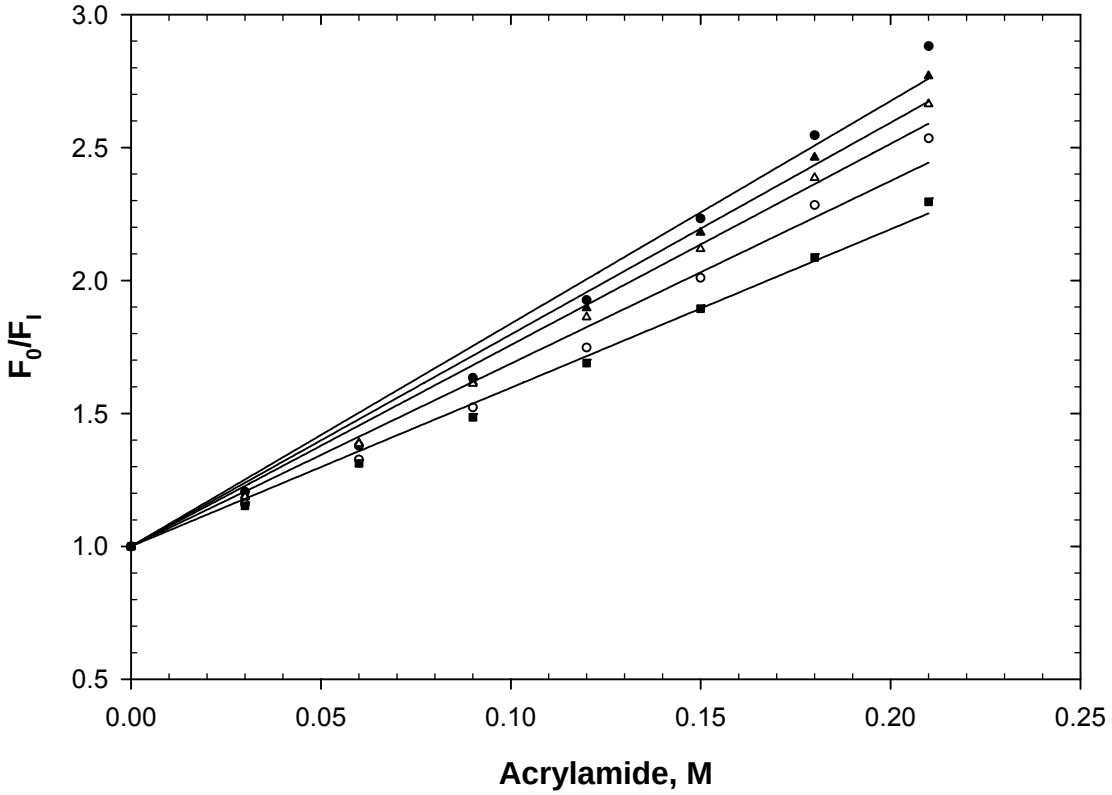

Figure 107. Acrylamide quenching of fluorescence (300 nm excitation, 350 nm emission) of the reduced, denatured RNase Sa tryptophan variants (10 μM) in the wild-type background in 3.8 M guanidine hydrochloride, 10 mM TCEP, pH 7.0, and 25 °C. The data represent the following variants: D1W (closed circles), Y52W (open circles), Y55W (closed triangles), T76W (open triangles), and Y81W (closed squares).

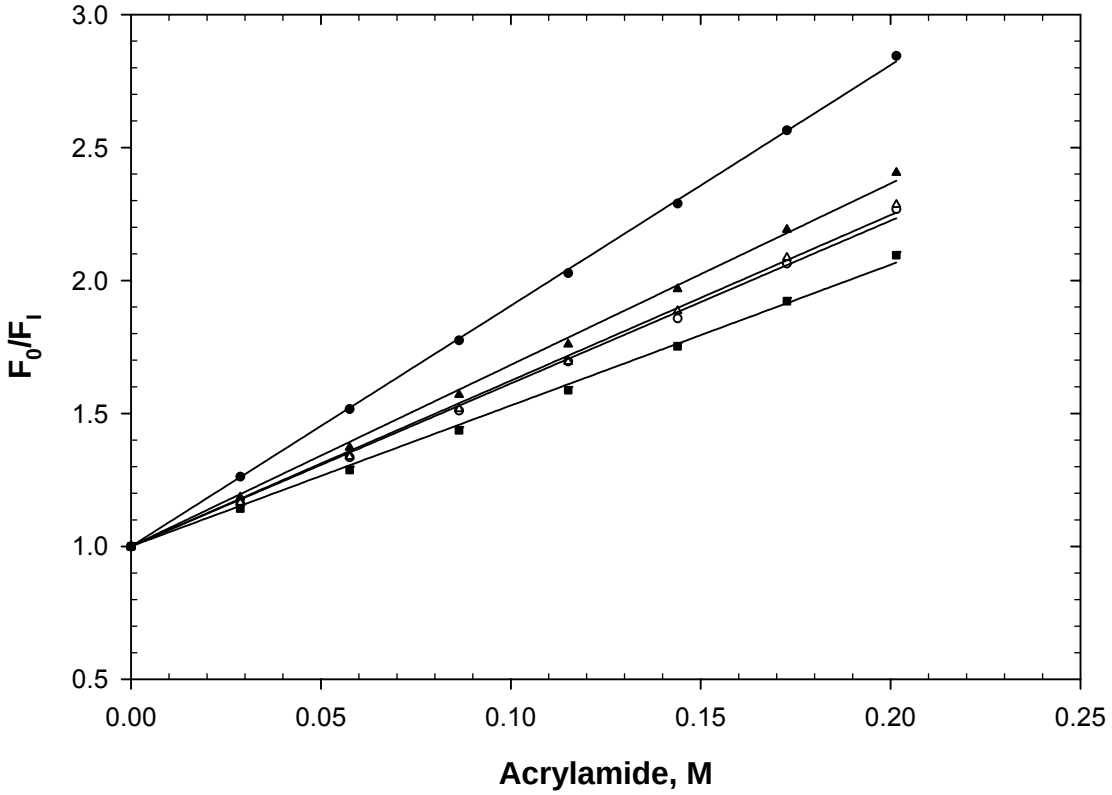

Figure 108. Acrylamide quenching of fluorescence (300 nm excitation, 350 nm emission) of the oxidized, denatured RNase Sa tryptophan variants (10 μM) in the wild-type background in 6 M guanidine hydrochloride, pH 7.0, and 25 °C. The data represent the following variants: D1W (closed circles), Y52W (open circles), Y55W (closed triangles), T76W (open triangles), and Y81W (closed squares).

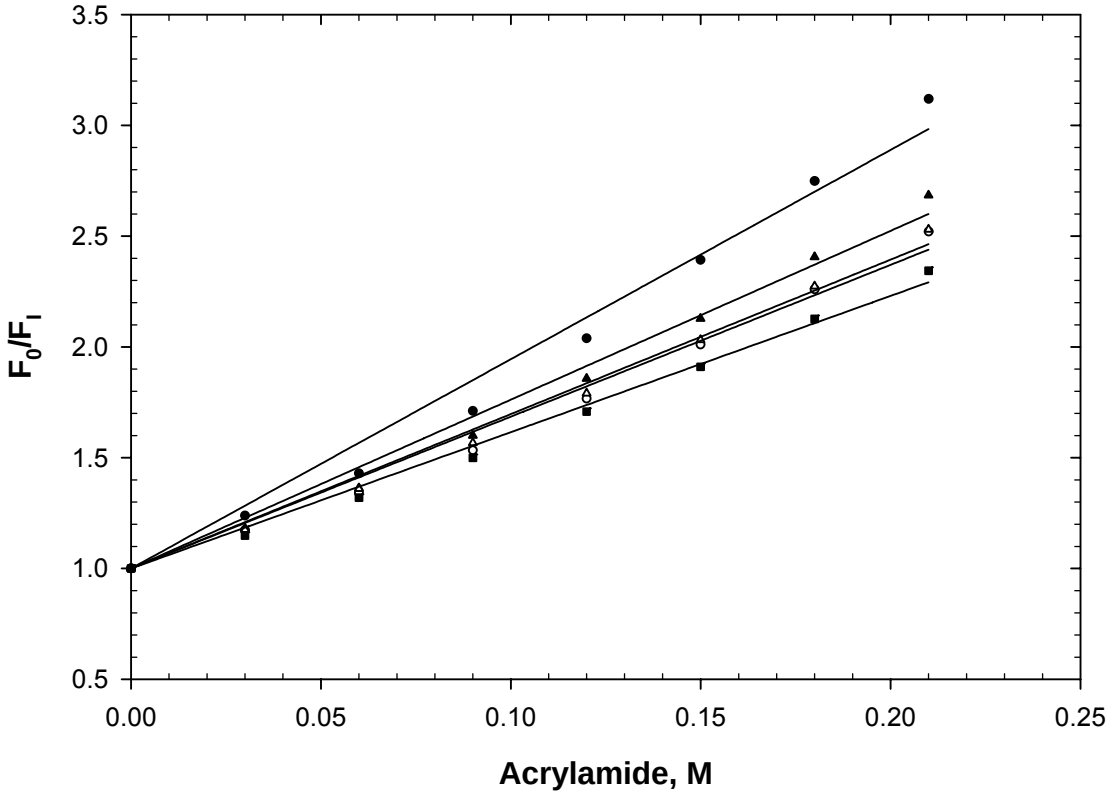

Figure 109. Acrylamide quenching of fluorescence (300 nm excitation, 350 nm emission) of the reduced, denatured RNase Sa tryptophan variants (10 μM) in the charge-reversal background in 3.8 M guanidine hydrochloride, 10 mM TCEP, pH 7.0, and 25 °C. The data represent the following variants: D1W (closed circles), Y52W (open circles), Y55W (closed triangles), T76W (open triangles), and Y81W (closed squares).

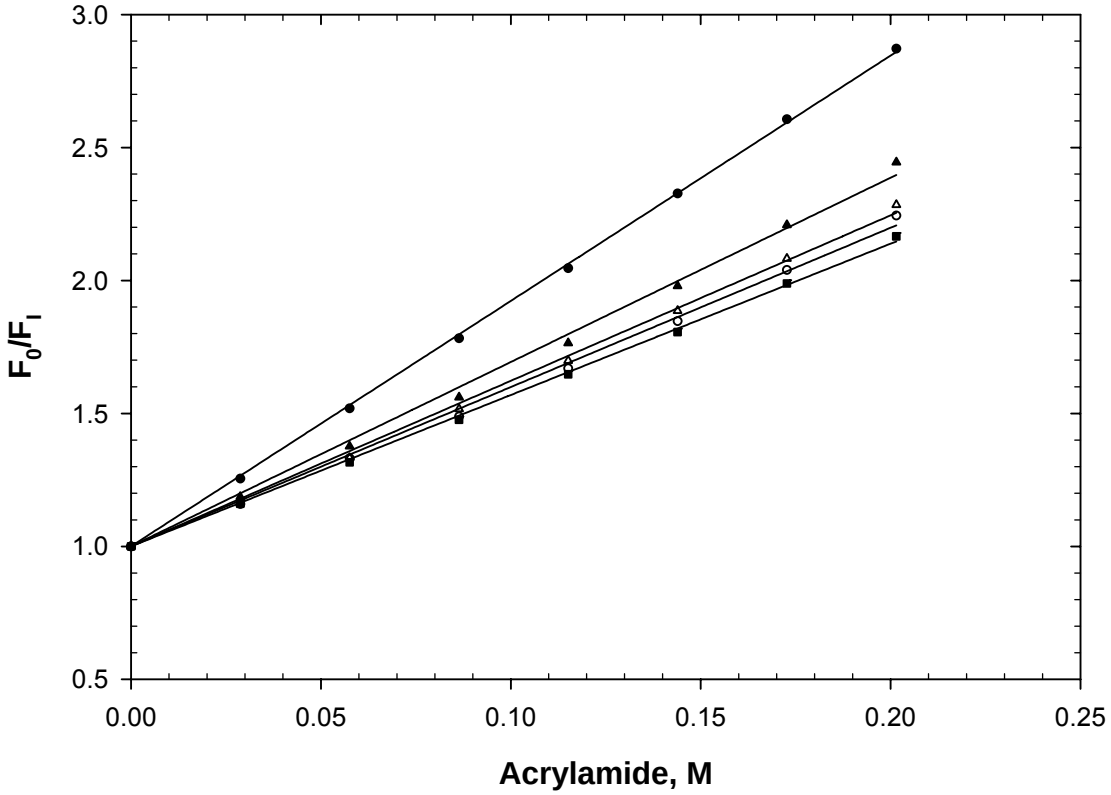

Figure 110. Acrylamide quenching of fluorescence (300 nm excitation, 350 nm emission) of the oxidized, denatured RNase Sa tryptophan variants (10 μM) in the charge-reversal background in 6 M guanidine hydrochloride, pH 7.0, and 25 °C. The data represent the following variants: D1W (closed circles), Y52W (open circles), Y55W (closed triangles), T76W (open triangles), and Y81W (closed squares).

VITA

Roy Willis Alston

503 Southwest Pkwy., #416

College Station, TX 77840

Roy Willis Alston was born in Trenton, Tennessee on April 15, 1963. After graduating from Harding Academy, Searcy, Arkansas, he graduated from the University of Arkansas, Fayetteville, Arkansas with a Bachelor's degree in secondary education. After graduation, he attended Indiana State University, Terre Haute, Indiana and graduated with a Master of Science degree in athletic training. He taught for four years and was the Head Athletic Trainer for the Texas City (Texas) Independent School District. Afterwards, he taught for three years and was the Head Athletic Trainer for the McKinney (Texas) Independent School District. After that, he enrolled in Harding University, Searcy, Arkansas, and in May of 1996 completed the degree requirements for a Bachelor's of Science in chemistry. He enrolled in Texas A&M University and was awarded a Master of Science degree in biochemistry in August of 1999. He continued his research under Dr. C. Nick Pace and was awarded a Ph.D. in biochemistry in May of 2004.